STRUCTURAL AND FUNCTIONAL STUDIES OF C2-DOMAIN PROTEINS INVOLVED IN NEUROTRANSMITTER RELEASE

APPROVED BY SUPERVISORY COMMITTEE

Jose Rizo-Rey, Ph.D., Advisor

Kevin Gardner, Ph.D., Committee Chair

Joseph Albanesi, Ph.D.

Hongtao Yu, Ph.D.

DEDICATION

To my family and friends who supported me through

STRUCTURAL AND FUNCTIONAL STUDIES OF C2-DOMAIN PROTEINS INVOLVED IN NEUROTRANSMITTER RELEASE

by

HAN DAI

DISSERTATION

Presented to the Faculty of the Graduate School of Biomedical Sciences

The University of Texas Southwestern Medical Center at Dallas

In Partial Fulfillment of the Requirements

For the Degree of

DOCTOR OF PHILOSOPHY

The University of Texas Southwestern Medical Center at Dallas

Dallas, Texas

April, 2007

ACKNOWLEDGEMENTS

First, I would like to offer a special thank to my dissertation advisor, Dr. Jose Rizo-Rey for his brilliant guidance and generous support during the past five years of my graduate studies. He is the person who initially persuaded me to join the Division of Cell and Molecular Biology (DCMB) in UT Southwestern Medical Center at Dallas when I decided to come to United States to pursue my Ph.D. degree. He is both a fantastic mentor and a great scientist. He has been persistently enthusiastic about my projects and always ready to provide sparkling novel ideas and in-depth discussions. He has been fearless to tackle challenging problems, yet at the same time, objective to answer scientific questions rigorously. He has been teaching me many fascinating biophysical skills and techniques, and more important, how to be a good scientist. My achievements would not have been possible without his guidance and encouragements. I could never thank him enough for his exceptional mentorship.

I would also like to give my thanks to all the members of the Rizo-Rey laboratory for establishing such a nice working environment and for their generous help and support to me. It has been really a great pleasure to work together with them. Dr. Irina Dulubova provided all kinds of helpful scientific advice and expertise in the laboratory. Dr. Xuelian (Sue) Luo, Dr. Jun Lu, Dr. Oleg Guryev, Xiaocheng Chen, Demet Arac, Rong Guan, Nan Shen, Timothy Craig, Minghua Wen, Iryna Huryeva and Tara Murphy have always been very friendly and supportive to me and provided me generous help and support.

I thank my dissertation committee members, Dr. Kevin Gardner, Dr. Joseph Albanesi, and Dr. Hongtao Yu for helpful discussions and insightful suggestions. I thank our collaborators Dr. Diana Tomchick and Dr. Mischa Machius in the Structural Biology Laboratory (SBL) of UT Southwestern for teaching and helping me with X-ray crystallography, and Nan Shen and Dr. George Whitesides in Harvard University for their help with microfluidic systems. I also want to thank our long-term collaborator Dr. Thomas Südhof in the Center for Basic Neuroscience of UT Southwestern for providing many constructive and helpful suggestions as well as Ok-Ho Shin and Jiong Tang in Dr. Südhof's laboratory for fruitful collaborations.

Finally, I would like to thank my parents, Zhenjia Dai and Xiumin Guo, as well as my wife, Rong Guan, for their love, encouragement and support throughout my graduate studies.

STRUCTURAL AND FUNCTIONAL STUDIES OF C2-DOMAIN PROTEINS INVOLVED IN NEUROTRANSMITTER RELEASE

Publication No. _____

Han Dai, Ph.D.

The University of Texas Southwestern Medical Center at Dallas, 2007

Supervising Professor: Jose Rizo-Rey, Ph.D.

Neurotransmitter release is mediated by synaptic vesicle exocytosis at presynaptic nerve terminals. This process is extremely fast and strictly regulated by the intracellular Ca^{2+} concentration. To achieve this exquisite regulation, many proteins are involved. The central fusion machinery includes the SNARE proteins synaptobrevin, syntaxin and SNAP-25, as well as Munc18. Besides these universal components, many other neuronal specific proteins are also involved in regulating Ca^{2+}-triggered release. Interestingly, most of these regulatory proteins contain C2 domains, versatile protein modules with Ca^{2+}-dependent and Ca^{2+}-independent activities. However, the mechanism of regulation by these C2-domain proteins

remains unclear. My research has focused on understanding the structural and functional properties of two types of C2-domain proteins, synaptotagmins and RIMs.

With NMR spectroscopy and biochemical assays, we demonstrated that synaptotagmin 4 is a Ca^{2+} sensor in *Drosophila* but not in rat, in contrast to the prediction based on sequence alignments. X-ray crystallography revealed that changes in the orientations of critical Ca^{2+}-ligands render the rat synaptotagmin 4 C2B domain unable to form full Ca^{2+}-binding sites.

We also analyzed the structural and biochemical properties of the RIM2 C2A domain. NMR spectroscopy and FRET experiments demonstrated no interaction between the RIM2 C2A domain and Ca^{2+}, phospholipid, synaptotagmin 1, and SNAP-25. However, the crystal structure of RIM C2A domain exhibits a strikingly dipolar distribution of the surface electrostatic potential. Several lines of evidence from the crystal structure suggested a potential target binding site around the bottom 3_{10}-helix.

With fluorescence microscopy and microfluidic channel technology, we demonstrated that synaptotagmin 1 binds simultaneously to phospholipids and the SNARE complex reconstituted in membranes in the presence of Ca^{2+}, forming a quaternary SSCAP complex, and that the membrane penetration of synaptotagmin 1 into phospholipids is independent of the reconstituted SNARE complex. We also showed that synaptotagmin 1 displaces complexin from the reconstituted SNARE complex in the presence of Ca^{2+}, and that the

synaptotagmin 1 C2B domain is primarily responsible for SNARE binding. Moreover, NMR spectroscopy and site-directed mutagenesis studies yielded structural information of the potential binding interface, allowing us to use computational modeling and docking to generate a preliminary model of the SSCAP complex.

TABLE OF CONTENTS

PRIOR PUBLICATIONS

Jun Zhong, Zhimei Qi, Han Dai, Chunhai Fan, Genxi Li, Naoki Matsuda. Sensing phenothiazine drugs at a gold electrode co-modified with DNA and gold nanoparticles. *Anal. Sci.*, 2003, 19, 653-657

Wenjun Zhang, Yinxi Huang, Han Dai, Xiaoyue Wang, Chunhai Fan, Genxi Li. Tuning the redox and enzymatic activity of glucose oxidase in layered organic films and its application in glucose biosensors. *Anal. Biochem.*, 2004, 329, 85-90

Han Dai, Ok-Ho Shin, Mischa Machius, Diana R Tomchick, Thomas C Südhof, Josep Rizo. Structural basis for the evolutionary inactivation of Ca^{2+} binding to synaptotagmin 4. *Nature Structural & Molecular Biology*, 2004, 11, 844 - 849

Han Dai, Diana R Tomchick, Jesus Garcia, Thomas C Südhof, Mischa Machius, Josep Rizo. Crystal structure of the RIM2 C2A domain at 1.4 Å resolution. *Biochemistry*, 2005, 44, 13533-13542

Jun Lu, Mischa Machius, Irina Dulubova, Han Dai, Thomas C Südhof, Diana R Tomchick, Josep Rizo. Structural basis for a Munc13-1 homodimer - Munc13-1/RIM heterodimer switch: C2-domains as versatile protein-protein interaction modules. *PLoS biology* 2006, 4, 1159-1172

Jiong Tang, Anton Maximov, Ok-Ho Shin, Han Dai, Josep Rizo, Thomas C Südhof. A complexin/synaptotagmin-1 switch controls fast synaptic vesicle exocytosis. *Cell* 2006, 126, 1175-1187

Han Dai, Nan Shen, Demet Arac, Josep Rizo. A quaternary SNARE-synaptotagmin - calcium-phospholipid complex in neurotransmitter release. *J. Mol. Biol.* 2007, 367, 848-863

Rong Guan, Han Dai, Diana R Tomchick, Irina Dulubova, Mischa Machius, Thomas C Südhof, Josep Rizo. Crystal structure of the RIM1α C2B domain at 1.7 Å resolution. *Structure* (Submitted)

Carlos M Roggero, Gerardo A De Blas, Han Dai, Claudia N Tomes, Joseph Rizo, Luis S Mayorga. Complexin/synaptotagmin interplay controls acrosomal exocytosis. *Nature Cell Biology* (Submitted)

Mikhail Khvotchev, Irina Dulubova, Jianyuan Sun, Han Dai, Josep Rizo, Thomas C Südhof. Dual modes of Munc18-1/SNARE interactions are coupled by functionally critical binding to syntaxin-1 N-terminus. (Manuscript in preparation)

LIST OF FIGURES

LIST OF TABLES

LIST OF DEFINITIONS

β-OG	octyl-β-D-glucopyranoside
1D	one -dimensional
2D	two-dimensional
3D	three-dimensional
AIR	ambiguous interaction restraint
APS	Advanced Photon Source
ASU	asymmetric unit
BCA	bicinchoninic acid
BODIPY	4,4-difluro-5,7-dimethyl-4-bora-3a,4a-diaza-s-indacene-3-propionic acid
BoNT	botulinum neurotoxin
BSA	bovine serum albumin
C.elegans	*Caenorhabditis elegans*
CCD	charged coupled device
CCP4	the collaborative computational project number 4
CD	circular dichroism
CMC	critical micellar concentration
CNS	crystallography and NMR system
CORD7	autosomal dominant cone-rod dystrophy
CSA	chemical shift anisotropy
DAG	diacylglycerol

Dansyl	5-(dimethylamino)naphthalene-1-sulfonyl
DD	dipole-dipole interaction
DLS	dynamic light scattering
d_{min}	high resolution limit (Å)
DMSO	dimethylsulfoxide
DOPE	1,2-dioleoyl phosphatidylethanolamine
DOPS	1,2-dioleoyl phosphatidylserine
DPPE	1,2- dipalmitoyl phosphatidylethanolamine
DTT	dithiothreitol
E. coil	*Eschericheria coli*
EDTA	ethylene diamine tetraacetic acid
EGTA	ethylene glycol-bis (β-aminoethyl ether)-tetraacetic acid
EM	electron microscopy
EPR	electron paramagnetic resonance
F_{calc}	calculated structure factors
F_{obs}	observed structure factors
FPLC	fast performance liquid chromatography
FRET	fluorescence resonance energy transfer
GAP	GTPase activating factor
GST	glutathione-S-transferase
HADDOCK	high ambiguity driven protein-protein docking

HEPES	N-(2-hydroxyethyl) piperizine-N’2-ethanesulphonic acid
HSQC	heteronuclear single quantum correlation
IPTG	isopropyl β-D-thiogalactopyranoside
ITC	isothermal titration calorimetry
Ka	association constant
Kd	dissociation constant
kDa	kilodalton
LB	luria broth
LDCV	large dense-core vesicle
LMV	large multilamellar vesicle
LTP	long-term potentiation
LUV	large unilamellar vesicle
MAD	multiple wavelength anomalous dispersion
MES	2-(N-morpholino)ethanesulfonic acid
MIR	multiple isomorphous replacement
NBD	N,N'-dimethyl-N-(iodoacetyl)-N'-(7-nitrobenz-2-oxa-1,3-diazol-4-yl) ethylenediamine
Ni-NTA	nickel-nitrilotriacetic acid
NMR	nuclear magnetic resonance
NOE	nuclear Overhauser effect
NOESY	nuclear Overhauser effect spectroscopy
NSF	N-ethylmaleimide-sensitive factor

NT	neurotransmitter
OD	optical density
PAGE	polyacrylamide gel electrophoresis
PBS	phosphate buffered saline
PC	phosphatidylcholine
PCR	polymerase chain reaction
PDB	protein data bank
PDMS	polydimethylsiloxane
PE	phosphatidylethanolamine
PEG	polyethylene glycol
PI	isoelectric point
PI3K	phosphoinositide-3 kinase
PKC	protein kinase C
PLCδ	phospholipase C-δ
POPC	1-palmitoyl, 2-oleoyl phosphatidylcholine
ppm	parts per million
PS	phosphatidylserine
PtdIns	phosphatidylinositol
R_{eff}	effective detergent to lipid molar ratio
RIM	Rab3-interacting molecule
RIM-BP	RIM-binding protein

rms	root mean square
rpm	revolutions per minute
R_{sat}	effective ratio at the onset solubilization of liposomes
R_{sol}	effective ratio at the total solubilization of liposomes
SAD	single wavelength anomalous dispersion
SBC	Structural Biology Center
SDS	sodium dodecylsulfate
SIR	single isomorphous replacement
SMR	the strongest methyl resonance
SN I	SNAP-25 (11-82-W)
SN III	SNAP-25 (141-203-W)
SNAP	soluble NSF attachment protein
SNAP-25	synaptosome-associated protein of 25 kDa
SNARE	SNAP receptor
TCA	trichloroacetic acid
TCEP	Tris(2-carboxyethyl) phosphine
TLS	translation/libration/skew
TM	transmembrane region
TOCSY	total correlation spectroscopy
Tris	tris (hydroxymethyl) aminomethane
TROSY	transverse-relaxation optimized spectroscopy

t-SNARE	target membrane SNARE
USF	Uppsala Software Factory
UV	ultraviolet
VAMP	vesicle-associated membrane protein
V_M	Matthew's coefficient
v-SNARE	vesicle SNARE

Chapter 1 General Introduction

1.1 Neurons and Interneuronal Communication

The nervous system in multicelluclar animals is a highly integrated and coordinated system to monitor and respond to the external environment and regulate all aspects of bodily functions. The brain is the control center of the nervous system to receive, store, interpret, integrate, and transmit information, which makes it a unique organ. The human brain contains more than 100 billion neurons, which are the elementary units of the nervous system and electrically excitable cells that function to receive, process, and transmit information. These neurons form an extremely complex and integrated communication network. The ability of neurons to communicate with each other is central for brain function and is perturbed in many neurological disorders such as schizophrenia, Huntington's disease and Parkinson's disease, *etc*.

1.1.1 The Neuron

Neurons are the elementary functional units of the nervous system. Neurons exhibit highly specialized shape and physiology in order to sense environmental stimuli and conduct electrochemical impulses. The high level of specialization costs the neurons to lose their ability to reproduce once formed.

In general, a typical neuron can be roughly divided into four morphologically distinct regions: the cell body, the dendrites, the axon, and the presynaptic terminals (Figure 1.1). The cell body, also known as the soma, usually occupies less than one tenth of the cell's

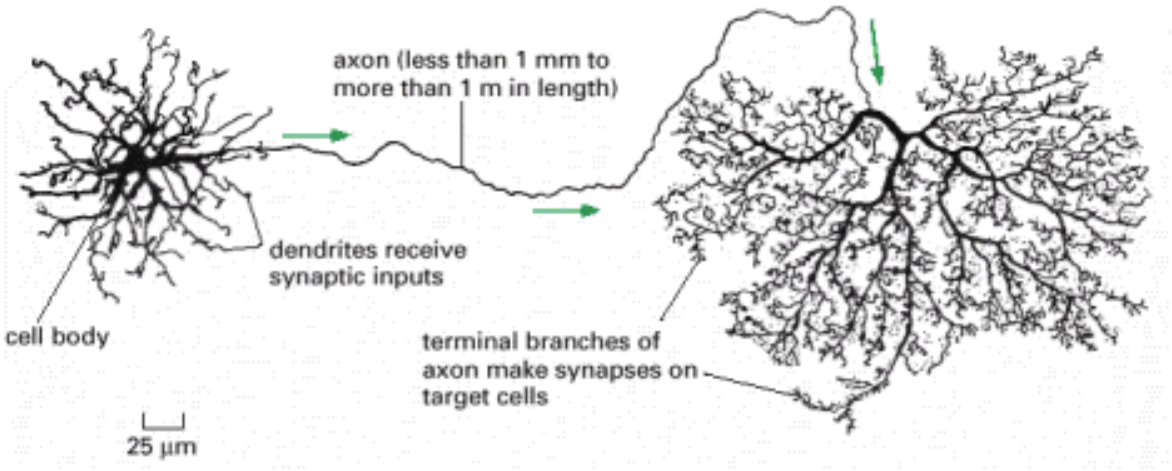

Figure 1.1 The diagram of a typical neuron of a vertebrate.

The neuronal cell body, dendrites, axons and the presynaptic terminals are labeled. The green arrows denote the direction of the information flow, from the dendrites to the presynaptic terminals (Molecular Biology of the Cell, fourth edition, Alberts et al., 2002).

volume and contains the nucleus and the organelles for the production of RNA, proteins and membranes, acting as the biosynthetic center of the cell. Dendrites and axons are specialized projections extended from the cell body, which are responsible for the interneuronal as well as intraneuronal information flow. The information flow is usually unidirectional, with dendrites sensing the changes in the cell environment, such as light, heat, injury and transmitted impulse from other neurons on one end, and axons propagating the information flow to the presynaptic terminals on the other end. Dendrites are usually highly ramified and establish contacts with many other neurons in order to receive signals from them. Axons usually exist singly in every neuron, assuming the morphology of a thin cylindrical projection that can extend up to 5 meters in some organisms. The presynaptic terminals are distinct structures located at the very end of an axon. Through its terminals, one neuron transmits information about its own activity to the dendrites of other neurons. This transmission is achieved by releasing in the terminal a specific chemical signal: the neurotransmitter.

1.1.2 The Synapse

Synapses are specialized cell-cell contacts where signals are reliably transmitted from a neuron to other neurons in a highly regulated manner. There are two major kinds of synapses in the nervous system: chemical synapse and electrical synapse. The chemical synapses are more common and much more flexible than electrical synapses. Chemical synapses are capable of amplifying neuronal signals as well as enduring changes in effectiveness, which is referred to as plasticity.

In chemical synapses, signal transduction is achieved by converting the electrical signal into a chemical signal: the neurotransmitter that diffuses between cells. The neuron sending out information is called the presynaptic cell and, correspondingly, the cell receiving information is called the postsynaptic cell. The conversion of the electrical signal into the chemical signal occurs at active zones, highly specialized sites of the presynaptic nerve terminal. Normally a presynaptic neuron terminates at the postsynaptic neuron's dendrites but communication may take place at the cell body, or even, although less often, at the initial or terminal portions of the axon. Electron microscopy (EM) ultrastructural studies revealed that electron dense proteinaceous material is present on both the presynaptic side and the postsynaptic side of many synapses, which corresponds to the so called active zone and postsynaptic density, respectively. The invasion of an action potential at the presynaptic active zone, where the neurotransmitter release machinery are localized, causes the opening of voltage-gated Ca^{2+} channels. Ca^{2+} influx triggers the synaptic vesicles loaded with neurotransmitters to fuse with the presynaptic plasma membrane and release the neurotransmitters into the interneuronal space, known as the synaptic cleft. The released neurotransmitters activate receptors on the postsynaptic density of the synapse, essentially allowing the action potential to "jump the gap" to the postsynaptic neurons (Figure 1.2).

1.1.3 Action Potential

Similar to all other types of cells, neurons possess an electric potential difference across the plasma membrane, so called the transmembrane potential, which arises from the uneven distribution of the carried charges of ions across the membrane through a

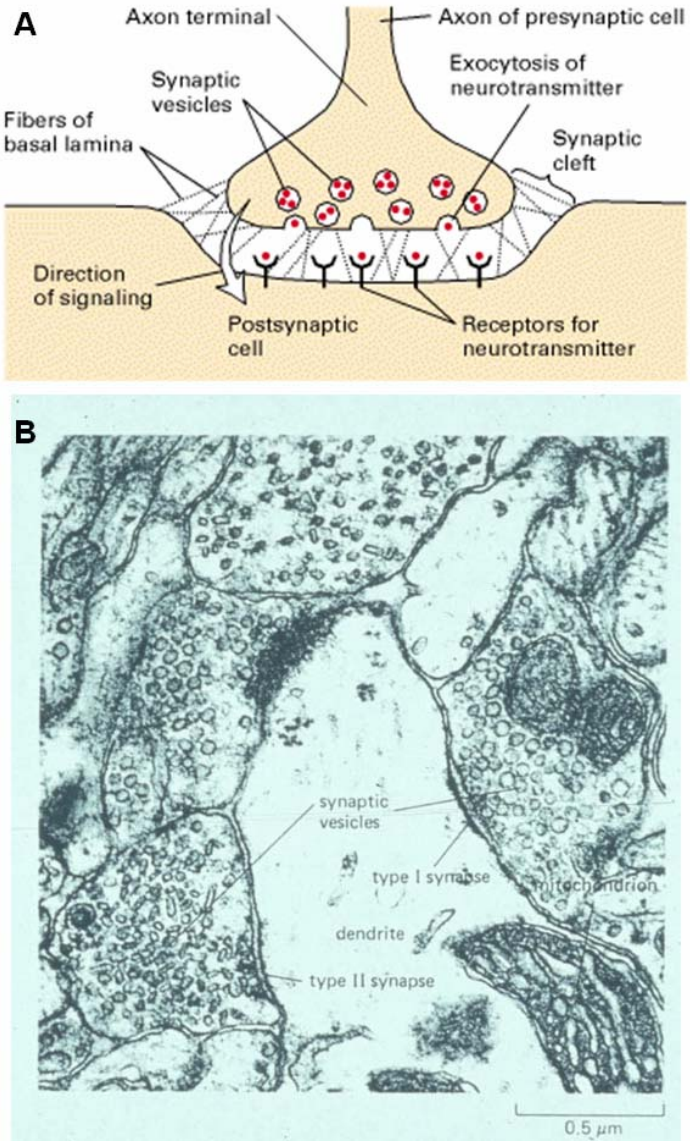

Figure 1.2 Schematic diagram and electron micrograph of chemical synapses.

(A) Schematic diagram of a chemical synapse. The synaptic cleft constitutes the narrow space between the plasma membranes of the presynaptic and postsynaptic cells. An action potential triggers synaptic vesicle exocytosis and neurotransmitter (red spots) release from the presynaptic cell. The released neurotransmitters diffuse across the synaptic cleft and bind to their cognate receptors on the plasma membrane of the postsynaptic cell to elicite downstream signal transduction events (Molecular Cell Biology, fourth edition, Lodish et al., 2000).

(B) Electron micrograph of chemical synapses. A cross section of a dendrite forming several chemical synapses with presynaptic axon terminals filled with synaptic vesicles.

combinational contribution by selective potassium channels and NaK ATPase pumps, maintaining a high potassium and low sodium concentration intracellularly.

At resting state, neurons maintain a transmembrane potential of approximately -70 mV with the intracellular side negative relative to the extracellular side. When a stimulus causes the transmembrane potential to depolarize toward 0 mV and reduce to the threshold of about -55 mV, a propagating electrical signal, the action potential, is evoked and the neuron fires. On the contrary, if the perturbation does not cause a reduction of transmembrane potential to the critical threshold level, no action potential will be elicited and the neuron will remain in the resting state. Moreover, when the critical threshold level is reached, the elicited action potential will be of a fixed size for any given neuron. Therefore, depending on whether or not the transmembrane potential of a neuron reaches the threshold of about -55 mV, a full action potential will be invoked in an all-or-none manner. The action potential is usually 100-110 mV in amplitude so as to cause the depolarization of membrane, a transient change of the transmembrane potential to +40 mV (Hodgkin, 1964; Huxley, 1964; Katz and Miledi, 1968). In about 1 millisecond, the membrane is repolarized rapidly to restore the transmembrane potential to its resting value, -70 mV (Jessell and Kandel, 1993). The action potential is conducted through the axon from the cell body toward the presynaptic terminals, where voltage-gated Ca^{2+} channels open in response to the action potential, allowing a drastic increase of intracellular Ca^{2+} concentration up to 200-300 μM and triggering the fusion of synaptic vesicles with the presynaptic plasma membrane and release of neurotransmitters (Llinas et al., 1992; Llinas et al., 1995).

1.2 Neurotransmitter Release and the Synaptic Vesicle Cycle

Neurotransmitter release is achieved through synaptic vesicle exocytosis. Initially, synaptic vesicles are filled with neurotransmitters and dock at the presynaptic active zone, likely through multiple protein-protein interactions. The docked vesicles undergo a priming process, which makes them ready for fusion. When the action potential invades the nerve terminal, voltage-dependent Ca^{2+} channels embedded in the presynaptic plasma membrane open in response to the membrane depolarization and Ca^{2+} rushes into the nerve terminal due to a greater extracellular Ca^{2+} concentration. Upon Ca^{2+} influx, the vesicles fuse with the plasma membrane and release the neurotransmitters into the synaptic cleft. The residual vesicles undergo endocytosis to sustain the synaptic vesicle cycle (Sudhof, 1995; Sudhof, 2004) (Figure 1.3).

Ca^{2+}-invoked neurotransmitter release exhibits a fast synchronous component that is triggered in less than 0.5 millisecond and a slower asynchronous component with a time scale of 10-50 milliseconds. The probability of release is modulated by plastic changes that depend on synaptic activity and shape the properties of neural networks. Such changes are thought to underlie some forms of information processing in the brain and include several forms of short- and long-term synaptic plasticity that are regulated by a variety of messengers such as Ca^{2+} and diacylglycerol (DAG). Many proteins involved in the neurotransmitter release have been identified, and extensive studies have yielded crucial insights into the molecular basis for the different steps that lead to release.

1.3 Membrane Trafficking and Membrane Fusion

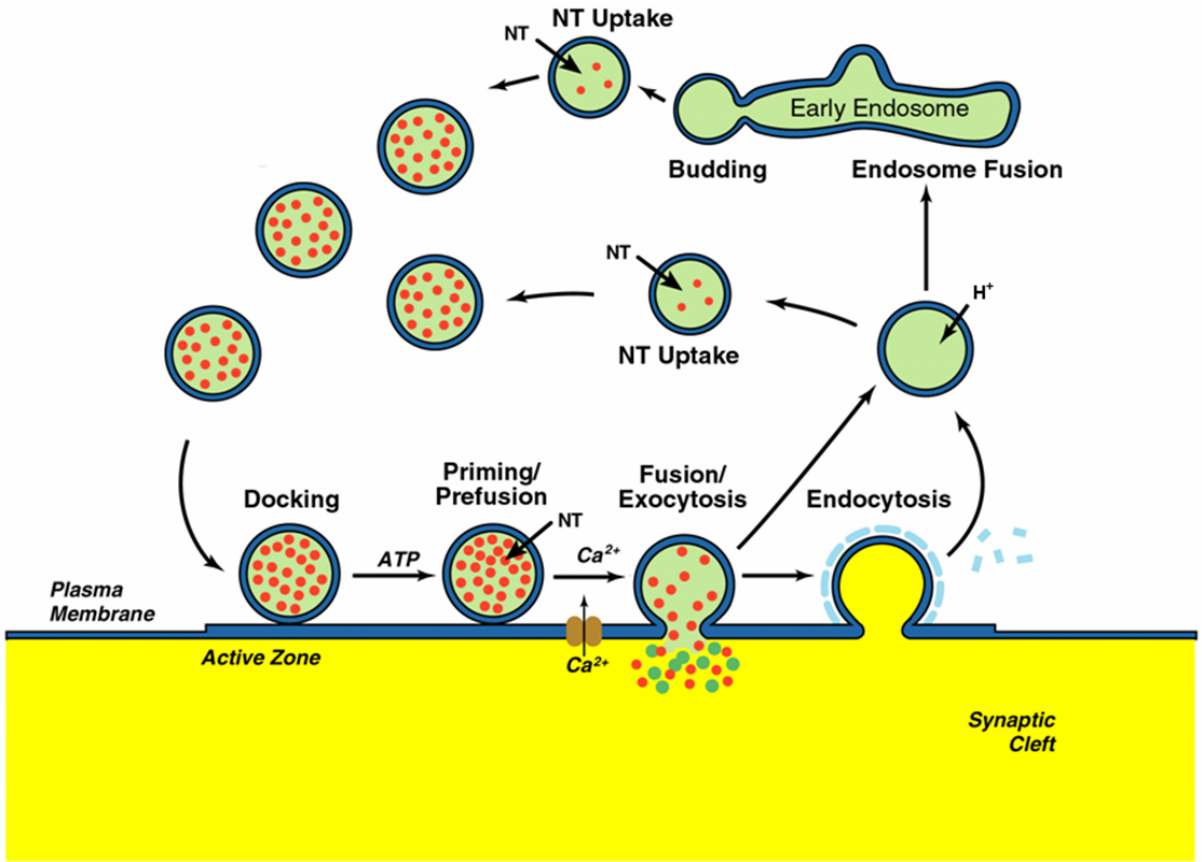

Figure 1.3 Synaptic vesicle cycle.

Neurotransmitter-filled synaptic vesicles are docked at the presynaptic active zone and undergo a priming process, which makes them ready for fusion. Ca^{2+} influx leads to the fusion of the synaptic vesicles with the presynaptic plasma membrane and release of the neurotransmitters. The residual vesicles are recycled through endocytosis to sustain the synaptic vesicle cycle (Sudhof, 1995; Sudhof, 2004).

Membrane trafficking within eukaryotic cells is a highly regulated process, which is vital for the maintenance of distinct subcellular compartments, and a variety of secretion processes (Rothman, 1994; Schekman and Orci, 1996). This process is conserved from unicellular yeast to mammalian cells (Bennett and Scheller, 1993; Clary et al., 1990). Membrane trafficking involves the continuous production and consumption of small transport vesicles. Cargo-laden transport vesicles act as intercompartmental shuttles, selectively docking to and fusing with their target membranes. The membrane fusion events are central to vesicular trafficking.

Membrane fusion is one of the major physiological processes in cellular activities. It is involved in a variety of cellular processes such as endocytosis, extracellular secretions, protein sorting, and viral budding and infection. Neurotransmitter release, a specialized form of extracellular secretion, is essentially a highly regulated membrane fusion event, which must be rapid, highly selective and leakage-free.

Under normal conditions, membrane fusion does not occur spontaneously. There is a thin layer of water molecules adhering on the hydrophilic surface of the two opposing membranes, which separate the membrane through hydration repulsion before fusion. Besides the hydration repulsion, other forces acting on the phospholipid bilayers include the electrostatic repulsion of negatively charged phospholipid headgroups as well as the van der Waals attraction. Before fusion occurs, the docking process first enables the two opposing membranes to come close enough for proteins protruding from the phospholipid bilayers to interact and adhere. Compared to docking, fusion requires a much closer apposition. The two opposing phospholipid bilayers need to approach within approximately 3 nm for the

membrane merger to occur (Helm and Israelachvili, 1993). When the phospholipid bilayers are in such a close apposition, the extremely high repulsion between the two opposing membranes creates a formidable energy barrier, which makes membrane fusion a highly energetically unfavorable process. Specialized fusion proteins are needed to catalyze membrane fusion by lowering the energy barrier. There must be certain local packing defects in the phospholipid bilayers to expose the hydrophobic interiors so that lipid mixing can occur and lipids can flow freely from one bilayer to the other. The defects can be created by insertion of membrane proteins, special lipid compositions and concomitant changes in membrane curvature.

When two membranes fuse together, an aqueous fusion pore forms to connect the opposing compartments. Fusion pore formation must involve transition states in which the phospholipid molecules are not arranged in lamellar bilayers and the phospholipid monolayers are highly bent. All transition states are essentially governed by the requirement to minimize exposure of hydrophobic surfaces to the aqueous environment. The currently most favored model of membrane fusion is the stalk hypothesis (Kozlov and Markin, 1983; Chernomordik et al., 1987). According to the stalk hypothesis, fusion of phospholipid membranes proceeds by an ordered sequence of distinct steps: local perturbation of the lipid structure and the merging of the proximal leaflets, stalk formation, generation of hemifusion intermediates, and fusion pore opening (Jahn et al., 2003) (Figure 1.4). A combination of thermal fluctuations of phospholipid, input of mechanical energy, and charge shielding allow the temporary reduction of the repulsive forces between the two opposing membranes and facilitate the dehydration and membrane approaching. Subsequently, relaxation may lead to

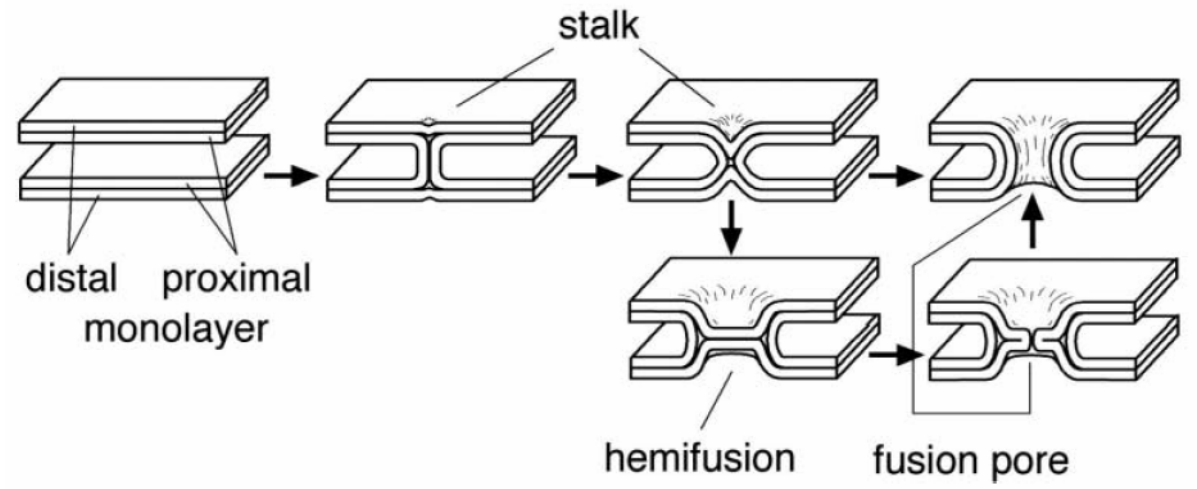

Figure 1.4 Transition states in membrane fusion.

The smooth and bendable sheets represent the phospholipid monolayers or leaflets. Initially, the two membrane bilayers are separated. The merging of the proximal leaflets but not the distal leaflet leads to the formation of the fusion stalk intermediate. The radial expansion of the proximal leaflets causes the distal leaflets to contact with each other and leads to the formation of the transmonolayer contact intermediate, which is also referred to as the hemifusion intermediate. The subsequent merging of the distal leaflets leads to fusion pore formation (Jahn et al., 2003).

the merging of the proximal leaflet and formation of metastable intermediates. The first intermediate is a stalk, an hourglass-shaped structure in which the proximal leaflets of the opposing membranes are merged while the distal leaflets are still separate. Once the highly bent stalk has formed, the radial expansion of the proximal leaflets pulls the two opposing distal leaflets toward each other and forms a transmonolayer contact intermediate, which is also referred to as the hemifusion intermediate. After establishment of the transmonolayer contact, relaxation of energetically unfavorable void interstices will lead to the fusion pore opening. Compared to other models of membrane fusion, the stalk hypothesis is the only coherent model, supported by both theoretical calculation and many lines of experimental evidence in a variety of model systems (Chernomordik, 1996; Lee and Lentz, 1997; Basanez et al., 1998).

1.4 C2 Domains

Interestingly, most of the regulatory proteins involved in neurotransmitter release contain C2 domains, which are autonomously folded protein modules of 120-150 amino acid residues. The C2 domain was initially identified as and named after the second conserved region of protein kinase C (PKC) and, similarly to other widespread modules such as SH2, SH3 and PDZ domains, has now been found in a wide variety of proteins that have modular architectures. Many of these proteins are involved in signal transduction and membrane traffic. Thus, research on C2 domains is broadly related to illnesses associated with defects in these processes, including cancer, neurological disorders, muscular dystrophies and heart diseases. Because of the large number of C2-domain proteins involved in synaptic

transmission, neurological diseases in which synapses are particularly affected, such as Parkinson's disease, Alzheimer's disease and myasthenia gravis may involve C2-domain proteins. A large percentage of C2 domains bind Ca^{2+} and phospholipids. This property is believed to underlie the Ca^{2+}-dependent membrane translocation of C2 domain containing enzymes involved in signal transduction, and the function of other proteins bearing C2 domains in Ca^{2+}-dependent membrane fusion events such as neurotransmitter release. However, some C2 domains do not bind Ca^{2+} and/or phospholipids, and probably act as protein-protein interaction domains. Thus, C2 domains are versatile protein modules with Ca^{2+}-dependent and Ca^{2+}-independent activities.

1.4.1 C2 Domain-Containing Proteins

C2 domains occur in the N-terminus, the C-terminus and the middle of protein sequences, and often are present in multiple copies with evolutionarily conserved differences that suggest functional differentiation. The different C2 domains of a given protein are usually referred to as C2A, C2B, C2C domains, *etc*, according to their location from the N- to the C-terminus of the sequence, as exemplified in synaptotagmins. Most C2-domain proteins involved in signal transduction contain a single C2 domain. These include proteins involved in the generation of lipid second messengers (e.g. phospholipases), in protein phosphorylation (e.g. PKC), in ubiquitin ligation (e.g. Nedd4) and in activation of GTPases (e.g. Ras-GAP). Phosphatidylinositol 3-kinases (PI3Ks), which are involved in signal transduction and membrane traffic, contain one or two C2 domains. Other C2-domain proteins involved in membrane traffic usually contain two C2 domains (e.g. synaptotagmins,

rabphilin, DOC2s, RIMs) or even three (e.g. Munc13s). In general, the functions of these proteins are not well understood but their critical roles in neurotransmitter release have been well established for the neuronal isoforms synaptotagmin 1, RIM1α, and Munc13-1, *etc*. Among the variety of additional C2-domain proteins that have been described, some contain up to six C2 domains. These include dysferlin and related proteins, which were identified because mutations in dysferlin result in limb girdle muscular dystrophy (Bashir et al., 1998).

1.4.2 Three-Dimensional Structures of C2 Domains

The structures of several C2 domains at atomic resolution have been determined by X-ray crystallography and nuclear magnetic resonance (NMR) spectroscopy. As illustrated by the structures of the synaptotagmin 1 C2A domain (Sutton et al., 1995) and the phospholipase C-δ (PLCδ) C2 domain (Essen et al., 1996; Rizo and Sudhof, 1998) (Figure 1.5), C2 domains share a common β-sandwich structure formed by two four-stranded antiparallel β-sheets with variable loops emerging at the top and the bottom. In some cases, the loops contain insertions that form α-helices, as seen in the synaptotagmin 1 C2B domain (Xu et al., 1998; Perisic et al., 1998; Ubach et al., 1999; Fernandez et al., 2001). Most intermolecular interactions of C2 domains have been mapped to the loops, and Ca^{2+} binding involves exclusively the top loops. Hence, the β-sandwich appears to constitute a scaffold for variable sequences that are specialized for distinct functions. Two different topologies resulting from a circular permutation of the β-strands have been observed in the structures of C2 domains. Different topologies may have functional consequences since they result in different orientations of the adjacent sequences with respect to the C2 domain. Thus, in

topology I (for instance, synaptotagmin 1 C2A domain, Figure 1.5A), the N- and C-termini are proximal to the Ca^{2+}-binding loops, whereas in topology II (for instance, PLCδ C2 domain, Figure 1.5B) the termini are at the opposite side of the domain.

1.4.3 Ca^{2+} Binding to C2 Domains

The Ca^{2+}-binding modes observed in different C2 domains exhibit both similarities and differences. In all cases studied, multiple Ca^{2+} ions bind in a cluster at the top of the domain. Four different Ca^{2+}-binding sites have been identified (Rizo and Sudhof, 1998) (Figure 1.6), although most C2 domains contain only two or three of these sites (Sutton et al., 1995; Shao et al., 1996; Essen et al., 1997; Sutton and Sprang, 1998; Shao et al., 1998; Xu et al., 1998; Perisic et al., 1998; Ubach et al., 1999; Fernandez et al., 2001). The Ca^{2+}-binding sites are formed primarily by aspartate side chains that often act as bidentate ligands, but also involve other oxygen-containing side chains and backbone carbonyl groups. Loops 1 and 3 at the top of the domain usually contribute all or most of the Ca^{2+}-coordinating ligands, while loop 2 sometimes contributes one ligand. These loops are distant in the sequence but closely clustered together in space. Thus, the Ca^{2+}-binding modes of C2 domains are topologically and structurally very different from the EF-hand, another widespread Ca^{2+}-binding motif that is formed by a contiguous polypeptide chain in a helix-loop-helix arrangement. Comparison of the high-resolution structures of the Ca^{2+}-free and Ca^{2+}-bound forms of the synaptotagmin 1 C2A domain and the PLCδ C2 domain shows that Ca^{2+} binding causes minimal structural changes (Shao et al., 1996; Essen et al., 1996). This observation indicates that these, and probably many other, C2 domains function by a very different mechanism to that observed in

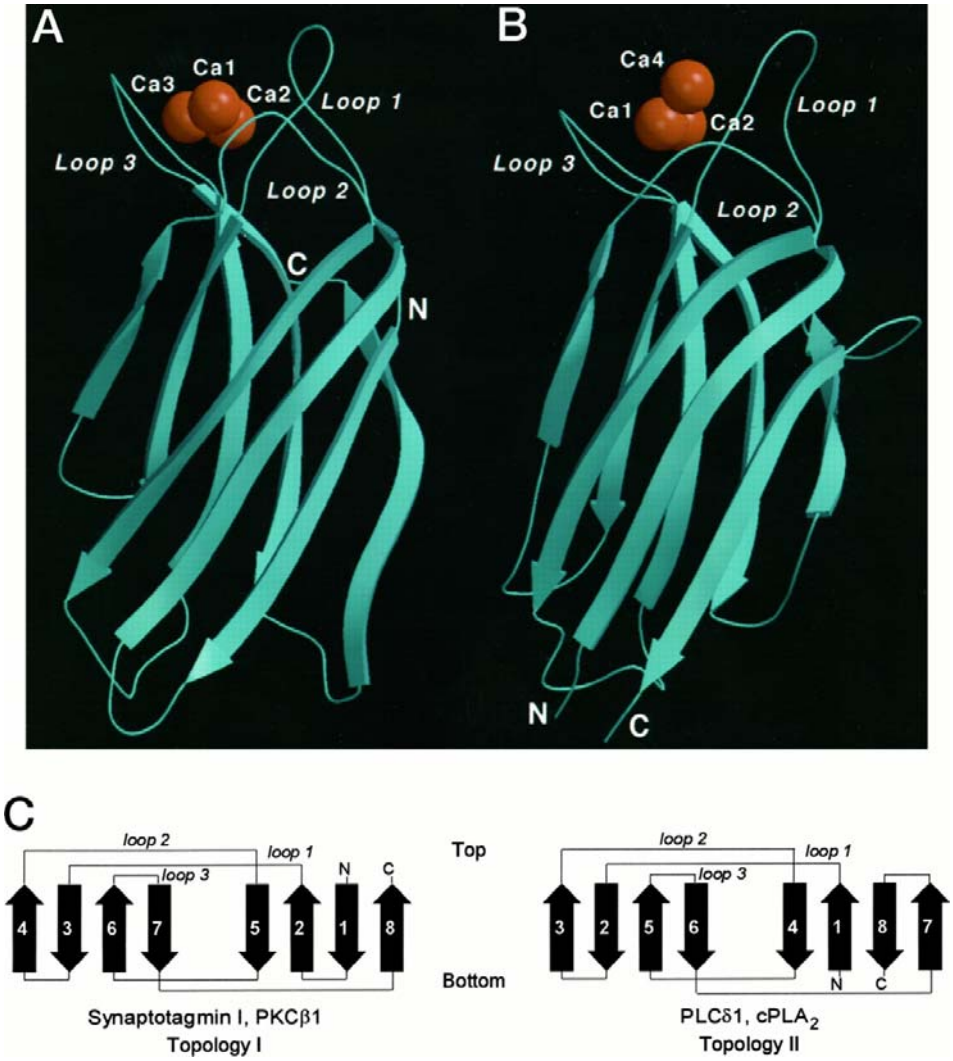

Figure 1.5 Three-dimensional structures of C2 domains.

(A) Ribbon diagrams of the structure of the C2A domain of synaptotagmin 1. The locations of the N and C termini and of the Ca^{2+}-binding loops are indicated. The bound Ca^{2+} ions are shown as orange spheres (Rizo and Sudhof, 1998).

(B) Ribbon diagrams of the structure of the C2 domain of PLCδ1. The locations of the N and C termini and of the Ca^{2+}-binding loops are indicated. The bound Ca^{2+} ions are shown as orange spheres (Rizo and Sudhof, 1998).

(C) Schematic drawing of the β-strand topologies of the C2A domain of synaptotagmin 1 and the C2 domain of PLCδ1. β-strands in the C2 domains from synaptotagmin 1 and PKCβ (left) and from PLCδ1 and cPLA2 (right) are numbered in the order of the primary sequences. The three Ca^{2+}-binding loops at the top of the C2 domains are indicated (Rizo and Sudhof, 1998).

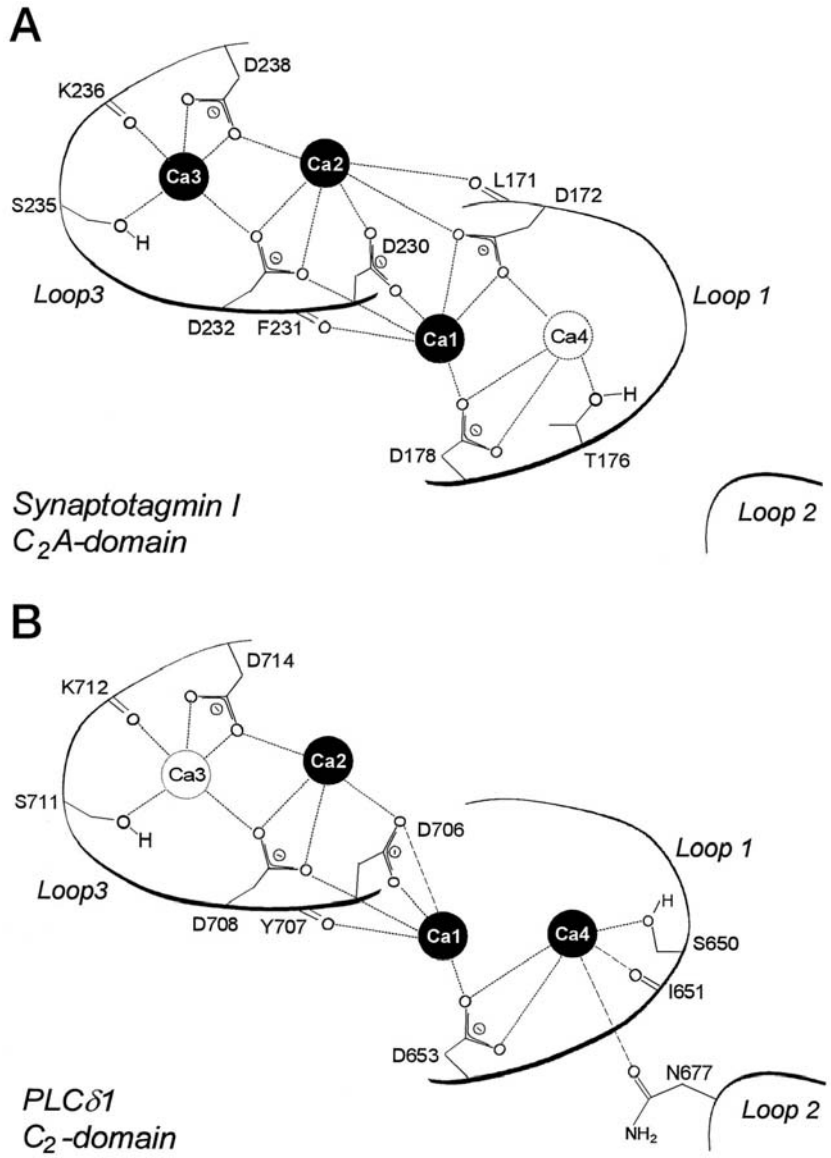

Figure 1.6 Schematic diagrams of the four Ca^{2+} binding sites in the Ca^{2+}-binidng loops of C2 domains.

(A) The Ca^{2+}-binding sites in the C2A domain of synaptotagmin 1. The side chains and carbonyl groups involved in binding are indicated. Sites actually observed in the structures are shown by solid circles, and potential additional sites by open circles (Rizo and Sudhof, 1998).

(B) The Ca^{2+}-binding sites in the C2 domain of PLCδ1. The side chains and carbonyl groups involved in binding are indicated. Sites actually observed in the structures are shown by solid circles, and potential additional sites by open circles (Rizo and Sudhof, 1998).

EF-hand proteins, where Ca^{2+} binding usually exposes hydrophobic surfaces that bind to target molecules. The intrinsic dissociation constants that have been measured for Ca^{2+}-binding sites of C2 domains range from low micromolar to more than 1 millimolar (Xu et al., 1998; Shao et al., 1998; Ubach et al., 1999; Fernandez et al., 2001). The low intrinsic Ca^{2+}-affinities arise in part from the fact that the bound Ca^{2+} ions usually contain empty coordination sites, which may be important for C2 domain function.

1.4.4 Phospholipid Binding to C2 Domains

A variety of C2 domains, including those of several synaptotagmins, PKCβ, PLCδ, Nedd4, and cPLA2, *etc*., bind phospholipid in a Ca^{2+}-dependent manner. This property is thus a hallmark of C2 domains and is the only C2 domain activity that has been unequivocally demonstrated to be physiologically relevant. Different phospholipid-binding preferences are exhibited, however, by different C2 domains. Hence, whereas the synaptotagmin and PKCβ C2 domains bind to negatively charged phospholipid, the cPLA2 C2 domain binds preferentially to electrically neutral, zwitterionic phospholipid (Shao et al., 1997; Zhang et al., 1998; Edwards and Newton, 1997; Nalefski and Falke, 1998). Ca^{2+}-dependent phospholipid binding to C2 domains occurs with much higher cooperativity and much higher apparent Ca^{2+} affinities (low micromolar) than intrinsic Ca^{2+} binding to C2 domains. These characteristics probably arise because occupation of all Ca^{2+}-binding sites available is required for phospholipid binding, and because the phospholipid head groups help to complete the coordinate ion spheres of the bound Ca^{2+} ions (Zhang et al., 1998; Verdaguer et al., 1999). In contrast to these Ca^{2+}-dependent phospholipid-binding C2

domains, the C2 domains from PI3K (phosphoinositide-3 kinase) and tumor suppressor protein PTEN were shown to bind phospholipids constitutively in a Ca^{2+}-independent manner. In the case of PI3K, this Ca^{2+}-independent binding to phospholipids may aid the constitutive activity of PI3K by properly orienting the catalytic domain similarly to cPLA2 and PLCδ.

The lack of a Ca^{2+}-induced conformational change in C2 domains also implies that their interactions with phospholipid do not involve opening of a hydrophobic cavity but rather a protein surface/lipid surface interaction that involves the C2 domain Ca^{2+}-binding region. Ca^{2+}-dependent phospholipid binding to the synaptotagmin 1 C2A domain seems to be driven by a Ca^{2+}-induced electrostatic switch mechanism, as shown by the salt sensitivity of this interaction (Zhang et al., 1998). Partial coordination of the Ca^{2+} ions by the phospholipid head groups and insertion of two exposed hydrophobic residues (methionine 173 and phenylalanine 234) from the Ca^{2+}-binding loops into the lipid bilayer are also likely to contribute to the binding energy. Other C2 domains probably share this mechanism, with the relative contributions of electrostatic and hydrophobic interactions depending on the nature of the Ca^{2+}-binding loops. For instance, these loops are much more hydrophobic in the cPLA2 C2 domain and its interaction with phospholipids is thus more hydrophobic in nature (Nalefski and Falke, 1998; Nalefski et al., 1998; Davletov et al., 1998). The interfacial nature of the C2 domain/phospholipid interactions is well suited for the function of the C2 domains of enzymes involved in signal transduction. Thus, the crystal structures of PLCδ and cPLA2 have shown that Ca^{2+}-dependent binding of their C2 domain to the membrane surface should

help to fix their catalytic domain in a productive orientation to perform their enzymatic activity (Essen et al., 1996; Dessen et al., 1999).

1.4.5 Other Interactions of C2 Domains

Besides their most general activities in Ca^{2+} and phospholipid binding, C2 domains are also involved in other types of interactions. Several C2 domains from different PKC isoforms have been shown to serve as protein-protein interaction modules (Ron et al., 1995; Gray et al., 1997; Dekker and Parker, 1997). In the neuronal system, as we have mentioned earlier, both Ca^{2+}-dependent and Ca^{2+}-independent interaction of synaptotagmin 1 C2 domains with SNARE proteins have been reported, but the specific structural features that mediate these interactions are still elusive. The first atomic resolution structure of a C2 domain engaged in protein-protein interactions was demonstrated for the Munc13-1 C2A domain, which can actually establish two different types of interaction modes that lead to either its homodimerization through one side of the β-sandwich or heterodimerization with the RIM2α zinc finger domain through the bottom tip of the β-sandwich, completely opposite to the canonical Ca^{2+}/phospholipid binding site (Lu et al., 2006). Moreover, the C2 domain of PKCδ was found to be able to bind to a phosphotyrosine-containing substrate peptide and the crystal structure of PKCδ with phosphotyrosine peptide bound revealed a novel mode of phosphotyrosine recognition, different from that observed in the classical phosphotyrosine-binding SH2 domain or PTB domain (Benes et al., 2005). These results demonstrate the diversity of interactions that can be mediated by various C2 domains. Undoubtedly, active

research on C2 domains will reveal additional aspects of the mechanisms of action of these versatile modules in the near future.

1.5 Proteins Involved in Neurotransmitter Release

Neurotransmitter release is mediated by exocytosis of synaptic vesicles at the presynaptic active zone of nerve terminals (Jahn and Sudhof, 1999). The Ca^{2+}-triggered release process *per se* is extremely fast, less than half a millisecond, and strictly regulated by the intracellular Ca^{2+} concentration. In order to achieve this highly precise spatial and temporal regulation, a complex hierarchy of protein machinery is involved. Extensive genetic and biochemical studies have led to the identification of numerous proteins that are involved in neurotransmitter release (Sudhof, 1995; Augustine et al., 1996; Jahn and Sudhof, 1999; Lin and Scheller, 2000). The central machinery consists of N-ethylmaleimide-sensitive factor (NSF), soluble NSF attachment proteins (SNAPs), SNAP receptors (SNAREs), Munc18-1, and Rab 3. These proteins share homologues in different membrane trafficking processes of a variety of organisms ranging from unicellular yeasts to humans, suggesting that synaptic vesicle exocytosis shares a common mechanism with many other types of constitutive intracellular membrane fusion events (Bennett and Scheller, 1993; Ferro-Novick and Jahn, 1994). In addition to these universal components, many other neuronal specific proteins are also involved in regulating Ca^{2+}-triggered neurotransmitter release such as the Ca^{2+} sensor synaptotagmins, key priming factors RIMs (Rab3-interacting molecules) and Munc13s, and the small SNARE-associating protein known as complexins. They are selectively essential

for neurotransmitter release, presumably contributing to the highly precise spatial and temporal regulation and complexity of nervous systems (Sollner, 2003).

Intriguingly, most of the regulatory proteins such as the synaptotagmins, RIMs, Munc13s, rabphilins, *etc*., contain a small globular domain, the C2 domain, which is an autonomously folded protein module of 120-150 amino acid residues. A large percentage of C2 domains bind Ca^{2+} and phospholipids while some C2 domains do not and probably act as protein-protein interaction domains. Thus, C2 domains are versatile protein modules with Ca^{2+}-dependent and Ca^{2+}-independent activities. All these properties are manifested in C2-domain proteins involved in neurotransmitter release. However, the mechanism of regulation by these C2-domain proteins remains unclear. My graduate research was mainly focused on the structural and functional studies of the C2-domain proteins involved in neurotransmitter release, particularly on the Ca^{2+} sensor synaptotagmins and the key priming factor RIMs. The proteins closely related to my graduate research are described below.

1.5.1 SNARE Proteins

SNARE proteins constitute a large evolutionarily conserved protein superfamily and are involved in a variety of intracellular membrane trafficking processes, mediating most if not all vesicular membrane fusion events in eukaryotic cells. SNARE proteins can be classified into two categories according to their differential distribution to distinct intracellular compartments, with v-SNAREs mainly present on vesicle membranes and t-SNAREs predominately on target membranes (Sollner et al., 1993b). The best characterized SNAREs are those involved in synaptic vesicle exocytosis, which include the synaptic

vesicle protein synaptobrevin/VAMP (vesicle-associated membrane protein) and the neuronal plasma membrane proteins syntaxin and SNAP-25 (Trimble et al., 1988; Baumert et al., 1989; Bennett et al., 1992; Oyler et al., 1989). The functional importance of these proteins was demonstrated by the observation that clostridial neurotoxins can inhibit neurotransmitter release by specific proteolysis of synaptobrevin, syntaxin or SNAP-25 (Schiavo et al., 1992; Link et al., 1992; Blasi et al., 1993a; Blasi et al., 1993b). Moreover, the essential role of SNARE proteins was also shown by the finding that synaptobrevin, syntaxin and SNAP-25 form a 20S complex with SNAPs and NSFs, which had been shown to be crucial for Golgi transport (Sollner et al., 1993a). Studies of different membrane trafficking processes in a variety of organisms, especially yeast, revealed that SNARE homologues are involved in a variety of intracellular membrane fusion events (Bennett and Scheller, 1993; Weimbs et al., 1998; Chen and Scheller, 2001; Burri and Lithgow, 2004).

Extensive biochemical and structural studies revealed many important characteristics of the SNARE proteins. All SNARE proteins share a common heptad repeat of about 60-70 residues, which is referred to as the SNARE motif and has a strong tendency to form a coiled coil structure (Hayashi et al., 1994; Bock et al., 2001; Jahn and Sudhof, 1999) (Figure 1.7). Synaptobrevin possesses one SNARE motif adjacent to its C-terminal transmembrane region. Besides one SNARE motif (H3) adjacent to its C-terminal transmembrane region, syntaxin also has a conserved N-terminal domain, known as the Habc domain, which forms an antiparallel three-helix bundle (Fernandez et al., 1998). It has been found that the N-terminal Habc domain of neuronal syntaxin 1 interacts with the C-terminal SNARE motif, forming a closed conformation that tightly binds to Munc18-1 and provides another level of regulation

through the switch between open and closed conformations (Dulubova et al., 1999). SNAP-25 contains two SNARE motifs (the N-terminal and the C-terminal SNARE motifs designated as SNAP-25N and SNAP-25C respectively), which are separated by a long cysteine-rich loop. Four cysteine residues in the loop are palmitoylated to anchor SNAP-25 to the plasma membrane (Hess et al., 1992).

The SNARE motifs of synaptobrevin, syntaxin and SNAP-25 (one from synaptobrevin, one from syntaxin and two from SNAP-25) form a highly stable four-helix bundle, named the core complex or the SNARE complex, which is proteolysis- and SDS-resistant, and only denatures above 90 ºC (Hayashi et al., 1994; Fasshauer et al., 1998a). The isolated SNARE motifs are unstructured in solution and form regular α-helical secondary structure upon core complex formation, which can be monitored as the increase of helicity by circular dichroism (CD) spectroscopy (Fasshauer et al., 1998a; Poirier et al., 1998a). Electron microscopy (EM), fluorescence resonance energy transfer (FRET) experiments, and electron paramagnetic resonance (EPR) spectroscopy showed that the SNARE motifs are aligned in a parallel configuration, with the membrane anchors of synaptobrevin and syntaxin located at the same end of the complex (Hanson et al., 1997; Lin and Scheller, 1997; Poirier et al., 1998b). The crystal structure of the neuronal SNARE core complex composed of synaptobrevin 2, syntaxin 1A and SNAP-25 revealed a highly twisted and parallel four-helix bundle structure with an overall length of 120 Å (Sutton et al., 1998) (Figure 1.8). The four-helix bundle is mainly stabilized by hydrophobic interactions except for a unique ionic layer in the center of the bundle, known as the zero-layer. This layer contains one arginine residue from synaptobrevin and three glutamine residues from each of the other SNARE motifs,

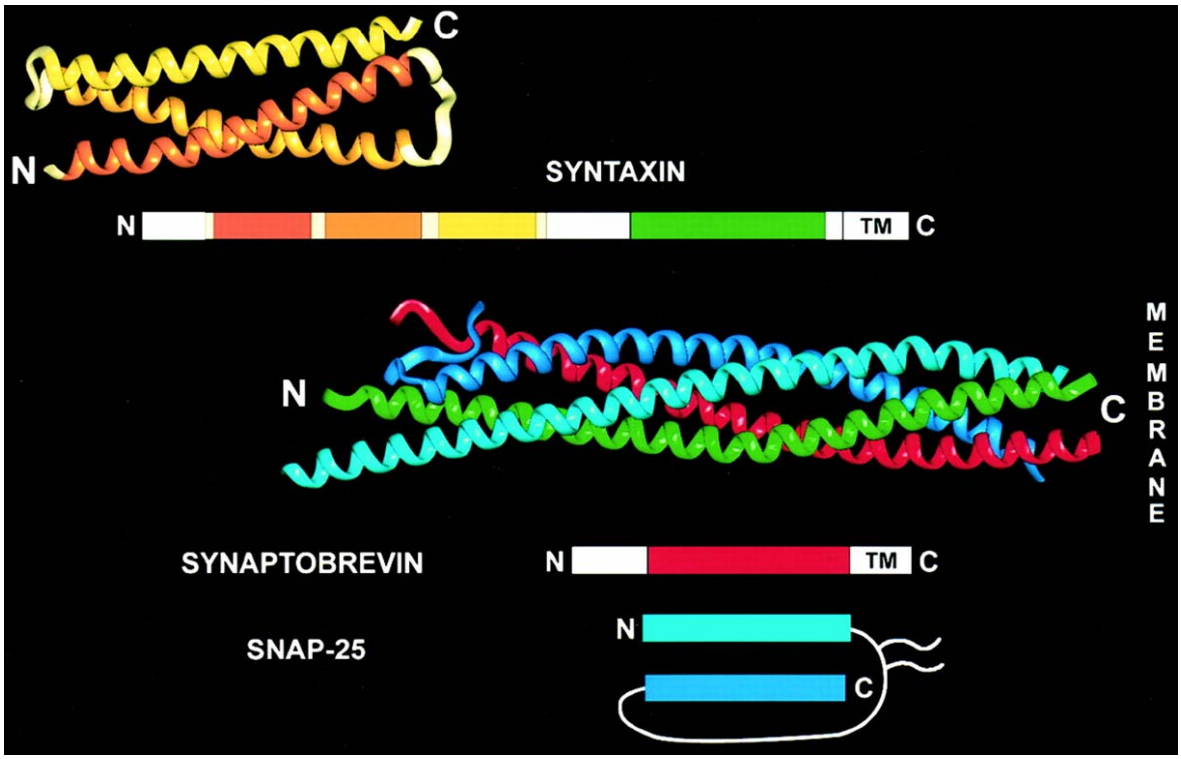

Figure 1.7 Schematic diagrams of the domain arrangement and structures of the neuronal SNARE proteins.

Syntaxin contains an N-terminal Habc domain, a C-terminal SNARE motif (green) and a transmembrane region (TM). The N-terminal Habc domain forms a three-helix bundle, shown on the top, with the three helices colored in orange, gold and yellow, respectively. Synaptobrevin contains a SNARE motif (red) followed by a transmembrane region (TM). SNAP-25 contains two SNARE motifs (cyan and blue) separated by a long loop, which is palmitoylated. The four SNARE motifs form a parallel four-helix bundle with the C-terminal transmembrane region of syntaxin and synaptobrevin close to the membranes, shown in the middle (Jahn and Sudhof, 1999).

which has been proposed to ensure the correct register during SNARE complex assembly. The interior residues of the SNARE complex are more conserved than the surface residues, and the zero-layer is conserved throughout the SNARE superfamily. The strict conservation of the zero-layer charged residues led to the reclassification of SNARE proteins as Q-SNAREs (containing glutamine in the zero-layer position) and R-SNAREs (containing arginine in the zero-layer position) and to the proposal that all core complexes are formed by one R-SNARE and three Q-SNAREs (Fasshauer et al., 1998b). The R/Q classification is preferable over the v/t classification because it correlates better with the structurally identified SNAREs than the localization criterion and the v/t classification does work for homotypic fusion. The surface electrostatic potential of the SNARE complex reveals a highly negatively charged surface throughout the middle region with positive charges clustered at the ends. The crystal structure of a distantly related mammalian endosomal SNARE complex shows a remarkable similarity to that of the neuronal SNARE complex despite the low level of sequence conservation (Antonin et al., 2002).

The most prevalent model of SNARE complex assembly is the zippering model: the SNARE motifs zipper from the distal N-termini to the proximal C-termini (Hanson et al., 1997; Lin and Scheller, 1997). It has been proposed that the formation of the core complex might be able to overcome the repulsion between the two fusion membranes and bring them into close proximity and facilitate or execute fusion (Hanson et al., 1997; Sutton et al., 1998) (Figure 1.8). Genetic studies have supported the involvement and functional importance of SNAREs in the membrane fusion, but did not seem to support their essential role for membrane fusion *per se*. Deletion of SNARE proteins in *Drosophila*, *C. elegans* and mice

abolishes Ca^{2+}-triggered release, yet at the same time maintaining at least some of the spontaneous miniature release events, indicating the fusion competence of the SNARE knockout neurons (Schoch et al., 2001; Washbourne et al., 2002; Schulze et al., 1995; Broadie et al., 1995).

In vitro reconstitution experiments with synaptobrevin and syntaxin/SNAP-25 incorporated into separate populations of synthetic liposomes led to the conclusion that SNAREs constitute the minimal machinery for executing the membrane fusion (Weber et al., 1998). However, these experiments only revealed lipid mixing at very slow rates (over a period of minutes to hours) and provided no evidence for other hallmarks of physiologically relevant fusion without disordered rupture, such as increase in vesicle size, absence of leakiness, content mixing and inhibition of fusion by inverted cone lipids. Another fundamental problem of the proposal of the SNARE complex as the minimal fusion machinery is that it provides no explanation for the strict requirement of Munc18-1, the knockout of which in mice causes a complete block in neurotransmitter release (Verhage et al., 2000). Moreover, reconstitution experiments with SNARE proteins under different conditions by several other groups revealed no occurrence of membrane fusion, in contrast to the results reported by Rothman and coworkers. Reconstitution experiments with synaptobrevin-containing native synaptic vesicles purified from brain and syntaxin/SNAP-25 reconstituted synthetic proteoliposomes revealed no SNARE complex formation and consequently no membrane fusion (Hu et al., 2002). Similar results were observed by independent studies, which provided a structural explanation for the restriction of synaptobrevin by the membrane (Kweon et al., 2003; Chen et al., 2004). Hence, the minimal

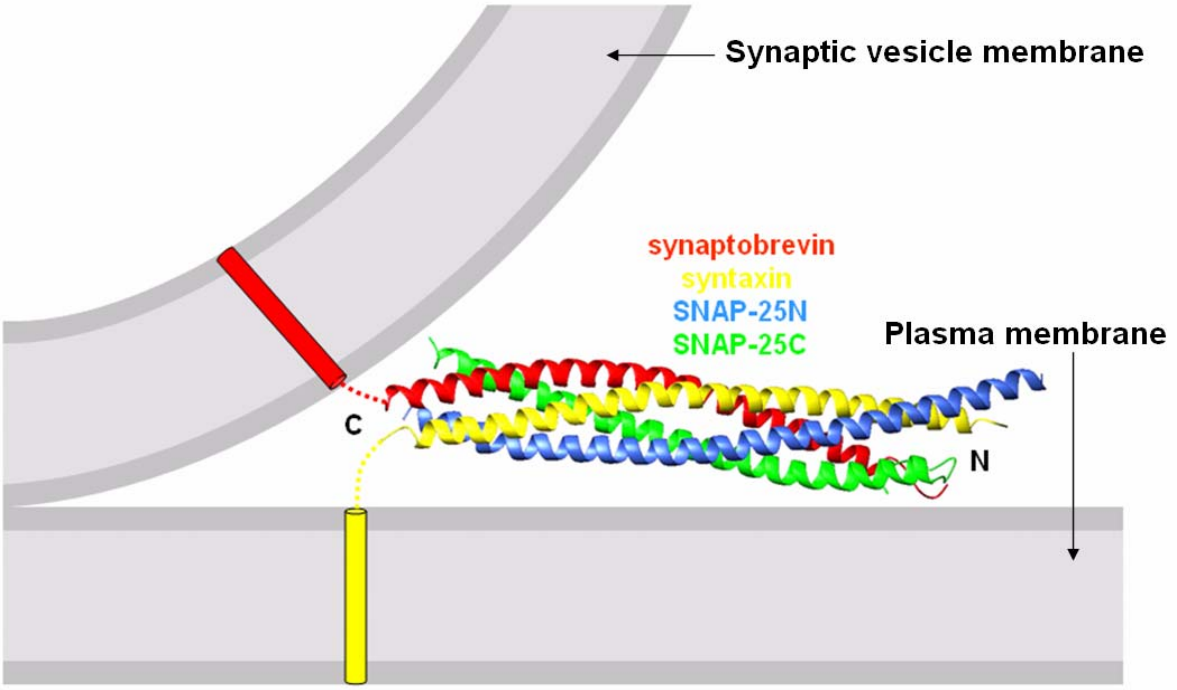

Figure 1.8 The formation of the SNARE complex brings the two opposing membrane to apposition.

The crystal structure of the neuronal SNARE complex is shown with respect to the synaptic vesicle membrane and the presynaptic plasma membrane. The SNARE motifs from syntaxin, synaptobrevin, N-terminal SNAP-25 and C-terminal SNAP-25 are colored in yellow, red, blue, and green, respectively. The cylinders inside the lipid bilayers represent the transmembrane regions of syntaxin and synaptobrevin with the linker regions shown as the dotted lines (Sutton et al., 1998; Rizo and Sudhof, 2002).

model of SNARE-mediated membrane fusion is likely to be under considerable debate for the coming years.

1.5.2 Synaptotagmins

Synaptotagmins are a large family of proteins implicated in membrane trafficking. Synaptotagmins contain a small N-terminal transmembrane region, a variable linker, and two C-terminal C2 domains (Perin et al., 1990). There have been at least fifteen synaptotagmin isoforms identified in mammals and eight in *Drosophila*.

1.5.2.1 Synaptotagmin 1

The most conserved and best characterized synaptotagmin isoform is synaptotagmin 1, which is also the first one discovered. Synaptotagmin 1 was initially discovered using monoclonal antibodies as p65 due to its migration in SDS-PAGE (Matthew et al., 1981). Purification and cloning revealed that synaptotagmin 1 is a type I membrane protein of 421 residues with a short intravesiclular amino terminus (Iv in Figure 1.9A), a short transmembrane region (TM in Figure 1.9A), and a linker followed by two tandem C2 domains (the C2A and C2B domain), which constitute the majority of the cytoplasmic sequence (Perin et al., 1990; Perin et al., 1991a; Perin et al., 1991b). Posttranslational modification analyses showed that its N-terminus is N-glycosylated and multiple cysteines at the cytoplasmic boundary of the transmembrane region are palmitoylated. Synaptotagmin 1 is anchored to the synaptic vesicle membrane and comprises about 7-8% of total vesicle proteins. Both C2 domains have been clearly shown to be able to bind to Ca^{2+} with low

intrinsic binding affinities (Shao et al., 1996; Ubach et al., 1998; Fernandez et al., 2001). It has also been shown that synaptotagmin 1 binds to phospholipids in a Ca^{2+}-dependent manner (Brose et al., 1992). These observations led to the proposal that this abundant synaptic vesicle protein could be a potential candidate for the Ca^{2+} sensor in neurotransmitter release (Brose et al., 1992; Ubach et al., 1998). Synaptotagmin 1 nulls in *Drosophila* and *C. elegans* exhibited severe impairment in Ca^{2+}-triggered neurotransmission, supporting the proposal of synaptotagmin 1 as the Ca^{2+} sensor (Nonet et al., 1993; Littleton et al., 1993; Littleton et al., 1994; DiAntonio and Schwarz, 1994). Knocking out synaptotagmin 1 in mice caused a selective abolishment of the fast synchronous release, whereas the slow asynchronous release was unaffected, strongly suggesting that synaptotagmin 1 functions as the Ca^{2+} sensor in fast synchronous release while asynchronous release might require other Ca^{2+} sensors (Geppert et al., 1994). All the aforementioned genetic studies provided direct evidence of the functional importance of synaptotagmin 1 in Ca^{2+}-trigger neurotransmitter release, but did not directly prove its role as the Ca^{2+} sensor. The most definitive and convincing data suggesting this notion was provided by the strong correlation between its *in vitro* Ca^{2+} affinity in the presence of phospholipids and *in vivo* Ca^{2+} sensitivity of neurotransmitter release. A single point mutation R233Q in synaptotagmin 1 caused the decrease of both values by about 50% (Fernandez-Chacon et al., 2001). Although it is widely believed that synaptotagmin 1 is the major Ca^{2+} sensor that triggers synchronous release, the mechanism of its action is still unclear.

X-ray crystallography and NMR spectroscopy have revealed the three dimensional structures of both C2 domains of synaptotagmin 1 (Sutton et al., 1995; Shao et al., 1998;

Fernandez et al., 2001). Both the C2A and C2B domains assume an eight-stranded, antiparallel β-sandwich core structure, which is typical of the C2-domain fold, with loops emerging from the top and bottom (Figure 1.9B). Unique structural features of the C2B domain, which are not observed in the C2A domain, are the insertion of an α-helix in the bottom of the β-sandwich between strands 7 and 8 and an extra C-terminal α-helix, (Fernandez et al., 2001). The α-helical insertion was first observed in the C2B domain of rabphilin and has been implicated in Ca^{2+}-independent protein-protein interactions (Ubach et al., 1999). Thus, the C2B domains may act as "Janus-faced modules" with a Ca^{2+}-dependent and a Ca^{2+}-independent face. The α-helix in the C-terminus has been implicated in endocytosis. The Ca^{2+}-binding sites of the synaptotagmin 1 C2 domains are formed by three loops at the top of the β-sandwich, and designated loop 1 (connecting strands 2 and 3), loop 2 (connecting strands 4 and 5) and loop 3 (connecting strands 6 and 7). The synaptotagmin 1 C2A domain binds three Ca^{2+} ions through the coordination of five aspartate side chains, one serine side chain and three backbone carbonyl groups contributed by loop 1 and loop 3 (Shao et al., 1996; Shao et al., 1998; Ubach et al., 1998). Loop 2 participates in the formation of the Ca^{2+}-binding sites by providing a hydrogen bond between its backbone amide and aspartate 178 from loop 1, which is critical for the proper orientation of aspartate 178 to coordinate Ca^{2+} ion. The three Ca^{2+}-binding sites are designated Ca1, Ca2, and Ca3, respectively. Both Ca1 and Ca2 sites are formed by six coordinating ligands and the Ca3 site is formed by five coordinating ligands, none of which fulfills the saturated seven-coordination sphere for Ca^{2+} ion. The incomplete coordination spheres result in the observed low intrinsic Ca^{2+} affinities measured by ^{1}H-^{15}N HSQC Ca^{2+} titration experiments, with Kds of 54 μM, 530 μM, and

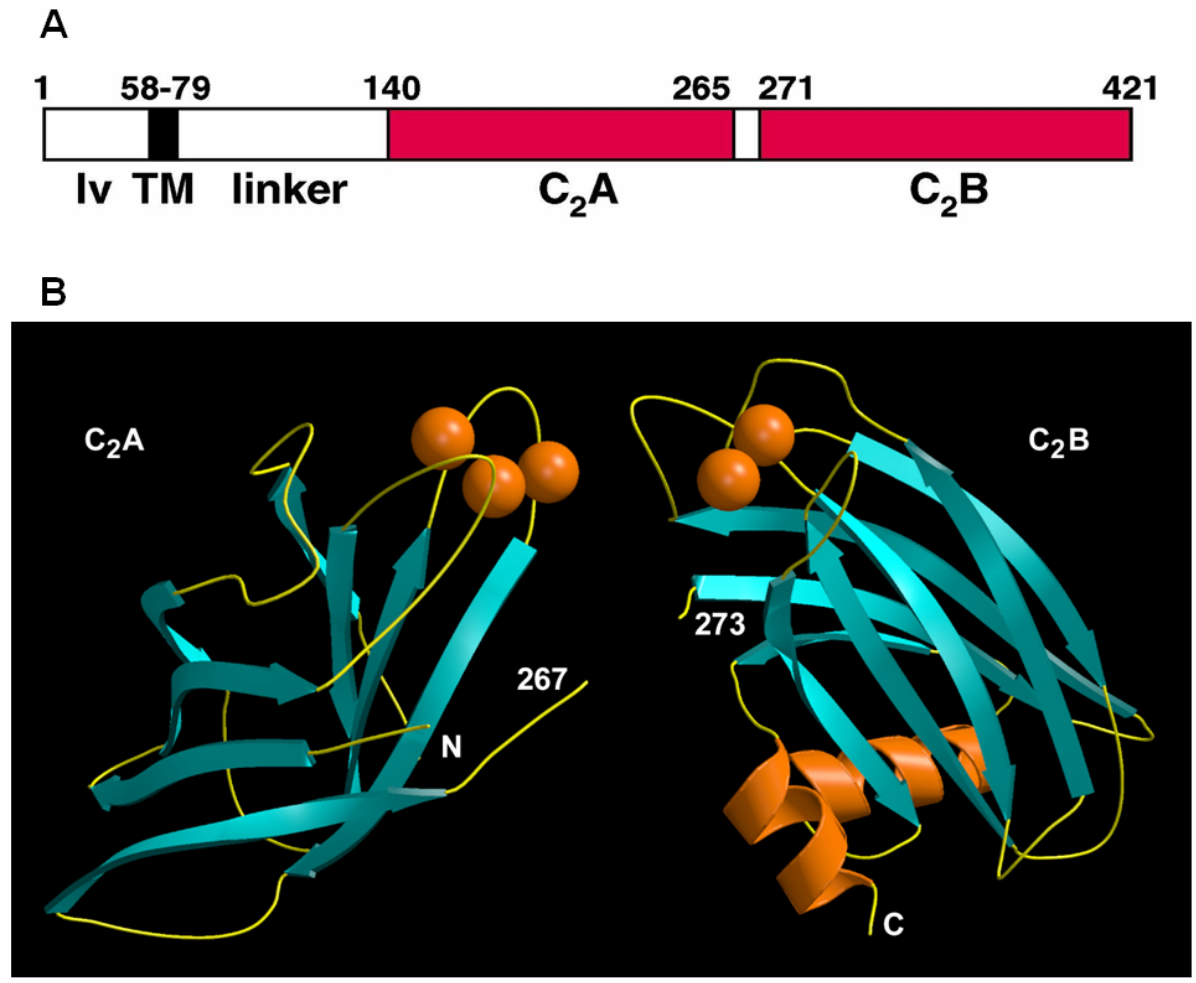

Figure 1.9 Schematic diagram of the domain arrangement and structures of synaptotagmin 1.

(A) The domain arrangement of synaptotagmin 1. The C2A and C2B domains are colored in red. Iv and TM stand for the intravesicular sequence and the transmembrane region, respectively. The residue numbers of the domain boundaries are labeled on the top.

(B) Ribbon diagrams of the synaptotagmin 1 C2A and C2B domains. β-strands and α-helices are colored in cyan and orange, respectively. The orange spheres on the top of the C2 domains represent the bound Ca^{2+} ions (three in the C2A domain and two in the C2B domain). The two C2 domains of synaptotagmin 1 can easily be oriented with their Ca^{2+}-binding sites in close proximity, which suggests the potential cooperativity between them (Fernandez et al., 2001).

>20 mM for sites Ca1, Ca2, and Ca3, respectively. The three Ca^{2+} ions bind to the active sites sequentially and binding of one Ca^{2+} ion will help to organize the shared aspartate ligands to facilitate the binding of the subsequent one. This notion was supported by the observation that mutation of the second aspartate ligand in loop 1 (aspartate 178 in C2A domain), which coordinates the first Ca^{2+}, causes much severer effects on Ca^{2+} binding than mutation of the last aspartate ligand in loop 3 (aspartate 238 in C2A domain), which coordinates the second Ca^{2+}. The Ca^{2+} binding sites of C2B domain exhibit remarkable similarities to those of the C2A domain. The C2B domain binds to two Ca^{2+} ions through the coordination of five aspartates and two backbone carbonyl groups (Fernandez et al., 2001). The absence of the hydroxyl side chain of the serine causes the loss of the weakest Ca3 coordination site. Similar to the C2A domain, both Ca1 and Ca2 sites of C2B domain formed by six coordinating ligands with Kds of 300-400 μM and 500-600 μM. Mutation of the second aspartate ligands in loop 1 (aspartate 309 in C2B domain, which coordinates the first Ca^{2+}) causes much severer effects on Ca^{2+} binding than mutation of the last aspartate ligands in loop 3 (aspartate 371 in C2B domain, which coordinate the second Ca^{2+}).

Comparison of the structures of the Ca^{2+}-free and Ca^{2+}-bound forms of either C2 domain of synaptotagmin 1 revealed very little conformational change on the overall structure. Instead, the positive charges introduced by the binding of multiple Ca^{2+} ions cause a dramatic switch in the electrostatic potential in the Ca^{2+}-binding sites from negative (due to the presence of multiple aspartate residues that form the Ca^{2+}-binding sites) to positive, which, together with the surrounding intrinsic positively charged residues, mediate the interaction between synaptotagmin 1 and negatively charged targets. Analysis of the Ca^{2+}-

dependent interaction of the synaptotagmin 1 C2A domain with syntaxin showed that the interaction is mediated by the Ca^{2+}-binding region of the C2A domain and is driven by a Ca^{2+}-induced switch in its electrostatic potential (Shao et al., 1997).

The first clue of the mechanism of synaptotagmin 1 action in neurotransmitter release came from the discovery that it binds to negatively charged phospholipids in a Ca^{2+}-dependent manner (Davletov and Sudhof, 1993). Initially, only the C2A domain of synaptotagmin 1 was shown to be capable of Ca^{2+}-dependent phospholipid binding whereas the C2B domain was not, which is quite unexpected given the high level of structural similarity of the Ca^{2+}-binding sites of both C2 domains (Schiavo et al., 1996; Sugita et al., 1996; Chapman et al., 1996; Bai et al., 2000). This puzzle was clarified later when it was shown by FRET experiments that extensively purified recombinant C2B domain can reproduce the Ca^{2+}-dependent phospholipid binding phenomenon observed for the C2A domain (Fernandez et al., 2001). The reason that the interaction was not detected earlier was due to the avid binding of acidic contaminants originated from bacteria, mostly nucleic acids, to the highly positively charged strand 4 in the C2B domain, the so called polybasic region, thus preventing the phospholipid interaction (Ubach et al., 2001). This finding also provided an explanation for another puzzling observation that mutations severely impair Ca^{2+}-dependent phospholipid binding to the C2A domain have only small effects on neurotransmitter release (Fernandez-Chacon et al., 2001). The ability of the C2B domain to bind phospholipid in response to Ca^{2+} compensates for the phospholipid binding-deficient mutation in the C2A domain. Indeed, in the context of a synaptotagmin 1 fragment containing the tandem C2 domains (C2AB fragment), mutations disrupting only Ca^{2+} binding

to the C2A domain exhibited little effect on the overall Ca^{2+}-dependent phospholipid binding ability (Fernandez-Chacon et al., 2001). This crucial result indicated that the two C2 domains of synaptotagmin 1 share a common Ca^{2+}-dependent activity and cooperate in phospholipid binding. The apparent affinity of the tandem C2AB fragment for negatively charged phospholipid is higher than those of individual C2 domains, showing a cooperativity in Ca^{2+}-dependent phospholipid binding. Extensive studies suggested that the Ca^{2+} binding on the top loops results in an electrostatic switch from negative to positive and the consequent formation of the positively charged surface together with basic residues in the vicinity. This positively charged surface interacts with the negatively charged phospholipid headgroups, which at the same time provide additional coordination sites for the bound Ca^{2+} ions to complete the coordination spheres (Rizo and Sudhof, 1998). Additional energetic contribution comes from the interaction of the nearby hydrophobic residues in the top loops with the phospholipid acyl chains. Hence, the C2 domains bind to negatively charged phospholipid through a combination of electrostatic and hydrophobic interactions. The completion of the coordination sphere of the Ca^{2+} ions by phospholipid headgroups was manifested by the observation that the apparent Ca^{2+} affinity of synaptotagmin 1 C2 domains increases dramatically (up to 5000 fold) to 5-10 μM in the presence of phospholipid (Davletov et al., 1993; Ubach et al., 1998).

The Ca^{2+}-dependent phospholipid binding activity is crucial for synaptotagmin 1 action in neurotransmitter release. Electrophysiological experiments performed in the calyx of held demonstrated that the apparent Ca^{2+} affinity of synaptotagmin 1 in the presence of phospholipid correlated very well with the requirement of Ca^{2+}-triggered neurotransmitter

release at the calyx of held, also supporting the role of synaptotagmin 1 as the major Ca^{2+} sensor (Schneggenburger and Neher, 2000; Bollmann et al., 2000). More convincing evidence came from the amazing finding, as mentioned above, that a single point mutation of R233Q in synaptotagmin 1 caused the decrease of apparent Ca^{2+} affinity of the tandem C2AB fragment in the presence of phospholipid by 50% and a corresponding decrease of Ca^{2+} sensitivity of neurotransmission in the knock-in mice.

Mutagenesis studies focused on the active sites of synaptotagmins 1 C2 domains have yielded tremendous information for as well as posed new puzzles. Knock-in mice bearing either D232N or D238N in the C2A domain exhibited little effect on neurotransmitter release, which was explained by the minimal effect of the mutations on the phospholipid binding affinities of the tandem C2AB fragment due to the compensation of the C2B domain (Fernandez et al., 2001; Fernandez-Chacon et al., 2002). In *Drosophila*, disruption of Ca^{2+}-binding sites in the synaptotagmins 1 C2A domain (corresponding to D178N in rat) only compromised the neurotransmission (Robinson et al., 2002) whereas, surprisingly and puzzlingly, disruption of Ca^{2+}-binding sites in the synaptotagmins 1 C2B domain in *Drosophila* (corresponding to D363N and D365N in rat) almost completely abolished (more than 95% decrease) neurotransmission, suggesting a preponderant role of the C2B domain in neurotransmission compared to the C2A domain (Mackler et al., 2002). The mechanistic basis for the dramatic asymmetric role of the two C2 domains of synaptotagmin 1 remains to be unraveled. Our results explained in chapter 5 suggested that the asymmetric role of the C2A domain and C2B domain of synaptotagmin 1 in neurotransmission results from their differential interaction with the SNARE complex and the C2B domain seemed to play a

preponderant role in the SNARE interaction (see details in chapter 5). Gain-of-function mutations in which exposed hydrophobic residues in the Ca^{2+}-binding loops of the C2 domains of synaptotagmin 1 were replaced with tryptophans led to correlated increases in the apparent Ca^{2+} affinity and the Ca^{2+} sensitivity of neurotransmission (Rhee et al., 2005). Together with the R233Q mutation and recent results of the C2B domain polybasic region mutation, these data revealed a remarkable correlation between the apparent Ca^{2+} affinity in the presence of phospholipid *in vitro* and the Ca^{2+} sensitivity of neurotransmission *in vivo* (Fernandez-Chacon et al., 2001; Rhee et al., 2005; Li et al., 2006).

Besides phospholipid binding, multiple studies have also reported Ca^{2+}-dependent and Ca^{2+}-independent interactions of synaptotagmin 1 with SNARE proteins (Sudhof and Rizo, 1996; Chapman, 2002). This type of interaction provides a very appealing way to couple Ca^{2+}-sensing and membrane fusion. Several studies have reported a Ca^{2+}-dependent interaction between synaptotagmin 1 and syntaxin (Bennett et al., 1992; Li et al., 1995; Chapman et al., 1995). However, mapping the binding sites on syntaxin by different methods yielded contradictory results. GST pulldown of deletion series of syntaxin mapped the binding site to the SNARE motif whereas NMR experiments mapped the binding site to the N-terminal Habc domain (Kee and Scheller, 1996; Shao et al., 1997). Other studies reported Ca^{2+}-dependent and/or Ca^{2+}-independent interaction between synaptotagmin 1 and SNAP-25 and the binding site on SNAP-25 was mapped to the C-terminus (Gerona et al., 2000; Banerjee et al., 1996). Many additional studies have described Ca^{2+}-dependent and/or independent binding of single or tandem C2 domains of synaptotagmin 1 to syntaxin, SNAP-25, syntaxin/SNAP-25 heterodimers and/or SNARE complexes, but it has been difficult to

unravel which of these interactions are physiologically relevant (Schiavo et al., 1997; Matos et al., 2000; Earles et al., 2001; Chieregatti et al., 2002; Zhang et al., 2002; Shin et al., 2003; Rickman and Davletov, 2003; Rickman et al., 2004; Bai et al., 2004). Thus, studies of which SNAREs bind to synaptotagmin 1, which sequences are involved in binding, and whether the interactions are promoted or decreased by Ca^{2+} have yielded contradictory data. Moreover, both synaptotagmin 1 and SNAREs are sticky proteins due to their highly charged composition, suggesting the possibility that at least some of the described interactions might have resulted from nonspecific electrostatic interactions. The most attractive interaction among all these is the interaction between synaptotagmin 1 and SNARE complexes since synaptotagmin 1 acts at the Ca^{2+} triggering step of release and SNARE complexes are believed to contribute to membrane fusion during this last step. Mechanistically, strong evidence has supported the notion that the binding of synaptotagmin 1 to phospholipids in response to Ca^{2+} influx is one of the mechanisms of synaptotagmin 1 action in neurotransmitter release (Shin et al., 2003; Rhee et al., 2005). However, the Ca^{2+}-dependence and physiological relevance of the interaction between the SNARE complex and synaptotagmin 1 as well as the relationship between SNARE binding and phospholipid binding of synaptotagmin 1, simultaneously or competitively, has been under a long-term debate. Our results explained in chapters 4 and 5 are focused on studies of the interaction of synaptotagmin 1 with the SNARE complex as well as with phospholipids, providing new insights into these long debated questions. Using fluorescence spectroscopy, confocal fluorescence microscopy, and microfluidic channel technology, we demonstrated that synaptotagmin 1 binds simultaneously to phospholipids and reconstituted SNARE complexes

in the presence of Ca^{2+}, and that the binding mode of synaptotagmin 1 to phospholipids is independent of the SNARE complexes. We also showed that synaptotagmin 1 competes with complexin (a SNARE-associating molecule, which will be introduced in more detail in section 1.5.3) for SNARE binding, which is dependent on the presence of Ca^{2+} and negatively charged phospholipid. Moreover, NMR spectroscopy and site-directed mutagenesis studies yielded structural information of the potential binding interface, allowing us to use computational modeling and docking to generate a hypothetical atomic model of synaptotagmin 1/SNARE complex (see details in chapters 4 and 5).

1.5.2.2 Synaptotagmin 4

Synaptotagmin 4 is the second most conserved synaptotagmin and shares a similar domain structure with synaptotagmin 1 (Sudhof, 2002). It has attracted much attention because its expression is developmentally regulated in mammals, with the highest expression at early stages during postnatal development. It is also strongly induced by seizures in adult brains and by increases in cAMP or Ca^{2+} in PC12 cells (Vician et al., 1995; Tocco et al., 1996; Ferguson et al., 1999; Berton et al., 2000). Synaptotagmin 4 knockout in mice caused defects in hippocampus-dependent learning and memory as well as fine motor coordination, suggesting its modulatory role in normal brain function (Ferguson et al., 2000). The human synaptotagmin 4 homologue was mapped to a region of chromosome 18, which was previously associated with the human psychiatric disorders, schizophrenia and bipolar disease, further supporting the requirement of synaptotagmin 4 for optimal brain functionality.

The localization of synaptotagmin 4 is still under debate. In mammals, it was originally found to localize at synaptic vesicles, but more recent studies by immunocytochemistry of brain sections, cultured neurons, and transfected cells revealed a localization to the Golgi apparatus, in distal parts of neurites and on large dense core vesicles (LDCVs) of NGF differentiated PC12 cells (Berton et al., 2000; Fukuda et al., 2001). In contrast, the *Drosophila* synaptotagmin 4 homologue was observed mainly on synaptic vesicles in the postsynaptic compartment (Littleton et al., 1999; Adolfsen et al., 2004). Another closely related isoform, synaptotagmin 11 was also identified in mammalian brains, the expression and localization of which is still under investigation (Sudhof, 2002). But the similarity between synaptotagmin 4 and 11 suggests that they might be functionally redundant.

The characteristic feature of synaptotagmins 4 and 11 (the hallmark of the synaptotagmin 4 subfamily) is the existence of a conserved substitution of one of the Ca^{2+}-coordinating aspartates for a serine residue in the C2A domain, suggesting that the C2A domain is deficient in Ca^{2+} binding and Ca^{2+}-dependent activities, such as phospholipid binding (von Poser et al., 1997). Together with the discovery of the preponderant role of synaptotagmin 1 C2B domain in Ca^{2+}-triggered neurotransmitter release and the fact that the synaptotagmin 4 C2B domain contains an intact Ca^{2+}-binding motif with a full complement of Ca^{2+} ligands, this observation led to the assumptions that the synaptotagmin 4 subfamily are Ca^{2+} sensors with a conserved function and that only their C2B domains function as a Ca^{2+}-binding module.

Several studies of regulated exocytosis of large dense core vesicles (LDCVs) in rat PC12 cells suggested that synaptotagmin 4 modulates fusion pore dynamics and the choice between kiss-and-run or full fusion, in a synaptotagmin 1-antagonistic fashion (Wang et al., 2001a; Wang et al., 2003a). Moreover, microinjection of synaptotagmin 4 fragments into PC12 cells inhibits Ca^{2+}-triggered neurotransmission (Thomas et al., 1999). These results suggested that synaptotagmin 4 is functionally antagonistic to synaptotagmin 1, acting as an inhibitor of Ca^{2+}-triggered neurotransmitter release. However, the Ca^{2+} and phospholipid binding properties of mammalian and *Drosophila* synaptotagmin 4 have not been systematically analyzed. To this end, we have used NMR spectroscopy and biochemical assays to analyze these properties systematically (see details in chapter 2). Surprisingly, we found that both C2 domains of *Drosophila* synaptotagmin 4 bind phospholipids in a Ca^{2+}-dependent manner while those of rat synaptotagmin 4 do not. NMR experiments also showed that the rat synaptotagmin 4 C2 domains do not bind Ca^{2+}. To understand the basis for the unexpected lack of Ca^{2+} binding by the rat synaptotagmin 4 C2B domain, we solved its crystal structure and found that it resembles the structure of the rat synaptotagmin 1 C2B domain but flexibility in the top loops and discrete changes in the orientation of the Ca^{2+}-coordinating ligands result in an inability to form full Ca^{2+}-binding sites. These results suggested that synaptotagmin 4 acts as a Ca^{2+} sensor in *Drosophila* but an evolutionary switch disabled Ca^{2+} binding to this isoform in vertebrates, resulting in a striking functional difference between two proteins that had been clearly identified as orthologues by sequence analyses.

1.5.2.3 Other Synaptotagmin Isoforms

Thirteen additional synaptotagmins have been identified besides synaptotagmin 1 and synaptotagmin 4, making this an unusually large family of trafficking proteins. All synaptotagmin isoforms exhibit similar overall domain structure as synaptotagmin 1 (Sudhof, 2002). However, the sequences of the N-terminal region, including the intravesicular region, the transmembrane region, and the linker, exhibit significant diversity. In contrast, the C-terminal tandem C2 domains are highly homologous to each other in all synaptotagmin isoforms. The fact that all C2B domains contain the α-helical insertion between strands 7 and 8 that is absent from the C2A domains indicates a common ancestry and suggests that the functional specialization between C2 domains in synaptotagmins is conserved.

All synaptotagmins are highly enriched in the brain. Extensive biochemical studies have suggested that they form a hierarchy of Ca^{2+} sensors with different Ca^{2+} affinities, performing complementary functions in Ca^{2+}-triggered exocytosis, and that the combination and relative abundance of different synaptotagmins could contribute to shaping the characteristic Ca^{2+} responses of various synapses (Sudhof, 2002). Among them, synaptotagmin 2 is highly similar to synaptotagmin 1 and is believed to function as an alternative Ca^{2+} sensor in fast synchronous neurotransmitter release in the more caudal areas of the brain that lack synaptotagmin 1, since their structures and properties are so similar and their distributions are in a complementary pattern, with synaptotagmin 1 primarily expressed in the forebrain and synaptotagmin 2 in the brain stem and spinal cord (Ullrich et al., 1994; Marqueze et al., 1995). Synaptotagmins 3 and 7 are the most abundant synaptotagmins after synaptotagmins 1 and 2. Together with synaptotagmins 5, 6 and 10, they form a class of

closely related synaptotagmins (Sudhof, 2002). In contrast to synaptotagmins 1 and 2, they are primarily localized to the plasma membrane instead of to synaptic vesicles and exhibit a 5- to 10-fold higher Ca^{2+} affinity in the presence of phospholipid than the vesicular synaptotagmins, suggesting their distinct functions (Butz et al., 1999; Sugita et al., 2001). Several studies have suggested that they function in Ca^{2+}-triggered exocytosis in permeabilized PC12 cells with a correspondingly higher Ca^{2+} sensitivity, leading to the hypothesis that plasma membrane synaptotagmins represent high-affinity Ca^{2+} sensors involved in slow Ca^{2+}-dependent exocytosis, whereas vesicular synaptotagmins function as low-affinity Ca^{2+} sensors specialized for fast Ca^{2+}-dependent exocytosis. As mentioned in the section above, synaptotagmin 11 is closely related to synaptotagmin 4 and their sequence similarity suggests they might share similar structures, properties and functional redundancy.

The other synaptotagmins are much less characterized, although many of them are abundantly co-expressed with synaptotagmin 1 in the brain and are evolutionarily conserved. However, they cannot substitute for the loss of synaptotagmin 1 functions, therefore they must bear other functions distinct from that of synaptotagmin 1, which are still under active investigations.

1.5.3 Complexins

Complexins, also known as synaphins, constitute a family of small (16-18 kDa) proteins of about 130 amino acids. The mammalian complexin family contains four isoforms, complexin I, complexin II, complexin III and complexin IV. The two major isoforms, complexins I and II, are soluble proteins, whereas complexins III and IV are C-terminally

farnesylated on a CAAX-box motif, which regulates their synaptic targeting (Reim et al., 2005). Complexins are enriched in neurons and mostly colocalize with syntaxin 1 and SNAP-25. Complexins were originally identified through their tight interaction with the SNARE complex (McMahon et al., 1995; Ishizuka et al., 1995; Takahashi et al., 1995). In contrast to many other SNARE-interacting molecules, complexins bind exclusively to the assembled SNARE complex, but very weakly or not at all to the individual SNARE proteins (McMahon et al., 1995; Pabst et al., 2000; Pabst et al., 2002). It has been shown that complexins compete with α-SNAP for binding to the SNARE complex, but the physiological relevance of this competition has not been well understood yet. The functional importance of complexins has been demonstrated by the lethal phenotype observed in the complexins I/II double knockout mice (Reim et al., 2001). Moreover, complexins are one of the few presynaptic proteins that have been found to be implicated in several types of neurological diseases, such as bipolar disorder, schizophrenia, Huntington's disease, and Alzheimer's disease (Eastwood and Harrison, 2000; Morton and Edwardson, 2001; Knable et al., 2002; Edwardson et al., 2003; Lee et al., 2005; Tannenberg et al., 2006). Therefore, understanding the molecular mechanism of complexins function is not only essential to elucidate the mechanism of how neurotransmitter release is tightly regulated, but also to potentially provide clues on therapeutic strategies and reagents for these human neurological diseases.

Complexins have been unequivocally implicated in Ca^{2+}-triggered neurotransmission, but exhibit double-sided effects, even though their binding to the SNARE complex is Ca^{2+}-independent. On one hand, complexin I/II double knockout in mice leads to a selective impairment of the Ca^{2+}-triggered step of fast neurotransmitter release, but not the hypertonic

sucrose-triggered release, which interestingly resembles a milder phenocopy of synaptotagmin 1 knockout (Reim et al., 2001). On the other hand, introduction of excess complexins or their fragments into cells, either by transfection or microinjection, inhibits neurotransmitter release (Tokumaru et al., 2001).

In solution, complexins lack a tertiary structure, but contain an α-helical region in the middle of the sequence that is responsible for its specific binding to the SNARE complex (Pabst et al., 2000). Previous nuclear magnetic resonance (NMR) spectroscopy and X-ray crystallography studies from our laboratory revealed that complexins assume an α-helical conformation and bind in an antiparallel fashion to the groove formed between syntaxin and synaptobrevin SNARE motifs (Bracher et al., 2002; Chen et al., 2002) (Figure 1.10). Deuterium exchange experiments suggested that complexin binding stabilizes the syntaxin/synaptobrevin interface, especially its C-terminal region, presumably through a combination of hydrogen bond network, salt bridges and hydrophobic interactions, as observed in the crystal structure. These observations led to a two-stage synaptic vesicle priming model, which provided an explanation for the observation that complexin I/II double knockout in mice caused a selective impairment in Ca^{2+}-triggered fast neurotransmitter release, while leaving the hypertonic sucrose-triggered release intact (Chen et al., 2002). In this model, the first priming stage involves a partially assembled SNARE complex whereas the second stage involves a fully assembled SNARE complex, which is stabilized by the selective binding of complexin; the two stages are interchangeable. Synaptic vesicles in both stages can be triggered to release by hypertonic sucrose treatment while only the vesicles in the second stage are ready for Ca^{2+}-triggered fast release.

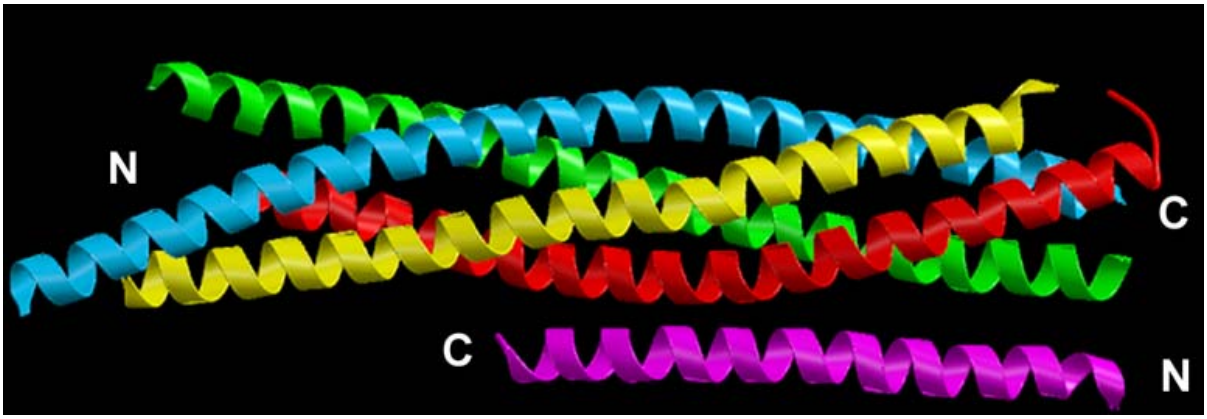

Figure 1.10 Crystal structure of the complexin/SNARE complex.

A ribbon diagram of the complexin/SNARE complex is shown. The SNARE motifs from syntaxin, synaptobrevin, N-terminal SNAP-25 and C-terminal SNAP-25 are colored in yellow, red, blue, and green, respectively. The complexin fragment (26-83) is colored in magenta. The SNARE complex forms a four-helix bundle with complexin assuming an α-helical conformation and binding antiparallel to the groove formed by syntaxin and synaptobrevin SNARE motifs (Chen et al., 2002).

1.5.4 RIMs

RIMs (Rab3-interacting molecules) were initially identified as Rab3 effectors, and include four genes in mammals (RIM1, RIM2, RIM3γ and RIM4γ), and one in *C. elegans* (unc10) (Wang and Sudhof, 2003; Wang et al., 1997). The mammalian RIM1 and RIM2 genes specify full-length transcripts encoding two closely related isoforms (RIM1α and RIM2α; referred to as α-RIMs) that contain an N-terminal zinc finger domain, a PDZ domain and two C-terminal C2 domains that are separated by long alternatively spliced sequences (referred to as the C2A domain and the C2B domain) (Wang et al., 1997; Wang and Sudhof, 2003). In addition, the RIM2 gene also specifies a shorter transcript lacking the N-terminal zinc finger (RIM2β), and an even shorter transcript (RIM2γ) that, like RIM3γ and RIM4γ, encodes only the C2B domain and adjacent sequences (Wang et al., 2000; Wang and Sudhof, 2003). *C. elegans* contains only one RIM protein, which is encoded by unc10, a gene first identified in the classic uncoordination mutant screen (Brenner, 1974; Koushika et al., 2001).

Genetic experiments have shown that RIMs are critical for normal priming of synaptic vesicles to a release-ready state, and control some forms of short-term and long-term presynaptic plasticity. Deletion of unc10 in *C. elegans* led to a drastic decrease in the level of neurotransmitter release (5-fold reduced level of fusion-competent vesicles despite normal levels of docked vesicles) that is associated to defects in synaptic vesicle priming (similar to unc13 nulls) and is more severe than the phenotype of Rab3 mutants, suggesting that unc10 is not merely a Rab3 effector (Koushika et al., 2001). Deletion of RIM1α in mice results in a milder phenotype compared to *C. elegans*, probably because of partial functional redundancy with RIM2α, but still results in less vesicle priming and impairment of synaptic

plasticity. In RIM1α knockout mice, the neurotransmitter release probability is significantly reduced, some forms of short-term synaptic plasticity, such as paired pulse facilitation, paired pulse depression, and post-tetanic potentiation, are altered, and a form of long-term synaptic plasticity known as mossy fiber long-term potentiation (LTP) is completely abolished (Schoch et al., 2002; Castillo et al., 2002; Calakos et al., 2004). RIM1α knockout mice exhibited severe defects in learning and memory that most likely arise from these defects in neurotransmitter release and its regulation (Powell et al., 2004). The later phenotype is also observed in Rab3A knockout mice (Castillo et al., 1997), suggesting that mammalian RIMs are *bona fide* Rab3 effectors *in vivo*.

RIMs are large (ca. 180 kDa for α-RIMs) proteins localized at presynaptic active zone, where Ca^{2+}-triggered neurotransmitter release occurs. The active zone of a synapse contains a network of large proteins, which include RIMs, Munc13s, Bassoon, piccolo, ELKS, and liprins, mediates Ca^{2+}-triggered neurotransmitter release, and integrates presynaptic signals that regulate neurotransmitter release (Schoch et al., 2002). Among these proteins, RIMs are particularly interesting because of their multiple roles in regulating release and organizing the active zone that have been suggested by extensive genetic and biochemical experiments. The different domains of α-RIMs have been implicated in multiple protein-protein interactions. Thus, the N-terminal zinc finger domain and adjacent regions are involved in binding to Rab3s and to Munc13-1 (Betz et al., 2001; Wang et al., 2001b; Schoch et al., 2002), an active zone protein with a key role in synaptic vesicle priming, while the central PDZ domain binds to ELKS (named after its high content of the amino acids glutamate, leucine, lysine and serine, and also known as ERC or CAST) (Wang et al., 2002).

On the other hand, the RIM C2A domain was reported to bind to the Ca^{2+} sensor synaptotagmin 1 and to SNAP-25 in a Ca^{2+}-dependent manner, whereas the C2B domain was also found to bind to synaptotagmin 1 and in addition to liprins (Coppola et al., 2001; Schoch et al., 2002). Finally, a proline-rich sequence between the two C2 domains binds to RIM-binding proteins (RIM-BPs) (Hibino et al., 2002). Besides these observed direct interactions, RIMs have also been found to interact indirectly with other synaptic proteins, for example with piccolo and bassoon via ELKS, and with receptor-tyrosine phosphatases via liprins (Serra-Pages et al., 1998; Zhen and Jin, 1999; Takao-Rikitsu et al., 2004). These observations suggested that α-RIMs may act as scaffolds that help to organize the active zone through its multiple interactions with active zone proteins, and at the same time may regulate neurotransmitter release by binding to key components of the release apparatus (Schoch et al., 2002). However, not all of these interactions have been reproducible, and their significance remains unclear at present. Moreover, little is known about the three-dimensional structures of the α-RIM domains. Due in part to this scarcity of structural and definitive biochemical information, there is currently a large gap between the extensive genetic and physiological data describing the functions of α-RIMs and the limited molecular understanding of these functions.

Interestingly, neither of the C2 domains of RIMs contains the consensus calcium binding sites that were defined in the synaptotagmin C2 domains and that are present in the C2 domains of another Rab3 effector, rabphilin. However, both RIM C2 domains are functional important. Previous studies of the *C. elegans* RIM homologue unc10 have shown that only the C2A domain of unc10 is necessary for its localization, while both the PDZ and

C2A domains are required for RIM-like localization along the nerve cords (Deken et al., 2005). Another clue of the physiological importance of the RIM C2A domain came from the finding that R844H substitution in the human RIM1 C2A domain segregates with autosomal dominant cone-rod dystrophy (CORD7), which is characterized by the early loss of visual acuity and color vision, followed by night blindness and peripheral visual field loss (Hunt et al., 2002; Johnson et al., 2003). The fact that the C2B domain exists in all six alternatively spliced isoforms of mammalian RIMs (RIM1α, RIM2α, RIM2β, RIM2γ, RIM3γ and RIM4γ) and its high degree of sequence conservation underlines the functional importance of the RIM C2B domain (Wang and Sudhof, 2003). Studies in *C. elegans* revealed that the introduction of unc10 constructs lacking the C2B domain into unc10 null animals failed to either restore aldicarb sensitivity or rescue behavioral deficits, in contrast to the full restoration of aldicarb sensitivity and rescue of the behavioral deficits by full length unc10 constructs, further supporting the physiological essentiality of the RIM C2B domain (Koushika et al., 2001).

The lack of consensus calcium binding sites of the RIM C2 domains suggests the lack of Ca^{2+}-dependent activities, raising the intriguing question of how these C2 domains facilitate the regulation of Ca^{2+}-triggered neurotransmitter release. To gain insight into this question, we have used NMR spectroscopy and X-ray crystallography to analyze structural and biochemical properties of the rat RIM2 C2A domain, which is closely related to the RIM1 C2A domain (see details in chapter 3). We confirmed that the RIM2 C2A domain does not bind to Ca^{2+} or negatively charged phospholipids in the presence of Ca^{2+}. Moreover, little binding of the RIM2 C2A domain to SNAP-25 or the C2 domains of synaptotagmin 1 was

detected by NMR experiments, suggesting that as-yet-unidentified interactions of the RIM C2A domain mediate its function. We also determined the crystal structure of the RIM2 C2A domain and revealed a β-sandwich fold that resembles those observed for other C2 domains, but exhibits a unique dipolar distribution of electrostatic charges whereby one edge of the β-sandwich is highly positive and the other edge is highly negative. The location of the mutation site (R805H) implicated in CORD7 at the bottom 3_{10}-helix of the domain and the pattern of sequence conservation suggested that, in contrast to most C2 domains, the RIM C2A domains may function through Ca^{2+}-independent interactions involving their bottom face.

Chapter 2 Structural Basis for the Evolutionary Inactivation of Ca^{2+} Binding to Synaptotagmin 4

(Parts of this chapter are adapted from Dai et al., 2004)

2.1 Introduction

Synaptotagmins are a family of proteins implicated in regulated neurotransmission, and are transmembrane proteins with two tandem C2 domains. Ca^{2+} binding and Ca^{2+}-dependent phospholipid binding constitute their most general activities. Up to now, at least eight isoforms have been identified in *Drosophila* and fifteen in mammals. Biochemical analyses of these isoforms have suggested that they form a hierarchy of Ca^{2+} sensors with different Ca^{2+} affinities (Sudhof, 2002; Sugita et al., 2002).

The most conserved and best characterized synaptotagmin is synaptotagmin 1. Synaptotagmin 1 has been strongly suggested by extensive genetic and biochemical studies to be the Ca^{2+} sensor in Ca^{2+}-triggered fast neurotransmitter release, as mentioned in chapter 1. The most definitive evidence supporting this notion came from the observation of a strong correlation between *in vitro* Ca^{2+} dependence of phospholipid binding and *in vivo* Ca^{2+} sensitivity of neurotransmitter release (Fernandez-Chacon et al., 2001). A single point mutation, R233Q, in the C2A domain of synaptotagmin 1 decreases both by about 50% (Fernandez-Chacon et al., 2001). The C2A and C2B domains of synaptotagmin 1 adopt similar β-sandwich structures (Sutton et al., 1995; Fernandez et al., 2001) and bind three or two Ca^{2+} ions, respectively, with low intrinsic Ca^{2+} affinity (Fernandez et al., 2001; Shao et al., 1996; Ubach et al., 1998). The Ca^{2+}-binding sites of the C2A domain are formed by one serine and five aspartate residues that are highly conserved and clustered in the top loops of

the β-sandwich (labeled S and D1−D5 in Figure 2.1A), whereas the C2B domain contains only the five aspartate residues (Figure 2.1B). Both C2 domains of synaptotagmin 1 exhibit Ca^{2+}-dependent phospholipid binding (Fernandez-Chacon et al., 2001; Fernandez et al., 2001; Davletov and Sudhof, 1993), which probably underlies the function of synaptotagmin 1 in triggering neurotransmitter release in response to Ca^{2+} influx (Fernandez-Chacon et al., 2001; Mackler et al., 2002; Shin et al., 2002). Phospholipids bind to hydrophobic and basic residues in the top loops of the synaptotagmin 1 C2 domains and markedly increase their apparent Ca^{2+} affinity (up to 5,000-fold), probably by completing the coordination of the Ca^{2+} ions (Fernandez-Chacon et al., 2001; Fernandez et al., 2001; Zhang et al., 1998; Chapman and Davis, 1998; Gerber et al., 2002).

Synaptotagmin 4, the second most conserved synaptotagmin, has attracted much attention because its expression is developmentally regulated in mammals and is strongly upregulated by seizures in the brains (Tocco et al., 1996). Synaptotagmin 4 knockout in mice caused defects in learning and memory as well as motor coordination. A closely related isoform, synaptotagmin 11, is also expressed in mammals (von Poser et al., 1997), whereas only one closely related synaptotagmin was identified in *Drosophila* as synaptotagmin 4 (Littleton et al., 1999). The C2A domains of all these synaptotagmins contain a conserved aspartate to serine substitution in one of the putative Ca^{2+} ligands at D3 position (Figure 2.1B) (von Poser et al., 1997). In contrast, the C2B domains of both mammalian and *Drosophila* synaptotagmin 4 contain a full Ca^{2+}-binding motif except for some conservative aspartate to glutamate or serine to threonine substitutions (Figure 2.1B). These observations have led to the assumptions that mammalian and *Drosophila* synaptotagmin 4 are Ca^{2+}

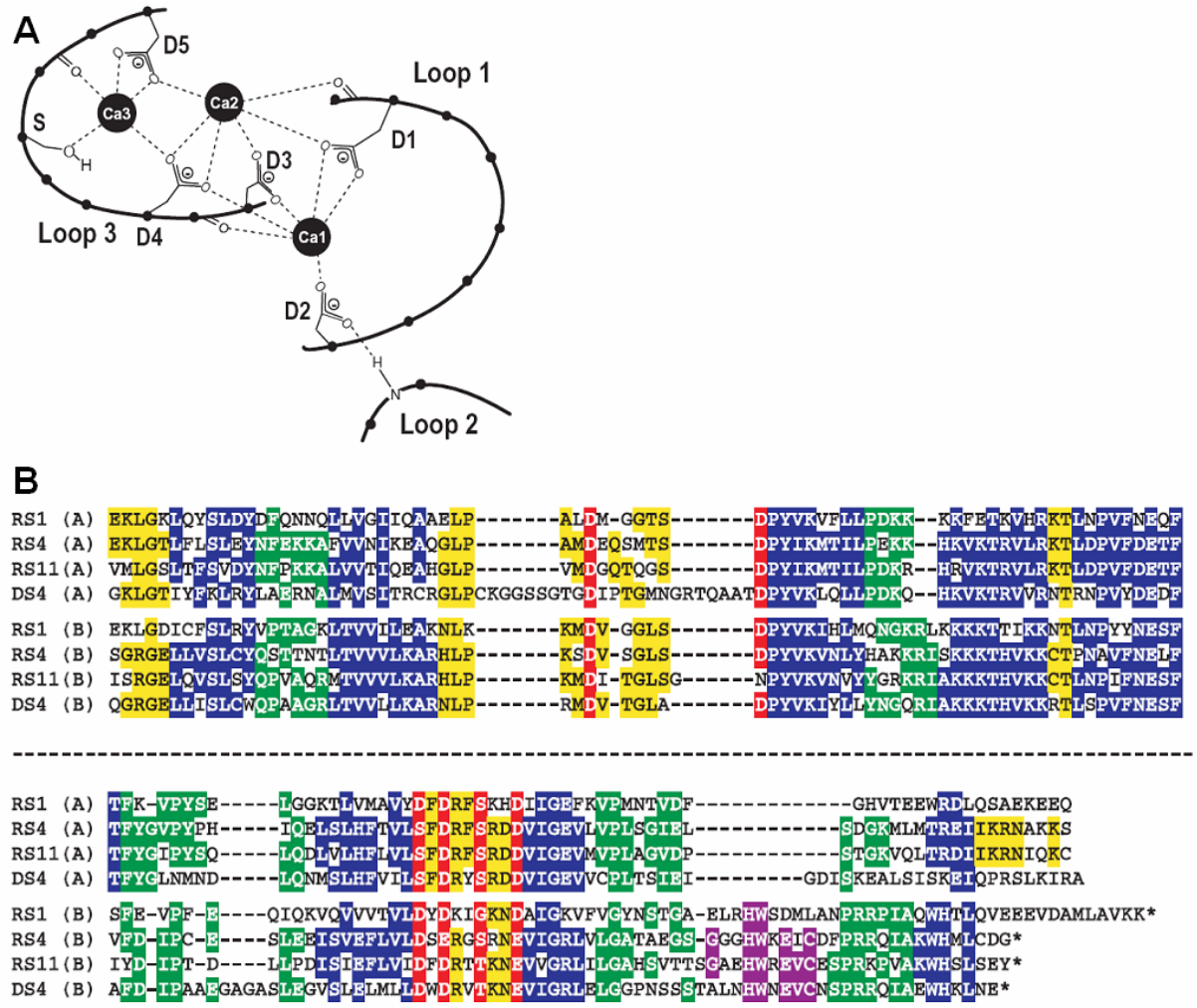

Figure 2.1 Sequence comparison of the synaptotagmins 1, 4 and 11 C2 domains.

(A) Schematic diagram summarizing the three Ca^{2+}-binding sites of the rat synaptotagmin 1 C2A domain (Ca1−Ca3, solid circles). The five aspartates and one serine involved in Ca^{2+} binding are labeled D1−D5 and S, respectively.

(B) Sequence alignment of the C2 domains from rat synaptotagmin 1 (RS1), rat synaptotagmin 4 (RS4), rat synaptotagmin 11 (RS11) and *Drosophila* synaptotagmin 4 (DS4). The C2A domains and C2B domains are designated as (A) and (B) after protein name abbreviations, respectively. Shown in red background are the residues that form the Ca^{2+}-binding sites of the synaptotagmin 1 C2 domains and conserved residues in the same positions from the synaptotagmins 4 and 11 C2 domains. Other background colors indicate conserved residues according to their location in the three-dimensional structures of C2 domains: blue, β-strands; yellow, top loops; green, bottom loops; purple, bottom helix present in the C2B domains but not in the C2A domains.

sensors with a conserved function (Littleton et al., 1999; Wang et al., 2001a; Wang et al., 2003a) and that only their C2B domains function as the Ca^{2+}-binding modules (Robinson et al., 2002). Based on this assumption, diverse controversial functions such as modulation of fusion pore dynamics, modulation of the selection of kiss-and-run or full fusion, *etc*., have been ascribed to synaptotagmin 4 (Wang et al., 2001a; Wang et al., 2003a). However, the Ca^{2+} and phospholipid binding properties of mammalian and *Drosophila* synaptotagmin 4 have not been systematically analyzed.

In this chapter, we analyzed the Ca^{2+} binding properties of rat and *Drosophila* synaptotagmin 4 subfamily through Ca^{2+} titrations monitored by ^{1}H-^{15}N HSQC spectra as well as their Ca^{2+}-dependent phospholipid binding properties using heavy liposome cosedimentation assay and FRET experiments. We found that, notably, both C2 domains of *Drosophila* synaptotagmin 4 bind to negatively charged phospholipids in a Ca^{2+}-dependent manner whereas neither of those from rat synaptotagmin 4 or 11 do. Moreover, the rat synaptotagmin 4 or 11 C2B domains do not even bind to Ca^{2+} in spite of the presence of a full complement of Ca^{2+}-coordinating residues. To investigate the structural basis for the unexpected observation of the inability to bind Ca^{2+} and negatively charged phospholipid of the rat synaptotagmin 4 C2B domain, we determined the crystal structure of the rat synaptotagmin 4 C2B domain in the presence or absence of Ca^{2+}, showing that its unexpected properties probably arise from an inability to form full Ca^{2+}-binding sites due to both the loop flexibility and the inappropriate orientation of key Ca^{2+}-coordinating side chains. These results suggest that synaptotagmin 4 functions as a Ca^{2+} sensor in *Drosophila*

but an evolutionary switch disabled Ca^{2+} binding to this isoform in vertebrates, resulting in a Ca^{2+}-independent synaptotagmin.

2.2 Materials and Methods

2.2.1 Recombinant Protein Preparation

DNA encoding GST fusion proteins of rat synaptotagmin 4 C2A domain (amino acids 152−285), rat synaptotagmin 4 C2B domain (amino acids 286−425), rat synaptotagmin 11 C2A domain (amino acids 155−288), rat synaptotagmin 11 C2B domain (amino acids 289−430), *Drosophila* synaptotagmin 4 C2A domain (amino acids 178−329) and *Drosophila* synaptotagmin 4 C2B domain (amino acids 330−474) subcloned in the pGEX-KG expression vector was generously provided by Dr. Ok-Ho Shin from Dr. Thomas C Südhof's laboratory. The rat synaptotagmin 4 C2B domain containing single point mutations E380D, E386D or double point mutations (E380D, E386D) were generated by the Quikchange® site-directed mutagenesis kit (Stratagene), which provides a simple and fast procedure to generate mutant DNA. Briefly, one pair of synthetic oligonucleotide primers was designed covering the mutation region with the intended nucleotide substitutions. The oligonucleotide primers were then extended during a temperature cycle. After the temperature cycling, the product was treated with Dpn I to specifically digest the parental DNA template that is derived from bacteria and thus methylated or hemimethylated, while leaving the newly synthesized DNA untouched. The resulting product was then transformed into *Escherichia coli* (*E. coli*) XL1-Blue supercompetent cells to repair the nicks and amplify the DNA. The plasmids encoding

the desired mutations were purified with Qiagen plasmid miniprep kit and the mutations were verified by DNA sequencing. All the plasmids were transformed into *Escherichia coli* BL21 competent cells for protein expression. Glycerol stocks (8% glycerol) of the transformed cells were kept in -80 ºC.

For a routine 1 liter bacteria culture, 50 ml luria broth (LB) media was inoculated with a single colony from an agar/ampicillin plate and incubated in the shaker at 250 rpm (revolutions per minute) overnight at 37 ºC. The next day, proper amount of culture (usually 10-20 ml) was transferred to 1 liter LB media to make sure that the starting OD_{600} was around 0.1. All the media contained 50 μg/ml ampicillin to maintain the presence of the transformed plasmids. Whenever isotope labeling was necessary, M9 minimal media were used instead of LB media. 1 liter M9 media contains: 6.8 g Na_2HPO_4, 3.0 g KH_2PO_4, 0.5 g NaCl, 1.0 g NH_4Cl, 2.0 mM $MgSO_4$, 100 μM $CaCl_2$, 2.5 mg thiamine, and 4.0 g D-glucose. Uniform ^{15}N labeling was achieved by using M9 minimal media prepared with $^{15}NH_4Cl$ instead of the unlabeled NH_4Cl as the sole nitrogen sources. Uniform ^{13}C labeling was achieved by replacing unlabeled glucose with $^{13}C_6$-D-glucose as the sole carbon sources, and 3.0 g $^{13}C_6$-D-glucose was used instead of 4.0 g due to the high cost of the $^{13}C_6$-D-glucose. The flasks were incubated at 37ºC and shaken at 250 rpm till OD_{600} reached 0.6-0.8, then the temperature was lowered to 25 ºC and 0.4 mM IPTG (isopropyl β-D-thiogalactopyranoside, from Sigma) was added to induce protein expression for overnight (about 15-16 hours). The cells were harvested by centrifugation at 4,000 rpm for 30 min in swing buckets with a rotor JS 4.2 (Model J6-MI centrifuge, Beckman Instruments) and resuspended into 35ml PBS (phosphate buffered saline) buffer (10 mM Phosphate, pH 7.4,

2.7 mM KCl and 137 mM NaCl) containing 10 µl/ml Sigma inhibitor cocktail (Sigma), 0.5 mM AEBSF (water soluble substitution of PMSF), 2 mM EDTA, and 5 mM EGTA. The cell suspension was frozen with liquid nitrogen and stored in -80 ºC for further protein purification.

The frozen cells from 1 liter culture were thawed and passed through a high pressure homogenizer (Model EmulsiFlex-C5, Avestin Inc.) for 3 to 4 times. The cell debris was spun down by centrifugation at 18,000 rpm for 30 minutes in a JA-20 rotor with the Beckman centrifuge (model J2-21). The supernatant was filtered with 0.45 µm syringe filter (Nalgene) and mixed with 1.0-1.5 ml slurry of the pre-washed glutathione Sepharose 4B resins (Amersham Pharmacia Biotech.) per liter of culture in the cold room at 4 °C overnight. GST fusion proteins were bound tightly to the glutathione resins, whereas unbound proteins and nonspecifically bound proteins were removed by washing sequentially with 50 ml PBS, 50 ml PBS containing 1% Triton X-100, and 50 ml PBS containing 1M NaCl for two to three times. In the cases of the purification of the C2B domains whose PI (isoelectric point) are significantly higher than 7, a benzonase (0.25 units/µl) nuclease treatment for one hour at room temperature in benzonase cleavage buffer (50 mM Tris, pH 8.0, 2 mM $MgCl_2$) with freshly added 1mM DTT was used to remove nonspecifically bound DNA followed by extensively washing with PBS containing 1M NaCl and PBS. The resin was then washed with 3 ml thrombin cleavage buffer (50 mM Tris, pH 8.0, 200 mM NaCl and 2.5 mM $CaCl_2$) with freshly added 1mM DTT for three times, followed by on-resin cleavage with 5-7 units/ml thrombin (from bovine plasma, Sigma) for three to four hours at room temperature to remove the GST tag and release the C2 domain proteins with N-terminal extra linker

residues from the construct. The proteins were eluted with elution buffers (200 mM NaPi, pH 6.2, 300 mM NaCl, 1mM DTT) and further purified by gel filtration chromatography through a Superdex 75 Hiload 16/60 column (Amersham Pharmacia Biotech.). The purity of the preparation was assessed by SDS-PAGE and Coomassie blue staining. The typical yield according to UV absorbance measurements at 280 nm was 3-5 mg per liter of culture.

2.2.2 NMR Spectroscopy

All NMR experiments were acquired at 27 °C on Varian INOVA500 or INOVA600 spectrometers (Varian, Palo Alto, California, USA) with C2 domain samples dissolved in 20 mM MES (pH 7.0 for rat synaptotagmin 4 C2A domain and rat synaptotagmin 11 C2A domain; pH 6.32 for *Drosophila* synaptotagmin 4 C2A domain, rat synaptotagmin 4 C2B domain, rat synaptotagmin 11 C2B domain and *Drosophila* synaptotagmin 4 C2B domain), and 150 mM NaCl, using H_2O/D_2O 95:5 (v/v) as the solvent. The 5% (v/v) D_2O was included to provide the lock signal for the control of the long term stability of the magnetic field. The resonance assignments for the rat synaptotagmin 4 C2B domain were obtained from triple-resonance experiments (HNCACB, CBCA(CO)NH and HNCO) in combination with 3D (three-dimensional) ^{1}H-^{15}N TOCSY-HSQC and ^{1}H-^{15}N NOESY-HSQC spectra. All NMR data were processed with the program NMRPipe (Delaglio et al., 1995) and analyzed with the program NMRView (Johnson and Blevins, 1994).

2.2.3 Ca^{2+} Titration Monitored by ^{1}H-^{15}N HSQC Spectra

The zero Ca^{2+} sample was assured by the addition of 1mM EDTA. The titration was done by adding to the sample a series of certain volume of high concentration $CaCl_2$ stock. The high concentration $CaCl_2$ stock was added on the top or the side of the eppendorf tube containing the sample and then mixed quickly and thoroughly. This strategy instead of directly adding $CaCl_2$ to protein sample was used to avoid the protein precipitation caused by the very high local Ca^{2+} concentration at the spot of Ca^{2+} addition. Since upon chelating Ca^{2+}, proton will be released from EDTA, the pH value of each titration sample was measured and adjusted to maintain the pH value constant. Appropriate concentrations for the further titration were estimated based on the already accomplished part of the titration. For rat synaptotagmin 4 C2A domain, the following calcium concentrations were used: 0 mM, 0.2 mM, 1 mM, 5 mM, 10 mM, 20 mM, 40 mM, and 80 mM Ca^{2+}. For rat synaptotagmin 4 C2B domain, the following calcium concentrations were used: 0 mM, 5 mM, and 20 mM Ca^{2+}. For *Drosophila* synaptotagmin 4 C2A domain, the following calcium concentrations were used: 0 mM, 5 mM, 10 mM, 20 mM, 40 mM, and 80 mM Ca^{2+}. For *Drosophila* synaptotagmin 4 C2B domain, the following calcium concentrations were used: 0 mM, 0.2 mM, 1 mM, 3 mM, 10 mM, 20 mM, and 40 mM Ca^{2+}. For rat synaptotagmin 11 C2A domain, the following calcium concentrations were used: 0 mM, 0.2 mM, 1 mM, 3 mM, 5 mM, 10 mM, 20 mM, 40 mM, and 80 mM Ca^{2+}. For rat synaptotagmin 11 C2B domain, the following calcium concentrations were used: 0 mM, 5 mM, 10mM, and 20 mM Ca^{2+}.

2.2.4 Preparation of Liposomes by Extrusion

Negatively charged liposomes (phospholipid vesicles) composed of 30% (w/w) DOPS, 65% (w/w) POPC, and 5% (w/w) Dansyl-DOPE or of 25% (w/w) DOPS and 75% (w/w) POPC were used for FRET (fluorescence resonance energy transfer) experiments and cosedimentation experiments, respectively. Synthetic1,2-dioleoyl phosphatidylserine (DOPS), 1-palmitoyl, 2-oleoyl phosphatidylcholine (POPC), and fluorescent 5-(dimethylamino)naphthalene-1-sulfonyl -1,2-dioleoyl phosphatidylethanolamine (Dansyl-DOPE) were obtained from Avanti Polar Lipids (Avanti Polar Lipids, Alabaster, AL, USA). The chloroform in the lipid mixture was evaporated under a stream of nitrogen gas in the hood to allow the formation of a thin lipid film, which was then thoroughly dried with a vacuum pump for two hours or overnight to remove residual chloroform. The dried lipid film was then hydrated by adding required amount of hydration buffer (40 mM HEPES, pH 7.5, and 100 mM NaCl) to give a final lipid concentration of 1 mg/ml and vigorous vortexing for at least five minutes to form large multilamellar vesicles (LMV). To prevent the membranes from fouling and improve the homogeneity of the size distribution of the final liposome suspension, the LMV suspension was disrupted by five times freeze/thaw cycles in liquid nitrogen. Mini extruder purchased from Avanti Polar Lipids was used to homogenize the lipids. The mini extruder is a system of two gas-tight syringes/plungers with a polycarbonate filter in between and assembled according to the procedure recommended by the manufacturer. After the initial pass through the polycarbonate filter, the particle size distribution will tend towards a bimodal distribution while after sufficient passes through the polycarbonate filter, a unimodal, normal distribution will be obtained. The lipid suspension was forced through a polycarbonate filter with 80 nm pore size for at least twenty-one times.

This procedure typically yields large unilamellar vesicles (LUV) of homogeneous size with a mean diameter of 100 nm as measured by dynamic light scattering (DLS). The liposomes were stored at 4 ºC and used within 1-3 days.

2.2.5 Phospholipid Binding by Cosedimentation Assay

Phospholipid binding to the isolated C2 domains and the tandem C2AB fragments from rat synaptotagmins 4 and 11 and *Drosophila* synaptotagmin 4 was analyzed by a cosedimentation assay with the C2 domains from rat synaptotagmin 1 as positive controls. Briefly, heavy liposomes (25% (w/w) DOPS, 75% (w/w) POPC) were prepared in hydration buffer (50 mM HEPES, pH 6.8, 100 mM NaCl, 4 mM EGTA) containing 0.5 M sucrose and isolated by centrifugation (100,000 g for 30 min) after adding 4 volumes of hydration buffer without sucrose. The heavy liposomes were then washed with hydration buffer, precipitated by microcentrifugation (13,000 rpm for 10 min), and resuspended in hydration buffer. GST fusion proteins containing the C2 domains (6 μg) were incubated with 100 μg of heavy liposomes with various concentrations of free Ca^{2+} clamped with Ca^{2+}/EGTA buffers, and microfuged at 13,000 rpm for 10 min. The pellets were washed with the corresponding Ca^{2+}/EGTA buffer, treated with chloroform:methanol (1:2, v/v), and centrifuged again (13,000 rpm for 15 min). The bound proteins were analyzed by SDS-PAGE and Coomassie blue staining.

2.2.6 Phospholipid Binding by Fluorescence Resonance Energy Transfer (FRET) Assay

FRET experiments were performed on a Perkin Elmer LS50B spectrofluorometer (Perkin Elmer, Uberlingen, Germany) with a 450 µl Quartz fluorometer cuvette (Nova Biotech), exciting at 280 nm and recording the emission spectra from 300 to 550 nm with 5nm excitation slit width and 5nm emission slit width. The experiments were performed at 25 ºC in 40 mM HEPES, pH 7.5, and 100 mM NaCl, with 0.1 mg/ml lipid (65% (w/w) POPC, 30% (w/w) DOPS, 5% (w/w) Dansyl-DOPE) concentration and 1 µM protein in the presence of either 1mM EDTA or 1mM Ca^{2+}. The fluorescence emission spectra of protein alone or liposome alone were acquired under identical conditions as references.

2.2.7 Crystallization of the Rat Synaptotagmin 4 C2B Domain in the Presence and Absence of Ca^{2+}

Rat synaptotagmin 4 C2B domain dissolved in 20 mM MES, pH 6.32, 150 mM NaCl and 1 mM EDTA was concentrated to 22 mg/ml and stored in small aliquots at -80 ºC. Crystals of the C2B domain were obtained by hanging-drop vapor diffusion technique. Briefly, a hanging drop containing protein, stabilizing buffers and precipitant, is allowed to equilibrate in a closed system with a much larger reservoir which contains the same chemicals but the protein. Because the precipitant concentration in the reservoir is higher than that in the hanging drop, water evaporates from the drop and consequently the protein concentration increases gradually, which leads to the formation of protein crystals in certain buffer conditions. Rat synaptotagmin 4 C2B domain in the absence of Ca^{2+} was crystallized in 4.5 M NaCl, 0.1 M HEPES, pH 7.5, at 20 °C. Hexagonal cylinder crystals appeared overnight and grew to a final size of 0.1 mm × 0.1 mm × 0.2 mm within 2 days

(Figure 2.2A). Rat synaptotagmin 4 C2B domain in the presence of 0.1 M $CaCl_2$ was crystallized in 2.5 M NaCl, 0.1 M HEPES, pH 7.5, at 20 °C. Similar hexagonal crystals except for extra hexagonal pyramidal caps on both ends appeared overnight and grew to a final size of 0.1 mm × 0.1 mm × 0.2 mm within 2 days (Figure 2.2B). Prior to data collection, crystals were transferred into a solution of 4.25 M NaCl, 0.1 M HEPES, pH 7.5, and 5% (v/v) ethylene glycol as cryoprotectant for crystals grown with no calcium, and 2.5 M NaCl, 0.1 M $CaCl_2$, 0.1 M HEPES, pH 7.5, and 20% (v/v) ethylene glycol as cryoprotectant for crystals grown in 0.1 M $CaCl_2$, and flash cooled in liquid propane, then stored in liquid nitrogen until used for data collection. The type and optimal amount of cryoprotectant used were chosen by testing the cryoprotection solution in the cryostream at 100K to ensure the lack of ice formation. Less amount of ethylene glycol was used for the Ca^{2+} free crystal, presumably because the high concentration of NaCl in the crystallization buffer also contributes to the cryoprotection.

2.2.8 X-ray Crystallographic Data Collection and Processing

The initial diffraction data of rat synaptotagmin 4 C2B domain in the absence of Ca^{2+} were collected to a Bragg spacing (d_{min}) of 2.5 Å in the capillary at room temperature using an Raxis IV imaging plate system (Molecular Structure Corporation, Houston, TX, USA) mounted on a Rigaku RU-200 rotating anode X ray generator (CuKα, wavelength 1.54Å) (Rigaku Corporation, Japan) operated at 100 mA and 50 kV. Subsequently, diffraction data were collected at the Structural Biology Center (SBC) beamlines 19BM and 19ID of the Advanced Photon Source (APS) at 100 K to a Bragg spacing (d_{min}) of ~2.3 Å for Ca^{2+}-free

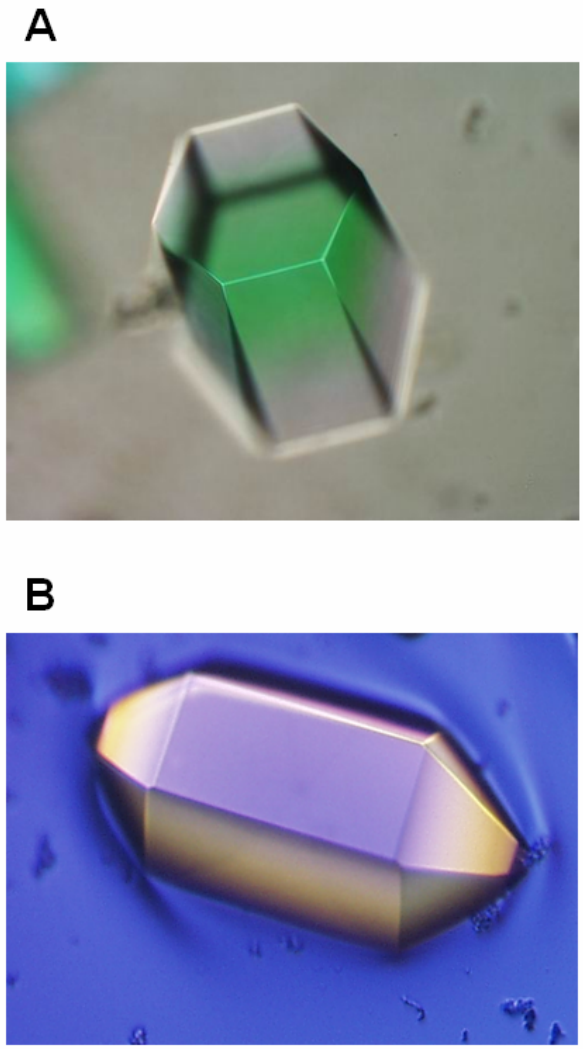

Figure 2.2 Crystallization of the rat synaptotagmin 4 C2B domain in the presence and absence of Ca^{2+}.

(A) Hexagonal cylinder crystals of the rat synaptotagmin 4 C2B domain in the absence of Ca^{2+} were obtained in 4.5 M NaCl, 0.1 M HEPES, pH 7.5, at 20 °C with a final size of 0.1 mm × 0.1 mm × 0.2 mm.

(B) Hexagonal crystals with extra hexagonal pyramidal caps on both ends of the rat synaptotagmin 4 C2B domain in the presence of Ca^{2+} were obtained in 0.1 M $CaCl_2$, 2.5 M NaCl, 0.1 M HEPES, pH 7.5, at 20 °C with a final size of 0.1 mm × 0.1 mm × 0.2 mm.

rat synaptotagmin 4 C2B domain and to ~1.93 Å for crystals containing 0.1 M Ca^{2+}. The Ca^{2+}-free crystal exhibited the hexagonal symmetry with space group $P6_322$ and unit cell parameters of a = b = 91.06 Å, c = 122.86 Å, α = β = 90°, γ = 120° and contained one molecule per asymmetric unit (ASU). Similarly, the crystal grown in 0.1 M $CaCl_2$ exhibited the same space group with slight different unit cell parameters of a = b = 91.49 Å, c = 122.14 Å, α = β = 90°, γ = 120° and thus also contained one molecule per asymmetric unit (ASU).

Data were processed and scaled in the HKL2000 suite using the programs DENZO and SCALEPACK (Otwinowski and Minor, 1997). Briefly, the program XDISPLAYF in the HKL2000 suite was used to display the diffraction pattern and identify reflections in the first frame. Once a reasonable number of reflections were found, the program DENZO can be used for autoindexing the diffraction pattern, and subsequently determining the unit cell parameters in the lowest symmetry Bravais lattice primitive triclinic lattice with space group P1 and the goodness of fit of these primitive triclinic unit cell parameters to the geometry and the symmetry constraints of all fourteen possible Bravais lattice, evaluated by the metric tensor distortion index. The appropriate Bravais lattice was chosen based on the criterion of the highest symmetry lattice with the lowest value of the distortion index (generally anything less than 2% is a good candidate), which, in our case, was primitive hexagonal lattice that contains actually five point groups: 3, 312, 321, 6, 622 with each containing its own set of enantiomer space groups. At this stage, the lowest symmetry space group P3 for the selected Bravais lattice was used. The correct space group was specified during the later scaling process with SCALEPACK. Initial refinement of the unit cell parameters, the rotation matrix of the crystal and the position of the direct beam by DENZO were performed to evaluate the

autoindexing and choice of the Bravais lattice as well as to improve the fit between the observed reflection positions and the predicted ones, followed by a more extensive refinement of all the crystal and detector parameters including the rotation matrix of the detector, the crystal-detector distance, crossfire position and mosaicity besides the basic parameters in the initial refinement.

The next step is integration of the entire dataset, which was done in a per-frame basis with preset spot size to integrate the diffraction spots according to their miller indices in the reciprocal space. Profile fitting, which involves the application of the spot profile leant from the strong spots to all spots local to it, performed by DENZO helps to identify spots with weak intensities and improve the integration accuracy. During integration, XDISPLAYF displayed the predicted reflection positions as empty circles, which should correspond to the observed reflection positions. The agreement between the predicted and observed reflection spots were also quantitatively evaluated by the position chi-squared parameters, chi-squared X and chi-squared Y while the partiality chi-squared reflected how good the estimation of the mosaicity is. Position chi-squared value at or close to 1 indicate good agreement between the predicted and observed spots and partiality chi-squared value at or close to 1 indicate good estimation of the mosaicity. During integration, each frame possesses slightly different values for the fitted crystal and detector parameters because DENZO only performed refinement during integration on a per-frame basis so that the fitted parameters are local optimal rather than global optimal values, but large variations of the parameters might indicate problems.

The integrated dataset on a per-frame basis was merged by the scaling with the global refinement of a number of parameters using the program SCALEPACK. The scaling process is based on the assumption that the intensities of symmetry related reflections, including the Friedel pairs (in the absence of anomalous scattering), are expected to be identical within errors. SCALEPACK merged all the symmetry-related reflections into sets of so called unique reflections. During scaling, the beam intensity variation and radiation damage are properly modeled by the per-frame scale factor and the per-frame B factor, respectively, which provided a lot of information about the data collection performance. Problematic reflections such as overloaded reflections, significantly non-match symmetry-related reflections, and reflections different excessively from the estimated mean value, *etc*. are usually written as rejections and excluded during the scaling process. Post-refinement was performed by SCALEPACK to optimize the unit cell parameters, the crystal orientation, and the mosaicity, *etc*., usually assuming small slippage of the crystal and an imperfect goniostat. Post-refined unit cell parameters by SCALEPACK are usually better than the locally refined ones by DENZO. The expected errors were modified to match the measured errors by adjusting the multiplicative error scale factor and a resolution shell specific error model so that the scaling chi-squared value for the data close to unity. Besides the chi-squared values, the traditional statistic parameter monitoring the data quality R_{sym} was computed during scaling, which reflects the percentage deviation of independently measured observations of each unique reflection from being equal to each other. R_{sym} is defined as:

$$R_{sym}(I) = \frac{\sum_{hkl}\sum_{i}\left|I_i(h,k,l) - \langle I(h,k,l)\rangle\right|}{\sum_{hkl}\sum_{i} I_i(h,k,l)}$$

where $I_i(h, k, l)$ is the intensity of the i-th measurement of the reflection (h, k, l), and <I(h, k, l)> is the average of all measurements for the reflection (h, k, l). Reflections measured only once were excluded from the R_{sym} calculation. Moreover, SCALEPACK provides a wealth of useful information such as I/σ (intensity/error), data completeness, and data redundancy, *etc*. in both overall and resolution shell specific fashion. The resolution limit of the crystal diffraction was determined at the resolution shell with I/σ greater than 2.

The point group symmetry was determined during the scaling by comparing the scaling statistics R_{sym} values and rejection percentage of scaling in different point groups. In our case, the primitive hexagonal lattice contain five possible point group with ascending symmetry 3<321=312=6<622. Basically, we tried all five possible point groups and chose the one with the highest symmetry and reasonable scaling statistics, which turned out to be P622 for the rat synaptotagmin 4 C2B domain crystals. In our case, R_{sym} actually increased when the data scaled in P622 point group compared to those scaled in P3 group, presumably because R_{sym} is dependent on the redundancy of the dataset and the data redundancy is four times higher in P622 point group than in P3 point group, therefore not necessarily indicate the decrease of data quality. After we knew it belongs to the P622 point group, there were still five possible enantiomers, which were distinguished through the observation of the systematic absences inherent for different enantiomers. For the C2B domain crytals, the systematic absences were 00*l* for odd *l*, indicating the exitense of a 6_3 screw axis and thus the space group of $P6_322$, which was confirmed during later moelcular replacement and refinement. Luckily, no ambiguity existed for $P6_322$ whereas the space group pairs $P6_122$ and

$P6_522$, $P6_222$ and P_422 were indistinguishable at this stage and could only be specificed during later phasing and refinement stages.

Scaled intensities from the diffraction data were converted to structure factor amplitudes and placed on an approximate absolute scale (which means the structure factor amplitudes are expressed in electrons) by the program TRUNCATE from the CCP4 (Collaborative Computational Project Number 4) package (French and Wilson, 1978; Bailey, 1994). The negative intensities resulting from the background correction of reflections were converted to small, positive structure factor amplitudes. The Wilson B values calculated for the observed data using the Wilson plot were as 56.32 $Å^2$ and 34.80 $Å^2$ for Ca^{2+}-free crystals and crystals containing 0.1 M Ca^{2+}, respectively.

2.2.9 Molecular Replacement

The three dimensional electron density in the real space is related to the diffraction pattern that includes both structure factor amplitude and phase information in the reciprocal space by the Fourier transformation since the diffraction arises from the scattering of X-ray by the electrons. However, diffraction data only provide the measurement of the intensity of the reflections from which the structure factor amplitude can be derived but not the phase information, therefore are not sufficient by themselves to mathematically reconstruct the three dimensional atomic structures. This is usually referred to as the phase problem in the crystallography. There are generally several ways to solve the phase problem and determine the structures such as molecular replacement, single/multiple isomorphous replacement (SIR/MIR), single/multiple wavelength anomalous dispersion (SAD/MAD) or their

combination. Since several C2 domain structures have been deposited in the PDB database, molecular replacement was used to solve the structure of rat synaptotagmin 4 C2B domain. There are generally two types of molecular replacement method, Patterson function-based and maximum likelihood-based. The Patterson function-based molecular replacement method was implemented in CNS (Crystallography and NMR System), AmoRe, Molrep, *etc*. and the maximum likelihood-based method was implemented in Phaser and BEAST.

The structure of rat synaptotagmin 4 C2B domain was solved via molecular replacement using AmoRe (Navaza, 1994). Initial model coordinates were obtained by modifying the coordinates of the rat synaptotagmin 1 C2B domain (PDB entry 1K5W) using the SEAMAN program from Uppsala Software Factory (USF) package (Fernandez et al., 2001). The model modification procedures are briefly listed as follows: 1) All the identical residues are preserved. 2) All the residues in synaptotagmin 1 C2B domain aligned with glycines in synaptotagmin 4 C2B domain are mutated to glycines. 3) All the non-glycine residues in synaptotagmin 1 C2B domain aligned with alanines in synaptotagmin 4 C2B domain are mutated to alanines whereas glycines are perversed even if they are aligned with alanines. 4) All the other non-identical residues in synaptotagmin 1 C2B domain aligned with residues larger than alanines in synaptotagmin 4 C2B domain are mutated to serines except where the minimalist substitution described in 5) can be applied whereas glycines and alanines are perversed even if they are aligned with residues larger than alanines. 5) All non-identical residues in synaptotagmin 1 C2B domain aligned with residues in accordance with the minimalist substitutions in synaptotagmin 4 C2B domain are mutated to those of synaptotagmin 4. The minimalist substitutions include tryptophans to phenylalanines,

tyrosines to histidines, glutamates to glutamines or vice versa, aspartates to asparagines or vice versa, arginines to lysines, isoleucines to valines or threonines, and threonines to valines or vice versa. 6) All the solvent molecules and non-protein atoms are removed from the pdb file.

Before the molecular replacement, we first estimated how many molecules to be expected in each asymmetric unit through the analysis of the Matthew's coefficient (Matthews, 1968). Matthew's coefficient (V_M) is the ratio of the volume of the unit cell and the molecular weight of all the protein molecules in the unit cell. It can be calculated as:

$$V_M = \frac{V_{unit\ cell}}{Z \times MW \times n}$$

where $V_{unit\ cell}$ is the volume of the crystal unit cell, Z is the number of asymmetric units (ASU) per unit cell, MW is the molecular weight of the macromolecule, and n is the number of molecules per asymmetric unit (ASU). Since the specific volume of protein molecules is always close to 0.74 cm^3/g, the solvent content can be calculate as $1-1.23/V_m$. Usually for protein crystals, the Matthews coefficient distributes from 1.7 to 3.5 $Å^3/Da$ with the highest probability around 2.15 $Å^3/Da$, which correspond to the solvent distribution from 28% to 65% with the highest probability around 43%. In our case, the unit cell volume and molecular weight are 888140 $Å^3$ and 16577 Da, respectively and therefore the calculated Matthews coefficient is 4.5/Z (Z is the number of synaptotagmin 4 C2B domains per asymmetric unit). The Matthews coefficients and the solvent contents corresponding to one, two or three molecules per asymmetric unit (ASU) are listed in table 2.1. The calculation suggested that the most probable situation was the existence of two rat synaptotagmin 4 C2B domains per asymmetric unit with 44.5% solvent content.

Molecular replace methods essentially try to place the search model within the unit cell of the target crystal in the similar orientation and position to that of the molecules with unknown structure, or the target molecules, through rotations and translations in the real space so that the calculated diffraction pattern from the search model will closely match the experimental diffraction pattern. In order to achieve this, six parameters with three rotational angles and three translational displacements need to be determined. However, direct search in the six dimensional parameter space will be too demanding computationally so that such a six-parameter search is usually broken down to two three-dimensional searches, firstly the three rotational angles for the correct orientation and then the three translational displacements for the position of the correctly-oriented molecules within the unit cell.

The program AmoRe performed the molecular replacement using Patterson function-based method. The Patterson function is defined as:

$$P(u,v,w) = \frac{1}{V}\sum_{hkl}\left|F(h,k,l)\right|^2 \cos[2\pi(hu+kv+lw)]$$

The Patterson function is essentially the Fourier transform of the reflection intensities that are equal to the squared structural factor amplitude. Therefore, the Patterson function of the target molecules with structure unknown, often referred to as the observed Patterson map, is only dependent on the structural factor amplitude but not at all on the phase information and can be easily calculated solely based on the measured reflection intensities. On the other hand, the Patterson function of the molecular replacement model, often referred to as the model Patterson map, can be calculated as the autocorrelation function of the electron density distribution, which essentially represent the interatomic distance vectors weighted by the

Table 2.1 Crystal cell content analysis

Nmol/ASU	Matthews coefficient	% solvent content
1	4.5	72.2
2	2.2	44.5
3	1.5	16.7

number of electrons in the atoms. The Patterson map contains two types of Patterson vectors, namely the self-Patterson vectors, or the intra-molecular vectors and the cross-Patterson vectors, or the inter-molecular vectors. The set of self-Patterson vectors contains the interatomic vectors formed within the molecule and therefore is dependent only on the orientation and independent of the position of the molecule whereas the set of cross-Patterson vectors contains the interatomic vectors formed from one molecule to another and is dependent on both the orientation and position of the molecule in the unit cell. The rotational angles can be determined by rotating the observed self-Patterson map with respect to the model self-Patterson map and finding the angles resulting in the best match between them, which is mathematically implemented in the rotation function introduced by Rossmann and Blow. The match between the observed and model self-Patterson map will give rise to a maximum value of the rotation function. As the rotation function calculation has to be based solely on the intra-molecular vectors and not on the inter-molecular ones, the choice of the integration radius is critical. Usually, in the case of a globular molecule, an integration radius corresponding to about 75% of the minimum diameter is used. After the correct orientation is determined, the translational displacement can be determined by maximizing the translation function, which reflects the correlation between the observed cross-Patterson map and the cross-Patterson vectors from the search model to its crystallographic symmetry-related molecules in the unit cell. Since the translation function involves the inter-molecular Patterson vectors arising from symmetry-related molecules, it is very sensitive to the correct assignment of the space group so that a comparison of translation function search performed on data scaled to different space group can help to determine or confirm the choice of correct

space group. After rotation and translation search, AmoRe also performed a rigid body refinement on the initial model from molecular replacement solution. For synaptotagmin 4 C2B domain, the rotation and translation function search was conducted with data between a dmin of 8.0 and 5.0 Å, and a single solution was obtained with a final correlation coefficient of 0.49. No further molecules can be found through molecular replacement or identified in the later refinements, indicating that only one rat synaptotagmin 4 C2B domain exists in one asymmetric unit and a corresponding solvent content of 72 percent, which is at the high-end tail of solvent content distribution observed in the PDB database.

2.2.10 Structure Refinement and Model Building

Refinement of the models was carried out using CNS (Brunger et al., 1998) as well as REFMAC (Murshudov et al., 1997) of the CCP4 package (Bailey, 1994) with a random subset of all data set aside for the cross-validation and the calculation of R_{free} factors. Interactive model building was carried out with O (Jones et al., 1991). After an initial rigid body refinement that optimizes the position of synaptotagmin 4 C2B domain in the asymmetric unit, the model was subjected to the simulated annealing, which applies torsion angle molecular dynamics to improve the model, especially to help remove the model bias common to molecular replacement solutions. Relatively large error that are not easily corrected by the conjugate gradient minimization refinement can be fixed by simulated annealing since it allows much larger changes in the atomic coordinates at the high temperatures during molecular dynamics and therefore the achievement of the global minima during the cooling stage instead of sticking to the local minima. The simulated annealing was

used in the initial several rounds of refinement for synaptotagmin 4 C2B domain and was omitted during later stages of refinement. The conjugate gradient minimization refinement and restrained, individual B-factor refinement were performed to refine the atomic coordinates and the atomic displacement parameters (also referred to as temperature factors or B factors) in the model, respectively. The progress of refinement was monitored by the crystallographic R factors and R_{free} factors, which reflect the agreement between the data and model by calculating the crystallographic residual between the observed structure factor amplitude and those calculated from the atomic model. R factor is defined as:

$$R = \frac{\sum_{hkl} \left| |F_{obs}| - K|F_{calc}| \right|}{\sum_{hkl} |F_{obs}|}$$

where F_{obs} and F_{calc} are the observed and calculated structure factors, respectively. R_{free} was introduced into crystallographic refinement as the method of statistical cross-validation to overcome the problem that lower R factors don't necessarily correspond to better models. The diffraction data were randomly divided into two sets: a working set which usually comprise 90% to 95% of the diffraction data and a complementary test set containing the remaining 10%-5% data. During the model building and refinement, only the diffraction data in the working set were used whereas those in the test set were not. The R factor calculated with the randomly assigned test set was referred to as the R_{free} factor, which essentially measures the degree to which the model predicts the diffraction data for the test set which was excluded from the model building and refinement process and has been shown to be correlated quite well with the quality of the atomic models.

The resulting model was used to calculate σA-weighted electron density maps. Two electron density maps were routinely calculated: 2Fo-Fc electron density map that displayed the current best estimate of the electron density for the target structure and Fo-Fc electron density map that is also referred to as the difference map with positive density indicating missing atoms to add and negative density indicating the misplaced atoms to remove. Both maps were visualized in the program O to guide the interactive model building of rat synaptotagmin 4 C2B domain. The rebuilt model was subjected to another round of conjugate gradient minimization refinement and restrained, individual B-factor refinement for refinement. In the crystal structure of rat synaptotagmin 4 C2B domain, several alternate conformations of side chains were observed in the electron density map such as threonine 305, isoleucine 408, glutamine 415, and isoleucine 416, and therefore were built into the model using CNS. The occupancy of the alternate conformation was refined by the grouped, unrestrained occupancy refinement routine in CNS. One trick in the occupancy refinement in CNS was the generated occupancies for the two alternate conformations were usually added up with a summation of more than unity and required normalization. After several rounds of refinement and model building of the protein part to almost completion, solvent molecules were added by either water_pick/water_delete routines in CNS or Arp/Warp where stereochemically reasonable and the added solvent molecules were inspected in the program O for their appropriate density and hydrogen bonding geometry and accordingly retained in or removed from the model. The ions were identified due to their high electron density as well as their coordination stereochemistry. A new type of TLS refinement implemented in the REFMAC was also performed to further improve the model. In contrast to isotropic

atomic displacement parameter refinement carried out in the earlier refinement stage, the TLS performed a rough anisotropic atomic displacement parameter refinement with limited numbers of parameters, therefore taking into account the anisotropic motion of the atoms in the model. The TLS (translation/libration/skew) parameters essentially described the anisotropic motion as the mean square displacement of rigid bodies, which are user-defined group of atoms in the target molecule. The rat synaptotagmin 4 C2B domain was divided into 3 TLS groups (residues 273-300, residues 308-331, and residues 336-409) according to the sequence connectivity and subjected to the TLS refinement. During the structure refinement and model building, structure validations were carried out by the program PROCHECK as well as the crystallographic model statistics routine in CNS in each cycle to examine the average deviation of model from ideal geometry derived from the statistics of high resolution structure deposited in the PDB database. Structure validation checked many parameters, such as the Ramachandran plot, Luzzati coordinate error plot, main-chain bond length and bond angle distributions, aromatic ring planarity, dihedral angle analysis, Cα chirality analysis, *etc*. The refined and validated atomic coordinates of the crystal structures of the rat synaptotagmin 4 C2B domain in the presence and absence 100 mM Ca^{2+} have been deposited in the the PDB database, with accession codes 1W15 and 1W16, respectively.

2.2.11 Backbone Resonance Assignment of Rat Synaptotagmin 4 C2B Domain

We performed the backbone resonance assignment of rat synaptotagmin 4 C2B domain using 3D HNCACB and CBCA(CO)NH triple-resonance experiments acquired on a uniform ^{15}N, ^{13}C-labeled sample. HNCACB and CBCA(CO)NH experiments are two

complementary experiments to assign the backbone resonances of a protein. The CBCA(CO)NH experiment provides interresidue connection by correlating the amide resonance of one residue with the Cα and Cβ carbons of the previous residue. The HNCACB correlates the amide resonance of one residue with both its own Cα and Cβ carbon atoms and those of the previous residue and generate both inter- and intraresidue connection. A combination of both experiments was used to obtain backbone resonance assignments and find the corresponding residue for each crosspeak in the ^{1}H-^{15}N HSQC spectra. Sequential HN/HN nuclear Overhauser effect (NOE) connectivities from ^{1}H-^{15}N NOESY-HSQC spectrum were used to confirm the assignments and resolve ambiguities. Residue type information from ^{1}H-^{15}N TOCSY-HSQC spectrum was also used to confirm the assignments and resolve ambiguities.

2.3 Results

2.3.1 Intrinsic Ca^{2+} Binding to Rat and *Drosophila* Synaptotagmin 4

To analyze the intrinsic Ca^{2+}-binding properties of the rat and *Drosophila* synaptotagmin 4 C2 domains, we used ^{1}H-^{15}N heteronuclear single quantum correlation (HSQC) spectra. ^{1}H-^{15}N HSQC spectra contain one crosspeak for the amide group of each non-proline residue in a ^{15}N labeled protein. The positions of the crosspeaks are very sensitive to the chemical environment. Therefore, perturbations in these crosspeaks (shifts or broadening) report on interactions with ligands or other proteins. If the interaction of protein and ligand has a fast exchange rate ($k\text{-}1 >> |\delta PL - \delta P|$, usually for $k\text{-}1 > 1000$Hz and $Kd > 10\mu M$),

it will be possible to follow the peaks of the residues in the binding site during the titration experiment as they are moving from the free to the bound state in the ^{1}H-^{15}N HSQC spectra. This is true in the case of Ca^{2+} binding of synaptotagmin C2 domains, which bind Ca^{2+} ion weakly and thus have a fast chemical exchange on the NMR time scale between the Ca^{2+}-free and Ca^{2+} bound forms. The positions of the ^{1}H-^{15}N HSQC crosspeaks corresponding to amide groups whose microenvironments are changed by Ca^{2+} binding reflect the average Ca^{2+} occupancy. As a result, Ca^{2+} titrations cause progressive movements of the crosspeaks from their Ca^{2+}-free to their Ca^{2+}-saturated positions. The crosspeak movements follow a straight line if there is only one Ca^{2+} binding site or multiple Ca^{2+} binding sites with identical affinities, while curved crosspeak movements demonstrate the presence of multiple binding sites with different affinities. Each component of the curve can then be associated with an individual site. The locations of the different Ca^{2+} binding sites can be approximately deduced from the structure of the protein and the observed chemical shift changes, and can be ascertained by the effects that mutations in putative ligands have on the specific components observed in the Ca^{2+} titrations. The Ca^{2+} affinity can be derived by curve fitting of the following function:

$$y = d0 + \frac{(df - d0) \times \left[(p + x + k) - \sqrt{(p + x + k)^2 - 4 \times p \times x} \right]}{2 \times p}$$

where p is the protein concentration, d0 is the chemical shift in the absence of Ca^{2+}, df is the chemical shift upon saturation with Ca^{2+}, k is the dissociation constant, x is the Ca^{2+} concentration, and y is the observed chemical shift during the Ca^{2+} titration. Amide chemical shift changes can be calculated as a weighted plot $\Delta\delta = [(\Delta\delta HN)^2 + (0.17 \times \Delta\delta N)^2]^{1/2}$, where

$\Delta\delta HN$ and $\Delta\delta N$ are the ^{1}H and ^{15}N amide chemical shift changes, respectively. The weighting factors are selected in such a way that differential chemical shift changes contributed by amide nitrogens and protons are normalized, based on the observation that the amide nitrogens and protons have typical chemical shift ranges of about 20 ppm and 3.5 ppm, respectively.

Ca^{2+} induced shifts in only a few crosspeaks of the ^{1}H-^{15}N HSQC spectrum of the rat synaptotagmin 4 C2A domain upon a series of titrations up to 80 mM, but Ca^{2+} titration of these shifts indicated a Kd of ~10 mM (Figure 2.3A). This result showed that the rat synaptotagmin 4 C2A domain retains residual Ca^{2+} binding, albeit with very low affinity. Similar results were obtained for the *Drosophila* synaptotagmin 4 C2A domain (Figure 2.3C). Notably, comparison of the ^{1}H-^{15}N HSQC spectra of the rat synaptotagmin 4 C2B domain in 0 and 20 mM Ca^{2+} revealed minimal changes (Figure 2.3B), indicating that this domain cannot bind Ca^{2+}. To test whether this result arises from the two aspartate to glutamate substitutions (glutamate 380 and glutamate 386) in the predicted Ca^{2+} ligands (Figure 2.1B), we analyzed rat synaptotagmin 4 C2B domain mutants in which both glutamates or one glutamate at a time were replaced by aspartates, but these mutants were also unable to bind Ca^{2+}. On the other hand, Ca^{2+} caused shifts in multiple crosspeaks of the ^{1}H-^{15}N HSQC spectrum of the *Drosophila* synaptotagmin 4 C2B domain (Figure 2.3D). Although a Ca^{2+} titration indicated a low Ca^{2+} affinity (Kd ~2 mM), the multiple crosspeak shifts observed for the *Drosophila* synaptotagmin 4 C2B domain are characteristic of Ca^{2+}-binding C2 domains (Fernandez et al., 2001; Shao et al., 1996) and are in sharp contrast with the behavior of the rat counterpart. This result suggested that critical differences exist in the

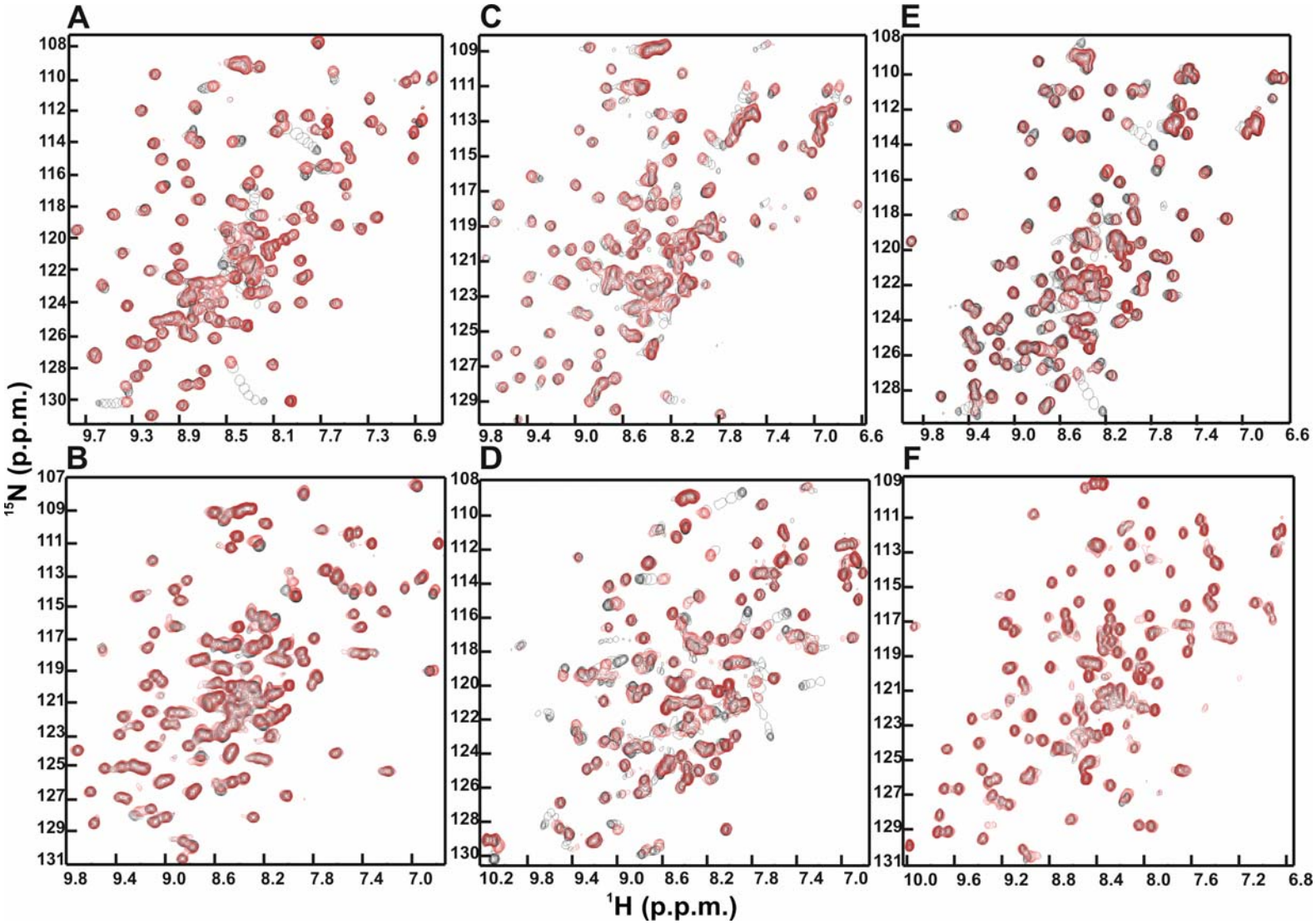
A
B
C
D
E
F
15N (p.p.m.)
1H (p.p.m.)

Figure 2.3 Intrinsic Ca^{2+}-binding properties of the synaptotagmin 4 and 11 C2 domains.

(A) ^{1}H-^{15}N HSQC spectra obtained at different Ca^{2+} concentrations for the rat synaptotagmin 4 C2A domain. The protein concentrations were 120 μM and the total Ca^{2+} concentrations used were: 0, 0.2, 1, 5, 10, 20, 40, 80 mM. The ^{1}H-^{15}N HSQC spectra acquired in the absence of Ca^{2+} and the highest Ca^{2+} concentrations are shown with multiple red contours and multiple black contours, respectively, whereas spectra obtained at intermediate Ca^{2+} concentrations are shown with single black contours.

(B) An analogous Ca^{2+} titration by ^{1}H-^{15}N HSQC spectra was done for the rat synaptotagmin 4 C2B domain. The protein concentrations were 120 μM and the total Ca^{2+} concentrations used were: 0, 20 mM.

(C) An analogous Ca^{2+} titration by ^{1}H-^{15}N HSQC spectra was done for the *Drosophila* synaptotagmin 4 C2B domain. The protein concentrations were 120 μM and the total Ca^{2+} concentrations used were: 0, 5, 10, 20, 40, 80 mM.

(D) An analogous Ca^{2+} titration by ^{1}H-^{15}N HSQC spectra was done for the *Drosophila* synaptotagmin 4 C2B domain. The protein concentrations were 120 μM and the total Ca^{2+} concentrations used were: 0, 0.2, 1, 3, 10, 20, 40 mM.

(E) An analogous Ca^{2+} titration by ^{1}H-^{15}N HSQC spectra was done for the rat synaptotagmin 11 C2B domain. The protein concentrations were 120 μM and the total Ca^{2+} concentrations used were: 0, 0.2, 1, 3, 5, 10, 20, 40, 80 mM.

(F) An analogous Ca^{2+} titration by ^{1}H-^{15}N HSQC spectra was done for the rat synaptotagmin 11 C2B domain. The protein concentrations were 120 μM and the total Ca^{2+} concentrations used were: 0, 20 mM.

functions of synaptotagmin 4 from rat and *Drosophila*. Because synaptotagmin 11 is closely related to synaptotagmin 4 and could be the actual rat orthologue of *Drosophila* synaptotagmin 4, we also analyzed the intrinsic Ca^{2+}-binding properties of the rat synaptotagmin 11 C2 domains (Figure 2.3E; Figure 2.3F), but we obtained similar results to those observed for the rat synaptotagmin 4 C2 domains.

2.3.2 Phospholipid Binding by Cosedimentation Assay

We next studied whether the C2 domains of rat synaptotagmin 4 and 11 and those of *Drosophila* synaptotagmin 4 are capable of forming Ca^{2+}-dependent complexes with negatively charged phospholipid. For this purpose, we used a cosedimentaiton assay and also tested the C2 domains of rat synaptotagmin 1 as positive controls. The cosedimentaiton assay was done by Dr. Ok-Ho Shin from Dr. Thomas C Südhof's laboratory. The schematic diagram of the cosedimentation assay is shown in Figure 2.4A. Extensively purified recombinant C2 domains were incubated with purified sucrose loaded heavy liposomes in the presence or absence of Ca^{2+} and centrifuged at high speeds. The C2 domains associating with the negatively charged phospholipids will be pelleted to the bottom, which can be analyzed by SDS-PAGE and thus the appearance of the C2 domain in the pellet fraction indicates its capability of phospholipid binding. We found that the rat synaptotagmins 4 and 11 C2A and C2B domains, and fragments containing both of their C2 domains (the C2AB fragment), were unable to bind to vesicles composed of phosphatidylserine (PS) and phosphatidylcholine (PC) in a Ca^{2+}-dependent manner (Figure 2.4B). These observations reinforced the conclusion drawn from the ^{1}H-^{15}N HSQC Ca^{2+} titration data that the rat

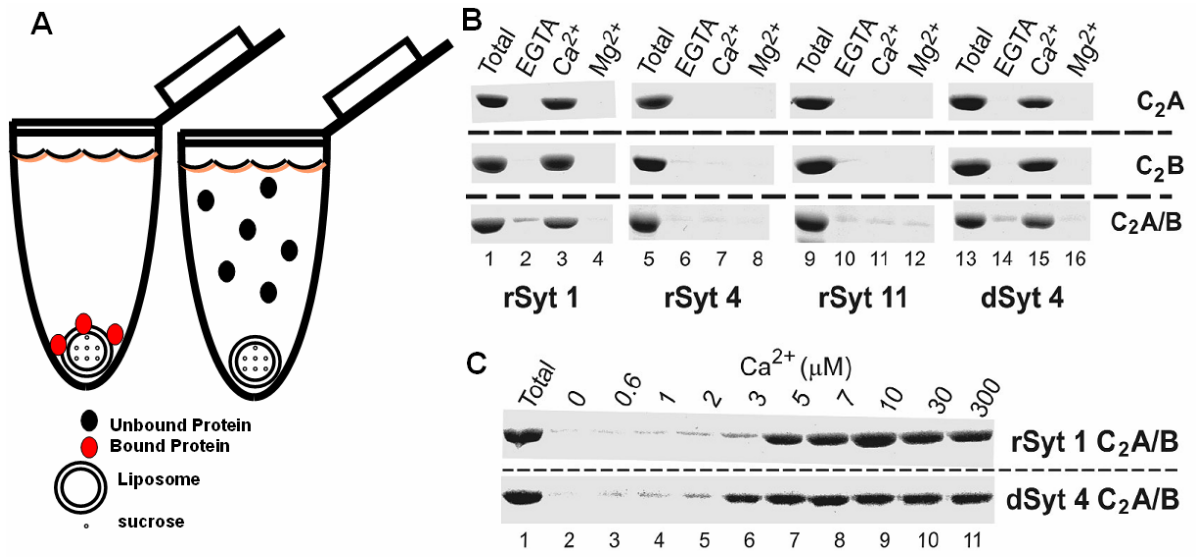

Figure 2.4 Ca^{2+}-dependent phospholipid binding properties of the synaptotagmins 4 and 11 C2 domains analyzed by the cosedimentation assay.

(A) Schematic diagram of the cosedimentation assay.

(B) Phospholipid binding to GST-fusion proteins of the C2 domains and the C2AB fragment from rat synaptotagmins 1, 4 and 11 (rSyt 1, rSyt 4 and rSyt 11, respectively) and *Drosophila* synaptotagmin 4 (dSyt 4) in the presence of 4 mM EGTA, 1 mM Ca^{2+} or 10 mM Mg^{2+} was analyzed by a cosedimentation assay with liposomes containing 25% (w/w) PS and 75% (w/w) PC. Proteins that cosedimented with the liposomes were analyzed by SDS-PAGE and Coomassie blue staining. The cosedimentaiton assay was done by Dr. Ok-Ho Shin from Dr. Thomas C Südhof's laboratory.

(C) Analogous phospholipid binding assays were done with GST fusions of the rat synaptotagmin 1 and *Drosophila* synaptotagmin 4 C2AB fragments in different Ca^{2+} concentrations. The cosedimentaiton assay was done by Dr. Ok-Ho Shin from Dr. Thomas C Südhof's laboratory.

synaptotagmin 4 and 11 C2B domains cannot bind Ca^{2+}. Notably, the *Drosophila* synaptotagmin 4 C2A and C2B domains both bound to PS-PC vesicles as a function of Ca^{2+} (Figure 2.4B). Ca^{2+} titrations showed that a *Drosophila* synaptotagmin 4 C2AB fragment in fact binds Ca^{2+}-phospholipids with a somewhat higher apparent Ca^{2+} affinity than the rat synaptotagmin 1 C2AB fragment (Figure 2.4C).

2.3.3 Phospholipid Binding by Fluorescence Resonance Energy Transfer (FRET) Assay

FRET is a technique in which non-radiative energy transfer between a donor and an acceptor fluorophore is measured. The efficiency of the transfer correlates inversely with the sixth power of the distance between the donor and acceptor so that FRET is highly sensitive to distance (Fung and Stryer, 1978). Endogenous tryptophans in proteins are natural fluorophores, absorbing light at 278 nm and emitting at 310-350 nm, depending on their environments, with more hydrophobic environment inducing further blue shift in the emission maxima. On the other hand, 5-(dimethylamino)naphthalene-1-sulfonyl (Dansyl) fluorescent dyes absorb light at 336 nm and emit at 513 nm. Significant overlap exists between tryptophan emission spectra and Dansyl excitation spectra and therefore, tryptophans and Dansyl fluorophores form a FRET pair with a Förster distance R_0 (the distance at which the FRET efficiency of the donor and acceptor pair is 50%) of 21-24 Å. By incorporating a Dansyl-labeled lipid probe (Dansyl-DOPE) in the bilayer, we can detect the membrane association of the selected C2 domains by monitoring the FRET between the tryptophans in the C2 domains and the Dansyl groups in the membrane. If the C2 domains bind to phospholipid, the Dansyl fluorophore will be able to accept non-radiant energy

transfer from the tryptophans and tyrosines of bound C2 domains, which can be measured as a decrease of the protein fluorescence emission and a concomitant increase of the Dansyl fluorescence emission. We could not use the FRET assay for the synaptotagmin 4 C2A domains because they do not contain any tryptophan in their sequences, but application of this assay to the C2B domains confirmed that the *Drosophila* synaptotagmin 4 C2B domain binds phospholipid in a Ca^{2+}-dependent manner whereas the rat synaptotagmin 4 C2B domain does not (Figure 2.5).

Our results were in contrast to those of previous studies using GST pulldown assays, which suggested that the *Drosophila* synaptotagmin 4 C2A domain and C2AB fragment do not bind phospholipid in a Ca^{2+}-dependent manner (Littleton et al., 1999). However, previous studies from our lab have shown that these assays can yield false negative results, probably because of the difficulty in removing bacterial contaminants from GST fusion proteins isolated with GST affinity resins and/or the solid-phase nature of these assays (Fernandez et al., 2001). Thus, weak or no Ca^{2+}-dependent phospholipid binding to the synaptotagmin 1 C2B domain was observed using GST pulldowns, whereas robust Ca^{2+}-dependent phospholipid-binding properties that resembled those of the synaptotagmin 1 C2A domain were observed for extensively purified synaptotagmin 1 C2B domain in solution using the fluorescence resonance energy transfer (FRET) assay and the cosedimentation assay used here to study synaptotagmins 4 and 11 (Fernandez et al., 2001). In our experience, the latter two assays yield more consistent and reliable results than GST pulldowns and, therefore, the discrepancies of our results with the previous studies of *Drosophila* synaptotagmin 4 (Littleton et al., 1999) most likely arise from the different assays used.

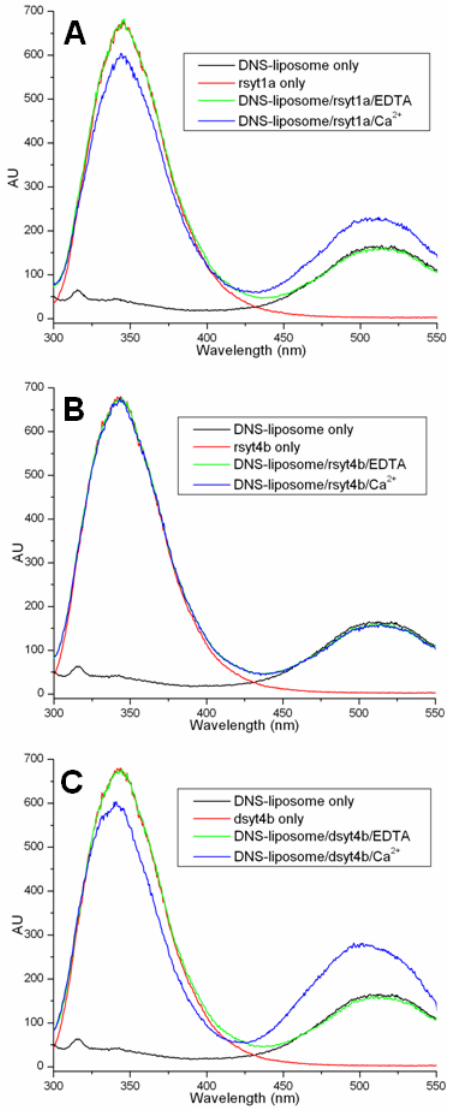

Figure 2.5 Ca^{2+}-dependent phospholipid binding properties of the synaptotagmin 4 and 11 C2 domains analyzed by the FRET assay.

(A) Phospholipid binding of rat synaptotagmin 1 C2A domain using the FRET assay. The emission spectra of Dansyl liposome or C2 domain alone are shown in black and red, respectively. The emission spectra of C2 domain together with Dansyl liposome in the presence of 1 mM EDTA or 1 mM Ca^{2+} are shown in green and blue, respectively.

(B) Analogous phospholipid binding assays were done with rat synaptotagmin 4 C2B domain.

(C) Analogous phospholipid binding assays were done with *Drosophila* synaptotagmin 4 C2B domain.

2.3.4 Structure of the Rat Synaptotagmin 4 C2B Domain

Our data revealed two unexpected observations, the ability of the *Drosophila* synaptotagmin 4 C2A domain to bind phospholipids in a Ca^{2+}-dependent manner (Figure 2.4B), and the inability of the rat synaptotagmin 4 C2B domain to bind Ca^{2+} and phospholipids (Figure 2.3B and Figure 2.4B). The Ca^{2+}-dependent phospholipid binding exhibited by the *Drosophila* synaptotagmin 4 C2A domain, despite the conserved aspartate to serine substitution in one of the Ca^{2+} ligands and its poor intrinsic Ca^{2+}-binding properties (Figure 2.3C), may arise from the distinctive properties associated with a 14-residue insertion in loop 1 that is not generally observed in C2 domains (Figure 2.1B). However, there is no apparent reason, based on the sequence alignments of rat and *Drosophila* synaptotagmins 1, 4 and 11, for the lack of Ca^{2+} binding to the rat synaptotagmin 4 C2B domain, considering its sequence similarity with the rat synaptotagmin 1 C2B domain and the *Drosophila* synaptotagmin 4 C2B domain (38% and 56% sequence identity, respectively), and the fact that it contains all the residues that form three Ca^{2+}-binding sites in the rat synaptotagmin 1 C2A domain (Figure 2.1B).

To investigate the structural basis for this unexpected behavior, we turned to X-ray crystallography. Crystals of the rat synaptotagmin 4 C2B domain were grown in the absence of Ca^{2+} and in the presence of 100 mM Ca^{2+}, and the corresponding structures were solved at resolutions of 2.3 and 1.93 Å, respectively (data collection and processing statistics are summarized in Table 2.2). The high Ca^{2+} concentration was used to try to detect even very weak Ca^{2+} binding to the C2 domain. One Ca^{2+} ion was found to bind to the canonical Ca1

site formed by the top loops in the crystal grown in the presence of 100 mM $CaCl_2$. The rat synaptotagmin 4 C2B domain is comprised of eight β-strands and one α-helix in a β-sandwich fold: two four-stranded antiparallel β-sheets (β1 (residues 290-298), β2 (residues 303-312), β5 (residues 353-361) and β8 (residues 415-421) forming one sheet, and β3 (residues 325-333), β4 (residues 336-342), β6 (residues 386-394), and β7 (residues 415-421) forming the other) with loops emerging at the top and the bottom. The α-helix (residues 399-411) is inserted between strands 7 and 8, which is characteristic of the C2B domain of synaptotagmins. Both structures were practically identical (0.18 Å rms deviation for 123 equivalent Cα carbons; Figure 2.6B) except for the presence of one bound Ca^{2+} ion in the latter and the observation of electron density for loop 2, which shows only spurious density in the absence of Ca^{2+}. No electron density for loop 1 was observed in either structure, indicating its flexibility. Figure 2.6A shows a ribbon diagram of the rat synaptotagmin 4 C2B domain structure obtained in the presence of 100 mM Ca^{2+}. The structure clearly resembles those of Ca^{2+}-binding C2 domains, and analysis with DALI (Holm and Sander, 1993) showed that it shares closest similarity with the NMR structures of the Ca^{2+}-bound forms of the rat synaptotagmin 1 C2B domain (Fernandez et al., 2001) (1.3 Å rms deviation for 126 equivalent Cα carbons; Figure 2.8A) and C2A domain (Shao et al., 1998) (1.6 Å rms deviation for 111 equivalent Cα carbons). These rms deviations are comparable to those observed among other C2 domains (Fernandez et al., 2001). The electron density around the Ca^{2+} ion observed in the crystal structure of the rat synaptotagmin 4 C2B domain shown in Figure 2.7 revealed that the Ca^{2+} ion occupies the canonical Ca1 site and is not fully coordinated, with only one water molecule and four of the six predicted Ca^{2+} coordinating

Table 2.2 Data collection and refinement statistics

	0 mM $CaCl_2$	100 mM $CaCl_2$
Data Collection		
space group	$P6_322$	$P6_322$
unit cell dimensions		
a, b, c (Å)	91.06, 91.06, 122.86	91.49, 91.49, 122.14
α, β, γ (°)	90, 90, 120	90, 90, 120
resolution (Å)	29.81-2.30 (2.34–2.30)	37.68-1.93 (1.96-1.93)
completeness	99.6 (95.2)	99.9 (99.9)
R_{merge} (%)	5.3 (72.5)	5.4 (71.9)
I/σ (I)	45.8 (1.8)	41.5 (2.3)
multiplicity	11.4 (4.7)	11.9 (8.5)
Wilson B value ($Å^2$)	56.32	34.80
Refinement		
resolution (Å)	19.96 – 2.30	19.96 – 1.93
no. of reflections R_{work}/R_{free}	12536/843	21831/1474
R_{work}/R_{free} (%)	23.71/27.45	20.57/24.18
no. of solvent molecules	44	90
no. of calcium ions	0	3
no. of sodium ions	2	2
no. of cloride ions	3	9
average B value ($Å^2$)	62.4	33.86
rmsd for bond lengths (Å)	0.020	0.020
rmsd for bond angles (°)	1.83	1.85

Notes: Data collection values are as defined in the program HKL2000. Values in parentheses are for the highest-resolution shell.

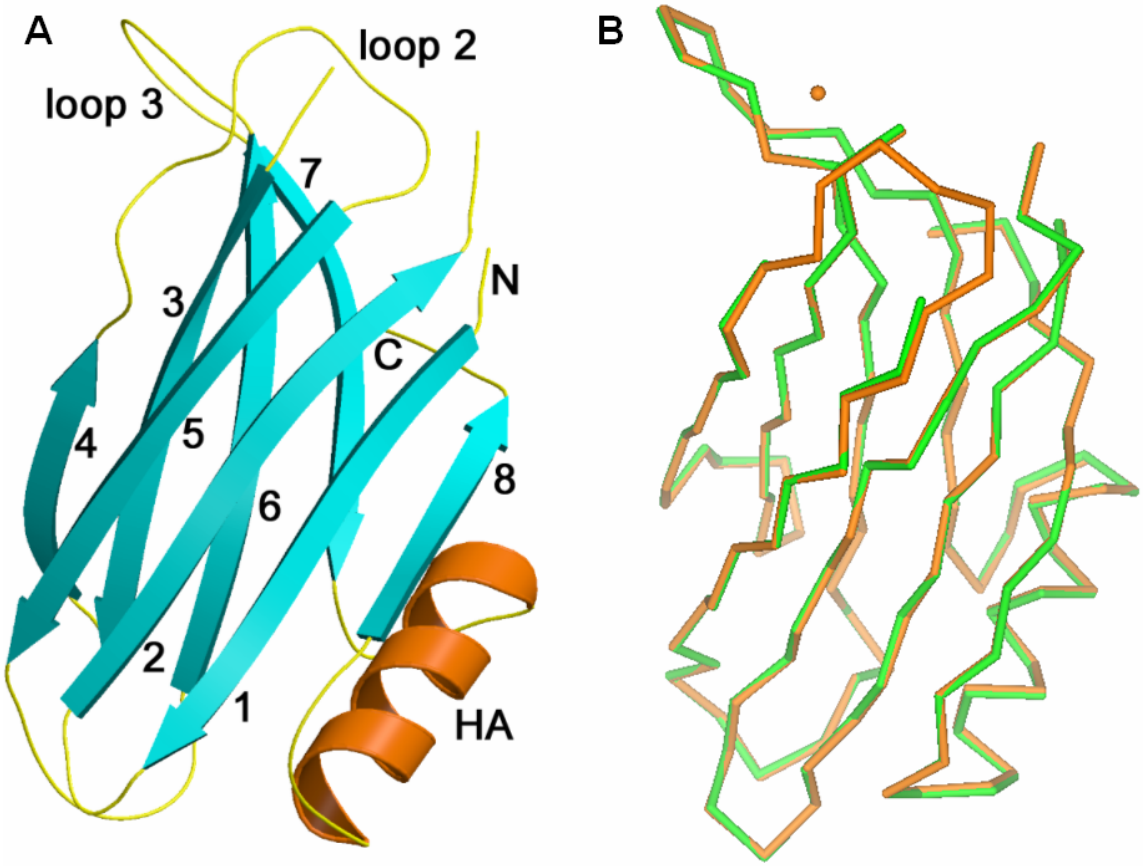

Figure 2.6 Crystal structure of the rat synaptotagmin 4 C2B domain in the presence or absence of Ca^{2+}.

(A) Ribbon diagram of the rat synaptotagmin 4 C2B domain. Strands (cyan) are labeled 1–8 and the single helix (orange) is labeled HA. The second and third Ca^{2+}-binding loops are labeled loop 2 and loop 3 whereas the first Ca^{2+}-binding loop is disordered and invisible in the crystal.

(B) Backbone superposition of the crystal structures of the rat synaptotagmin 4 C2B domain determined in the presence (orange) or absence (green) of Ca^{2+}. The Ca^{2+} ion bound in the active site of the first structure is shown as an orange sphere.

protein ligands forming its coordination sphere, and one of these ligands (E4) exhibiting poor electron density.

Even though the overall structure of the rat synaptotagmin 4 C2B domain is very similar to those of Ca^{2+}-binding C2 domains, comparison with the synaptotagmin 1 C2 domain, especially their top loops, revealed that none of the three predicted Ca^{2+}-binding sites is fully formed in the rat synaptotagmin 4 C2B domain crystals even in the presence of 100 mM Ca^{2+} (Figure 2.8B; Figure 2.8C). Most conspicuous in this comparison is the absence of loop 1 in the rat synaptotagmin 4 C2B domain, which does not exhibit electron density and hence is probably flexible. This flexibility was confirmed by assigning the backbone resonances of the rat synaptotagmin 4 C2B domain in solution using triple-resonance experiments, which showed that the residues of loop 1 are generally characterized by sharp resonances in the absence of Ca^{2+} and after addition of 20 mM Ca^{2+} (see for instance serine 320, glycine 321 and aspartate 324 amide crosspeaks in Figure 2.9). Loop 1 contains a predicted Ca^{2+} ligand (D1) that contributes to form sites Ca1 and Ca2 in the synaptotagmin 1 C2 domains, which is disordered in the rat synaptotagmin 4 C2B domain (Figure 2.1A). Hence, the Ca^{2+} ion observed in the crystal structure of the rat synaptotagmin 4 C2B domain, which binds to the predicted Ca1 site, is not fully coordinated. The lack of Ca^{2+} binding to sites Ca2 and Ca3 of the rat synaptotagmin 4 C2B domain may arise in part from the inability to fully form site Ca1, as Ca^{2+} binding to site Ca1 is necessary to properly organize the contiguous Ca^{2+}-binding sites in the synaptotagmin 1 C2 domains (Ubach et al., 1998; Fernandez et al., 2001). In addition, differences in the backbone conformation of loop 3 of the rat synaptotagmin 4 C2B domain with respect to the synaptotagmin 1 C2 domains

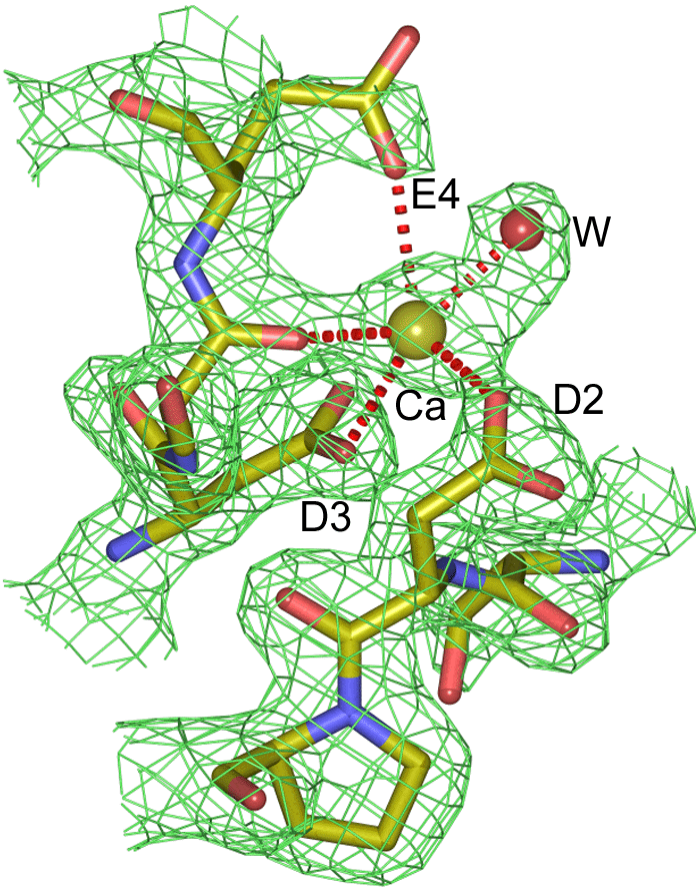

Figure 2.7 Electron density map of the Ca^{2+}-binding site of the rat synaptotagmin 4 C2B domain.

A $2F_o$ - F_c electron density map is contoured at 1σ. Oxygen atoms are colored in red, nitrogen atoms in blue and carbon atoms in yellow. The Ca^{2+} ion is labeled Ca, the protein Ca^{2+}-ligands are labeled D2, D3 and E4, and a coordinating water molecule is labeled W.

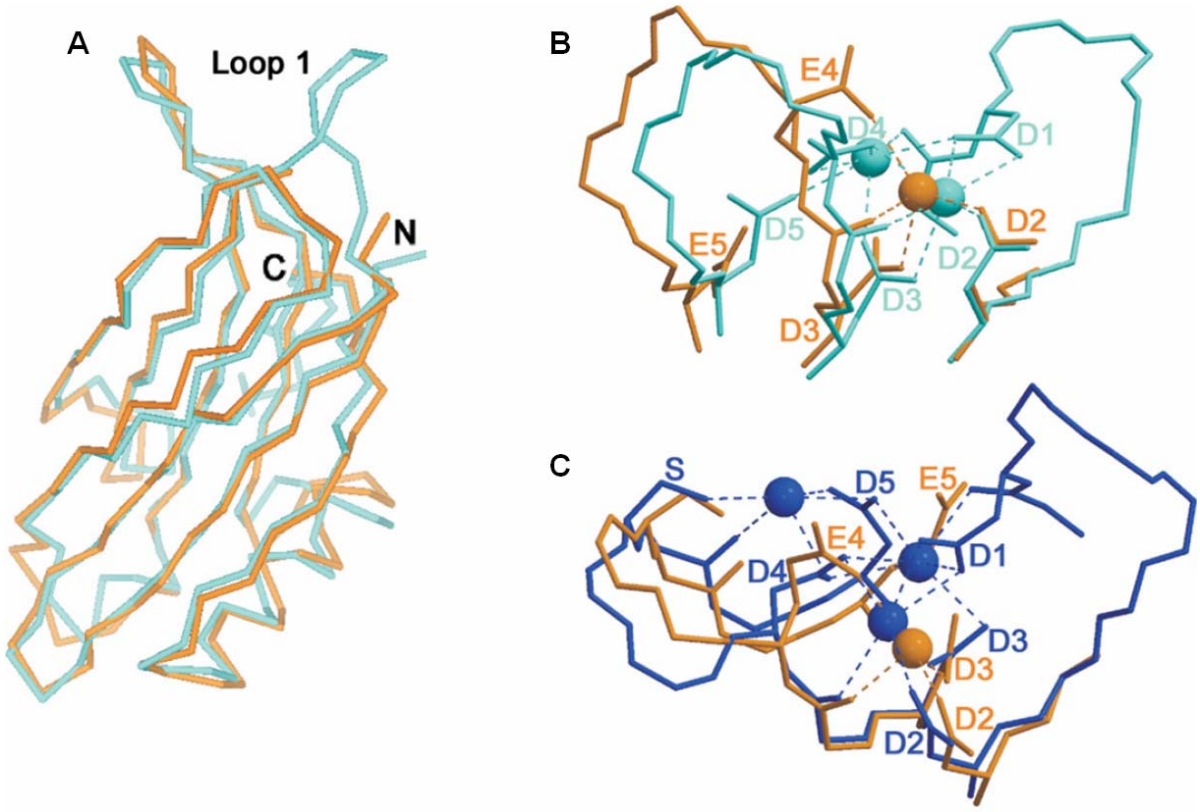

Figure 2.8 Comparison of the crystal structure of the rat synaptotagmin 4 C2B domain with those of the rat synaptotagmin 1 C2A and C2B domain.

(A) Backbone superposition of the structures of the rat synaptotagmin 4 C2B domain (orange) and the rat synaptotagmin 1 C2B domain (cyan).

(B) Superposition of the Ca^{2+}-binding loops of the rat synaptotagmin 4 C2B domain (orange) and the rat synaptotagmin 1 C2B domain (cyan). The Ca^{2+} ions are in the same color as the protein.

(C) Superposition of the Ca^{2+}-binding loops of the rat synaptotagmin 4 C2B domain (orange) and the rat synaptotagmin 1 C2A domain (dark blue). The Ca^{2+} ions are in the same color as the protein.

probably prevent the putative Ca^{2+} ligands, particularly E5, from adopting the proper orientation for Ca^{2+} coordination.

These observations explained the minimal changes induced by 20 mM Ca^{2+} in the ^{1}H-^{15}N HSQC spectrum of the rat synaptotagmin 4 C2B domain (Figure 2.2B). Indeed, the slight HSQC crosspeak shifts induced by 20 mM Ca^{2+} correspond to the amide groups around the surface of the rat synaptotagmin 4 C2B domain (Figure 2.9), as is commonly observed for most proteins at these high Ca^{2+} concentrations because of nonspecific Ca^{2+} binding to small oxygen-rich clusters in their surface. Although some of the crosspeak shifts correspond to the amide groups in the top loops of the rat synaptotagmin 4 C2B domain, the small magnitudes of these shifts compared with those induced by full saturation of Ca^{2+}-binding sites in the synaptotagmin 1 C2 domains (Fernandez et al., 2001; Ubach et al., 1998) indicated that the putative Ca^{2+}-binding sites of the top loops of the rat synaptotagmin 4 C2B domain are marginally populated (<5−10%) in solution even at 20 mM Ca^{2+}. Hence, it is highly unlikely that the observation of one bound Ca^{2+} ion in the crystals grown in 100 mM Ca^{2+} has any physiological significance.

2.3.5 Backbone Resonance Assignment of the Rat Synaptotagmin 4 C2B Domain

The backbone resonance assignment of rat synaptotagmin 4 C2B domain were determined mainly through 3D HNCACB and CBCA(CO)NH triple-resonance experiments, which are two complementary experiments to assign the backbone resonances of a protein. The CBCA(CO)NH experiment provides interresidue connection by correlating the amide resonance of one residue with the Cα and Cβ carbons of the previous residue. The HNCACB

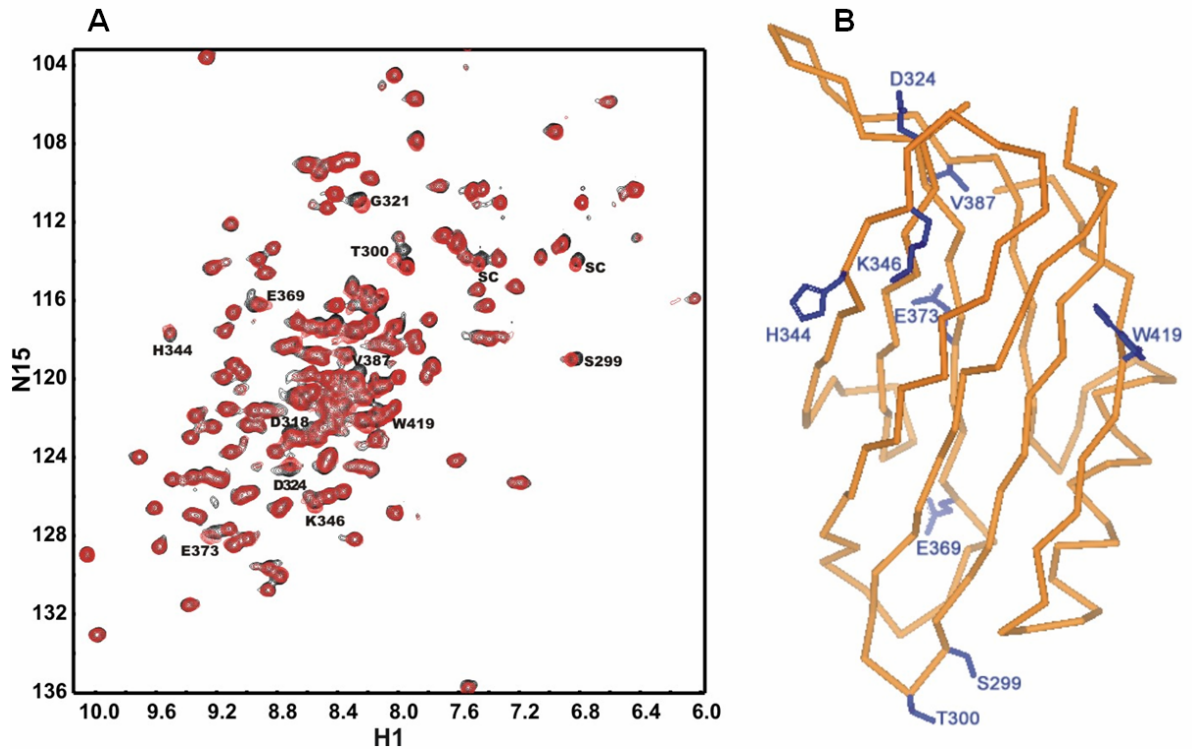

Figure 2.9 Slight Ca^{2+}-induced shifts in the ^{1}H-^{15}N HSQC spectrum of the rat synaptotagmin 4 C2B domain.

(A) Superposition of ^{1}H-^{15}N HSQC spectra of the rat synaptotagmin 4 C2B domain in the presence (black contours) and absence (red contours) of 20 mM Ca^{2+}. The crosspeaks with the most significant Ca^{2+}-induced shifts are labeled.

(B) Diagram of the crystal structure of the rat synaptotagmin 4 C2B domain illustrating the location of the residues corresponding to crosspeaks exhibiting the most significant crosspeak shifts (side chains shown in blue). Note that some of the crosspeaks correspond to residues in loop 1, which was not observed in the crystal structure.

experiment correlates the amide resonance of one residue with both its own Cα and Cβ carbon atoms and those of the previous residue due to the similar magnitude of the one-bond $J_{NC\alpha}$ coupling constant (-11 Hz) and the two-bond $J_{NC\alpha}$ coupling constant (7 Hz), therefore generating both inter- and intraresidue connection. A combination of both experiments was used to obtain backbone resonance assignments and find the corresponding residue for each crosspeak in the ^{1}H-^{15}N HSQC spectrum. Since prolines are imino acids and don't contain an amide proton, the sequential assignment connectivity is broken into fragments at positions where proline residues exist. The backbone resonance assignment results are summarized in table 2.3 with the chemical shifts of amide nitrogen, amide proton, Cα and Cβ carbons of its own and previous residue of all assignable non-proline residues. The sequential assignment was usually initiated at some particular sequence containing tandem "special" residues with distinct chemical shifts such as glycines that don't contain Cβ carbons, alanines whose Cβ carbon chemical shifts are aournd 20 ppm or serines/threonines whose Cβ carbon chemical shifts are larger than their Cα carbon chemical shifts due to their connection to electronegative oxygen atoms. For example, the Cα /Cβ carbon chemical shifts of the sequence GAT (residues 122-124) are 43.614 ppm/none, 54.512 ppm/19.397 ppm and 60.181 ppm/68.952 ppm, which immediately identify this tri-peptide fragment are GAS/T and help to localize their position in the primary sequence. Sequential HN/HN nuclear Overhauser effect (NOE) connectivities from ^{1}H-^{15}N NOESY-HSQC spectrum were used to confirm the assignments and resolve ambiguities. Residue type information from a ^{1}H-^{15}N TOCSY-HSQC spectrum was also used to confirm the assignments and resolve ambiguities.

Table 2.3 Backbone resonance assignments of rat synaptotagmin 4 C2B domain

Residue	Nitrogen	Proton	ca, i	cb, i	ca, i-1	cb, i-1
03P	N/A	N/A	N/A	N/A	N/A	N/A
04G	109.001	8.409	45.325	0	63.614	32.048
05I	120.018	7.999	61.046	38.91	45.308	0
06S	119.802	8.463	58.412	63.753	61.195	38.919
07G	111.19	8.474	45.478	0	58.401	63.86
08G	109.274	8.501	45.389	0	45.389	0
09G	109.024	8.33	45.141	0	45.141	0
10G						
11G						
12I	121.724	8.076	58.652	38.726	45.051	0
13P	N/A	N/A	N/A	N/A	N/A	N/A
14S(trans)	116.127	8.408	58.406	64.184	63.259	32.144
14S	116.52	8.679	58.689	64.078	63.083	34.698
15G	110.5	8.426	45.803	0	58.445	64.095
16R	120.459	8.428	54.661	31.025	45.797	0
17G	104.478	8.026	44.878	0	54.585	31.067
18E	117.056	8.676	55	36.614	44.924	0
19L	122.919	9.384	53.635	48.854	55.068	36.598
20L	130.684	8.863	53.658	40.102	53.658	48.878
21V	119.695	7.822	58.356	36.03	53.863	39.85
22S	117.457	9.148	55.766	65.124	58.347	36.061
23L	125.765	8.372	54.153	48.141	55.82	65.02
24C	117.509	8.281	58.417	29.9	54.213	48.073
25Y	132.983	9.99	54.708	39.325	58.331	29.857
26Q	130.033	8.787	54.514	27.282	54.514	39.293
27S	118.954	6.839	60.366	62.449	54.414	27.347
28T	113.562	7.982	64.657	68.439	60.286	62.333
29T	107.231	6.973	60.415	68.898	64.837	68.898
30N	119.254	7.789	54.878	37.244	60.383	68.861
31T	107.696	7.884	59.877	72.788	54.929	37.297
32L	124.814	9.262	53.317	47.659	59.787	72.916
33T	124.998	9.368	62.611	69.599	53.269	47.518
34V	128.487	9.586	60.802	35.877	62.609	69.593
35V	126.533	9.621	60.348	33.413	60.348	35.786
36V	127.57	9.12	62.226	31.606	60.176	33.27
37L	128.102	8.288	59.007	41.079	62.131	31.474
38K	113.852	7.346	55.079	38.715	58.912	40.845
39A	121.767	9.343	50.627	23.425	55.081	38.666
40R	116.496	9.095	54.25	34.617	50.638	23.3

41H	114.525	8.876	55.293	26.972	54.483	34.57
42L	117.02	8.181	53.669	39.777	55.323	26.964
43P	N/A	N/A	N/A	N/A	N/A	N/A
44K	121.033	8.467	56.016	33.446	63.147	31.854
45S	117.345	8.457	58.332	63.963	55.978	33.439
46D	122.709	8.717	55.273	41.064	58.385	63.991
47V	117.239	8.008	62.958	32.526	55.322	40.985
48S	116.02	8.129	58.759	64.019	62.977	32.591
49G	110.772	8.275	45.655	0	58.799	64.066
50L	121.767	8.161	55.104	42.931	45.543	0
50L	122.017	8.165	55.121	42.915	45.584	0
51S	117.023	8.426	58.242	64.454	55.156	42.91
52D	124.516	8.727	52.176	41.8	58.229	64.482
53P	N/A	N/A	N/A	N/A	N/A	N/A
54Y	113.521	8.831	55.863	40.837	62.837	34.079
55V	118.769	8.343	60.145	34.385	55.711	40.621
56K	126.94	9.314	55.676	35.295	60.136	33.819
57V	122.934	8.523	60.406	33.753	55.709	35.156
58N	123.712	9.113	51.034	42.773	60.377	33.594
59L	124.404	8.246	53.191	45.513	51.046	42.728
60Y	125.094	9.187	56.626	41.505	53.274	45.516
61H	119.657	9.032	54.135	33.595	56.716	41.305
62A	131.477	9.394	54.019	16.566	54.019	33.384
63K	115.52	8.301	57.004	30.92	54.013	16.473
64K	121.9	8.1	55.1	34.3	57.2	31.2
65R	128.065	8.993	56.816	29.745	55.106	34.317
66I	122.196	8.96	61.621	39.637	56.921	29.94
67S	115.346	7.475	58.738	64.984	61.813	39.444
68K	123.266	8.16	55.193	35.465	58.682	64.898
69K	122.296	9.003	53.446	37.023	55.167	35.404
69K'	123.234	9.034	53.461	36.736	55.12	35.423
70K	118.882	8.501	55.465	36.192	53.61	37.098
71T	112.272	9.12	61.25	71.976	55.466	36.351
72H	117.7	9.51	57	31	72	55
73V	120.268	8.296	62.247	32.589	57.083	30.995
74K	126.291	8.546	53.23	35.345	62.328	32.784
75K	116.898	7.789	55.321	33.904	53.4	35.655
76C	120.925	8.689	58.68	27.182	58.7	34.037
77T	115.52	8.193	59.576	69.94	59.576	27.266
78P	N/A	N/A	N/A	N/A	N/A	N/A
79N	120.231	8.082	52.207	39.266	64.276	34.369
80A	124.471	8.492	51.073	20.96	52.365	39.385

81V	124.428	8.513	62.287	32.284	50.739	20.954
82F	124.713	8.2	59.865	40.292	62.533	32.083
83N	118.297	8.76	54.097	37.667	59.862	40.124
84E	118.519	8.039	56.627	32.997	54.065	37.644
85L	126.781	8.017	54.753	44.832	56.5	33.118
86F	125.034	9.505	55.786	43.295	54.465	44.946
87V	121.517	8.407	61.717	33.458	55.937	43.284
87V'	121.9	8.45	62.3	32.6	57.1	30.1
88F	125.015	9.209	56.626	42.337	61.568	33.36
89D	123.033	8.653	54.757	41.866	56.551	42.444
90I	123.791	8.455	55	36.781	55.039	41.679
91P	N/A	N/A	N/A	N/A	N/A	N/A
92C	116.27	7.414	55.492	30.402	63.671	30.402
93E	118.269	8.708	57.776	0	55.506	30.158
94S	112.574	7.702	56.594	65.112	57.944	29.987
95L	120.7	8.6	55	41	56.9	65.2
96E	121.267	8.466	60.35	29.794	54.493	41.038
97E	116.2	8.941	55.604	29.962	60.265	29.962
98I	124.122	7.629	56.907	37.213	55.62	30.1
99S	118.717	8.553	56.726	66.224	56.726	37.117
100V	119.768	8.584	59.933	34.71	56.696	66.359
101E	128.489	9.09	53.299	35.982	60.009	34.632
102F	123.921	9.719	55.424	40.67	53.423	35.976
103L	122.326	9.23	53.079	44.611	55.416	40.689
103L'	122.337	9.335	53.16	44.779	55.347	40.652
104V	123.634	8.814	61.865	31.335	53.044	44.533
105L	129.606	8.865	54.116	45.201	61.748	31.333
106D	117.32	8.573	53.739	43.201	53.739	45.126
106D	117.269	8.543	53.739	43.038	53.739	44.895
107S	118.682	8.592	60.471	63.98	53.409	43.168
108E	122.955	8.572	57.186	30.122	60.416	64.014
109R	121.267	8.371	57.242	30.022	57.103	30.35
110G						
111S	116.147	8.2	58.985	63.734	46.168	0
112R	121.002	8.2	56.804	30.335	59.269	64.149
112R'	120.831	8.241	56.938	30.282	58.769	63.696
113N	117.518	8.271	53.649	38.806	56.692	29.959
114E	120.293	8.144	56.962	31.03	53.45	38.874
115V	119.518	8.256	62.446	32.584	56.995	30.998
116I	127.775	9.204	63.35	38.251	62.172	32.39
117G	102.527	7.537	45.858	0	63.589	38.46
118R	121.501	8.949	54.424	35.213	45.845	0

119L	125.765	8.987	54.213	47.281	54.213	35.066
120V	125.765	8.469	60.981	34.432	54.175	47.221
121L	126.036	9.056	53.031	44.731	61.046	34.443
122G	105.798	6.604	43.614	0	53.192	44.74
123A	121.57	8.871	54.512	19.397	43.551	0
124T	105.583	7.9	60.181	68.952	54.735	19.303
125A	125.24	7.189	52.628	19.026	60.329	69.145
126E	120.518	8.567	56.4	30.753	52.645	19.06
127G	109.031	8.609	45.833	0	56.361	30.767
128S						
129G	114.271	9.239	47.74	0	62.053	67.071
130G	110.047	7.716	46.82	0	48.127	0
131G	109.711	8.181	47.141	0	47.141	0
132H	122.284	8.453	57.683	34.204	47.196	0
133W	118.007	8.107	59.874	30.616	58.054	34.082
134K	117.269	8.192	59.611	32.356	59.611	30.61
135E	117.791	7.9	60.79	30.518	59.413	32.344
136I	112.973	7.615	63.932	37.42	60.799	30.392
137C	115.219	7.232	62.564	27.219	64.124	37.412
138D	119.844	8.403	56.011	41.031	62.699	27.289
139F	118.312	7.878	55.063	38.738	56.023	40.968
140P	N/A	N/A	N/A	N/A	N/A	N/A
141R	113.771	8.931	59.329	28.383	63.905	32.051
142R	121.42	8.04	55.617	32.318	59.459	28.163
143Q	126.515	8.783	55.477	28.815	55.477	32.175
144I	126.515	8.783	60.479	40.254	55.477	28.815
145A	104.429	9.265	50.406	20.725	60.382	40.074
146K	119.872	8.302	55.207	37.599	50.367	20.674
147W	122.007	8.234	57.291	30.853	55.299	37.571
148H	119.896	9.165	55.331	37.581	57.164	30.874
149M	121.498	9.141	55.652	33.103	55.652	37.544
150L	122.517	8.513	54.372	42.913	55.903	32.915
151C	119.276	9.091	57.642	30.226	54.441	42.727
152D	121.069	8.64	54.977	41.24	57.634	30.235
153G	114.123	7.947	46.423	0	54.985	41.233

2.4 Discussion

Our results showed that the Ca^{2+}-binding properties of C2 domains cannot be reliably predicted from sequence analyses, and suggested that the general assumption that rat synaptotagmin 4 functions as a Ca^{2+} sensor (Wang et al., 2003a) should be revised. Furthermore, past research on rat and *Drosophila* synaptotagmin 4 generally assumed that these two proteins are orthologues that carry out a conserved function in both species based on phylogenetic analyses and the conservation of the aspartate to serine substitution in the C2A domain (Wang et al., 2001a; Wang et al., 2003a; Littleton et al., 1999; Robinson et al., 2002). The different Ca^{2+}-binding properties of the rat and *Drosophila* synaptotagmin 4 C2 domains described here indicate that the two proteins, although homologues, are not true orthologues, and that they experienced a marked functional alteration during evolution. To our knowledge, this is the first known example in which two proteins were identified as clear orthologues from sequence analyses and yet may have changed function in evolution. Previous genetic studies of *Drosophila* and mammalian synaptotagmin 4 should be reinterpreted considering the differential Ca^{2+}-binding properties uncovered here.

Overall, our results emphasized the danger of assuming protein properties based solely on sequence comparisons without experimental verification (Wang et al., 2003a). Prediction of the functional activities of proteins from a given family generally focuses on the conservation of particular residues that have been shown to be critical for such activities in other members of the family, ignoring the potential importance of other residues that are not conserved in the family. Thus, the assumption that the *Drosophila* and rat synaptotagmin

4 C2A domains share an inability to form complexes with Ca^{2+}-phospholipids was based on the conservation of the aspartate to serine substitution in one of the putative Ca^{2+} ligands, but ignored the presence of a 14-residue insertion in loop 1 of the *Drosophila* C2A domain (Figure 2.1B) that is not observed in other C2 domains and could substantially alter its properties. Similarly, the expectation that the C2B domains from both *Drosophila* and rat synaptotagmin 4 bind Ca^{2+} focused on the conservation of the residues that coordinate Ca^{2+} in other C2 domains such as those of synaptotagmin 1. However, our data clearly showed that, although this prediction was correct for the *Drosophila* synaptotagmin 4 C2B domain, the rat synaptotagmin 4 C2B domain cannot fully form Ca^{2+}-binding sites. This marked distinction in their Ca^{2+}-binding properties must arise from specific features determined by residues that are not conserved in their sequences. The crystal structure of the rat synaptotagmin 4 C2B domain showed that nonconserved residues cause only subtle changes in its structure, and perhaps in its dynamic properties, compared with those of the synaptotagmin 1 C2 domains. However, these subtle changes have profound consequences for the functional properties of the rat synaptotagmin 4 C2B domain. These observations emphasize the notion that protein function is not only governed by residues directly involved in specific activities but also by specific structural details that cannot be predicted with current sequence analysis and structure modeling methods.

Chapter 3 Crystal Structure of the Rat RIM2 C2A Domain at 1.4 Å

(Parts of this chapter are adapted from Dai et al., 2005)

3.1 Introduction

Neurotransmitter release is mediated through Ca^{2+}-triggered synaptic vesicle exocytosis at the presynaptic plasma membrane, and is a central event in interneuronal communication. This process exhibits exquisite spatial and temporal regulation and involves several steps, which include docking of the synaptic vesicles to the presynaptic plasma membrane, one or more priming reactions that prepare the synaptic vesicles in a release-ready state, and the actual Ca^{2+}-evoked release of neurotransmitters upon Ca^{2+} influx caused by the invasion of the action potential at the presynaptic terminal (Sudhof, 1995). The release of neurotransmitters is extremely fast, occurring in less than half a millisecond, and is restricted to specialized sites of the presynaptic plasma membrane known as the active zones. The different steps that lead to exocytosis are controlled by a complex protein machinery. This machinery is formed in part by components that have homologues in all types of intracellular membrane traffic such as the SNARE proteins synaptobrevin, syntaxin, and SNAP-25, which play a key role in membrane fusion, and Rab3s, which are small GTPases that regulate neurotransmitter release (Lin and Scheller, 2000; Rizo and Sudhof, 2002). In addition, neurotransmitter release is controlled by specialized proteins such as the Ca^{2+} sensor synaptotagmin 1, the essential priming factors RIMs and Munc13s, and other components of the active zones (Sudhof, 2002; Tucker and Chapman, 2002).

The active zones of a synapse mediate Ca^{2+}-triggered neurotransmitter release, and integrate presynaptic signals that regulate neurotransmitter release. Electron microscopy

(EM) ultrastructural studies revealed that the active zones at the presynaptic plasma membrane are characterized by electron dense proteinaceous materials, which are formed by a network of large proteins, including RIMs, Munc13s, Bassoon, piccolo, ELKS, and liprins (Garner et al., 2000). Among these proteins, RIMs are particularly interesting because of their multiple roles in regulating neurotransmitter release and organizing the active zone that have been suggested by extensive genetic and biochemical experiments. RIMs were initially identified as Rab3 effectors (Wang et al., 1997) and include four genes in mammals (RIM1, RIM2, RIM3γ, and RIM4γ) (Wang and Sudhof, 2003) and one in *Caenorhabditis elegans* (unc10) (Koushika et al., 2001). The mammalian RIM1 and RIM2 genes specify full-length transcripts encoding two closely related protein products (RIM1α and RIM2α, respectively) that contain an N-terminal zinc finger domain, a central PDZ domain, and two C-terminal C2 domains (referred to as the C2A domain and the C2B domain, respectively) that are separated by long alternatively spliced sequences. In addition, through transcription from different internal promoters, the RIM2 gene specifies a shorter transcript lacking the N-terminal zinc finger (RIM2β) and an even shorter transcript (RIM2γ) that, like RIM3γ and RIM4γ, only encodes the C-terminal C2B domain and adjacent sequences (Wang and Sudhof, 2003). Unc10 mutants in *C. elegans* exhibit a drastic decrease in the level of release (5-fold reduced level of fusion-competent vesicles in spite of normal levels of docked vesicles) that is associated with a defect in synaptic vesicle priming (Koushika et al., 2001). Deletion of RIM1α in mice leads to a milder phenotype, probably due to redundancy with RIM2α, but still results in less vesicle priming and alteration of short-term synaptic plasticity, such as paired pulse facilitation, paired pulse depression, and post-tetanic potentiation

(Schoch et al., 2002; Calakos et al., 2004). Moreover, a form of long-term synaptic plasticity known as mossy fiber long-term potentiation (LTP) is completely abolished in these mice (Castillo et al., 2002). RIM1α knockout mice exhibit severe defects in learning and memory (Powell et al., 2004) that most likely arise from these defects in neurotransmitter release and its regulation.

The different domains of α-RIMs have been implicated in multiple protein-protein interactions. For example, the N-terminal zinc finger domain and adjacent regions are involved in binding to Rab3s (Wang et al., 1997) and to Munc13-1 (Betz et al., 2001), an active zone protein with an essential role in synaptic vesicle priming, while the central PDZ domain interacts with ELKS (also known as ERC or CAST) (Wang et al., 2002). On the other hand, the RIM C2A domain was reported to bind to synaptotagmin 1 and to SNAP-25 (Coppola et al., 2001), whereas the C2B domain was also found to bind to synaptotagmin 1 as well as to liprins (Schoch et al., 2002). Furthermore, a proline-rich sequence between the two C2 domains was found to bind to the SH3 domain-containing RIM-binding proteins (RIM-BPs) (Wang et al., 2000). These observations suggested that α-RIMs might act as protein scaffolds that help to organize the active zone through its multiple interactions with active zone proteins, and at the same time might regulate neurotransmitter release by binding to key components of the release apparatus. However, some of the biochemical studies that described these interactions relied largely on GST pulldown experiments, which are prone to artifacts (Fernandez et al., 2001); for instance, no binding of synaptotagmin 1 to the RIM C2A domain was observed in GST pulldown experiments performed in a separate study (Schoch et al., 2002). Moreover, little is known about the three-dimensional structures of the

α-RIM domains. Due in part to this scarcity of structural and definitive biochemical information, there is currently a large gap between the extensive genetic and physiological data describing the functions of α-RIMs and the limited molecular understanding of these functions.

In this chapter, we carried out studies on the structure and interactions of the RIM C2A domain. This domain plays a critical role in the proper localization of unc10 in *C. elegans* (Deken et al., 2005), and its functional importance is further emphasized by the observation that an R844H point mutation in the human RIM1α C2A domain segregates with autosomal dominant cone-rod dystrophy (CORD7), a severe visual disease that is characterized by the early loss of visual acuity and color vision, followed by night blindness and peripheral visual field loss (Johnson et al., 2003; Hunt et al., 2002). However, the RIM C2A domain is only distantly related to the C2 domains that have been more thoroughly studied such as those from synaptotagmins and PKCs, and therefore it is unclear to what extent the RIM C2A domain shares their properties. C2 domains are widespread protein modules that usually bind phospholipids in a Ca^{2+}-dependent manner and have a β-sandwich structure with loops emerging at the top and bottom of the sandwich, as mentioned in chapter 1. Multiple Ca^{2+} ions commonly bind to a motif formed by five conserved aspartate residues located at the top loops (Sutton et al., 1995; Shao et al., 1996; Essen et al., 1997; Ubach et al., 1998), which also mediate Ca^{2+}-dependent phospholipid binding (Zhang et al., 1998; Chapman and Davis, 1998). However, some C2 domains do not bind Ca^{2+} or phospholipid. The RIM C2A domain does not contain the full complement of aspartate residues that form the C2 domain Ca^{2+}-binding motif. This observation suggests that the RIM C2A domain does

not bind Ca^{2+}, but this prediction has not been tested. Moreover, because of the limited degree of sequence identity with C2 domains of known three-dimensional structure, it is unknown whether the RIM C2A domain contains specific structural features that may be critical for its function. To shed light on these questions and provide a structural basis for understanding the role(s) of the C2A domain of RIMs, we have analyzed the biochemical properties of the rat RIM2 C2A domain using NMR spectroscopy, and we have determined its crystal structure using data to 1.4 Å resolution. We found that the rat RIM2 C2A domain does not bind to Ca^{2+}, phospholipid, synaptotagmin 1, or SNAP-25 with significant affinity, suggesting that other interactions mediate its function. The rat RIM2 C2A domain adopts a β-sandwich structure that resembles those of other C2 domains such as the C2A domain of synaptotagmin 1, but exhibits a striking dipolar distribution of electrostatic potential, with a highly positive potential on one edge of the β-sandwich and a highly negative potential on the opposite edge. The location of the conserved arginine side chain implicated in CORD7 at the bottom of the domain and the pattern of sequence conservation in RIM C2A domains suggest that these domains may function through Ca^{2+}-independent interactions mediated by its bottom face, in contrast to the common involvement of Ca^{2+}-dependent interactions of the top loops in C2 domain function.

3.2 Materials and Methods

3.2.1 Recombinant Protein Preparation

DNA encoding GST fusion proteins of various fragments spanning the rat RIM2α C2A domain were made using custom-designed primers and standard PCR cloning techniques and subcloned into the pGEX-KG expression vector. The rat RIM2α C2A domain (amino acids 722-859) R805H point mutant was generated by the Quikchange® site-directed mutagenesis kit (Stratagene), according to the manufacturer's protocol.

The expression and purification procedures of rat RIM2 C2A domain wild type and R805H mutant were similar to those for synaptotagmin C2 domains described in chapter 2. Briefly, the fusion proteins were expressed at 25 ºC in Escherichia coli BL21 and isolated by affinity chromatography on glutathione-Sepharose followed by on-resin cleavage with thrombin. The eluted proteins were further purified by gel filtration chromatography through a Superdex 75 Hiload 16/60 column (Amersham Pharmacia Biotech.). The purity of the preparation was assessed by SDS-PAGE and Coomassie blue staining. The typical yield according to UV absorbance measurements at 280 nm was 5-7 mg per liter of culture. Uniform ^{15}N labeling was achieved by growing the bacteria in $^{15}NH_4Cl$ as the sole nitrogen source.

3.2.2 NMR Spectroscopy

All NMR experiments were carried out at 27 ºC on Varian INOVA500 or INOVA600 spectrometers with samples containing approximately 100 μM C2 domains dissolved in 20 mM MES, pH 6.0, and 150 mM NaCl, using H_2O/D_2O 95:5 (v/v) as the solvent. The 5% (v/v) D_2O was included to provide the lock signal for the control of the long term stability of the magnetic field. Ca^{2+} titrations monitored by ^{1}H-^{15}N HSQC experiments were performed

as described in chapter 2. All the NMR binding experiments were carried out at 27 ºC on Varian INOVA500 or INOVA600 spectrometers with samples containing 60 μM ^{15}N-labeled proteins and 80 μM nonlabeled proteins dissolved in 20 mM MES, pH 6.0, and 150 mM NaCl in the presence or absence of 10 mM $CaCl_2$, using H_2O/D_2O 95:5 (v/v) as the solvent. All NMR data were processed with NMRPipe (Delaglio et al., 1995) and analyzed with NMRView (Johnson and Blevins, 1994).

3.2.3 X-ray Crystallography

Rat RIM2α C2A domain (amino acids 722-859) dissolved in 20 mM MES, pH 6.0, 150 mM NaCl, and 1 mM EDTA was concentrated to 25 mg/mL and crystallized in 17.5% (w/v) PEG 4000, 0.2 M $(NH_4)_2SO_4$, and 0.1 M sodium acetate, pH 4.5 at 20 ºC using the hanging-drop vapor diffusion method. Crystals appeared overnight and grew to a final size of 0.05 mm × 0.05 mm × 0.1 mm within 2 days. Prior to data collection, crystals were transferred into a solution of 20% (w/v) PEG 4000, 0.15 M NaCl, 0.2 M $(NH_4)_2SO_4$, 0.1 M sodium acetate, pH 4.5, and 15% (v/v) ethylene glycol, and then flash-cooled in liquid propane. Diffraction data were collected at Structural Biology Center (SBC) beamlines 19BM and 19ID of the Advanced Photon Source (APS) at 100 K to a Bragg spacing (d_{min}) of ~1.41 Å. The crystals exhibited the monoclinic symmetry of space group $P2_1$, contained one molecule per asymmetric unit, and had the following unit cell parameters: a = 25.45 Å, b = 44.81 Å, c = 55.76 Å and α=90°, β= 103.86°, γ=90°. Data were processed and scaled in the HKL2000 program suite (Otwinowski and Minor, 1997) as described in chapter 2. The rat RIM2 C2A domain structure was determined via molecular replacement using AMoRe

(Navaza, 1994). Initial model coordinates were obtained by modifying the coordinates of the human RIM2 C2A domain (PDB entry 1V27). The rotation and translation function search was conducted with data between a d_{min} of 8.0 and 4.0 Å, and a single solution was obtained with a final correlation coefficient of 0.50. Model refinement was carried out with Refmac (Murshudov et al., 1997; Bailey, 1994) of the CCP4 package (Bailey, 1994) with a random subset of all data set aside for the calculation of R_{free}. Manual adjustments to the models were carried out with O (Jones et al., 1991). The electron density clearly showed the presence of two sulfate ions. After refinement of the protein part was complete, solvent molecules were added where stereochemically reasonable. The model has good stereochemistry, with 87.7% of residues in the most favored region of the Ramachandran plot and none in disallowed regions. Data collection and refinement statistics are listed in Table 3.1.

3.2.4 Phospholipid Binding by Fluorescence Resonance Energy Transfer (FRET) Assay

FRET experiments were performed on a Perkin Elmer LS50B spectrofluorometer (Perkin Elmer, Uberlingen, Germany) with a 450 µl Quartz fluorometer cuvette (Nova Biotech), exciting at 280 nm and recording the emission spectra from 300 to 550 nm with 5nm excitation slit width and 5nm emission slit width. The experiments were performed at 25 ºC in 20 mM Tris, pH 7.2, 100 mM NaCl, with 0.1 mg/ml lipid (65% (w/w) POPC, 30% (w/w) DOPS, 5% (w/w) Dansyl-DOPE) concentration and 1 µM protein in the presence of either 1mM EDTA or 1mM Ca^{2+}. The fluorescence emission spectra of protein alone or liposome alone were acquired under identical conditions as references.

Table 3.1 Data collection and refinement statistics

Data Collection	
space group	$P2_1$
unit cell dimensions	
a, b, c (Å)	25.45, 44.81, 55.76
α, β, γ (°)	90, 103.86, 90
resolution (Å)	20.92-1.41 (1.43-1.41)
completeness	98.5 (82.0)
R_{merge} (%)	2.2 (18.3)
I/σ (I)	52.9 (5.2)
multiplicity	4.0 (2.8)
Wilson B value ($Å^2$)	15.98
Refinement	
resolution (Å)	20.00-1.41
no. of reflections R_{work}/R_{free}	21884/1383
R_{work}/R_{free} (%)	18.10/21.35
no. of solvent molecules	104
no. of sulfate ions	2
average B value ($Å^2$)	17.74
rmsd for bond lengths (Å)	0.019
rmsd for bond angles (°)	1.92

Notes: Data collection values are as defined in the program HKL2000. Values in parentheses are for the highest-resolution shell.

3.2.5 Thermal Denaturation by CD Spectroscopy

CD spectra and thermal denaturation curves of both the rat RIM2 C2A domain wild type and R805H mutant were recorded on an Aviv model 62DS spectropolarimeter using a CD cuvette of 1 mm path length. The CD spectra were recorded from 190 nm to 260 nm with 1 nm increment. The temperature denaturation curves were recorded from 25 °C to 95 °C with 1 °C increment, monitoring the CD signal at 210 nm. The rat RIM2 C2A domain wild type and R805H mutant samples for thermal denaturation was about 5 μM in 20 mM MES, pH 6.0, 150mM NaCl, and 1 mM EDTA. The fraction of unfolded protein at each temperature was calculated by using the formula $(I_{obs} - I_f)/(I_u - I_f)$, where I_{obs} is the observed signal intensity, and I_u and I_f are the signal intensities of the unfolded and folded states, respectively, which were calculated by extrapolation of the linear regions at the extremes of the temperature denaturation curves.

3.3 Results

3.3.1 Definition of Domain Boundaries and Biochemical Analysis

The region of rat RIM2 that contains the predicted C2A domain exhibits only a limited degree of sequence similarity with C2 domains of known structure, particularly at the C-terminus where C2 domains tend to be more variable. For instance, the synaptotagmin 1 C2B domain contains two C-terminal α-helices that are not present in the synaptotagmin 1 C2A domain and, as a result, is 20 residues longer (Fernandez et al., 2001; Sutton et al., 1995). To experimentally define the correct boundaries of the rat RIM2 C2A domain, we

expressed several constructs spanning residues 662-869 of rat RIM2α, performed limited proteolysis experiments with trypsin and chymotrypsin, and identified proteolytically resistant fragments by mass spectrometry. On the basis of these experiments, we focused on a minimal fragment containing residues 722-859 of rat RIM2α. A ^{1}H-^{15}N HSQC spectrum of a uniformly ^{15}N-labeled sample of this fragment in the absence of Ca^{2+} (Figure 3.1, black contours) revealed an excellent chemical shift dispersion, demonstrating that the fragment is properly folded and thus contains the rat RIM2 C2A domain. All experiments described below were performed with this fragment, which hereafter will be called the rat RIM2 C2A domain for simplicity.

In addition to providing information about the proper folding of a protein, ^{1}H-^{15}N HSQC spectra are also useful in analyzing interactions of a ^{15}N-labeled protein in solution, as we have mentioned in chapter 2. ^{1}H-^{15}N HSQC spectra contain one crosspeak for the amide group of each non-proline residue in the protein. The positions of the crosspeaks are very sensitive to the chemical environment of the amide groups. Hence, perturbations in these crosspeaks (shifts or broadening) can report on interactions with ligands or other proteins. To analyze whether the rat RIM2 C2A domain binds Ca^{2+}, we acquired additional ^{1}H-^{15}N HSQC spectra in the presence of 1 and 20 mM Ca^{2+} (Figure 3.1, red and green contours, respectively). Addition of 1 mM Ca^{2+} did not induce significant perturbations, showing that the rat RIM2 C2A domain does not bind Ca^{2+} at this concentration. A few crosspeaks exhibited small shifts in the presence of 20 mM Ca^{2+}. This behavior is characteristic of C2 domains that do not bind Ca^{2+} with significant affinity and can be attributed to weak binding

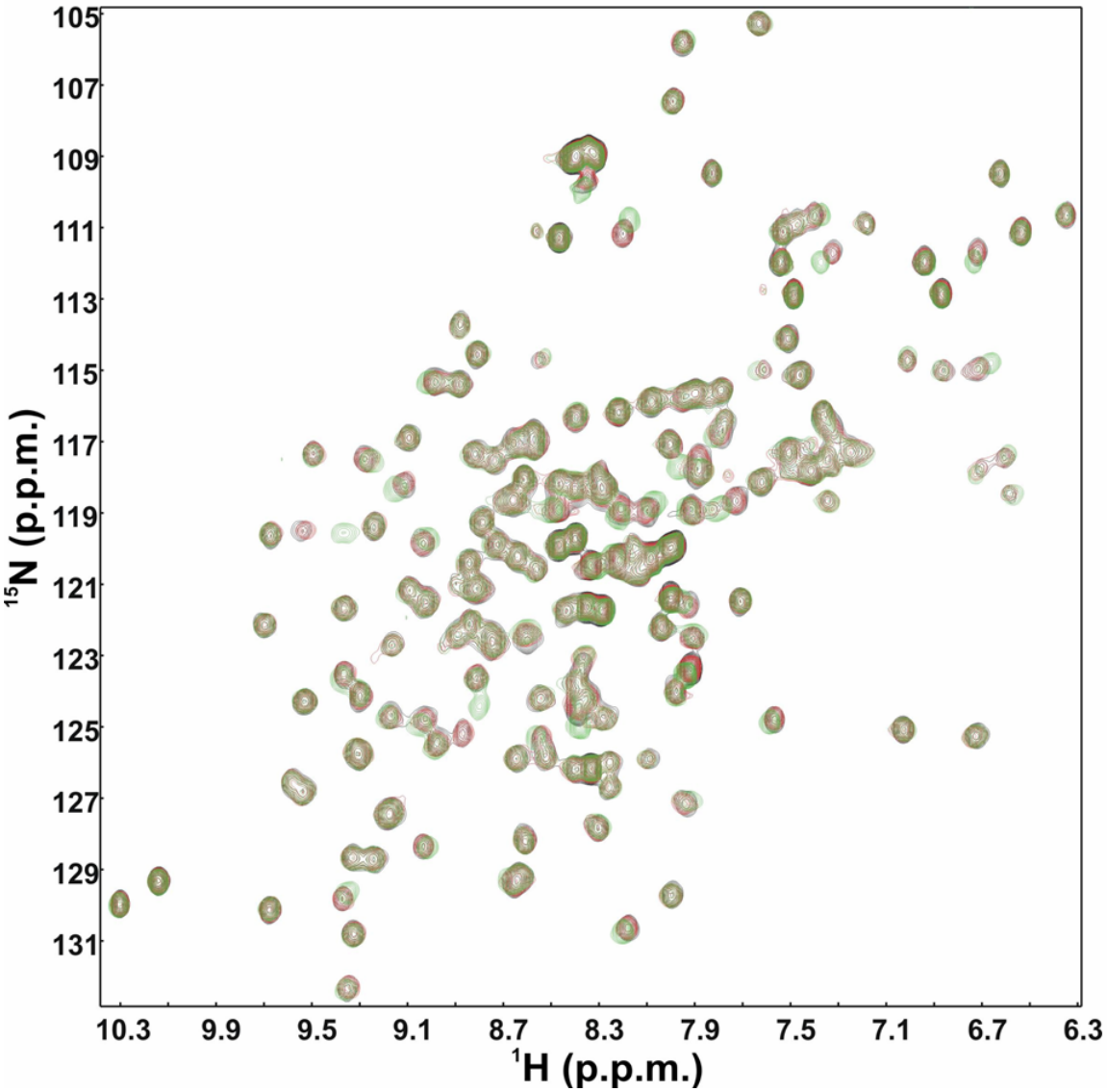

Figure 3.1 The RIM2 C2A domain does not bind Ca^{2+}.

^{1}H-^{15}N HSQC spectra of the RIM2 C2A domain in the absence (black contours) and presence of 1 mM Ca^{2+} (red contours) or 20 mM Ca^{2+} (green contours) are shown.

of Ca^{2+} to oxygen-rich clusters at the surface of a protein (Dai et al., 2004; Chen et al., 2005). We also investigated whether the rat RIM2 C2A domain binds to negatively charged phospholipid using a similar fluorescence resonance energy transfer (FRET) based assay as described in chapter 2 (Fernandez et al., 2001), but we did not observe any significant binding in the presence or absence of Ca^{2+} (Figure 3.2). In principle, the FRET effect can be monitored by either the decrease of tryptophan emission or the sensitized enhancement of Dansyl emission, but practically the Dansyl emission enhancement is more reliable since tryptophan fluorescence is very sensitive to the environmental change and therefore might change independent of FRET, as shown in Figure 3.2 for the rat RIM2 C2A domain. No Dansyl emission enhancement was observed when the rat RIM2 C2A domain and Dansyl-labeled liposomes were incubated, indicating no binding, in spite of the observed decrease of tryptophan fluorescence upon Ca^{2+} addition, which probably resulted from the quenching of tryptophan fluorescence by Ca^{2+}.

The interactions of the RIM C2A domain with SNAP-25 and synaptotagmin 1 were identified using GST pulldown experiments with GST fusion proteins immobilized on GST affinity resins (Coppola et al., 2001). However, GST pulldown experiments are prone to artifacts that can yield false positive or false negative results. For instance, we previously described that immobilized GST fusion proteins of the synaptotagmin 1 C2B domain have a strong tendency to bind to polyacidic compounds that are very difficult to remove even with extensive washes of the resins and that can induce artifactual binding or mask relevant interactions (Ubach et al., 2001). To test whether the rat RIM2 C2A domain binds to SNAP-25 and synaptotagmin 1 by an independent method, we used NMR spectroscopy. Addition of

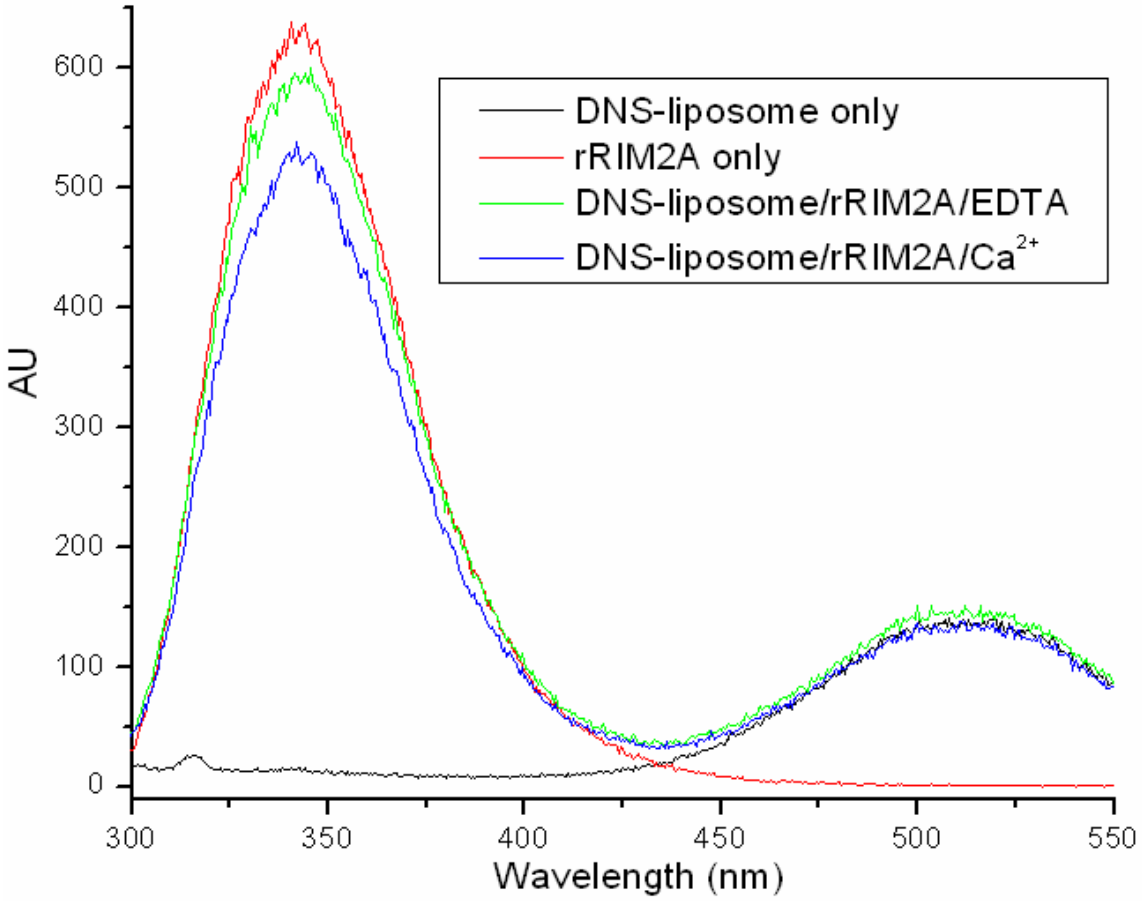

Figure 3.2 Ca^{2+}-dependent phospholipid binding properties of the RIM2 C2A domain analyzed by the FRET assay.

Phospholipid binding of the RIM2 C2A domain using the FRET assay. The emission spectra of Dansyl liposomes or C2 domain alone are shown in black and red, respectively. The emission spectra of the C2 domain together with Dansyl liposomes in the presence of 1 mM EDTA or 1 mM Ca^{2+} are shown in green and blue, respectively.

unlabeled SNAP-25 did not cause significant perturbation of the ^{1}H-^{15}N HSQC spectrum of the ^{15}N-labeled RIM2 C2A domain in the absence of Ca^{2+} (Figure 3.3A), showing that the RIM2 C2A domain and SNAP-25 do not interact under these conditions. Only minor spectral changes were observed in analogous experiments performed in the presence of 10 mM Ca^{2+} (Figure 3.3B). These minor changes may reflect a very low affinity interaction that is likely to be nonspecific and that contrasts with the nanomolar affinity observed in previous GST pulldown experiments (Coppola et al., 2001). To test for interactions between the RIM2 C2A domain and synaptotagmin 1, we prepared ^{15}N-labeled samples of the synaptotagmin 1 C2A domain and C2B domain and recorded the effects that addition of the unlabeled RIM2 C2A domain has on their ^{1}H-^{15}N HSQC spectra in the presence or absence of 10 mM Ca^{2+} since we already had the backbone resonance assignments for the ^{1}H-^{15}N HSQC spectra of synaptotagmin 1 C2A and C2B domains (Figure 3.3 C-F). The RIM2 C2A domain did not cause any significant perturbations in these spectra, showing that it does not bind to the synaptotagmin 1 C2 domains. It should be noted that these experiments were performed in solution with purified fragments that do not contain any tags (such as GST) and that have been extensively characterized by NMR spectroscopy. In addition, these experiments were performed at protein concentrations of 60-80 μM that favor the formation of protein complexes even if they have low affinity. Hence, we conclude that the rat RIM2 C2A domain does not form binary complexes with SNAP-25 and the synaptotagmin 1 C2 domains either in the presence or absence of Ca^{2+} with significant affinity.

3.3.2 Three-Dimensional Structure of the Rat RIM2 C2A Domain

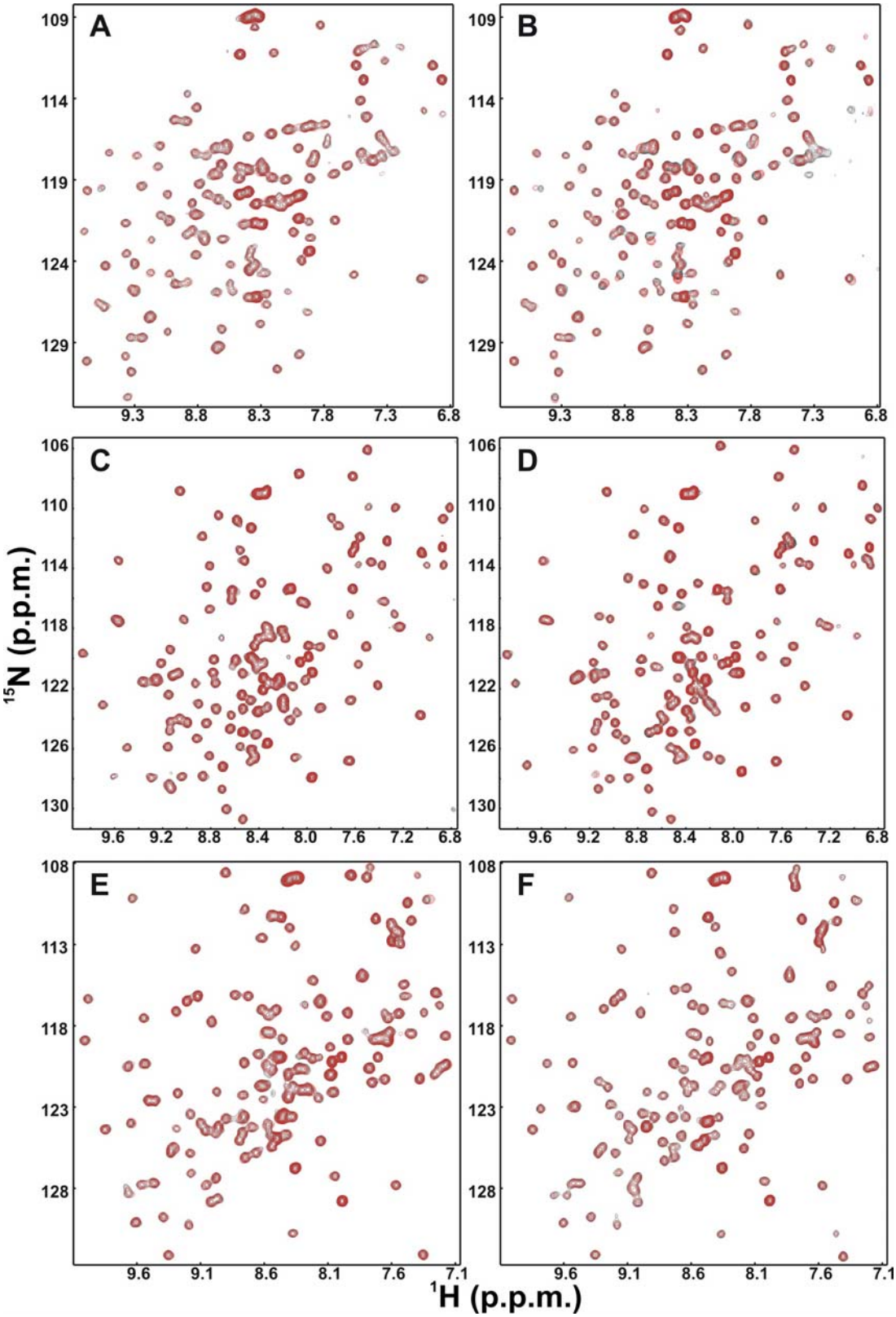
A
B
C
D
E
F
^{15}N (p.p.m.)
^{1}H (p.p.m.)

Figure 3.3 The RIM2 C2A domain does not bind to SNAP-25 and the synaptotagmin 1 C2 domains.

(A) ^{1}H-^{15}N HSQC spectra of the RIM2 C2A domain before (black) and after (red) addition of unlabeled SNAP-25 in the absence of Ca^{2+}.

(B) ^{1}H-^{15}N HSQC spectra of the RIM2 C2A domain before (black) and after (red) addition of unlabeled SNAP-25 in the presence of 10 mM Ca^{2+}.

(C) ^{1}H-^{15}N HSQC spectra of the synaptotagmin 1 C2A domain before (black) and after (red) addition of unlabeled RIM2 C2A domain in the absence of Ca^{2+}.

(D) ^{1}H-^{15}N HSQC spectra of the synaptotagmin 1 C2A domain before (black) and after (red) addition of unlabeled RIM2 C2A domain in the presence of 10 mM Ca^{2+}.

(E) ^{1}H-^{15}N HSQC spectra of the synaptotagmin 1 C2B domain before (black) and after (red) addition of unlabeled RIM2 C2A domain in the absence of Ca^{2+}.

(F) ^{1}H-^{15}N HSQC spectra of the synaptotagmin 1 C2B domain before (black) and after (red) addition of unlabeled RIM2 C2A domain in the presence of 10 mM Ca^{2+}.

To investigate whether the RIM2 C2A domain has specific structural features accounting for its functional importance, we turned to X-ray crystallography. Crystals of the rat RIM2 C2A domain grew overnight in 17.5% (w/v) PEG 4000 (polyethylene glycol 4000), 0.2 M $(NH_4)_2SO_4$, and 0.1 M sodium acetate, pH 4.5 at 20 °C (Figure 3.4). The structure was determined by molecular replacement using as a search model an NMR structure of the human RIM2 C2A domain that was deposited in the PDB database (PDB entry 1V27) as part of a structural genomics initiative, but has not been described in the literature. The crystal structure was refined using data to 1.4 Å resolution and the data collection and refinement statistics are summarized in Table 3.1. The ribbon diagram of the rat RIM2 C2A domain shown in Figure 3.5 revealed that like other C2 domains, the structure of the RIM2 C2A domain consists of a β-sandwich formed by two four-stranded antiparallel β-sheets (β1 (residues 730-738), β2 (residues 743-752), β5 (residues 793-800) and β8 (residues 846-851) forming one sheet, and β3 (residues 765-772), β4 (residues 779-784), β6 (residues 812-819), and β7 (residues 829-837) forming the other) with loops emerging at the top and the bottom. The bottom of the domain contains a short 3_{10}-helix in the loop connecting strands 5 and 6, which often contains a short α-helix in other C2 domains, too. No electron density was observed for the loop connecting strands 6 and 7, which is usually called loop 3 and is commonly involved in binding of Ca^{2+} to C2 domains (Rizo and Sudhof, 1998). This loop is ordered in most C2 domains whose structures have been elucidated, but it is highly charged and somewhat longer in the RIM2 C2A domain, which likely results in its greater flexibility.

Two prominent, tetrahedrally shaped difference electron density peaks observed near the bottom loop of the rat RIM2 C2A domain that contains the 3_{10}-helix were attributed to

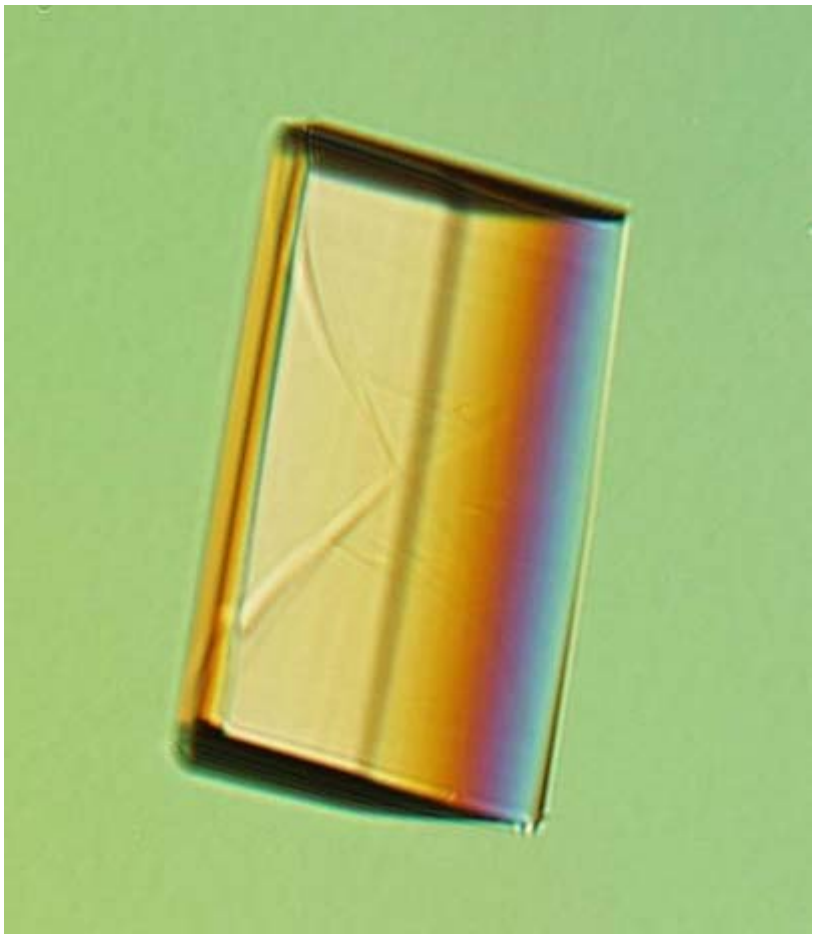

Figure 3.4 Crystallization of the rat RIM2 C2A domain.

Crystals of the rat RIM2 C2A domain were obtained in 17.5% (w/v) PEG 4000, 0.2 M $(NH_4)_2SO_4$, and 0.1 M sodium acetate, pH 4.5 at 20 ºC with a final size of 0.05 mm × 0.05 mm × 0.1 mm.

two sulfate anions (Figure 3.6A). One sulfate ion interacts with the backbone amide nitrogens of arginine 805 and arginine 806, two nitrogens NE and NH2 from the guanidine group of the arginine 806 side chain, and two water molecules. The other sulfate ion is also stabilized by a hydrogen bond with the nitrogen NH1 from the guanidine group of arginine 806 side chain and is coordinated by an additional water molecule. With positively charged residues such as histidine 742, histidine 804, arginine 805, arginine 806, and arginine 809, the electrostatic potential surrounding the bottom loops helps to stabilize the binding of anions. The presence of the two sulfate anions in the crystal structure of the rat RIM2 C2A domain suggested that the region around the bottom 3_{10}-helix might have the potential to participate in electrostatic interactions and provide a suitable environment for binding to the negative charged residues of interacting molecules. The bottom 3_{10}-helix exhibits a highly charged amino acid composition of RRDFRE. Figure 3.6B shows a ribbon-and-stick diagram illustrating the relative orientations of the side chains in this region, which includes the arginine 805 side chain, with the three arginine residues residing on the outside whereas one hydrophobic and two acidic residues pointing to the interior. Interestingly, the arginine 805 of the rat RIM2α C2A domain is in a position equivalent to arginine 844 of the human RIM1α C2A domain, which has been identified as a mutation site (to histidine) in CORD7 patients (Johnson et al., 2003). The exposed nature of this side chain suggests that the arginine to histidine mutation should not affect the proper folding of the RIM2 C2A domain. Indeed, most of the resonances in the ^{1}H-^{15}N HSQC spectrum of the ^{15}N-labeled R805H mutant RIM2 C2A domain are identical to those of wild type, demonstrating the similarity of the structure of the mutant and wild type proteins (Figure 3.7). Introduction of the R805H

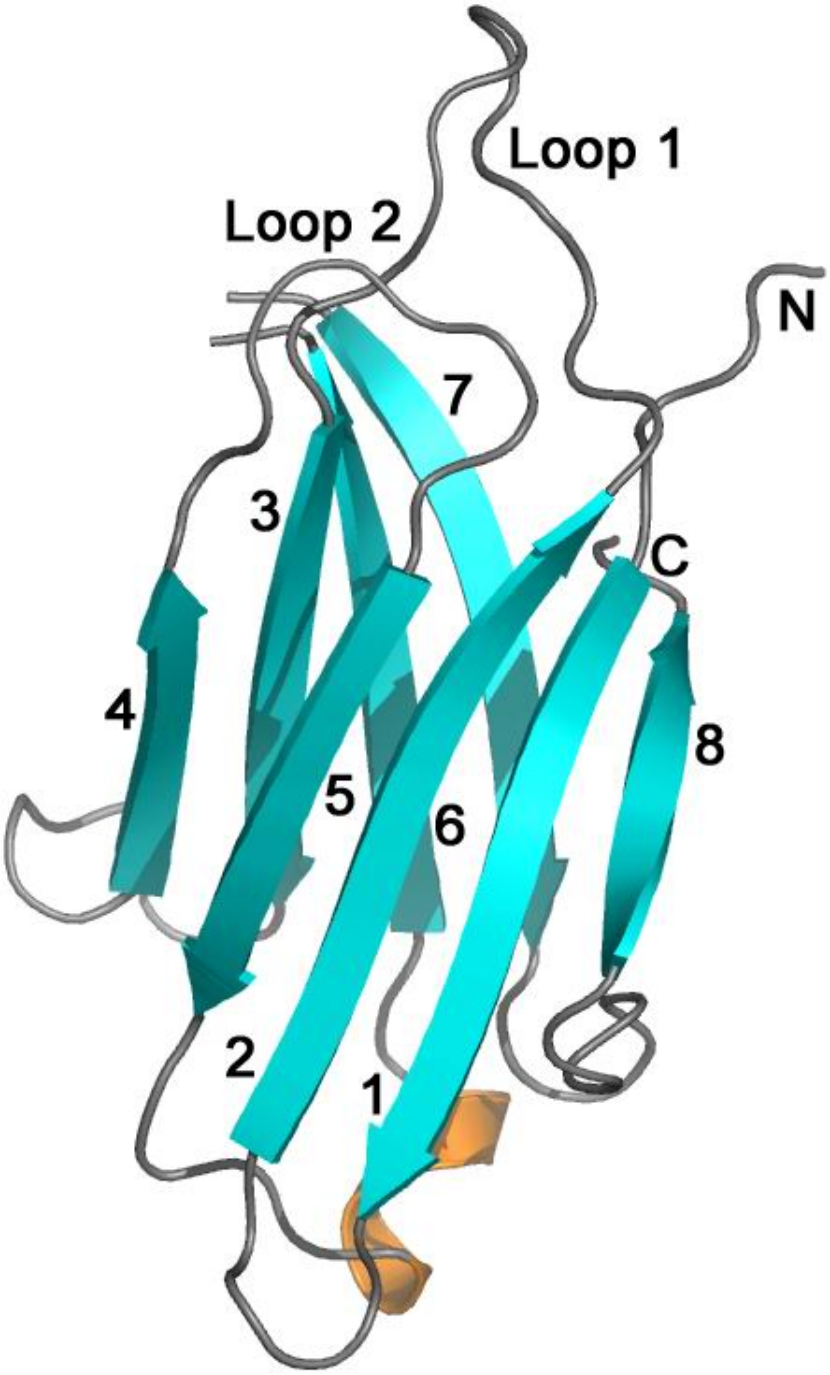

Figure 3.5 Ribbon diagram of the rat RIM2 C2A domain.

The β-strands are colored in cyan and labeled from 1 to 8. The 3_{10}-helix is colored in orange. The canonical Ca^{2+}-binding loops are labeled loop 1 and loop 2 (loop 3 is disordered). N and C indicate the N- and C-termini, respectively.

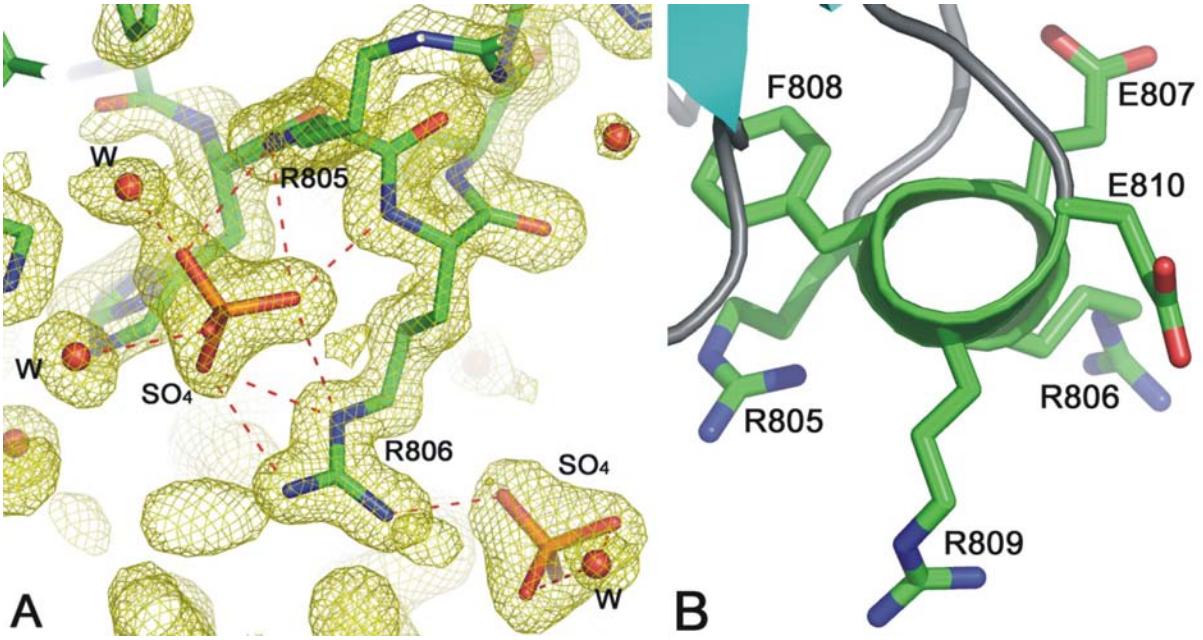

Figure 3.6 Binding of sulfate ions to a positively charged region at the bottom of the RIM2 C2A domain.

(A) A $2F_o$ - F_c electron density map contoured at 1σ of the bottom loop of the rat RIM2 C2A domain where two sulfate ions bind. Oxygen atoms are colored in red, nitrogen atoms in blue, sulfur atoms in orange, and carbon atoms in green. Water molecules hydrogen bonded to the two sulfate ions are labeled W.

(B) Ribbon-and-stick representation of the bottom 3_{10}-helix viewed along the helix axis.

mutation only induced minor perturbations in a few crosspeaks of the ^{1}H-^{15}N HSQC spectrum of the rat RIM2 C2A domain, which are probably corresponding to residues in close proximity to arginine 805 in the structure of the wild type protein (Figure 3.7). The thermal denaturation profiles of both wild type and the R805H mutant RIM2 C2A domain monitored by CD spectroscopy revealed only about 2-3 °C decrease of the denaturation transition temperature for the R805H mutant compared to the wild type, confirming that the overall structural and stability perturbation caused by the R805H mutation was minimal (Figure 3.8). Thus, it is most likely that the mutation causes disease by interfering with an interaction(s) of the RIM C2A domain with a target molecule. The observation of the two bound sulfate ions in the crystal structure of the rat RIM2 C2A domain, which might mimic the negative charges of a target, also suggests that this region may act as an interaction site through its multiple positively charged residues.

The potential importance of electrostatic forces for the interactions of the RIM C2A domain was further emphasized by examination of its surface electrostatic potential. Intriguingly, this analysis revealed a striking dipolar distribution, with a highly positively charged surface on the edge of the β-sandwich that includes the 3_{10}-helix region at the bottom, and a highly negatively charged surface on the opposite edge (Figure 3.9). The positively charged edge is formed by strands 4 and 5, and its highly positive potential is due in part to the abundance of basic residues in strand 4. The opposite edge of the β-sandwich is formed by strands 7 and 8, both of which contain negatively charged residues. Overall, the basic and acidic residues that lead to the dipolar character of the rat RIM2 C2A domain are generally conserved in the RIM C2A domains (Figure 3.10). Correspondingly, analysis of the

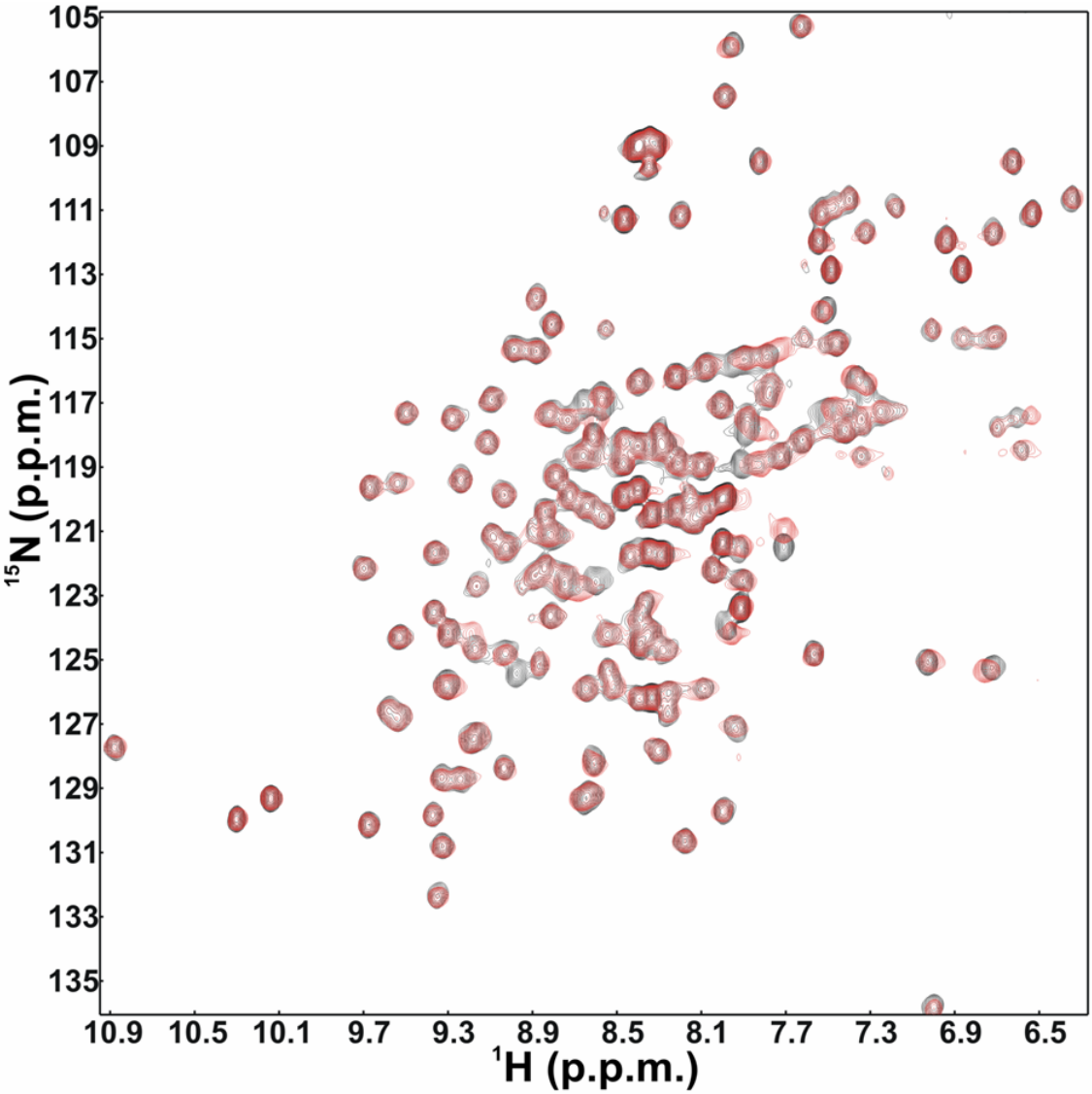

Figure 3.7 R805H mutation in RIM2 C2A domain does not affect its proper folding.

^{1}H-^{15}N HSQC spectra of the RIM2 C2A domain wild type (black contours) and R805H mutant (red contours) are shown.

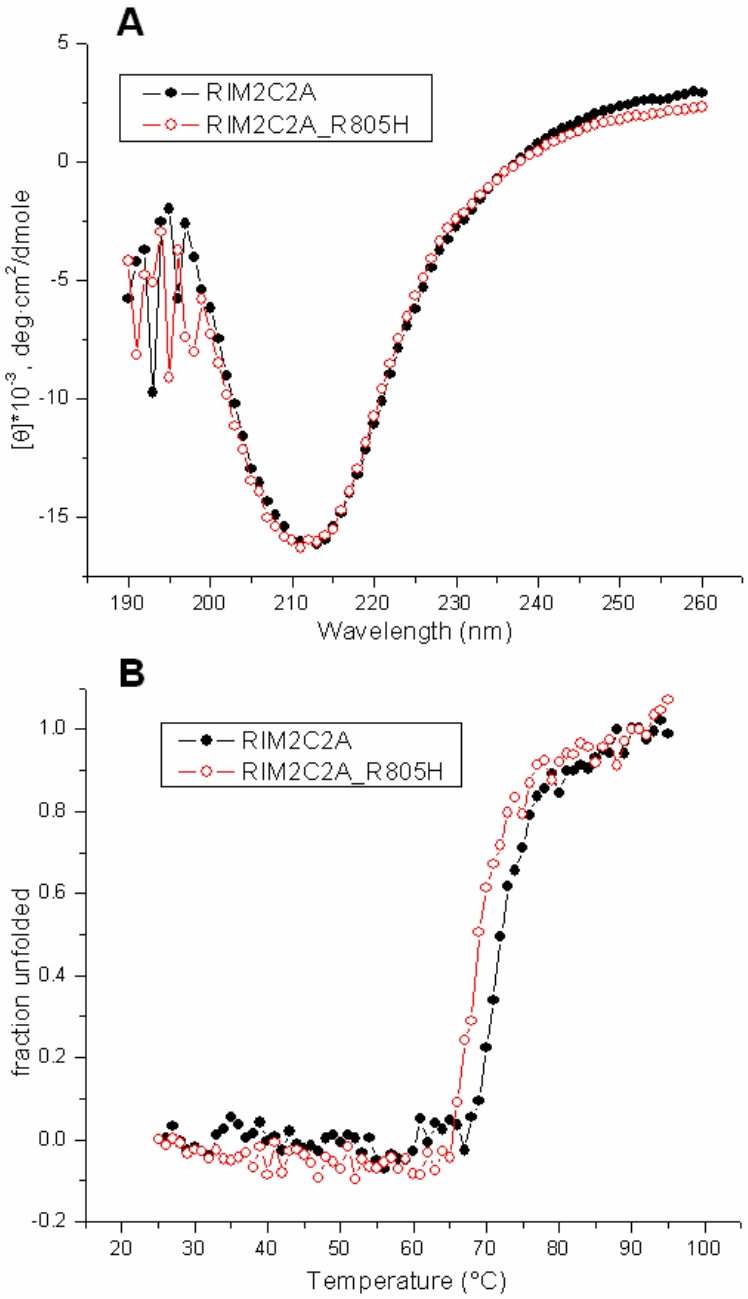

Figure 3.8 The far-UV circular dichroism (CD) spectra and the thermal denaturation profiles monitored by CD spectroscopy of the wild-type RIM2 C2A domain and R805H mutant.

(A) The CD spectra of the wild type RIM2 C2A domain (black solid circles) and R805H mutant (red open circles).

(B) The thermal denaturation profiles monitored by CD spectroscopy of the wild type RIM2 C2A domain (black solid circles) and R805H mutant (red open circles).

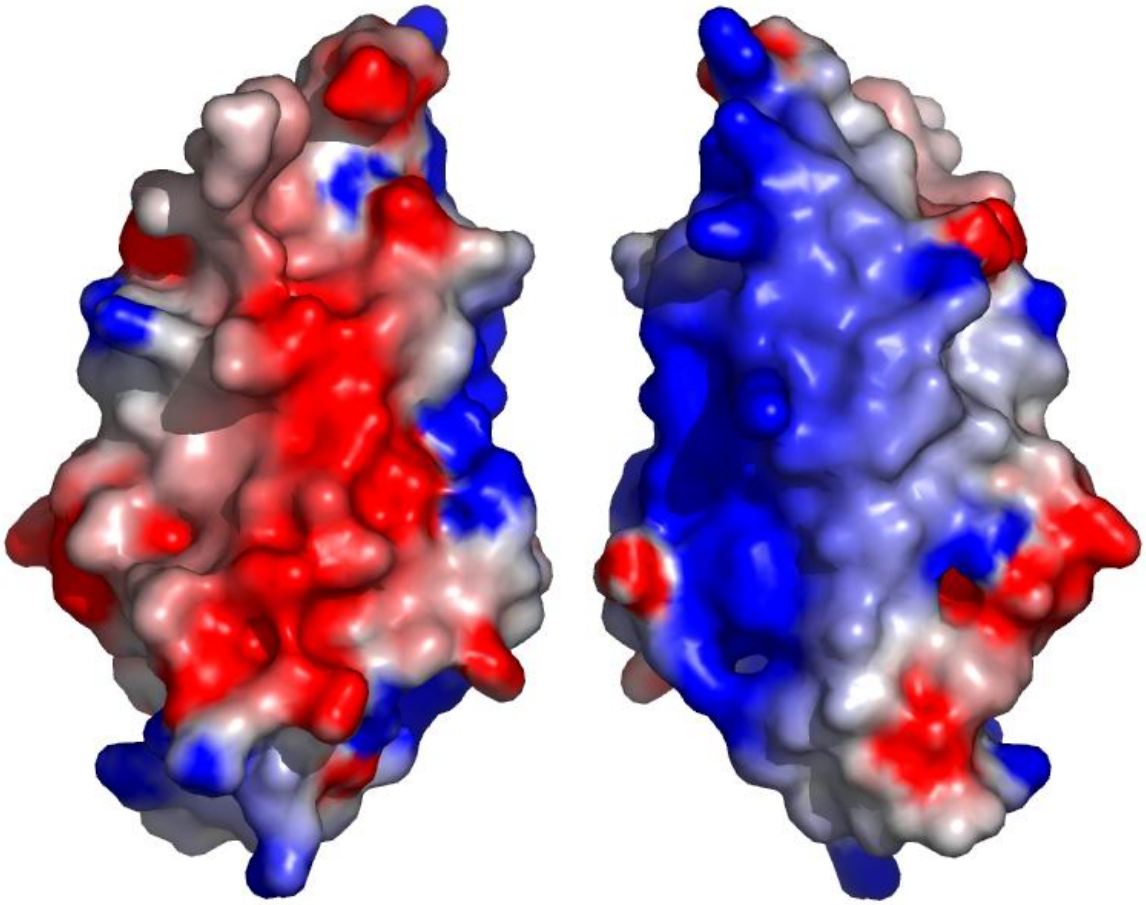

Figure 3.9 RIM2 C2A domain with a dipolar distribution of electrostatic charges.

Two views of the surface electrostatic potential of the rat RIM2 C2A domain rotated 180° with respect to the vertical axis are shown. In the left panel, strands 7 and 8 are in the front; while in the right panel, strands 4 and 5 are in the front. Hydrogen atoms were generated using CNS, and the surface electrostatic potential was computed with GRASP and rendered with PyMol. The electrostatic potential is contoured at the 5 kT/e level, with red denoting negative potential and blue denoting positive potential.

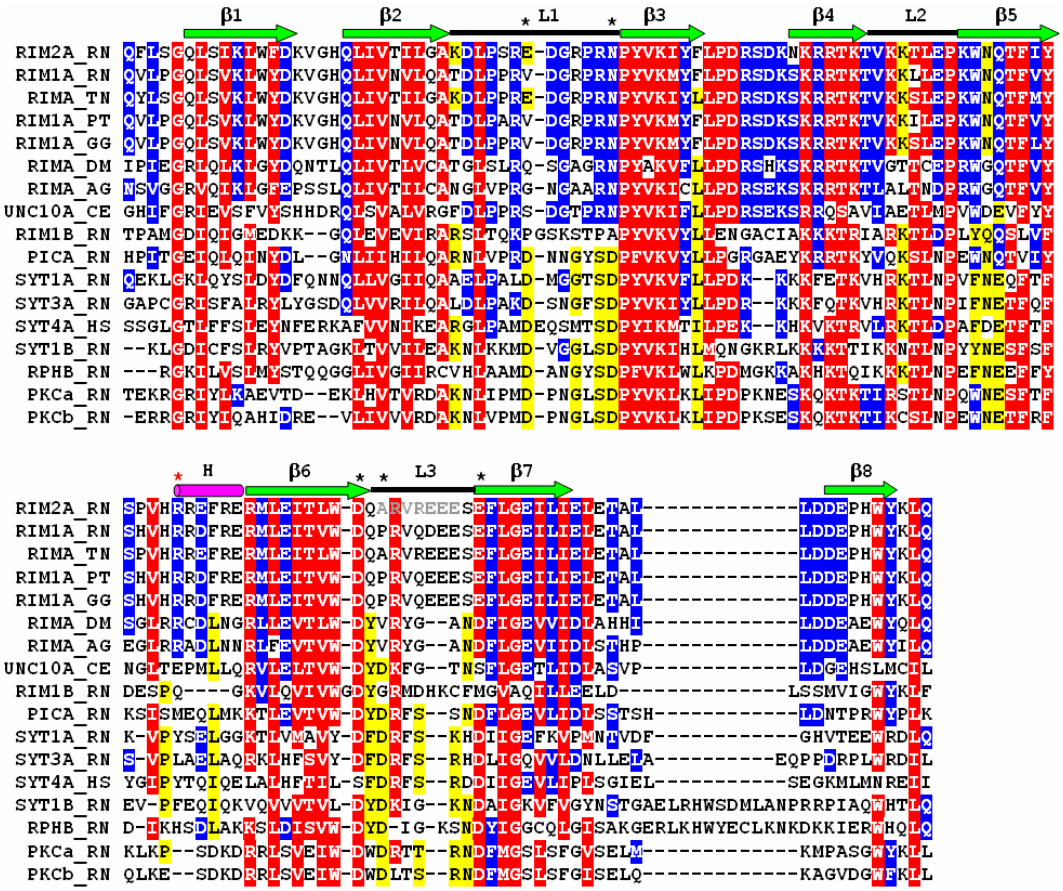

Figure 3.10 Sequence alignment of the RIM C2A domains from different species and selected rat C2 domains.

Residues conserved in most C2 domains (>80% of the sequences displayed; E = D, K = R, N = Q, L = V = I = M, F = Y, and S = T) are colored white with a red background. Residues that appear to be selectively conserved in RIM C2A domains are colored white with a blue background. Residues that appear to be selectively conserved in other C2 domains, but not in RIM C2A domains, are colored black with a yellow background. Residues invisible in the rat RIM2 C2A domain structure are colored gray. The secondary structure elements of the rat RIM2 C2A domain are shown at the top of the alignment. The three top loops that are usually involved in binding of Ca^{2+} to C2 domains, the 3_{10}-helix, and the β-strands are represented by black bars, a magenta cylinder, and green arrows, respectively. The black asterisks indicate the positions of the five aspartate residues that are commonly involved in binding of Ca^{2+} to C2 domains. The red asterisk indicates the position corresponding to the mutation site involved in CORD7. Piccolo, synaptotagmin, and rabphilin are abbreviated PIC, SYT, and RPH, respectively. A and B at the end of the protein name refers to the C2A domain and the C2B domain, respectively. Species abbreviations: RN, rat; HS, human; PT, chimpanzees; GG, chicken; TN, spotted green puffer fish; DM, fruit fly; AG, mosquito; and CE, round worm.

surface electrostatic potential in models of the RIM C2A domains from different species, built by homology modeling with the crystal structure of the rat RIM2 C2A domain, also revealed a dipolar charge distribution, although this dipolar character is less pronounced in the unc10 C2A domain because of a lower degree of conservation of the charged residues.

3.3.3 Comparison of the RIM C2A Domains with Other C2 Domains

C2 domains usually form β-sandwiches that can have two different topologies resulting from a circular permutation of the β-strands, referred to as topology I and II, as mentioned in chapter 1 (Rizo and Sudhof, 1998; Nalefski and Falke, 1996). The structure of the RIM C2A domain conforms to topology I, which is also observed in other C2 domains involved in intracellular membrane traffic such as those from synaptotagmins (Fernandez et al., 2001; Sutton et al., 1995; Dai et al., 2004; Shao et al., 1998; Sutton et al., 1999) and rabphilin (Ubach et al., 1999), as well as in some C2 domains involved in signal transduction such as those of PKCs (Sutton and Sprang, 1998; Verdaguer et al., 1999). A structural comparison performed with DALI (Holm and Sander, 1993) revealed that, as expected, the RIM2 C2A domain is closely structurally similar to other C2 domains. The highest Z score yielded by DALI in the search (18.2) corresponds to the crystal structure of the synaptotagmin 1 C2A domain (Sutton et al., 1995), which exhibits a trace rms deviation of 1.7 Å for 119 equivalent Cα atoms with respect to the RIM2 C2A domain. A trace superposition of the synaptotagmin 1 and RIM2 C2A domains (Figure 3.11A) shows that there is a remarkable similarity between the two structures in the β-sheets, and that differences occur largely at a few loops connecting the β-strands, particularly at the C-

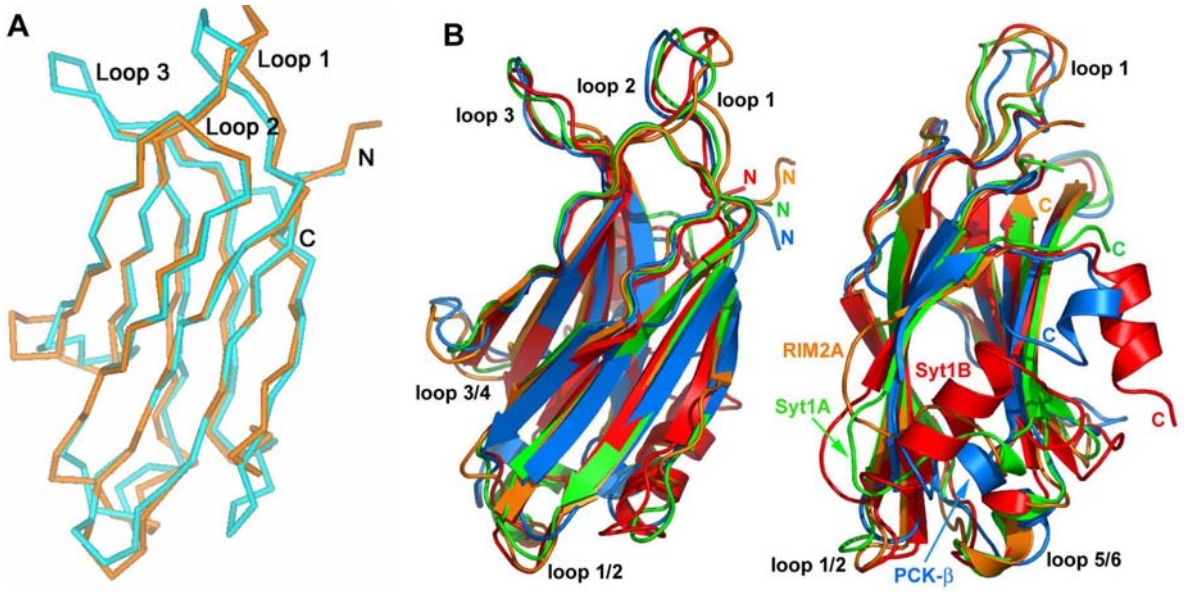

Figure 3.11 Comparison of the structures of the RIM2 C2A domain and other C2 domains.

(A) Cα trace superposition of the RIM2 C2A domain (orange) and the synaptotagmin 1 C2A domain (cyan).

(B) Two different views of ribbon superpositions of the RIM2 C2A domain (orange), the synaptotagmin 1 C2A domain (green) and C2B domain (red), and the PKCβ C2 domain (blue). The positions of the top loops commonly implicated in Ca^{2+} binding, as well as the N- and C-termini, are indicated in panels A and B. In panel B, the positions of the loops connecting strands 1 and 2, strands 3 and 4, and strands 5 and 6 are labeled as loop 1/2, loop 3/4, and loop 5/6, respectively, and the position of the loop connecting strands 7 and 8 is indicated with the color-coded name of the protein.

terminal loop connecting strands 7 and 8. Indeed, ribbon superpositions of the known C2 domain structures revealed that the conformation of this loop is highly variable in C2 domains, as illustrated with the RIM2 C2A domain, the synaptotagmin 1 C2A domain and C2B domain, and the PKCβ C2 domain in Figure 3.11B. Note that some degree of diversity is observed in the structure of most loops and, in some cases, they can diverge considerably; for instance, the cPLA2 C2 domain contains an α-helix inserted in loop 1 (Perisic et al., 1998). However, the high variability of the loop connecting strands 7 and 8 in basically all C2 domains is particularly pronounced.

The alignment shown in Figure 3.10 compares the sequences of the RIM C2A domains from different species together with those of the rat RIM C2B domain and of other rat C2 domains with type I topology. The alignment illustrates that the C-terminal sequences of C2 domains are in general more variable than the remaining sequences, particularly in the region connecting strands 7 and 8. This observation correlates with the structural diversity in this region. However, it is noteworthy that this region exhibits a relatively high degree of conservation in RIMs, and is included among several regions that are conserved in RIMs but differ in other C2 domains (highlighted in blue in Figure 3.10; note that these regions may still be conserved in different species for a given C2 domain). Interestingly, the strand 7-strand 8 region contains several acidic residues that are selectively conserved in RIM C2A domains and that contribute to their dipolar character. Strand 4 and adjacent sequences, which also contribute substantially to this dipolar character, contain several basic residues that are selectively conserved in RIM C2A domains. However, this region is basic in most C2 domains, particularly in the synaptotagmin 1 C2B domain (Fernandez et al., 2001), and

thus includes basic residues that are conserved throughout the C2 domain family (highlighted in red in Figure 3.10). Overall, these observations suggested that the striking dipolar nature is a unique property of the RIM C2A domains. A survey of the surface electrostatic potential of different C2 domains with known three-dimensional structure revealed that some degree of charge separation is actually observed in several of them, although it is generally not as marked as that observed in the RIM C2A domain (Figure 3.12).

It is also worth noting that loop 3 at the top of the domain, which usually contains three of the aspartate side chains that coordinate Ca^{2+} in Ca^{2+}-dependent C2 domains (Shao et al., 1996) and is directly involved in phospholipid binding (Zhang et al., 1998; Chapman and Davis, 1998), exhibits a relatively low level of sequence conservation in RIM C2A domains. This contrasts with the high level of conservation of residues in the strand 3-strand 4 and strand 7-strand 8 regions at the bottom half of the domain, which also contains the arginine 805 residue that is mutated in RIM1α of CORD7 patients. These observations suggested that the bottom part of the RIM C2A domains might play a key role in their function, in contrast to the preponderant role that the top half plays in Ca^{2+}-dependent C2 domains.

The differences between the RIM C2A domains and the C2 domains from synaptotagmins, rabphilin, and PKCs are emphasized in the dendogram shown in Figure 3.13, which was constructed on the basis of the sequence alignment of Figure 3.10. The dendogram shows that the synaptotagmin, rabphilin, and PKC C2 domains are more closely related to each other than to the RIM C2A domains. This finding does not correlate strictly with the inability of the RIM C2A domains to bind Ca^{2+}, since the synaptotagmin 4 C2A domain is also unable to bind Ca^{2+} (Dai et al., 2004). In addition, the piccolo C2A domain

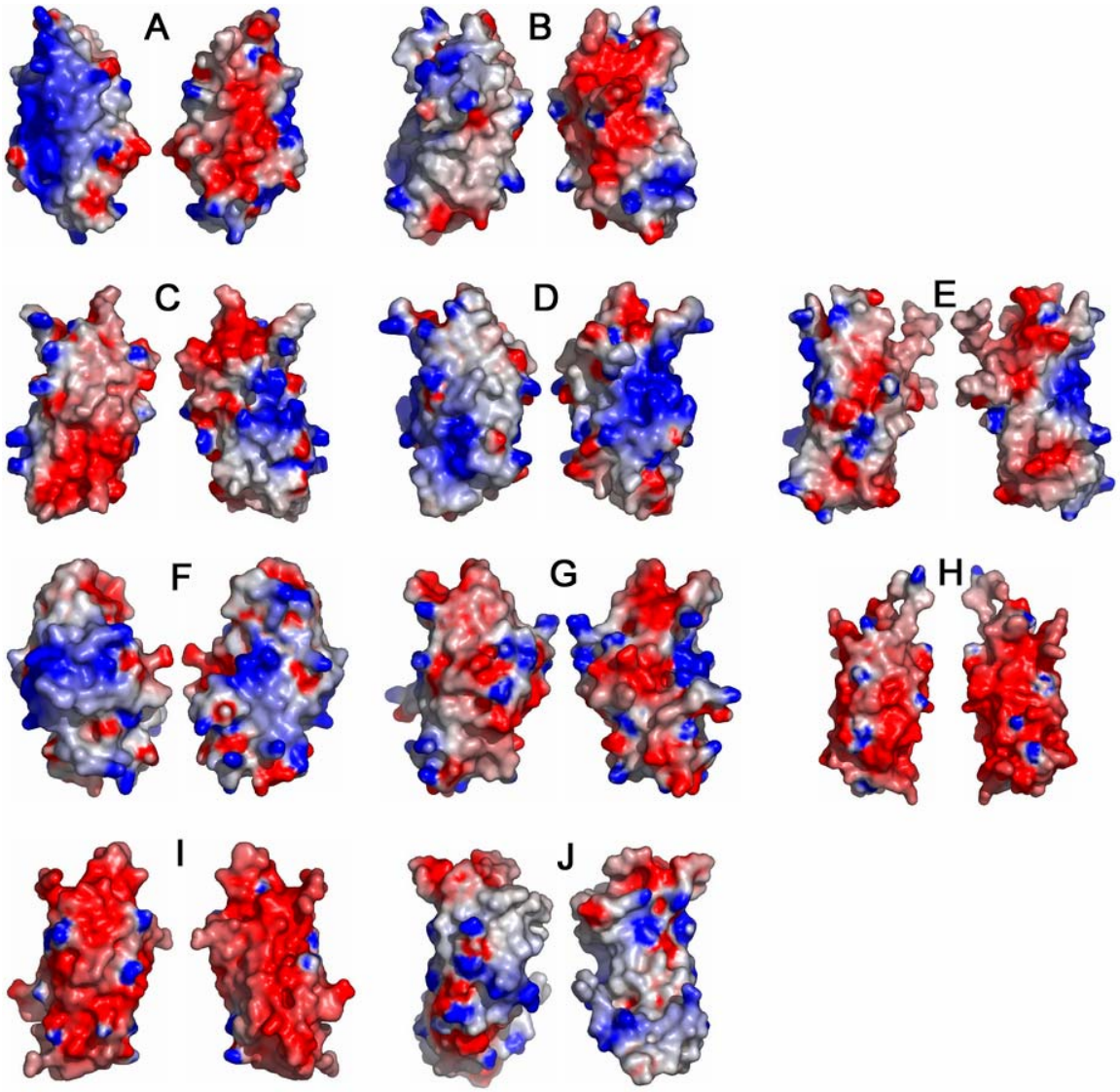

Figure 3.12 Gallery of the surface electrostatic potential of different C2 domains.

Two views of the surface electrostatic potential of each C2 domain are shown (180° rotation around the vertical axis). Hydrogens were generated using CNS, and the surface electrostatic potential was computed with GRASP and rendered with PyMol. The electrostatic potential is contoured at the 5 kT/e level, with red denoting negative potential and blue denoting positive potential. (A) RIM2 C2A domain; (B) Piccolo C2A domain (PDB id 1RH8); (C) Synaptotagmin 1 C2A domain (PDB id 1BYN); (D) Synaptotagmin 3 C2A domain (PDB id 1DQV); (E) Synaptotagmin 4 C2A domain (PDB id 1UGK); (F) PKCα C2 domain (PDB id 1DSY); (G) PKCβ C2 domain ((PDB id 1A25); (H) PKCε C2 domain (PDB id 1GMI); (I) cPLA2 C2 domain (PDB id 1RLW); (J) PLC-δ C2 domain (PDB id 1QAS).

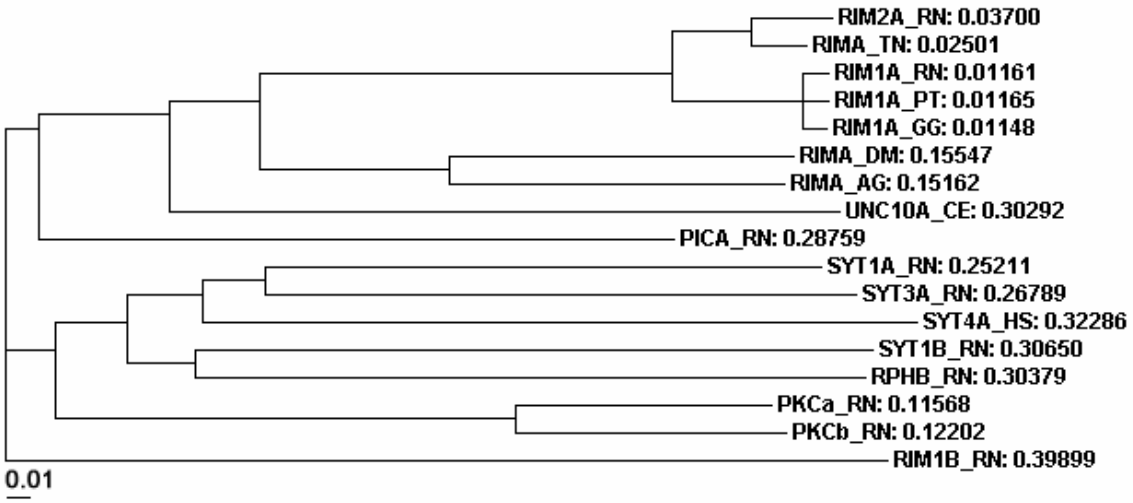

Figure 3.13 Phylogram of RIM C2A domains from different species and selected rat C2 domains.

The tree was generated with ClustalW using the sequence alignment of Figure 3.10. The branch lengths are proportional to the inferred evolutionary change. The scores given at the right reflect the inferred evolutionary change from the closest branch point.

binds Ca^{2+} (Garcia et al., 2004) but is more closely related to the RIM C2A domains than to the synaptotagmin, rabphilin, and PKC C2 domains (Figure 3.13). The rat RIM C2B domain, which is also predicted to be unable to bind Ca^{2+}, appears to be equally distant from the RIM C2A domains and the synaptotagmin, rabphilin, and PKC C2 domains.

3.4 Discussion

RIMs are large, multidomain proteins of the presynaptic active zone that play key roles in synaptic vesicle priming and regulation of short- and long-term presynaptic plasticity (Koushika et al., 2001; Schoch et al., 2002; Calakos et al., 2004; Castillo et al., 2002). These multiple roles are most likely associated with interactions of RIMs with target molecules. Indeed, multiple interactions of the RIM domains with active zone proteins and with proteins implicated in Ca^{2+}-dependent membrane fusion have been described (Wang et al., 1997; Schoch et al., 2002; Betz et al., 2001; Wang et al., 2002; Coppola et al., 2001; Wang et al., 2000), suggesting that RIMs help to organize the active zone and regulate neurotransmitter release by directly influencing the membrane fusion apparatus. However, there is little information about the nature and the relevance of these interactions, as well as about the three-dimensional structures of the RIM domains. This scarcity of structural and biochemical information hinders the development of a molecular understanding of the functions of RIMs, which on the other hand have been extensively characterized by genetic and physiological experiments.

To help develop such an understanding, in this chapter we have focused on the structure and interactions of the rat RIM2 C2A domain. We found that this domain does not

bind Ca^{2+}, as predicted on the basis of the observation that the rat RIM2 C2A domain does not contain the full complement of aspartate residues that form the canonical C2 domain Ca^{2+}-binding motif (Figure 3.10). In addition, our data revealed no significant binding of the rat RIM2 C2A domain to SNAP-25 or to the synaptotagmin 1 C2 domains either in the presence or in the absence of Ca^{2+}. Binding of the RIM C2A domain to SNAP-25 and synaptotagmin 1 had been previously investigated using GST pulldown assays with immobilized GST fusion proteins (Coppola et al., 2001). These experiments were motivated by the observation that the RIM C2A domain contains multiple basic residues in strand 4, which are also present in the synaptotagmin 1 C2B domain and were implicated in its oligomerization as well as in interactions with other targets. However, this polybasic region of the synaptotagmin 1 C2B domain was shown to bind avidly to polyacidic compounds such as DNA and RNA, which are very difficult to remove from immobilized GST fusion proteins and could induce artifactual interactions (Ubach et al., 2001). For instance, the purified synaptotagmin 1 C2B domain was shown to be monomeric in solution (Ubach et al., 2001). Thus, it seems likely that interactions of the RIM C2A domain with synaptotagmin 1 and SNAP-25 observed with GST pulldown experiments (Coppola et al., 2001), which we could not confirm with our NMR experiments, may arise from incomplete removal of acidic contaminants in the immobilized proteins. Indeed, mutations in the polybasic region of the RIM C2A domain abolished binding to synaptotagmin 1 (Coppola et al., 2001), consistent with this proposal. Our NMR data cannot rule out the possibility that the RIM C2A domain interacts with synaptotagmin 1 sequences outside its C2 domains, but it should be noted that no interaction between the RIM C2A domain and synaptotagmin 1 from brain extracts was

observed in separate GST pulldown experiments (Schoch et al., 2002). On the basis of the crucial importance of the RIM C2A domain for proper localization (Deken et al., 2005), it is tempting to speculate that an as yet unidentified interaction with another active zone protein may underlie the primary function of the RIM C2A domain.

The crystal structure of the rat RIM2 C2A domain and the comparison with other C2 domains described in this chapter further emphasize the pattern of conservation and divergence that has been emerging from structural studies of these intriguing protein modules. On one hand, the similarity between the structures of the RIM2 C2A domain and the synaptotagmin 1 C2A domain (Figure 3.11A) shows the high degree of structural conservation of the core of the β-sandwich. On the other hand, this and other structural comparisons between C2 domains (Figure 3.11B) illustrate the variability in the loops connecting the strands of the β -sandwich, which thus appears to act as a scaffold for diverse sequences emerging at the top and the bottom. Particularly striking is the diversity of the loop connecting strands 7 and 8 at the bottom of the domain. While the significance of this diversity remains to be established, the functional importance of the bottom of the RIM C2A domain is supported by the selective conservation of several residues in the strand 7-strand 8 region of the RIM C2A domain, and by the implication of the RIM1α R844H mutation in CORD7 disease. A key functional role for the bottom of the RIM C2A domains would represent a new paradigm for the range of mechanisms of action of C2 domains, which until now have been largely shown to function through the Ca^{2+}-dependent interactions mediated by their top loops. A distinct mechanism of action for the RIM C2A domains would not be surprising, given the observation that the C2 domains of synaptotagmins, rabphilin, and

PKCs are more closely related to each other than to the RIM C2A domains (Figure 3.13). The finding that the RIM2 C2A domain exhibits an unusual dipolar distribution of electrostatic charges that is conserved in most RIM C2A domains suggests that this dipolar character may be critical for its role in neurotransmitter release. In particular, the presence of a highly positively charged surface that includes the arginine mutated in CORD7 patients suggests that an interaction of the RIM C2A domain with a highly acidic target may be crucial for its function. Further research will be needed to test these ideas and identify which interaction(s) mediates the function of the RIM C2A domain. The crystal structure of the rat RIM2 C2A domain described in this chapter provides a framework for understanding the structural basis of its function.

Chapter 4 Studies of the Interaction between Synaptotagmin 1 and the SNARE Complex in Solution

4.1 Introduction

The release of neurotransmitters by synaptic vesicle exocytosis is acutely triggered by Ca^{2+}, exhibiting a fast, synchronous component that emerges in less than half a millisecond after Ca^{2+} influx into a presynaptic terminal, and a slower, asynchronous component (Sudhof, 2004). Extensive genetic and biochemical studies have suggested that synaptotagmin 1 acts as the major Ca^{2+} sensor in fast, synchronous release through both of its cytoplasmic C2 domains (the C2A and C2B domains) (Fernandez-Chacon et al., 2001; Mackler et al., 2002; Rhee et al., 2002), which form similar eight-stranded antiparallel β-sandwich structures and bind three and two Ca^{2+} ions, respectively, via the three top loops at one tip of the β-sandwich (Sutton et al., 1995; Shao et al., 1996; Ubach et al., 1998; Shao et al., 1998; Fernandez et al., 2001). Also critical for neurotransmitter release are the SNARE proteins synaptobrevin/VAMP, syntaxin and SNAP-25, which are central components of the exocytotic machinery. The SNARE proteins form a tight four-helix bundle, which is referred to as the SNARE complex, through their characteristic heptad repeat sequences called SNARE motifs (Sollner et al., 1993a; Poirier et al., 1998b; Sutton et al., 1998). Assembly of this complex brings the synaptic vesicle and plasma membranes together (Hanson et al., 1997) and is likely key for membrane fusion (Rizo and Sudhof, 2002; Brunger, 2005). Complexins, small soluble proteins that bind tightly to SNARE complexes and are selectively required for normal Ca^{2+}-triggered synchronous release (McMahon et al., 1995;

Reim et al., 2001), appear to be involved in the last step(s) of neurotransmitter release in response to Ca^{2+}.

Both synaptotagmin 1 C2 domains bind to negatively charged phospholipid in a Ca^{2+}-dependent manner through their Ca^{2+}-binding loops (Fernandez et al., 2001; Zhang et al., 1998; Chapman and Davis, 1998; Frazier et al., 2003; Rufener et al., 2005), and mutations that decrease or increase their apparent Ca^{2+} affinity in the presence of phospholipid led to parallel changes in the Ca^{2+} sensitivity of neurotransmitter release, as mentioned in chapter 1 (Fernandez-Chacon et al., 2001; Rhee et al., 2005). Hence, there is little doubt that the Ca^{2+}-dependent phospholipid binding activity of synaptotagmin 1 is crucial for its function in neurotransmitter release. However, a key observation that cannot be explained solely by this activity is that mutating the Ca^{2+}-binding sites of the C2B domain impairs release much more severely than disrupting Ca^{2+} binding to the C2A domain, whereas analogous mutations in the C2A or C2B domain in the context of the tandem C2AB fragment have only mild effects on overall phospholipid binding because the remaining intact C2 domain can still mediate Ca^{2+}-dependent phospholipid binding (Mackler et al., 2002; Fernandez-Chacon et al., 2002; Robinson et al., 2002; Stevens and Sullivan, 2003; Nishiki and Augustine, 2004). A potential explanation for these findings was provided by reports of Ca^{2+}-dependent synaptotagmin 1 oligomerization mediated by the C2B domain (Wu et al., 2003), but extensive evidence has shown that a fragment including both synaptotagmin 1 C2 domains (the C2AB fragment) does not oligomerize in solution or on membranes (Arac et al., 2006; Ubach et al., 2001; Garcia et al., 2000). More recently, studies from our lab revealed a new property that is more likely to underlie the preponderant role of the C2B domain in neurotransmitter release,

namely its ability to bind to two membranes simultaneously upon Ca^{2+} binding, which is not shared by the C2A domain and could cooperate with the SNAREs in promoting membrane fusion (Arac et al., 2006). However, such cooperation could also involve direct synaptotagmin 1/SNARE interactions.

Extensive studies have supported the notion that the binding of synaptotagmin 1 to phospholipid in response to Ca^{2+} influx is one of the mechanisms of synaptotagmin 1 action in neurotransmitter release (Shin et al., 2003; Rhee et al., 2005). However, the existence and significance of the interaction between synaptotagmin 1 and SNARE proteins or the SNARE complex in the presence or absence of Ca^{2+} is still under debate. Many studies have described binding of synaptotagmin 1 to syntaxin, to SNAP-25, to syntaxin/SNAP-25 heterodimers and/or to SNARE complexes (Sudhof, 2004; Rizo et al., 2006), but it has been difficult to unravel which of these interactions are physiologically relevant. Thus, studies of which SNAREs bind to synaptotagmin 1, which sequences are involved in binding, and whether the interactions are promoted or decreased by Ca^{2+} have yielded contradictory data (Li et al., 1995; Chapman et al., 1995; Kee and Scheller, 1996; Gerona et al., 2000; Zhang et al., 2002). Moreover, synaptotagmin 1 and the SNAREs are sticky proteins that have been reported to bind to many different targets (for instance, more than 40 interacting molecules for syntaxin have been reported in the literature), suggesting that at least some of the described synaptotagmin 1/SNARE interactions arise from these sticky properties. Nevertheless, Ca^{2+}-dependent interactions between synaptotagmin 1 and the SNARE complexes (Gerona et al., 2000; Zhang et al., 2002; Davis et al., 1999; Bai et al., 2004; Bowen et al., 2005) are attractive from a mechanistic point of view because synaptotagmin 1 acts at the Ca^{2+}

triggering step of neurotransmitter release and SNARE complexes are believed to contribute to membrane fusion during this last step. On the other hand, Ca^{2+}-independent interactions between synaptotagmin 1 and SNARE complexes might be required for positioning of the synaptotagmin 1 on the docked synaptic vesicle close to the presynaptic plasma membrane before Ca^{2+} influx, ready to trigger the membrane fusion and enabling the fusion event to be extremely fast and precise. As Ca^{2+} enters the presynaptic nerve terminal, synaptotagmin 1 can quickly bind to the nearby membranes, dissociate from the SNARE complex or remain associated with the SNARE complex (in a similar or different mode compared to that in the absence of Ca^{2+}), and lead to the occurrence of membrane fusion and release of neurotransmitters. Our aim is to study the interactions between synaptotagmin 1 and the SNARE complex in the presence or absence of Ca^{2+} and their roles in neurotransmission.

In this chapter, we carried out studies on the interactions between synaptotagmin 1 and the SNARE complex in the presence or absence of Ca^{2+} in solution using their soluble fragments, trying to understand how the functions of synaptotagmin 1 and SNAREs might be coupled. We found that the synaptotagmin 1 C2AB fragment can interact with longer versions (compared to the core complex which consists of solely the SNARE motifs) of SNARE complex: SC, composed of syntaxin 1A (180-264), synaptobrevin 2 (1-96), SNAP-25 (11-82-W)/ SN I, and SNAP-25 (141-203-W)/ SN III or SC2, containing synaptobrevin (29-93) instead of synaptobrevin (1-96), using ^{15}N-edited one-dimensional (1D) NMR method. However, using size exclusion chromatography, we only observed the interactions between synaptotagmin 1 and SC/SC2 in the presence, but not in the absence of Ca^{2+}. In addition, we found that introduction of complexin I (26-83) into the ^{15}N-edited 1D NMR

binding experiment could cause the partial recovery of the amide proton signal of ^{15}N-labeled synaptotagmin 1 C2AB fragment, suggesting that complexin competes with synaptotagmin 1 for SNARE complex interaction in solution. This observation also suggested a possible role of the synaptobrevin C-terminus in binding to synaptotagmin 1. Indeed, the SNARE complex containing a C-terminal truncated synaptobrevin 2 (29-76) is unable to interact with synaptotagmin 1 in the ^{15}N-edited 1D NMR binding assay. We also tried to use isothermal titration calorimetry (ITC) to determine the binding stoichiometry and affinity of the interaction between synaptotagmin 1 and the SNARE complex, which failed to yielded meaningful results, yet unexpectedly, revealed a weak interaction between GST and the SNARE complex.

4.2 Materials and Methods

4.2.1 Recombinant Protein Preparation

DNA construct encoding GST fusion proteins of the SNARE motif of rat syntaxin 1A (amino acids 180-264) subcloned in the pGEX-KT expression vector was generously provided by Jiong Tang from Dr. Thomas C Südhof's laboratory. DNA constructs encoding GST fusion proteins of the SNARE motifs of rat synaptobrevin 2 (amino acids 1-96 or amino acids 29-93), and human SNAP-25 (amino acids 11-82 and amino acids 141-203, both containing an additional tryptophan residue at the C terminus to facilitate detection by UV absorption; abbreviated as SN I and SN III respectively) as well as rat complexin I (amino acids 26-83) were prepared using custom-designed primers and standard PCR cloning

techniques, and subcloned into the pGEX-KT expression vector previously in our lab. DNA constructs encoding GST fusion proteins of synaptotagmin 1 C2A domain (amino acids 140-267), C2B domain (amino acids 271-421) and C2AB fragment (amino acids 140-421) were subcloned into the pGEX-KG expression vector previously in out lab. Rat synaptobrevin 2 truncation constructs (amino acids 29-56 or amino acids 29-76) were generated by site-directed mutagenesis (Stratagene) to mutate the residue after the truncation site to a stop codon, according to the manufacturer's protocol. Each plasmid was transformed into *Escherichia coli* BL21 cells for protein expression. Glycerol stocks (8% glycerol) of the transformed cells were kept at -80 ºC.

For a routine 1 liter bacteria culture of the SNARE motifs, 50 ml luria broth (LB) media was inoculated with a single colony from an agar/ampicillin plate and incubated in the shaker at 250 rpm (revolutions per minute) overnight at 37 ºC. The next day, proper amount of culture (usually 10-20 ml) was transferred to 1 liter LB media to make sure that the starting OD_{600} was around 0.1. All the media contained 50 μg/ml ampicillin to maintain the presence of the transformed plasmids. Whenever isotope labeling was necessary, M9 minimal media were used instead of LB media. 1 liter M9 media contains: 6.8 g Na_2HPO_4, 3.0 g KH_2PO_4, 0.5 g NaCl, 1.0 g NH_4Cl, 2.0 mM $MgSO_4$, 100 μM $CaCl_2$, 2.5 mg thiamine, and 4.0 g D-glucose. Uniform ^{15}N labeling was achieved by using M9 minimal media prepared with $^{15}NH_4Cl$ instead of the unlabeled NH_4Cl as the sole nitrogen sources. Perdeuteration was achieved by growing bacteria using D2O as the solvent. The flasks were incubated at 37ºC and shaken at 250 rpm till OD_{600} reached 0.6-0.8, then the temperature was lowered to 25 ºC and 0.4 mM IPTG (isopropyl β-D-

thiogalactopyranoside, from Sigma) was added to induce protein expression for overnight (about 15-16 hours). The cells were harvested by centrifugation at 4,000 rpm for 30 min in swing buckets with a rotor JS 4.2 (Model J6-MI centrifuge, Beckman Instruments) and resuspended into 35ml PBS (phosphate buffered saline) buffer (10 mM Phosphate, pH 7.4, 2.7 mM KCl and 137 mM NaCl) containing 10 µl/ml Sigma inhibitor cocktail (Sigma), 0.5 mM AEBSF, 2 mM EDTA, and 5 mM EGTA. The cell suspension was frozen with liquid nitrogen and stored in -80 ºC for further protein purification.

The frozen cells from 1 liter culture were thawed and passed through a high pressure homogenizer (Model EmulsiFlex-C5, Avestin Inc.) for 3 to 4 times. The cell debris was spun down by centrifugation at 18,000 rpm for 30 minutes in a JA-20 rotor with the Beckman centrifuge (model J2-21). The supernatant was filtered with 0.45 µm syringe filter (Nalgene) and mixed with 1.0-1.5 ml slurry of the pre-washed glutathione Sepharose 4B resins (Amersham Pharmacia Biotech.) per liter of culture in the cold room at 4 °C overnight. GST fusion proteins were bound tightly to the glutathione resins, whereas unbound proteins and nonspecifically bound proteins were removed by washing sequentially with 50 ml PBS, 50 ml PBS containing 1% Triton X-100, and 50 ml PBS containing 1M NaCl for two to three times. In the cases of the purification of synaptobrevin 2 fragments and SN I, a benzonase (0.25 units/µl) nuclease treatment for one hour at room temperature in benzonase cleavage buffer (50 mM Tris, pH 8.0, 2 mM $MgCl_2$) was used to remove nonspecifically bound DNA followed by extensively washing with PBS containing 1M NaCl and PBS. The resin was then washed with 3 ml thrombin cleavage buffer (50 mM Tris, pH 8.0, 200 mM NaCl and 2.5 mM $CaCl_2$) for three times, followed by on-resin cleavage with 5-7 units/ml thrombin (from

bovine plasma, Sigma) for three to four hours at room temperature to remove the GST tag and release the proteins with N-terminal extra two residues (GS) from the constructs. The proteins were eluted with elution buffers (20 mM HEPES, pH 7.4, 150 mM NaCl) and further purified by gel filtration chromatography through a Superdex 75 Hiload 16/60 column (Amersham Pharmacia Biotech.). The purity of the preparation was assessed by SDS-PAGE and Coomassie blue staining. The typical yield according to UV absorbance measurements at 280 nm was 3-5 mg per liter of culture.

The expression and purification procedures of complexin I (26-83) were similar to those for the SNARE motifs, except that the complexin I (26-83) was eluted with 20 mM sodium acetate, pH 4.5 after the thrombin cleavage, followed by further purification with cation exchange chromatography through a Source S column (Amersham Pharmacia Biotech.) and gel filtration chromatography through a Superdex 75 Hiload 16/60 column (Amersham Pharmacia Biotech.). The purity of the preparation was assessed by SDS-PAGE and Coomassie blue staining. The typical yield according to UV absorbance measurements at 280 nm was 3-5 mg per liter of culture. The expression and purification procedures of synaptotagmin 1 C2A domain, C2B domain and C2AB fragment were similar to those for the synaptotagmin 4 C2 domains, described in chapter 2, except that synaptotagmin 1 C2AB fragment was expressed at 23 °C overnight and 1% Triton X-100 was included in its resuspension buffer and that the purification of synaptotagmin 1 C2B domain and C2AB fragment included an additional cation exchange chromatography step through a Source S column (Amersham Pharmacia Biotech.). The purity of the preparation was assessed by

SDS-PAGE and Coomassie blue staining. The typical yield according to UV absorbance measurements at 280 nm was 5-7 mg per liter of culture.

4.2.2 NMR Spectroscopy

All NMR experiments were acquired at 27 °C on Varian INOVA500 or INOVA600 spectrometers (Varian, Palo Alto, California, USA) using H_2O/D_2O 95:5 (v/v) as the solvent. The 5% (v/v) D_2O was included to provide the lock signal for the control of the long term stability of the magnetic field. All NMR data were processed with the program NMRPipe (Delaglio et al., 1995) and analyzed with the program NMRView (Johnson and Blevins, 1994).

4.2.3 ^{15}N-edited 1D NMR Experiments

The first increment of a gradient-enhanced ^{1}H-^{15}N HSQC spectrum was acquired to obtain the 1D ^{15}N-edited ^{1}H NMR spectra with both ni (number of t1 increments in the ^{15}N dimension) and phase set to 1. The 1D ^{15}N-edited ^{1}H NMR spectra were acquired at 27 °C on Varian INOVA500 with 3000 transients for total acquisition time of about an hour. A typical experiment was performed by acquiring the 1D ^{15}N-edited ^{1}H NMR spectra of 5 μM ^{15}N labeled sample with or without the addition of 10 μM non-labeled binding partner of interest.

4.2.4 Size Exclusion Chromatographic Binding Assay

Size exclusion chromatographic binding assay was performed with a Superdex S200 10/300 GL column (Amersham Pharmacia Biotech.) on an ÄKTA FPLC™ protein

purification system. The sample of 300 μL was injected into a 500 μL sample loop and eluted through the size exclusion column. The final concentrations of injection samples were usually 5 or 10 μM. The typical binding assay buffer was 20 mM HEPES, pH 7.4, 150 mM NaCl with either 1mM EDTA or 5mM $CaCl_2$. Binding reactions were usually incubated at 4 ºC for two hours before injection into the FPLC system. The fractions were concentrated by trichloroacetic acid (TCA) precipitation and analyzed by SDS-PAGE and Coomassie blue staining.

4.2.5 Isothermal Titration Calorimetry (ITC)

ITC experiments were performed using a VP-ITC system (MicroCal, Northampton, Massachusetts, United States) at 20 °C in a buffer composed of 25 mM HEPES, pH 7.4, 50 mM KCl, 1 mM EDTA, and 0.3 mM TCEP. The proteins were extensively dialyzed against the ITC buffer, centrifuged, and degassed before the experiment. Typically, 500 μM synaptotagmin 1 C2AB fragment was injected in 35 aliquots of 8 μl into a 1.8 ml sample cell containing 25–35 μM SNARE complexes. Data were fitted with a nonlinear least squares routine using a single-site binding model with the software MicroCal Origin™ for ITC, varying the stoichiometry (n), the enthalpy of the reaction (ΔH) and the association constant (Ka), whose reciprocal is the dissociation constant (Kd).

4.2.6 Dynamic Light Scattering (DLS)

Dynamic light scattering (DLS) analysis was performed on a DynaPro dynamic light scattering model 99D instrument equipped with a temperature controlled microsampler

(DynaPro International) using 20 second acquisition time at 20 °C. The purified SNARE complex, synaptotagmin 1 C2AB fragment or equal molar mixture of synaptotagmin 1/SNARE complex were diluted to 1 mg/ml and microfuged at 13,000 rpm for 15 min in a microcentrifuge (Fisher Scientific) before DLS data acquisition. The laser power was adjusted to keep the intensity between 500,000 counts and 2,000,000 counts. The results were then processed with the program Dynamics V6 (DynaPro International). The radii and the size distribution were calculated with the regularization algorithm provided by the program.

4.2.7 Bicinchoninic Acid (BCA) Assay for Protein Concentration Measurement

The constructs synaptobrevin 2 (29-56) and synaptobrevin 2 (29-76) contain no tryptophan and thus their concentrations could not be determined by UV absorbance measurements at 280 nm. Therefore, the protein concentrations of these synaptobrevin truncation constructs were measured with the BCA™ protein assay kit (Pierce). A series of standard bovine serum albumin (BSA) solutions with increasing concentrations (0, 5, 25, 50, 100, 150, 200, and 250 μg/ml) were prepared freshly from the 2 mg/ml BSA stock. Aliquots (0.05 ml) of each standard or the protein samples of unknown concentration were pipetted into appropriately labeled test tubes individually. 1.0 ml of the working reagent (mixture of 50 parts of BCA™ Reagent A with 1 part of BCA™ Reagent B) was added to each tube and thoroughly mixed. All the tubes were then covered by parafilms and incubated at 60 °C for 30 minutes. After incubation, the tubes were cooled to room temperature and the absorbance at 562 nm (OD_{562}) was measured within 10 minutes. The calibration curve was generated by

plotting the OD_{562} values versus the BSA concentrations. The protein concentration in each sample was then determined according to the calibration curve.

4.3 Results

4.3.1 Purification of the SNARE Motifs and Assembly of the SNARE Complex

Previous ^{13}C-edited 1D NMR data from our lab have shown that the SNARE core complex, which contains the SNARE motifs only, doesn't bind to synaptotagmin 1 C2AB fragment efficiently in the absence of Ca^{2+}. The core complex used in the previous binding studies was composed of syntaxin 1A (191-253), synaptobrevin 2 (29-93), SN I, and SN III, which correspond to the minimal sequences involved in the SNARE complex assembly (Sutton et al., 1998) except that the syntaxin SNARE motif was truncated at residue 253. The deletion of six residues at the C terminus of the syntaxin SNARE motif dramatically reduced the aggregation of the assembled SNARE complex (Margittai et al., 2001) and facilitated the NMR study of the core complex, as illustrated in the complexin/SNARE complex studies (Chen et al., 2002). C-terminal tryptophans in SN I and SN III were added to the sequence artificially to enable the UV detection and quantification. We have demonstrated that the C-terminal truncation of syntaxin and the artificial tryptophan appendages do not affect the assembly and stability of the core complex, allowing stoichiometric amounts of the SNARE proteins to assemble almost quantitatively into a SDS-resistant SNARE complex.

Interestingly, GST pulldown experiments performed by Jiong Tang from Dr. Thomas C Südhof's lab showed that both in the presence and absence of Ca^{2+}, the GST fusion protein

of synaptotagmin 1 C2AB fragment (GST-C2AB) is capable of binding to a longer SNARE complex (SC) composed of syntaxin 1A (180-264), synaptobrevin 2 (1-96), SN I, and SN III, which contain longer N- and C- termini than the minimal SNARE motifs in syntaxin and synaptobrevin (Figure 4.1). Therefore, we started trying to characterize the interaction between the synaptotagmin 1 C2AB fragment and this type of SNARE complex (SC) in solution using biochemical and biophysical methods.

In order to assemble the SNARE complex, the SNARE proteins/motifs were expressed and purified separately. The gel filtration chromatograms of the SNARE proteins through the Superdex 75 Hiload 16/60 column (Amersham Pharmacia Biotech.) are shown in Figure 4.2. Syntaxin 1A (180-264) eluted with an apparent molecular weight of 100 kDa, which was consistent with the observation that the SNARE motif of syntaxin formed homotetramers in solution (Misura et al., 2001b) (Figure 4.2A). The synaptobrevin 2 (1-96), SN I, and SN III also eluted earlier than globular proteins with the corresponding molecular weights (Figure 4.2B, 4.2C and 4.2D) due to their lack of secondary and tertiary structures (Fasshauer et al., 1997).

A typical SNARE complex assembly reaction was carried out by mixing 1:1.2:1.2:1.2 stoichiometry (or for some experiments at higher concentration such as those for isothermal titration calorimetry (ITC) experiment, 1:1.5:1.5:2 stoichiometry) of syntaxin 1A (180-264), SN I, SN III, and synaptobrevin 2 (1-96), and incubating overnight. Samples were taken at different time points (5 minutes, 10 minutes, 30 minutes, 1 hour, 2 hours, and overnight) to check the assembly level of the ternary SNARE complex. Since the ternary SNARE complex is SDS-resistant and only denatures above 90 ºC, the assembly of the ternary SNARE

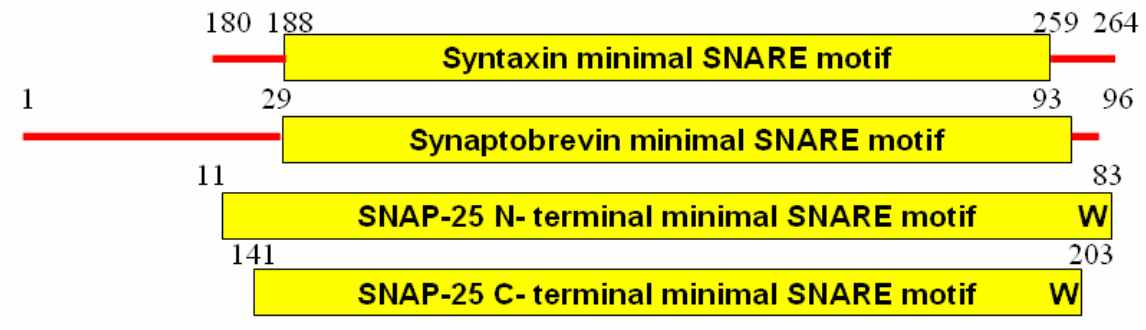

Figure 4.1 Constructs used to assemble the SNARE complex.

The minimal SNARE motifs of rat syntaxin 1A, synaptobrevin 2, SNAP-25 are shown as yellow boxes while the N- and C- terminal extensions of syntaxin and synaptobrevin are shown as red lines. The starting and ending residue numbers of the constructs and the SNARE motifs are labeled. The Ws at the end of SNAP-25 SNARE motifs are trpytophans introduced to facilitate detection by UV absorption.

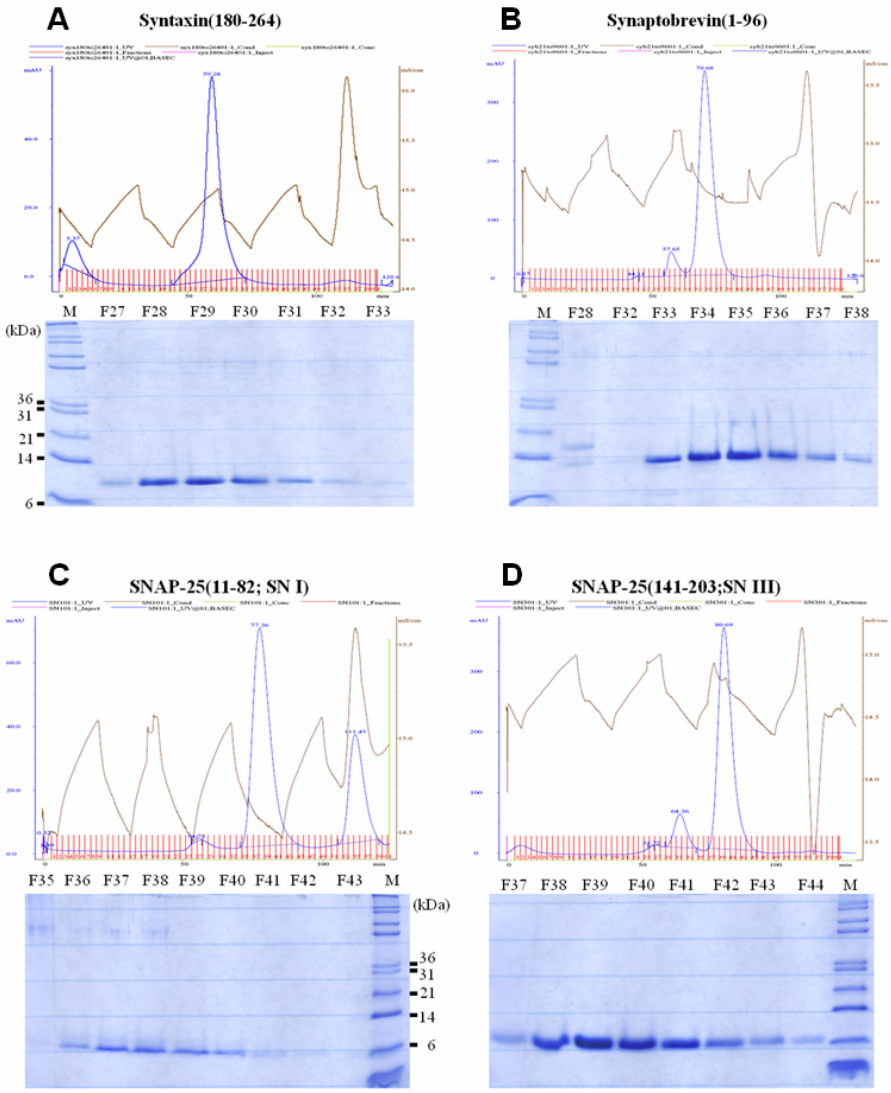

Figure 4.2 Purification of the SNARE proteins used for the SNARE complex assembly.

(A) Gel filtration chromatogram of syntaxin 1A (180-264) and the purified fractions analyzed by SDS-PAGE and Coomassie blue staining.

(B) Gel filtration chromatogram of synaptobrevin 2 (1-96) and the purified fractions analyzed by SDS-PAGE and Coomassie blue staining.

(C) Gel filtration chromatogram of SNAP-25 (11-82-W)/ SN I and the purified fractions analyzed by SDS-PAGE and Coomassie blue staining.

(D) Gel filtration chromatogram of SNAP-25 (141-203-W)/ SN III and the purified fractions analyzed by SDS-PAGE and Coomassie blue staining.

complex can be easily evaluated by comparing the sample with or without boiling and observing the existence of SDS-resistant SNARE complex at about 37 kDa in the non-boiled sample (the lane next to the marker in Figure 4.3A). The assembly efficiency for the SC type of SNARE complex is relatively low, only about 25%, in contrast to >80% assembly efficiency of the core complex. The low assembly efficiency is most likely due to the existence of extra residues in syntaxin and synaptobrevin, especially the C-terminus of syntaxin, which has been shown to oligomerize and tend to induce nonspecific aggregation.

The assembled SNARE complex was firstly purified by cation exchange chromatography with a Mono S column (Amersham Pharmacia Biotech.). Four major peaks were eluted with a gradient of increasing NaCl concentration at 270 mM, 370 mM, 500 mM, and 700 mM NaCl. The cation exchange chromatogram was shown in Figure 4.3A. All of these peaks contained the assembled SNARE complex. The third peak was most enriched with pure SDS-resistant ternary SNARE complex (Figure 4.3A), and thus was pooled and subjected to further purification by gel filtration chromatography with a Superdex 75 Hiload 16/60 column (Amersham Pharmacia Biotech.). The gel filtration chromatogram is shown in Figure 4.3B. Anion exchange chromatography with a Mono Q column was also tested, but didn't give much separation. The purity of the SNARE complex was judged by SDS-PAGE (Figure 4.3B). The absence of isolated SNARE protein bands in the gel demonstrated the purity of the complex.

It has been shown that the syntaxin SNARE motif and SN I can also form a very tight 2:2 parallel four-helix bundle complex (Misura et al., 2001a). Even though the assembly rate of this syntaxin/SN I complex is slow, this type of complex is highly stable once formed and

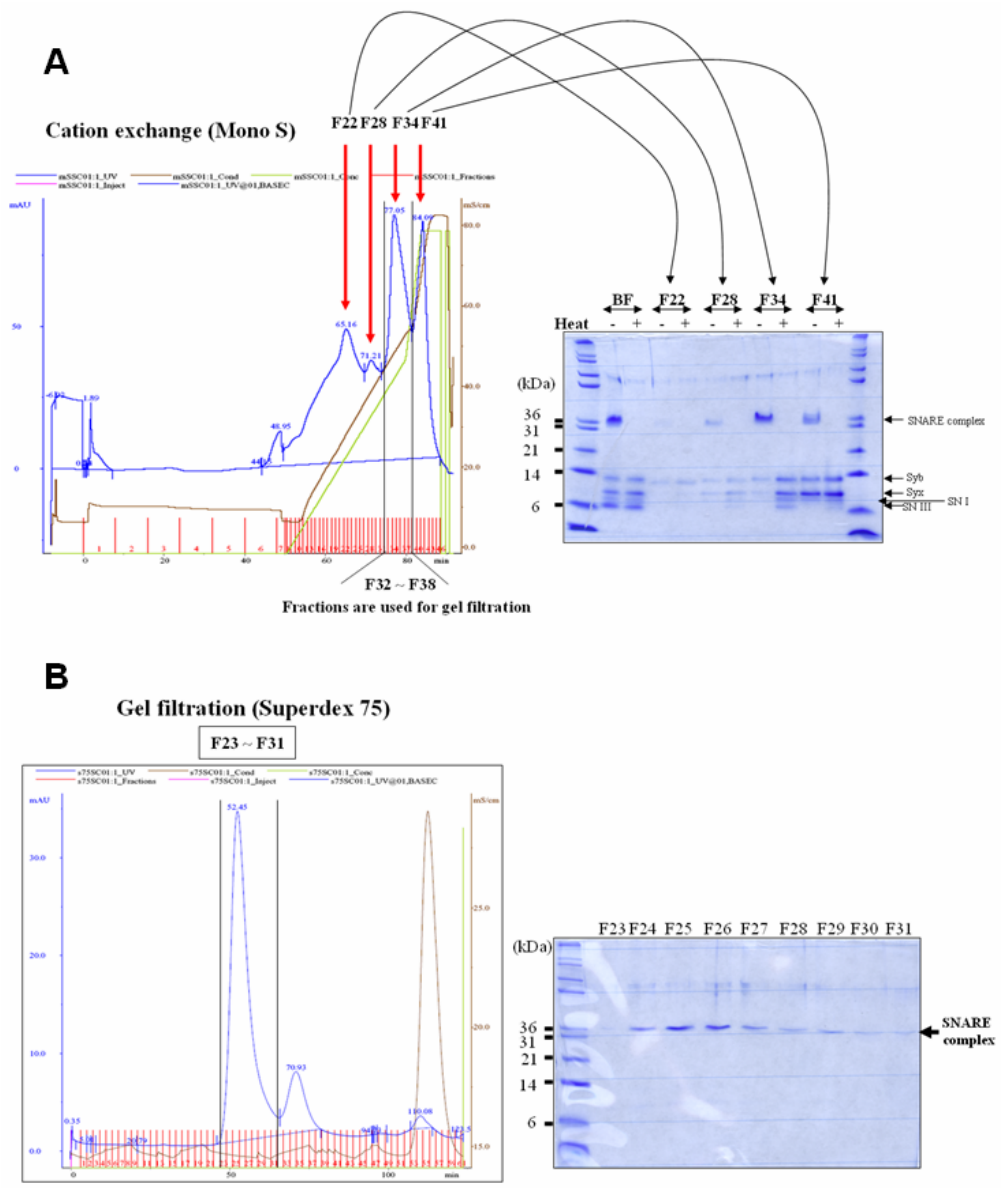

Figure 4.3 Assembly and purification of the SNARE complex SC.

(A) Cation exchange chromatogram of the assembled SNARE complex on a Mono S column and the fractions analyzed by SDS-PAGE and Coomassie blue staining. Four major elution peaks were observed on the Mono S column elution. The SDS-resistant SNARE complex was most enriched in the third peak, which was pooled and subjected to further purification. The fraction BF denotes the sample before chromatographic purification.

(B) Gel filtration chromatogram of the Mono S purified SNARE complex on a Superdex 75 column and the fractions analyzed by SDS-PAGE and Coomassie blue staining.

can function as a kinetic trap for the ternary SNARE complex assembly so that its formation will hinder the formation of the right type of ternary SNARE complex. Bearing this in mind, we need to pay special attention to the order of mixing SNARE proteins for the assembly reaction to avoid the coexistence of the syntaxin SNARE motif and SN I without the presence of the synaptobrevin SNARE motif. A typical order of the mixing in an assembly reaction was firstly, the synaptobrevin SNARE motif, then, SN I, followed by SN III, and finally, the syntaxin SNARE motif.

Another complication came from the observation of the existence of the ternary SNARE complexes in both parallel and antiparallel configurations with a ratio about 3:1 by single molecule fluorescence studies of the SNARE complex assembly in solution even though several biophysical studies, including EM, FRET, EPR and X-ray crystallography showed that the SNARE complex exists in a parallel configuration (Weninger et al., 2003). It has also been shown in this study that the antiparallel configuration is less stable than the parallel configuration and could be almost completely eliminated by high concentration urea treatment. Since the antiparallel configuration is less stable, the corresponding SNARE complex is no longer resistant to SDS and therefore can not be evaluated by the SDS-PAGE even if it forms. To evaluate how much the bi-configuration will affect the longer SNARE complex assembly as well as to improve the poor assembly efficiency of this type of SNARE complex, additional treatment with 5-6 M urea for 2 hours was performed after the assembly reaction and followed by extensive dialysis to remove urea before further chromatographic purification. This treatment did increase the assembly efficiency to a certain level, about 30-35%, but not substantially; therefore this step was not incorporated into the standard

assembly and purification procedure of the longer version SNARE complex SC. Actually, addition of urea in the very beginning of the assembly reaction almost completely abolished the SDS-resistant ternary SNARE complex formation (Dulubova I, personal communication).

4.3.2 Binding Studies of Synaptotagmin 1 and the SNARE Complex by ^{15}N-edited 1D NMR Experiments

^{1}H-^{15}N HSQC experiments, when applicable, constitute a very powerful tool to study protein-protein interactions. For weak interactions, which usually fall into the fast exchange time regime, the binding affinity can be measured by titration of a series of concentrations of a non-labeled protein into a ^{15}N-labeled protein and monitoring the chemical shift perturbations in the ^{1}H-^{15}N HSQC spectra. However, one intrinsic weakness of two-dimensional (2D) NMR spectra is their relatively low sensitivity so that high protein concentrations (typically 50-100 μM) are required for the acquisition of a high quality spectrum in a reasonable amount of time. This problem is especially severe for macromolecules of large molecular weight. The high protein concentrations required tend to promote nonspecific interactions as well as to cause solubility problems. To minimize the nonspecific interactions yet at the same time maintain sufficient sensitivity to study the interaction between synaptotagmin 1 and the SNARE complex, we use a ^{15}N-edited 1D NMR method instead of the commonly used 2D spectra. In a ^{15}N-edited 1D HSQC experiment, only the first trace of a regular 2D ^{1}H-^{15}N HSQC spectrum was recorded so that the resonances that spread out in the nitrogen dimension of 2D ^{1}H-^{15}N HSQC spectra were

merged together and therefore the overall signal intensity was enhanced. In combination with longer acquisition time to boost the signal to noise ratio, low protein concentrations could be used to observe signals even without the help of cold probes. Furthermore, the introduction of higher magnetic fields and cold probes (the radio frequency coils, preamplifier, and other parts of the probe are chilled to approximately 20 K with helium gas) could further shorten the required acquisition time and even lower the required protein concentration.

In a regular 1D proton NMR spectrum, all types of protons can be observed. In contrast, in a ^{15}N-edited 1D HSQC spectrum, only those protons directly bonded to nitrogen nuclei, typically the backbone amide protons of non-proline residues in proteins as well as side chain amide protons of asparagines, glutamines, arginines and tryptophans, are observed around 6-9 ppm (parts per million). When a non-labeled protein is added to the ^{15}N-labeled protein, complex formation will cause an increase of the overall molecular weight and a consequent decrease of overall tumbling rate and increase of transverse relaxation rates. These effects will lead to an increase of the resonance linewidths and a decrease of the resonance intensities. Since the titrant is non-labeled and only contains natural abundance amount of ^{15}N isotopes (about 0.36%), the addition of the titrant won't make any significant contribution to the amide proton signals in the ^{15}N-edited 1D HSQC spectrum and thus no ambiguous compensation will be introduced by the titration. Therefore, the decrease of the amide proton resonance intensities upon addition of non-labeled potential binding partners in the ^{15}N-edited 1D HSQC spectrum indicates binding of non-labeled proteins to the ^{15}N-labeled proteins, whereas no change in the amide proton resonance intensities indicates that no interaction is observed at the concentration tested (Figure 4.4A). This is in sharp contrast

to a closely related 1D NMR method in which the methyl resonances from the aliphatic side chains such as valines, leucines and isoleucines observed around 0.8-0.9 ppm, referred to as the strongest methyl resonance (SMR), is monitored and used to evaluate interactions. In the SMR method, no labeling is involved, which is advantageous. When an interacting titrant is added, the increase of the resonance linewidth caused by the complex formation is compensated by the increase of aliphatic side chain methyl signals introduced by the titrant, resulting in essentially no significant change of the SMR signal upon titration (Figure 4.4B). On the contrary, when a non-interacting titrant is added, only the increase of aliphatic methyl signals takes effect, which is not compensated by the increase of resonance linewidth, resulting in actually gradual increase of the SMR signal upon titration (Figure 4.4B). The disadvantage of the SMR method is that it is difficult to differentiate the contributions from the free binding partners and the binary complex to the signals, which is obviated in the ^{15}N-edited 1D HSQC experiment through selective isotope labeling. However, since the SMR method doesn't require isotope labeling, it is always good to check the SMR signals during the ^{15}N-edited 1D HSQC experiment by acquiring the regular 1D proton NMR spectra.

Previous NMR studies in our lab suggested that the high protein concentration might promote nonspecific interaction between synaptotagmin 1 and the SNARE complexes. Therefore, we decided to apply the ^{15}N-edited 1D NMR method to study the synaptotagmin 1/SNARE complex interaction in solution using low micromolar concentration of proteins. The ^{15}N-edited 1D HSQC spectrum of 5 μM ^{15}N-labeled synaptotagmin 1 C2AB fragment was acquired on a 500 MHz NMR spectrometer for about one hour (Figure 4.5A, spectrum in blue). Addition of 10 μM purified longer SNARE complex (SC) into 5 μM ^{15}N-labeled

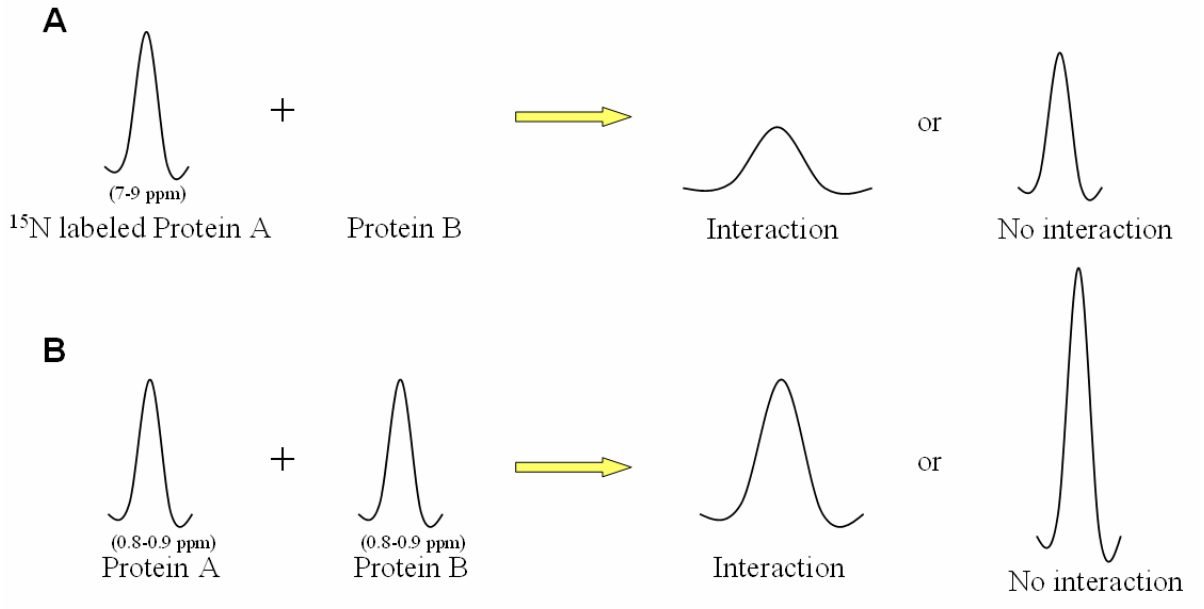

Figure 4.4 Schematic diagrams of the ^{15}N-edited 1D NMR binding assay and the SMR 1D NMR binding assay.

(A) In a ^{15}N-edited 1D NMR experiment, the ^{15}N-labeled protein is mixed with an unlabeled potential binding partner. The amide proton resonances can only be observed for the ^{15}N-labed protein A, as shown on the left. Complex formation between the ^{15}N-labeled protein and the unlabeled protein will result in a decrease of the amide proton resonance intensity, whereas no interaction will not cause any change, as shown on the right.

(B) In a SMR 1D NMR experiment, the strongest methyl resonances can be observed for both protein A and protein B. When equal amounts of protein A and protein B are mixed, no interaction will result in the addition the SMR signals of both proteins into a higher intensity resonance, whereas 100% complex formation will result in comparable resonance intensity to those of the individual proteins.

synaptotagmin 1 C2AB fragment in the absence of Ca^{2+} led to a significant reduction of the amide proton resonance intensities, indicating the binding of synaptotagmin 1 to this type of SNARE complex (Figure 4.5A, spectrum in green). The molecular weights of both the SNARE complex and the synaptotagmin 1 C2AB fragment are roughly 30 kDa so that the formation of their 1:1 stoichiometry complex will double the overall molecular weight. The signal reduction caused by addition of this SNARE complex was actually more than 50%. Thus, at first sight, these data seemed to suggest a more than 1:1 stoichiometry. However, considering the elongated cylindrical shape of the SNARE complex and the known oligomerization of the SNARE complex, which will cause a much slower overall tumbling rate than a globular protein of similar size, the interpretation of the binding stoichiometry was not straightforward. Similarly, in the presence of 5 mM Ca^{2+}, the addition of this SNARE complex also caused the reduction of the amide proton resonance intensities of ^{15}N-labeled synaptotagmin 1 (Figure 4.5B, spectrum in red for before SNARE complex addition and spectrum in orange for after SNARE complex addition), which was more severe than that observed in the absence of Ca^{2+}, suggesting the binding might be stronger in the presence of Ca^{2+}. These results suggested that synaptotagmin 1 C2AB fragment interacts with SNARE complex at low micromolar concentration both in the presence and absence of Ca^{2+}.

4.3.3 Binding Studies of Synaptotagmin 1 and the SNARE Complex by Size Exclusion Chromatographic Binding Assay

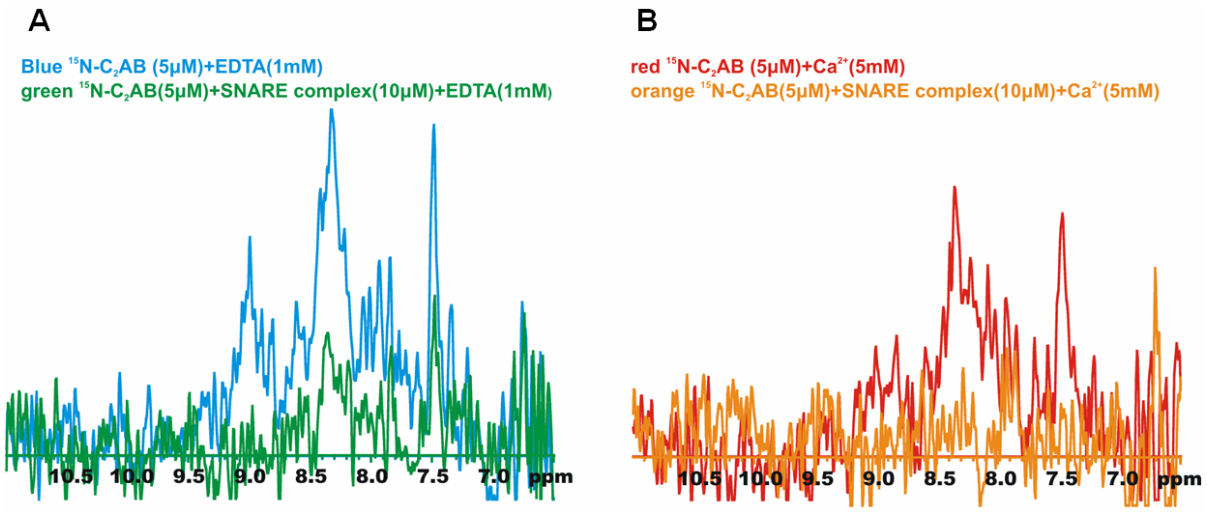

Figure 4.5 Interaction between synaptotagmin 1 C2AB fragment and the SNARE complex analyzed by ^{15}N-edited 1D NMR experiment.

(A) ^{15}N-edited 1D HSQC of 5μM ^{15}N-labeled synaptotagmin 1 C2AB fragment before (blue) and after (green) addition of 10 μM unlabeled SNARE complex in the presence of 1 mM EDTA.

(B) ^{15}N-edited 1D HSQC of 5μM ^{15}N-labeled synaptotagmin 1 C2AB fragment before (red) and after (orange) addition of 10 μM unlabeled SNARE complex in the presence of 5 mM Ca^{2+}.

To use a different method to test the interaction between synaptotagmin 1 and the SNARE complex independently, we performed a size exclusion chromatographic binding assay. 5 μM of synaptotagmin 1 and 5 μM SNARE complex were incubated in the presence of either 1 mM EDTA or 5 mM Ca^{2+} at 4 ºC for two hours before injection into the Superdex S200 10/300 GL size exclusion column (Amersham Pharmacia Biotech.). Synaptotagmin 1 alone or the SNARE complex alone were also injected separately to obtain their elution volumes as references, shown in Figure 4.6. In the absence of Ca^{2+}, synaptotagmin 1 and the SNARE complex migrated separately and did not form a stable binary complex (Figure 4.6A, 4.6B) whereas in the presence of 5 mM Ca^{2+}, synaptotagmin 1 could form complex with the SNARE complex and elute earlier from the column, as shown in the size exclusion chromatograms and the fractions analyzed by SDS-PAGE and Coomassie blue staining (Figure 4.6C, 4.6D). Therefore, the interaction between synaptotagmin 1 and the SNARE complex could only be observed by size exclusion chromatographic binding assay in the presence, but not in the absence of Ca^{2+}. The apparently contradictory results with respect to the synaptotagmin 1/SNARE complex interaction in the absence of Ca^{2+} from the ^{15}N-edited 1D HSQC experiment and the size exclusion chromatographic binding assay might be due to the high off rate of the synaptotagmin 1/SNARE complex binary complex formed in the absence of Ca^{2+}.

4.3.4 Binding Studies of Synaptotagmin 1 and the SNARE Complex Containing a Shorter Synaptobrevin

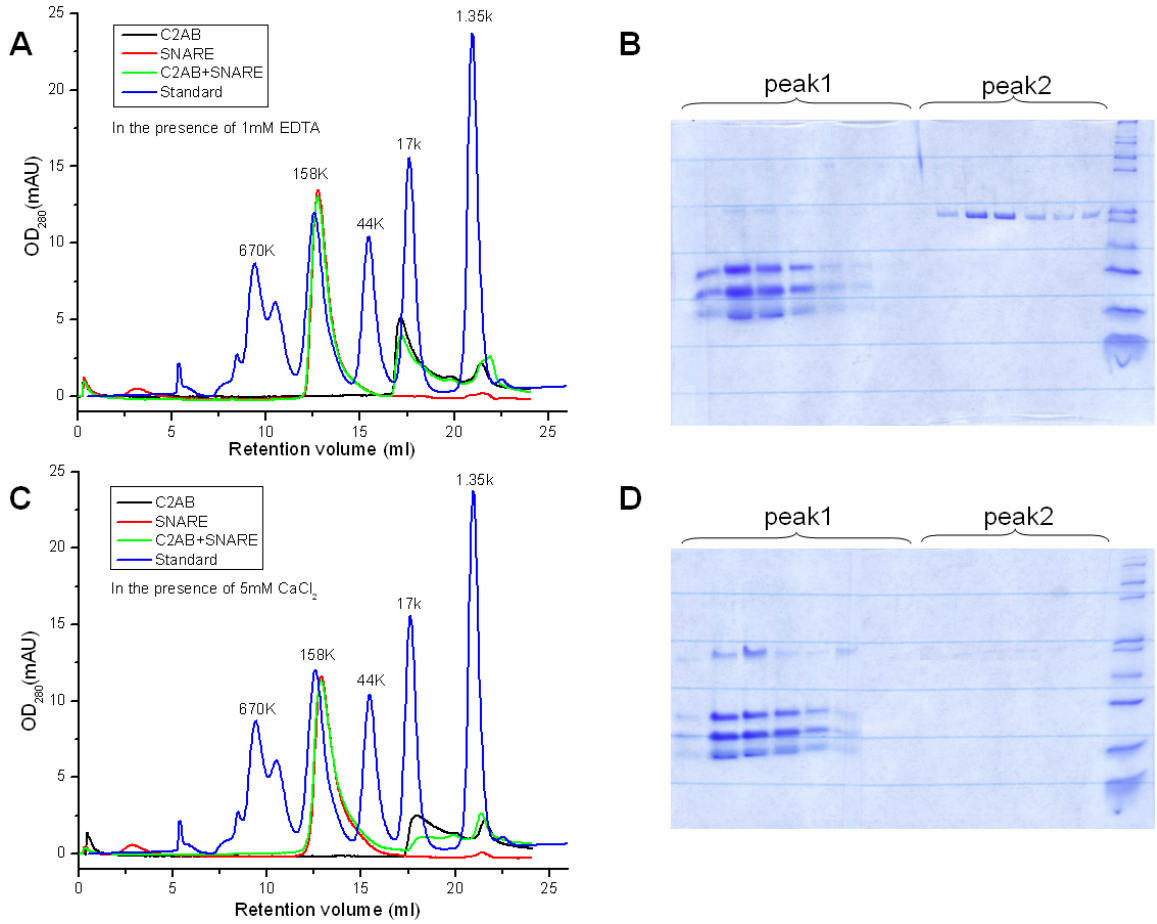

Figure 4.6 Interaction between synaptotagmin 1 C2AB fragment and the SNARE complex by size exclusion chromatographic binding assay.

(A) Size exclusion chromatograms of C2AB alone (black), the SNARE complex alone (red), and the equalmolar mixture of C2AB and SNARE complex (green) in the presence of 1 mM EDTA.

(B) The fractions from the size exclusion chromatographic elution of the equalmolar mixture of C2AB and SNARE complex in the presence of 1 mM EDTA, analyzed by SDS-PAGE and Coomassie blue staining.

(C) Size exclusion chromatograms of C2AB alone (black), the SNARE complex alone (red), and the equalmolar mixture of C2AB and SNARE complex (green) in the presence of 5 mM Ca^{2+}.

(D) The fractions from the size exclusion chromatographic elution of the equalmolar mixture of C2AB and SNARE complex in the presence of 5 mM Ca^{2+}, analyzed by SDS-PAGE and Coomassie blue staining.

After studying the interaction between synaptotagmin 1 and the longer SNARE complex (SC) in solution, we tried to use a shorter synaptobrevin 2 (29-93) that contains merely the SNARE motif instead of the synaptobrevin 2 (1-96) fragment that contains the entire cytoplasmic region to assemble the SNARE complex and test the interaction between the synaptotagmin 1 C2AB fragment and this type of SNARE complex (SC2) by ^{15}N-edited 1D NMR experiment at low micromolar concentration. We decided to carry out this modification due to two reasons: 1) The assembly efficiency for the longer SNARE constructs was low (~25%), which probably resulted from the existence of extra residues in syntaxin and synaptobrevin. 2) The syntaxin 1A (180-264) C-terminal 10 residues tend to cause the oligomerization of the ternary SNARE complexes and consequently a significant increase of their molecular weight, which might hinder further studies via NMR spectroscopy such as binding sites mapping. Removal of about 30 residues from synaptobrevin, if not affecting the binding to synaptotagmin 1 observed for the longer SNARE complex, will decrease the molecular weight of the oligomeric SNARE complex and make further experiments easier.

Similar procedures used for SC assembly and purification were used to assemble and purify the SNARE complex containing the shorter synaptobrevin (SC2). Indeed, removing the 30 extra residues help to increase the assembly efficiency, but only mildly, to about 35%. The ^{15}N-edited 1D NMR results suggested that removal of the sequences outside the synaptobrevin SNARE motif didn't affect the synaptotagmin 1 binding and that the addition of the SNARE complex containing this shorter synaptobrevin (SC2) caused a similar reduction of the amide proton resonance intensities of ^{15}N-labeled synaptotagmin 1 C2AB

fragment (Figure 4.7A, 4.7B). This observation motivated us to try to use deuterium-labeling and ^{1}H-^{15}N TROSY-HSQC based NMR experiments (the principles of which will be explained in more details in chapter 5) to map the binding sites for synaptotagmin 1 on this type of SNARE complex in the absence of Ca^{2+}. This attempt was not successful, presumably due to the large size of the oligomeric SNARE complex. The size exclusion chromatographic binding assay also suggested that SC2 behaved similarly to SC in terms of synaptotagmin 1 binding. SC2 bound to synaptotagmin 1 in the presence, but not in the absence of Ca^{2+}. Even though we couldn't obtain a stable binary complex of SC2 and synaptotagmin 1 by gel filtration chromatography in the absence of Ca^{2+}, dynamic light scattering (DLS) analyses showed that a 1:1 molar ratio mixture of SC2 and the synaptotagmin 1 C2AB fragment at 1 mg/ml concentration in the presence of 1 mM EDTA appeared as a nicely monodispersed single species with a polydispersity index of 15.2%. The equalmolar mixture of C2AB and SNARE complex exhibited a larger average hydrodynamic radius (6.68 nm) and apparent molecular weight (286.5 kDa) than SC2 alone (5.8 nm and 205.9 kDa), suggesting the formation of a synaptotagmin 1/SNARE complex 'hypercomplex' (Figure 4.8). This observation motivated us to set up some preliminary crystallization trials to see if we could obtain the crystal of the synaptotagmin 1/SNARE complex 'hypercomplex', hoping that the high concentrations used in the crystallization trials would favor the complex formation. We did get crystals from our initial screening, which diffracted to about 2.9 Å. Unfortunately, it turned out that the crystals contained only the SNARE complex.

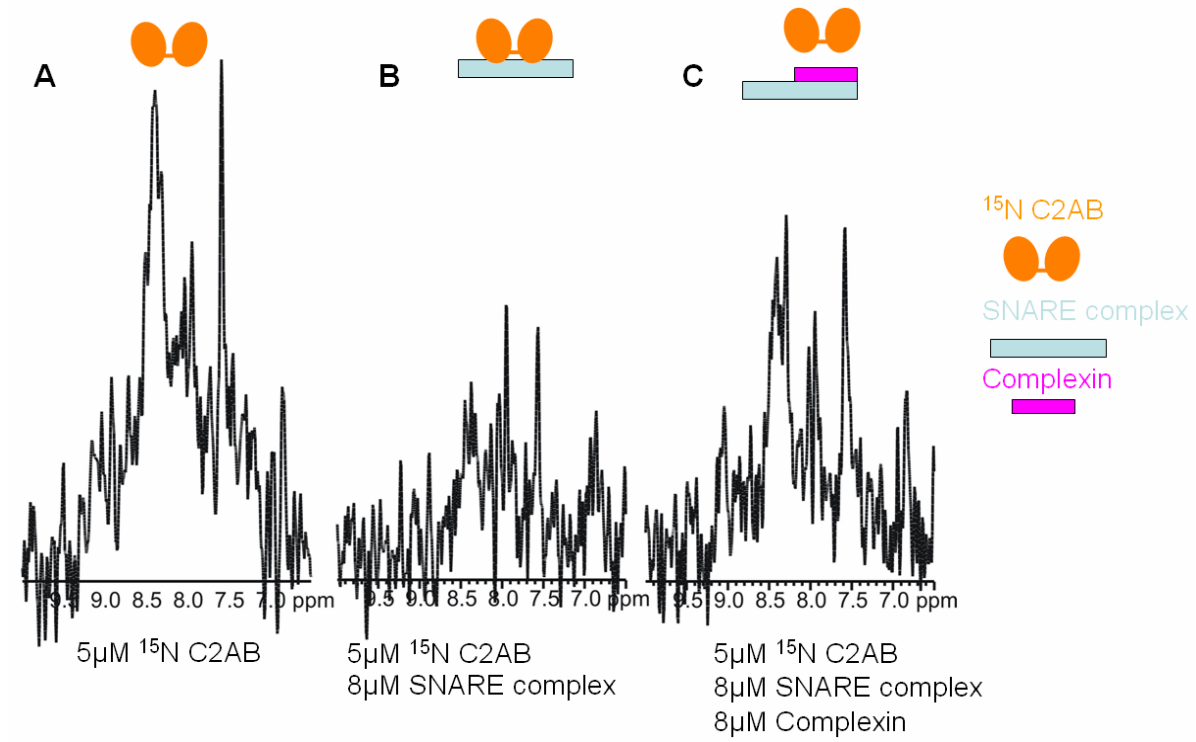

Figure 4.7 Complexin competes with synaptotagmin 1 C2AB fragment for SNARE complex binding in solution.

(A) ^{15}N-edited 1D HSQC of 5μM ^{15}N-labeled synaptotagmin 1 C2AB fragment in the presence of 1 mM EDTA.

(B) ^{15}N-edited 1D HSQC of 5μM ^{15}N-labeled synaptotagmin 1 C2AB fragment after addition of 8 μM unlabeled SNARE complex (SC2) in the presence of 1 mM EDTA.

(C) ^{15}N-edited 1D HSQC of (B) after addition of 8 μM complexin in the presence of 1 mM EDTA.

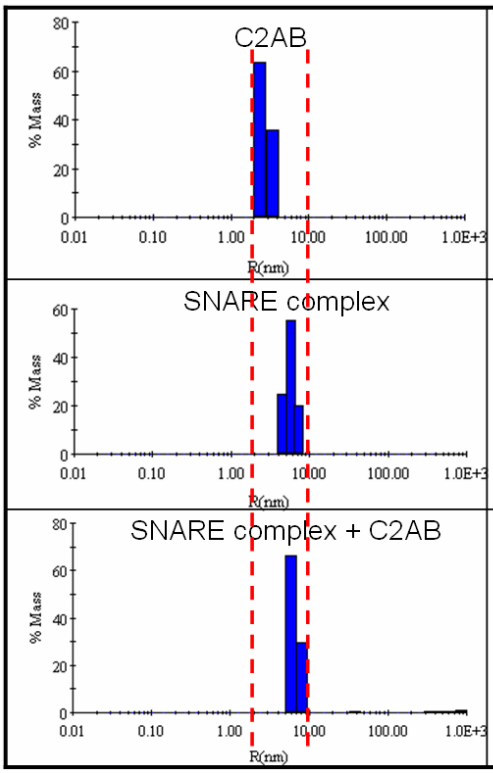

Item	R (nm)	Pd (nm)	%Pd	MW-R (kDa)	%Int	%Mass
Peak 1	2.77507	0.6	20	36.673	6.9	99.3
Peak 2	231.295	46	19.9	1145130	40.6	0
Peak 3	5607.54	2518.3	44.9	1988640000	52.5	0.7

Item	R (nm)	Pd (nm)	%Pd	MW-R (kDa)	%Int	%Mass
Peak 1	5.80133	0.9	16.3	205.912	88.2	99.9
Peak 2	29.6851	3.1	10.4	9389.1	8.1	0.1
Peak 3	357.206	0	0	3165900	3.7	0

Item	R (nm)	Pd (nm)	%Pd	MW-R (kDa)	%Int	%Mass
Peak 1	6.68114	1	15.2	286.526	5.7	96
Peak 2	38.9758	0	0	17755	6.7	0.6
Peak 3	394.101	61.5	15.6	3984570	29	0.7
Peak 4	916.727	207.3	22.6	28722900	58.6	2.6

Figure 4.8 Dynamic light scattering (DLS) analyses.

The DLS analyses show the size distribution of purified synaptotagmin 1 C2AB fragment (top panel), the SNARE complex (middle panel), and an equalmolar mixture of C2AB and SNARE complex (bottom panel) with radii, polydispersity (Pd) and apparent molecular weights corresponding to globular molecules.

4.3.5 Complexin Competes with the Synaptotagmin 1 C2AB Fragment for SNARE Complex Interaction

In the meantime, we also tried to add complexin into the binding assays to test its potential influence on the interaction between the synaptotagmin 1 C2AB fragment and the SNARE complex. Complexins are a family of small brain-specific proteins of about 130 amino acids with four isoforms, complexin I, II, III and IV. Extensive studies have shown that complexins bind stoichiometrically and tightly to the SNARE core complex in a Ca^{2+}-independent manner and suggested that they play a role just before Ca^{2+} triggering of membrane fusion. Clues that complexins might be related to synaptotagmin 1 function came from the observation that complexin I/II double knockout in mice resulted in a selective impairment of the Ca^{2+}-triggered step of fast neurotransmitter release, which was similar to the phenotypes of synaptotagmin 1 knockout mice, but much milder (Reim et al., 2001). It is quite puzzling that the interaction between complexin and the SNARE complex is Ca^{2+}-independent whereas the involvement of complexins in neurotransmitter release occurs in a Ca^{2+}-dependent fashion. Will synaptotagmin 1 be the bridge for the discrepancy? For example, do complexin and synaptotagmin 1 interact synergistically with the SNARE complex and form a ternary 'hypercomplex'? Do complexin and synaptotagmin 1 compete for SNARE complex binding?

In our ^{15}N-edited 1D NMR experiments, addition of 8 μM non-labeled complexin into the mixture of 5 μM ^{15}N-labeled synaptotagmin 1 C2AB fragment and 8 μM non-labeled SC2 in the presence of 1mM EDTA caused the attenuated amide proton signals of synaptotagmin 1 to be partially recovered, suggesting that complexin competes with

synaptotagmin 1 for SC2 binding in the absence of Ca^{2+} (Figure 4.7B, 4.7C). However, in the crystal structure of complexin/SNARE complex, complexin binds to the middle and toward the C-terminus of the groove formed in between the synaptobrevin and syntaxin SNARE motifs (Chen et al., 2002), which is actually opposite to the putative synaptotagmin 1 binding sites on the syntaxin/SNAP-25 side. Therefore, the observation that complexin competed with synaptotagmin 1 for SNARE complex binding implied a potential role of the synaptobrevin C-terminus in synaptotagmin 1 interaction. To test this possibility, we made two truncation constructs of synaptobrevin 2 (29-56 and 29-76) and used them to assemble the SNARE complex (SC3 and SC4, respectively) and studied their interactions with synaptotagmin 1 C2AB fragment using the ^{15}N-edited 1D NMR experiments. These two constructs were chosen based on the observations that synaptobrevin 2 (29-56) was capable of reducing the initial rate of fusion in a dose-dependent manner, presumably by reversibly binding to syntaxin/SNAP-25 (Melia et al., 2002) and that synaptobrevin 2 (29-76) terminates at the cleavage site of botulinum toxin type B (BoNT/B) and has been shown by EPR to be capable of forming ternary SNARE complex with syntaxin and SNAP-25 (Margittai et al., 2001). In our hands, synaptobrevin 2 (29-56) was unable to assemble into an SDS-resistant ternary SNARE complex with syntaxin and SNAP-25, and therefore was not further studied. The by-product of this assembly reaction was the binary 2:1 syntaxin/SNAP-25 complex (SC5), which also could bind to the synaptotagmin 1 C2AB fragment, shown in Figure 4.9B. On the other hand, synaptobrevin 2 (29-76) was capable of ternary SNARE complex formation, but the SNARE complex containing synaptobrevin 2 (29-76) (SC4) lost the ability to interact with the synaptotagmin 1 C2AB fragment in our ^{15}N-edited 1D

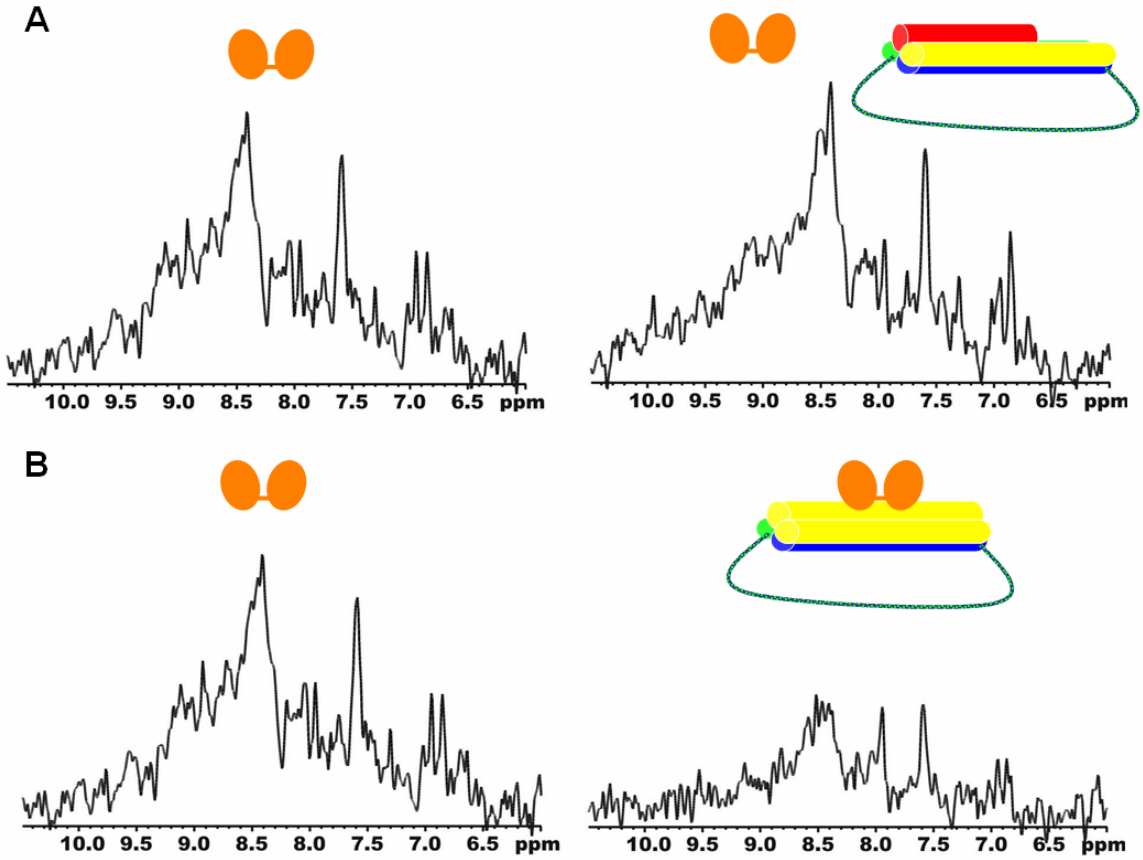

Figure 4.9 Interaction between synaptotagmin 1 C2AB fragment and the SNARE complex assembled with truncated synaptobrevins by ^{15}N-edited 1D NMR experiment.

(A) ^{15}N-edited 1D HSQC of 5μM ^{15}N-labeled synaptotagmin 1 C2AB fragment before (left) and after (right) addition of 10 μM unlabeled SNARE complex assembled with synaptobrevin (29-76), syntaxin and SNAP-25 in the presence of 1 mM EDTA. The SNARE motifs from syntaxin, synaptobrevin, N-terminal SNAP-25 and C-terminal SNAP-25 are colored in yellow, red, blue, and green, respectively. The synaptotagmin 1 C2AB fragment is colored in orange.

(B) ^{15}N-edited 1D HSQC of 5μM ^{15}N-labeled synaptotagmin 1 C2AB fragment before (left) and after (right) addition of 10 μM unlabeled SNARE complex assembled with syntaxin and SNAP-25 in the presence of 1 mM EDTA.

NMR binding assay (Figure 4.9A), suggesting a direct or indirect involvement of the synaptobrevin C-terminus in synaptotagmin 1 interaction.

4.3.6 Binding Studies of Synaptotagmin 1 and the SNARE Complex by Isothermal Titration Calorimetry

Since reproducible binding of the GST fusion protein of synaptotagmin 1 C2AB fragment (GST-C2AB) to the SNARE complex in the presence or absence of Ca^{2+} was observed in GST pulldown experiments performed by Jiong Tang from Dr. Thomas C Südhof's lab, we tried to use isothermal titration calorimetry (ITC) to determine the binding stoichiometry and affinity, which would be helpful to understand whether it is a specific and meaningful interaction. ITC is an ideal tool to measure the stoichiometry and Kd for binding at constant temperature and pressure. It is a procedure performed in two side-by-side cells: the sample cell contains buffer and the target molecule, and the reference cell contains only buffer. A ligand is added to the sample cell (in some instruments, ligands can be added simultaneously into both cells) in aliquots. The temperatures of the two cells are kept equal to each other using feedback from thermopile temperature sensors. ITC measures the amount of heat change upon ligand binding to target molecule, which in theory is equivalent to the apparent heat enthalpy due to the change of $[\Delta L]_{bound}$ between the corresponding steps *i* and *i-1*. The heats of dilution of the titrants can be subtracted from the titration data for baseline correction. The software MicroCal Origin™ for ITC can be used to analyze the baseline-corrected data to determine the enthalpy (ΔH), dissociation constant (Kd), and stoichiometry of binding (n). The amount of heat change at each consecutive ligand additions is the area

integrated under the curves observed at each step. Plots of the ratio of integrated heat change to the amount of ligand ($\Delta Q/\Delta L$) against the molar ratio of ligand and target molecule will give a sigmoidal binding isotherm curve, the transition point of which corresponds to the stoichiometry number (n). The isothermal titration calorimetric data can be fitted to different association models available in the software such as "single set of identical sites", "two sets of independent sites", and "sequential binding sites", *etc*. The models were evaluated by visual inspection of the fitted curves and by comparing the χ^2 values obtained after the fitting. The model resulting in the lowest value of χ^2 was considered the best model to describe the molecular mechanism of binding. The enthalpy (ΔH), dissociation constant (Kd), and stoichiometry of binding (n) were determined from the best fit model. The free energy change for binding (ΔG) can be calculated from $\Delta G = -RT\ln Kd$. (R is gas constant and T is the absolute temperature). The entropy change (ΔS) can be calculated using standard free energy relationships $\Delta G = \Delta H - T\Delta S$.

In our ITC experiments, 0.5 μM affinity and 1:2 stoichiometry were observed for GST-C2AB/SNARE complex interaction (Figure 4.10A, 4.10B). However, titration of GST alone into the SNARE complex yielded a fit with 62.5 μM affinity and 1:1 stoichiometry (Figure 4.10D) whereas titration of C2AB alone into the SNARE complex couldn't generate a reasonable binding isotherm fit (Figure 4.10C), probably due to multiple processes occurring during the titration such as binding, oligomer dissociation, and conformational change. The finding that GST alone binds weakly to the SNARE complex is quite interesting and provided an explanation for the observed relatively strong Ca^{2+}-independent interaction between synaptotagmin 1 and the SNARE complex by GST pulldown experiments.

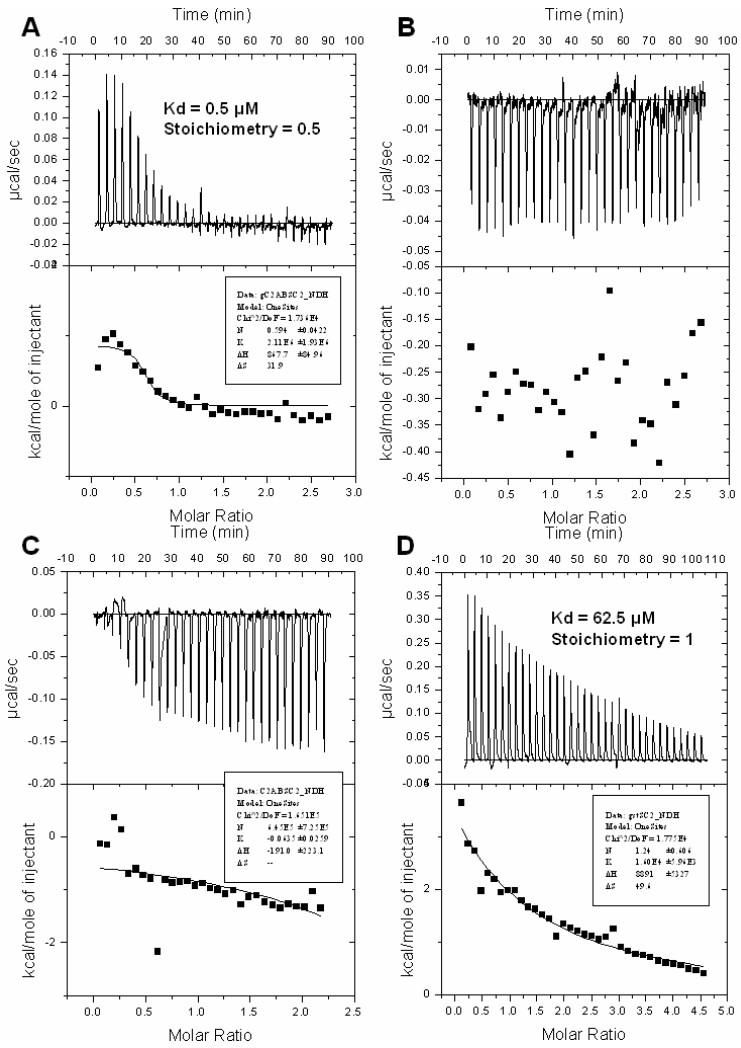

Figure 4.10 Isothermal titration calorimetry (ITC) reveals a weak interaction between GST and the SNARE complex.

(A) ITC isotherm of 512.1 μM GST-C2AB titrated into 35.2 μM SNARE complex. The data suggested a 1:2 stoichiometry and a dissociation constant of 0.5 μM.

(B) ITC isotherm of the control experiment where 512.1 μM GST-C2AB was titrated into ITC buffer.

(C) ITC isotherm of 426.9 μM C2AB titrated into 36.22 μM SNARE complex, which failed to generate a reasonable binding isotherm fit.

(D) ITC isotherm of 512 μM GST-C2AB titrated into 24.5 μM SNARE complex. The data suggested a 1:1 stoichiometry and a dissociation constant of 62.5 μM, although this value must be considered an estimate because of experimental limitations of this method.

4.4 Discussion

In contrast to the well characterized properties of Ca^{2+}-binding and Ca^{2+}-dependent phospholipid binding of synaptotagmin 1, the interaction between synaptotagmin 1 and SNAREs, which could couple the two key players, the Ca^{2+} sensor and the central fusion machinery, and hence might be crucial for neurotransmitter release, is much less defined. In this chapter, we focused on studies of the interaction between synaptotagmin 1 and the SNARE complex in solution using their soluble fragments with ^{15}N-edited 1D NMR, size exclusion chromatography and ITC. Both ^{15}N-edited 1D NMR experiments and size exclusion chromatography suggested that the synaptotagmin 1 C2AB fragment interacts with the SNARE complex in the presence of Ca^{2+}. However, attempts to unravel the structural basis of the Ca^{2+}-dependent interaction by 2D NMR spectroscopy or ITC were hindered by the severe precipitation problem even at 12 μM protein concentrations. On the other hand, for the synaptotagmin 1/SNARE complex interaction in the absence of Ca^{2+}, we could detect the interaction using ^{15}N-edited 1D NMR experiments, but failed to detect stable complex formation by size exclusion chromatography. Attempts to characterize this interaction by ITC failed to yield meaningful results yet, unexpectedly, revealed a weak interaction between GST and the SNARE complex. These observations suggest that the interaction between synaptotagmin 1 and the SNARE complex in the absence of Ca^{2+}, if it exists, is very weak. The observation of GST/SNARE complex interaction suggested that fusing GST to synaptotagmin 1 might artificially enhance its Ca^{2+}-indpendent interaction with the SNARE complex in the GST pulldown assay. Another interesting observation revealed in this chapter

is the competition between complexin and synaptotagmin 1 for SNARE complex binding. This observation suggested that Ca^{2+}-triggered fast synchronous neurotransmitter release might result form the exquisitely regulated interplay between complexin, synaptotagmin 1 and the SNARE complex, which turned out to be crucial from our studies described in chapter 5.

Chapter 5 Studies of the Interaction between Synaptotagmin 1 and the SNARE Complex in a Membrane Environment

(Parts of this chapter are adapted from Dai et al., 2007)

5.1 Introduction

The inconsistency and contradiction about the existence, the Ca^{2+}-dependence, and the physiological relevance of the interaction between synaptotagmin 1 and the SNARE complex have been well documented in the literature. Our studies of the interaction in solution using soluble fragments with several different methods described in chapter 4 also yielded inconsistent results and failed to be conclusive in spite of all our efforts. A possible explanation for this might be that both native synaptotagmin 1 and SNARE proteins are normally embedded in the membranes, which might affect the strength or the mode of the synaptotagmin 1/SNARE complex interaction, in contrast to the experiments in chapter 4, which were performed in a nonmembranous environment. As such, we decided to study the interaction in a physiological membrane environment using reconstituted SNARE complexes, both in the presence and absence of Ca^{2+}. To study the synaptotagmin 1/SNARE complex interaction in a membrane environment, we used confocal fluorescence microscopy and microfluidic channel systems. SNARE proteins with transmembrane regions were purified and reconstituted into liposomes and then deposited into microfluidic channels to form a supported proteolipid bilayer, constituting a platform to detect interactions on the membrane. Fluorescently-labeled proteins bound to the reconstituted SNAREs or the membranes within microfluidic channels could be observed and quantified with confocal fluorescence microscopy.

In this chapter, we have studied the interaction of the synaptotagmin 1 C2AB fragment with the SNARE complex attached to single phospholipid bilayers that were deposited within microfluidic channels. We demonstrated that the synaptotagmin 1 C2AB fragment binds simultaneously to phospholipids and the SNARE complex reconstituted in membrane in the presence of Ca^{2+}, forming an intimate, specific quaternary complex with Ca^{2+}, phospholipids and the SNARE complex, which we referred to as the SSCAP complex (for SNAREs, Synaptotagmin, Ca^{2+}, Phospholipid). Further, we determined that the binding mode of the synaptotagmin 1 C2AB fragment to the phospholipid is independent of the presence of the SNARE complex. We also showed that the synaptotagmin 1 C2AB fragment competes with complexin for binding to reconstituted SNARE complex in the presence of Ca^{2+}. Using the complexin displacement assay, we demonstrated that the preponderant role of the synaptotagmin 1 C2B domain in neurotransmitter release compared to the C2A domain arises from the fact that the C2B domain is primarily responsible for SNARE binding. Additional mutagenesis studies showed that the effects of several point mutations on the interaction between synaptotagmin 1 and reconstituted SNARE complex and hence the formation of the quaternary SSCAP complex correlated with their effects on synaptic vesicle exocytosis. Together with the binding site mapping studies by NMR spectroscopy, this yielded structural information of the potential binding interface, allowing us to use computational modeling and docking to generate a preliminary model of the SSCAP complex. Examination of the preliminary model of the SSCAP complex revealed a potential mechanism whereby the highly positive electrostatic potential created by the synaptotagmin 1 C2B domain and the C-terminus of the SNARE complex after displacement of complexin

helps to induce membrane fusion and neurotransmitter release. Overall, our data suggested the following mechanism of Ca^{2+}-triggered fast neurotransmitter release: complexin helps to fully assemble the SNARE complex, yet suspends primed vesicles in a metastable state; Ca^{2+}-binding to synaptotagmin 1 triggers fast neurotransmitter release by displacing complexin from the SNARE complex and forming the quaternary SSCAP complex.

5.2 Materials and Methods

5.2.1 Recombinant Protein Preparation

The expression and purification procedures of the SNARE motifs of syntaxin 1A (amino acids 191-253), synaptobrevin 2 (amino acids 29-93), SNAP-25 (amino acids 11-82-W and 141-203-W) and the cytoplasmic fragment of synaptobrevin 2 (amino acids 1-96) were essentially the same as described in chapter 4. The expression and purification procedures of the complexin I (amino acids 26-83) V61C mutant and the synaptotagmin 1 (amino acids 140-421) single mutants D178N, D309N and double mutants (C277S, V419C), (F234C, C277S), (C277S, V304C), (K326C, K327C) were essentially the same as those of the wild type proteins described in chapter 4.

The SNAP-25 full length double or triple mutants (D186K, D193K), (D51K, E52K, E55K) were generated by site-directed mutagenesis (Stratagene), according to the manufacturer's protocol. Both the double and triple mutation sites were close in sequence (8 amino acids apart for the double mutant and 5 amino acids apart for the triple mutant, respectively), therefore only one pair of synthetic oligonucleotide primers was designed

covering each mutation region with all the intended substitutions at the same time. The GST fusion proteins of wild type and mutant SNAP-25 were expressed in *Escherichia coli* BL21 at 23 °C, isolated by affinity chromatography on glutathione Sepharose 4B (Amersham Pharmacia Biotech.) and cleaved with thrombin (from bovine plasma, Sigma) with the same protocols as those for SNARE motifs described in chapter 4. The proteins were then eluted with the thrombin cleavage buffer (50 mM Tris, pH 8.0, 200 mM NaCl, 2.5 mM $CaCl_2$, and 1mM DTT) and further purified by anion exchange chromatography through a Mono Q column and gel filtration chromatography through a Superdex 75 Hiload 16/60 column (Amersham Pharmacia Biotech.). The purity of the preparation was assessed by SDS-PAGE and Coomassie blue staining. The typical yield according to UV absorbance measurements at 280 nm was about 4 mg per liter of culture.

The construct expressing a hexameric His tag fusion protein of syntaxin 1A fragment that contains the SNARE motif and the transmembrane region (amino acids 183-288) was generously provided by Dr. Reinhard Jahn's laboratory. The plasmid was transformed into *Escherichia coli* BL21 (DE3) cells for protein expression since the transcription was driven by a T7 promoter. Glycerol stocks (8% glycerol) of the transformed cells were kept at -80 ºC. For a routine 1 liter bacteria culture, 50 ml LB media was inoculated with a single colony from an agar/kanamycin plate and incubated in a shaker at 250 rpm overnight at 37 ºC. The next day, a proper amount of culture (usually 10-20 ml) was transferred to 1 liter LB media to make sure that the starting OD_{600} was around 0.1. All media contained 30 μg/ml kanamycin to maintain the presence of the transformed plasmids. The flasks were incubated at 37 ºC and shaken at 250 rpm till OD_{600} reached 0.6-0.8, then 0.5 mM IPTG was added to

induce protein expression for 5-6 hours at 37 ºC. The cells were harvested by centrifugation at 4,000 rpm for 30 minutes in swing buckets with a rotor JS 4.2 (Model J6-MI centrifuge, Beckman Instruments) and resuspended into 10 ml resuspension buffer (100 mM Tris, pH 7.4, 500 mM NaCl, and 8 mM imidazole) containing 0.5 mM AEBSF and 5mM β-mercaptoethanol (EDTA and EGTA were not added since they would chelate the nickel ions in the Ni-NTA agarose resins; Sigma inhibitor cocktail was not added because it also contained EDTA; β-mercaptoethanol was used instead of DTT since low concentration of DTT would reduce the nickel ions in the Ni-NTA agarose resins). To facilitate cell disruption, the cell suspension was frozen with liquid nitrogen and then thawed before protein purification. 10 ml resuspension buffer containing 10% (w/v) sodium cholate was added into the thawed cell suspension, followed by 15 minute incubation at room temperature. Next, solid urea was added to the cell suspension till the final concentration reached 6 M. The mixture was incubated at room temperature for additional 15 minutes and then passed through the high pressure homogenizer (Model EmulsiFlex-C5, Avestin Inc.) for three times. The cell debris was spun down by centrifugation at 18,000 rpm for 30 minutes in a JA-20 rotor with the Beckman centrifuge (model J2-21). The supernatant was filtered with 0.45 μm syringe filter (Nalgene) and mixed with 1.0-1.5 ml slurry of the pre-washed nickel-nitrilotriacetic acid (Ni-NTA) agarose (Qiagen) per liter of culture in the cold room at 4°C overnight. The next day, unbound proteins and nonspecifically bound proteins were removed by washing extensively with washing buffer (50 mM Tris, pH 7.4, 250 mM NaCl, 4 mM imidazole, 5mM β-mercaptoethanol and 1.5% (w/v) sodium cholate). The resins were then washed with 3 ml thrombin cleavage buffer (50 mM Tris, pH 8.0, 200 mM NaCl, 2.5 mM

$CaCl_2$, and 1% (w/v) β-OG) containing freshly added 5mM β-mercaptoethanol for three times. The N-terminal His tag was removed with 5-7 units/ml thrombin (from bovine plasma, Sigma) for four hours at room temperature. The syntaxin (183-288) fragment was very sticky onto the Ni-NTA agarose resins and therefore 8 M urea was included in the elution buffer (20 mM Tris, pH 7.4, 5mM β-mercaptoethanol, 1% (w/v) β-OG, and 8 M urea) to help the elution since this syntaxin fragment is unstructured. The eluted syntaxin (183-288) was further purified by anion exchange chromatography using a Vivapure Q spin column (Vivascience). The eluted syntaxin (183-288) was loaded onto the Q spin column pre-equilibrated with QA buffer (20 mM Tris, pH 7.4, 0.3 mM TCEP, and 1% (w/v) β-OG) and extensive wash with QA buffer was used to remove the residual urea. QB buffer (20 mM Tris, pH 7.4, 0.5 M NaCl, 0.3 mM TCEP, and 1% (w/v) β-OG) was used to elute the bound syntaxin (183-288) from the Q spin column. The purity of the preparation was assessed by SDS-PAGE and Coomassie blue staining. The typical yield according to UV absorbance measurements at 280 nm was about 1-2 mg per liter of culture.

5.2.2 Labeling Proteins with Fluorescent Dyes

Lysines and cysteines are the residues commonly used for labeling with amino-reactive and thiol-reactive fluorescent probes, respectively. Because lysines are very abundant on protein surfaces, cysteines are usually used for single homogenous labeling. To label complexin, valine 61 was mutated to cysteine on the wild type background since there are no intrinsic cysteines in the complexin fragment (amino acids 26-83). While for synaptotagmin 1 C2AB fragment, the single intrinsic cysteine residue (cysteine 277) in the

C2B domain was mutated to serine to yield a mutant for introduction of single cysteine mutations at specific sites. The ^{1}H-^{15}N HSQC of the C277S mutant resembles that of the wild type, indicating that the C277S mutation doesn't affect the proper folding of the synaptotagmin 1 C2B domain.

The proteins were dialyzed against the labeling buffer (40 mM HEPES, pH 7.4, 100 mM NaCl, and 0.3 mM TCEP). Extensive buffer exchanges were performed to remove any residual DTT or β-mercaptoethanol which might inhibit the labeling reaction due to their free thiol groups. Instead, Tris(2-carboxyethyl) phosphine (TCEP) was used to ensure the reducing state of the thiol group of the cysteine side chain because it does not contain any thiol groups like DTT or β-mercaptoethanol and thus will not interfere with the labeling process. To prevent disulfide bond formation, the buffers used were deoxygenated using a nitrogen stream and the labeling reactions were carried out under an inert nitrogen atmosphere. The fluorescent dyes were dissolved in dimethylsulfoxide (DMSO) to make a 5 mM stock solution immediately prior to use. All samples containing the fluorescent probes were wrapped in aluminum foil to protect from light at all times. Specified amounts of fluorescent dyes were added dropwise to the protein solution (0.5 or 1 ml of approximately 50-100 μM protein) while stirring, to reach a dye to protein ratio of 10:1 to 20:1 (molar ratio). The labeling reactions were incubated at room temperature for six hours, followed by addition of 10 mM DTT to consume the excess thiol-reactive fluorescent dyes and stop the reaction. The fluorescently-labeled proteins were subjected to extensive dialysis as well as gel filtration chromatography to remove the excess fluorescent dyes. Labeling efficiencies were calculated by measuring the final concentrations of proteins and fluorescent dyes in the

purified samples, and were typically 80% to 85%. The fluorescently-labeled proteins were frozen and stored in small aliquots wrapped in aluminum foil at -80 °C, protected from light to prevent photobleaching.

5.2.3 Reconstitution of the SNARE Complex into the Preformed Liposomes

Previous studies from our lab have characterized and compared two different detergent mediated reconstitution methods: the standard comicellization method and the direct method. In the standard comicellization method, the mixture of the purified membrane proteins, detergents and phospholipids are diluted to allow the decrease of the detergent concentration below its critical micelle concentration (CMC) and consequent removal by dialysis. This method usually generates inhomogeneous liposome size distribution and differential protein insertion. In contrast, in the direct method, the membrane proteins are directly inserted into preformed liposomes saturated with detergents and subsequently the detergents are removed to allow the formation of reconstituted proteoliposome. This method usually generates relatively homogeneous liposome size distribution.

The direct method is based on the assumption that the reconstitution of membrane proteins and the liposome solubilization by detergents constitute reverse reactions and therefore they should share similar intermediate states (Rigaud et al., 1995; Rigaud and Levy, 2003). Studies of liposome solubilization by detergents revealed three major stages with the increasing detergent concentrations: 1) detergents are inserted into the liposomes until the liposomes are saturated with detergents without membrane solubilization; 2) liposomes start to solubilize with the transition of liposomes saturated with detergents to mixed micelles

composed of detergents and phospholipid until the complete solubilization of the liposomes; and 3) the detergent fraction in the micelles increases with the increasing detergent concentration. For a certain detergent/phospholipid system, the key factor determining the stage of the system is the molar ratio of detergent to phospholipid in the aggregates (mixed liposomes and mixed micelles), which is defined as:

$$R_{eff} = (D_{total} - D_{water}) / [lip]$$

where D_{total}, D_{water} and [lip] are the total detergent concentration, the aqueous monomeric detergent concentration and the total phospholipid concentration, respectively. The R_{eff} corresponding to the two transitions between the three different stages are referred to as R_{sat} and R_{sol}, respectively, which mark the onset and complete solubilization of the liposome. Assuming that reconstitution takes the reverse pathway of the liposome solubilization, reconstitution can be achieved by incubating the preformed liposome saturated with detergents and purified membrane protein in detergents, followed by removal of detergents by dialysis and hydrophobic adsorption.

In our experiments, liposomes of synaptic vesicle composition (composed of 41% (w/w) 1-palmitoyl, 2-oleoyl phosphatidylcholine (POPC), 32% (w/w) 1,2- dipalmitoyl phosphatidylethanolamine (DPPE), 12% (w/w) 1,2-dioleoyl phosphatidylserine (DOPS), 5% (w/w) phosphatidylinositol (PtdIns), and 10% (w/w) cholesterol) were prepared by extrusion methods, as described in chapter 2. In a typical reconstitution experiment, 100 μl of the preformed liposomes (15 mM phospholipid) and 200 μl of the preassembled SNARE complex were mixed at room temperature. The protein solution contained 1% (w/v) β-OG. Thus, the final concentrations of phospholipid and β-OG in the mixture were 5 mM and

0.66% (w/v), respectively. Under these conditions, the R_{eff} value is around 1.2, which is very close to the R_{sat} value for β-OG (~1.3). Such reconstitution conditions were chosen based on systematic studies of β-OG mediated reconstitution (Rigaud et al., 1995). For preparation of the SNARE-incorporated proteoliposomes, the typical protein to lipid ratio used was 1:500 or 1:1000 (molar ratio). The mixture was kept at room temperature for 30 minutes under gentle stirring. Then detergent was removed by a three-step dialysis as follows. First, the mixture was dialyzed against 1 liter reconstitution buffer (25 mM HEPES, pH 7.4, 100 mM KCl, 0.1 mM EGTA, and 1mM DTT) containing 1 g Biobeads SM2 polystyrene beads (Bio-Rad Laboratories) at room temperature for one hour. Next, the dialysis was continued against 1 liter fresh reconstitution buffer containing 1 g Biobeads at room temperature for two more hours. Finally, the sample was transferred to 2 liter fresh reconstitution buffer containing 2 g Biobeads and dialyzed at 4 ºC overnight.

5.2.4 Preparation of Planar Supported Proteolipid Bilayer and Microfluidic Channels

Purified recombinant syntaxin (183-288), full length SNAP-25 and synaptobrevin (1-96) were used to assemble the SNARE complex in the presence of 1% (w/v) β-OG. The assembled SNARE complexes were reconstituted into preformed liposomes with a molar protein to lipid ratio 1:1000 as described above. Microfluidic channels of 200 μm width, 200 μm height, and 2.5 cm length were formed using standard soft lithography techniques (Xia and Whitesides, 1998) (Figure 5.1). Briefly, a layer of negative photoresist (SU-8, micrometers to ~1 mm thick) was spin-coated onto silicon wafers, exposed to UV light through a high-resolution transparency photomask of the designed pattern, and developed to

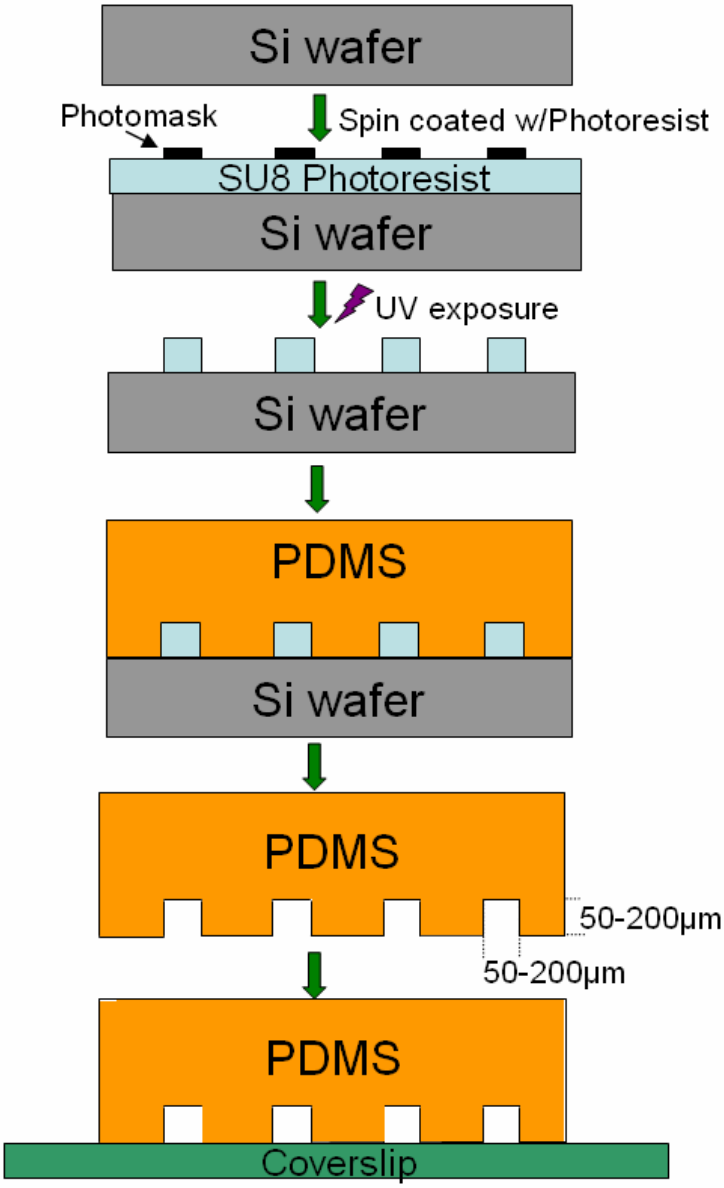

Figure 5.1 Schematic diagrams of microchannel fabrications with polydimethylsiloxane (PDMS).

A layer of negative photoresist (SU-8) was spin-coated onto silicon wafers, exposed to UV light through a high-resolution transparency photomask of the designed pattern, and developed to produce masters for molding channels. PDMS prepolymer was cast on silicon masters and cured thermally at 65 °C for 5 hours. Cured PDMS stamps were cut out with a scalpel blade, peeled away from the silicon master and then firmly pressed down against the thoroughly cleaned coverslips to form a reversible, leak-tight seal.

produce masters for molding channels. poly dimethylsiloxane (PDMS) prepolymer (Sylgard 184, Dow Corning) was cast on silicon masters and cured thermally at 65 °C for 5 hours. Cured PDMS stamps were cut out with a scalpel blade, and peeled away from the silicon master, and inlets and outlets were punched with an 18 gauge blunt needle. Coverslips were plasma oxidized with a glow discharge unit in the EM facilities for 3 minutes under vacuum. PDMS stamps were then firmly pressed down against the coverslips to form a reversible, leak-tight seal. The microchannel system for the partition experiments (Figure 5.2) used a torque-actuated screw valve (TWIST valve) to switch on and off the connection between the channels because it is easy to fabricate and operate. To fabricate the valve, a hole of about 4 mm in diameter was drilled to about 2–3 mm deep. A smaller hole was drilled right above the channel to hold the screw in place; the diameter of the hole was similar to that of the screws (about 1 mm). The device was plasma oxidized for 1 minute to render the PDMS hydrophilic and prevent polyurethane from flowing onto the device. The screw was then pushed into the smaller hole until it made contact with the underlying PDMS. Polyurethane (NOA81) was filled around the screw and cured by UV for 6–8 minutes. The whole device was then incubated at 60 °C for 6 hours to improve the adhesion between the polyurethane and PDMS. Parallel lanes of supported bilayers containing or lacking reconstituted SNARE complexes were formed using the vesicle fusion method (Brian and Mcconnell, 1984) in the microfluidic channels.

5.2.5 Equilibrium Partition Experiments

Liposomes (1 mM of phospholipid) containing or lacking reconstituted SNARE complexes were deposited into the separate exterior channels (Figure 5.2) with the screw valve closed. After deposition and removal of excess unfused liposomes, the valve was opened to connect all the microchannels. BODIPY (4,4-difluro-5,7-dimethyl-4-bora-3a,4a-diaza-s-indacene-3-propionic acid) –FL-labeled C277S, V419C double mutant of synaptotagmin 1 C2AB fragment (40 nM) was injected through the middle inlet in reconstitution buffer (25 mM HEPES, pH 7.4, 100 mM KCl, 0.1 mM EGTA, 0.3mM TCEP) containing 1 mM EDTA or 1 mM Ca^{2+}. After incubating for one hour and washing the microchannels with the same buffer, BODIPY-FL fluorophores that remained bound to the membranes were imaged on a Leica (Wetzlar, Germany) confocal fluorescence microscope (TCS SP2) using a HC PL FLUOTAR 10×, 0.3 numerical aperture confocal scanning objective, and a 488 nm argon laser excitation with BODIPY-FL filter set. The amount of synaptotagmin 1 associated with the membranes was quantified with Image J (NIH, MD). Briefly, fluorescence intensity in separate squares of 100 μm × 100 μm within the same image was integrated and the resulting values were averaged.

5.2.6 Complexin Displacement Assays

A complexin I fragment (amino acids 26-83) containing a V61C mutation was labeled with BODIPY-FL. In a typical experiment, 50 nM BODIPY-FL-labeled complexin was incubated with a deposited supported bilayer containing assembled wild type or mutant SNARE complexes for 15 minutes, and unbound complexin was washed out with the reconstitution buffer (25 mM HEPES, pH 7.4, 100 mM KCl, 0.1 mM EGTA, 0.3mM TCEP).

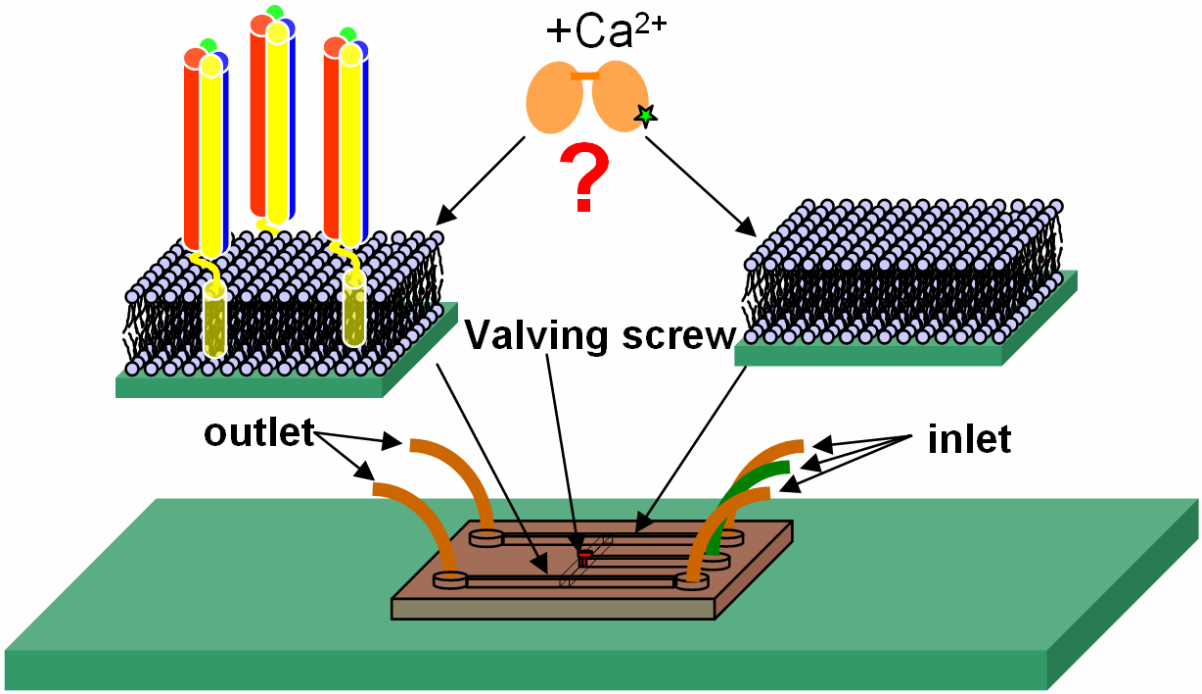

Figure 5.2 Schematic diagram of the valved microfluidic channels for the equilibrium partition experiments.

A PDMS stamp with grooves inscribed on the bottom was sealed tightly on top of a coverslip, forming channels in between the coverslip and PDMS stamp. External tubings were connected to the channels to facilitate the delivery and flushing process. In the valved microfluidic channels, a valving screw was put in the middle to control the connection between the left channel and the right channel. Supported proteolipid bilayer can be deposited inside the channel, forming the platform to detect interaction on the membrane. The valved microfluidic channels were used to test whether the synaptotagmin 1 C2AB fragment partitions preferentially to membranes containing the reconstituted SNARE complex formed by the syntaxin SNARE motif and TM region (yellow), the synaptobrevin SNARE motif (red) and the SNAP-25 N-terminal (blue) and C-terminal (green) SNARE motifs (molar protein to lipid ratio 1:1000). The V419C-C2AB fragment is represented by two orange ellipses with a green star depicting the site labeled with BODIPY-FL.

An unlabeled synaptotagmin 1 fragment containing its two C2 domains (amino acids 140-421) at the desired concentration was then added in the presence of either 1 mM EDTA or 1 mM Ca^{2+} and incubated with the bilayer for 10 minutes, followed by a wash with buffer containing either 1 mM EDTA or 1 mM Ca^{2+} correspondingly. Similar experiments were performed for different synaptotagmin 1 C2AB mutants or its individual C2 domains. Control experiments where complexin was added to supported bilayers lacking reconstituted SNARE complexes were used to measure the background fluorescence that might result from nonspecific binding of complexins to the phospholipid bilayers. Supported lipid bilayer lacking the negatively charged phospholipid contains 58% (w/w) POPC, 32% (w/w) DPPE, and 10% (w/w) cholesterol. BODIPY-FL fluorophores that remained bound to the membranes were imaged on a Leica (Wetzlar, Germany) confocal fluorescence microscope (TCS SP2) using a HC PL FLUOTAR 10 ×, 0.3 numerical aperture confocal scanning objective, using a 488 nm argon laser excitation with BODIPY-FL filter set. The amount of complexin bound to SNARE complexes on the bilayer was quantified with Image J (NIH, MD). Briefly, fluorescence intensities in separate squares of 100 μm × 100 μm within the same image were integrated and the resulting values were averaged. The competition titration data were analyzed with Origin 6.0 and fitted to a Dose-response model.

5.2.7 NBD Fluorescence Experiments

Fluorescence emission measurements of the NBD (N,N'-dimethyl-N-(iodoacetyl)-N'-(7-nitrobenz-2-oxa-1,3-diazol-4-yl) ethylenediamine) fluorophore from 480 nm to 580 nm, were performed at 25 °C on a PTI spectrofluorometer (Photon Technology Incorporated,

Lawrenceville, NJ) with excitation at 478 nm using 0.1 μM NBD-labeled C277S, F234C double mutant or C277S, V304C double mutant of synaptotagmin 1 C2AB fragment dissolved in reconstitution buffer (25 mM HEPES, pH 7.4, 100 mM KCl, 0.1 mM EGTA, and 0.3mM TCEP) containing 1 mM EDTA or 1 mM $CaCl_2$, and 0.1 mg/ml of liposomes lacking or containing SNARE complexes reconstituted as described above (molar protein to lipid ratio 1:1000) for the microchannel experiments. Analogous experiments were performed in the absence of phospholipids with 0.125 μM soluble SNARE complexes (the syntaxin (183-288) fragment was replaced with a syntaxin (180-264) fragment, which lacks the transmembrane region).

5.2.8 NMR Spectroscopy

^{1}H-^{15}N TROSY-HSQC spectra were acquired at 27 ˚C on a Varian INOVA800 spectrometer with samples dissolved in 20 mM Tris, pH 7.4, 100 mM NaCl, 1 mM EDTA, and 0.3mM TCEP, using H_2O/D_2O 95:5 (v/v) as the solvent. The 5% (v/v) D_2O was included to provide the lock signal for the control of the long term stability of the magnetic field. All NMR data were processed with the program NMRPipe (Delaglio et al., 1995) and analyzed with the program NMRView (Johnson and Blevins, 1994).

5.2.9 Computational Docking of the C2B Domain on the SNARE Complex

The models were generated using HADDOCK (High Ambiguity Driven protein-protein DOCKing) (Dominguez et al., 2003) in conjunction with CNS (Brunger et al., 1998). The starting structures used in HADDOCK were the SNARE complex from

complexin/SNARE complex (PDB entry 1KIL) and synaptotagmin 1 C2B domain with the two Ca^{2+} ion removed (PDB entry 1K5W). The active residues used to define the ambiguous interaction restraints (AIRs) were solvent-accessible (as calculated by NACCESS (Hubbard et al., 1991)) and demonstrated strong effects during mutagenesis analysis using complexin displacement assay. Ambiguous interaction restraints (AIRs) were used to force proximity between K326, K327 of the synaptotagmin 1 C2B domain and D186, D193 of SNAP-25 with the 2Å upper distance limit for AIRs (maximum distance between any atom of an active residue of one molecule to any atom of an active or passive residues of the second molecule). Passive residues were chosen as those that were surface neighbors of the active residues within 6Å and that have a high level of solvent accessibility (>50%). Rigid body energy minimization generated an initial set of 1000 rigid body docking solutions, which were sorted by the intermolecular energy of each complex (sum of van der Waals, electrostatic, AIRs). The standard docking protocol also includes additional semi-flexible simulated annealing and explicit solvent refinement. However, the semi-flexible simulated annealing step caused the SNARE complex to splay at the N-terminal ends, therefore, only the solutions from the rigid body energy minimization were examined.

Docking was also carried out using another fast Fourier transform-based docking program FTDock (Fourier Transform rigid-body Docking) (Gabb et al., 1997) with further refinement of the resulting complex using the MultiDock (Multiple copy side-chain refinement of protein-protein interfaces) program (Jackson et al., 1998). Firstly, a global scan of translational and rotational space of possible positions of the two molecules, limited by surface complementarity and an electrostatic filter, was performed by FTDock. Next, the

integrated RPScore (Residue level Pair potential Scoring) program (Moont et al., 1999) generated an empirical scoring of the possible complexes using residue level pair potentials to screen the output from FTDock. The resulting complexes were further screened using restraints from the mutagenesis data to force proximity (4.5 Å) between K326, K327 of the C2B domain and D186, D193 of SNAP-25. Finally, MultiDock performed an energy minimization and removal of steric clashes on the side-chains of the interface.

5.3 Results

5.3.1 Synaptotagmin 1 Binds Simultaneously to Phospholipids and the SNARE Complex

To study the synaptotagmin 1/SNARE complex interaction in the membrane environment, a key question to answer is whether synaptotagmin 1 can bind simultaneously to the phospholipid and the SNARE complex. It has been reported that the immunoprecipitated synaptotagmin 1/SNARE complex could bind to phospholipids (Davis et al., 1999), but the synaptotagmin 1 fragment used in this study contained a mutation that prevented correct folding of the C2B domain (Ubach et al., 2001). In contrast, ^{13}C-edited 1D NMR studies from our lab demonstrated that phospholipid displaced the soluble SNARE complex from the synaptotagmin 1 C2AB fragment in the presence of Ca^{2+} (Arac et al., 2003), but it is possible that this result arose because the SNARE complex was not attached to membranes. Therefore, we could not exclude the possibility that the reconstituted SNARE complex might act synergistically with phospholipids in binding to synaptotagmin 1 in the presence of Ca^{2+}. The finding that synaptotagmin 1 enhanced the rate of assembly of

membrane-attached syntaxin/SNAP-25 heterodimers provided evidence for simultaneous interactions of synaptotagmin 1 with phospholipid and reconstituted SNAREs, leading to the proposal that, upon Ca^{2+} influx, synaptotagmin 1 induces formation of the heterodimers followed by the SNARE complex formation (Bhalla et al., 2006). However, the observed rate enhancement was rather modest (ca. 5-fold) and it seemed unlikely that all of these events could occur in the fast time scale of release. Simultaneous binding of synaptotagmin 1 to SNAREs and phospholipids was also proposed to underlie the observed enhancement of SNARE-dependent proteoliposome fusion by synaptotagmin 1 in the presence of Ca^{2+} (Tucker et al., 2004), but the increase was rather modest (2-4 fold) and was more severely impaired by disruption of Ca^{2+}-binding to the C2A domain than to the C2B domain (Bhalla et al., 2005), in sharp contrast with the critical role of Ca^{2+}-binding to the C2B domain for release *in vivo* (Mackler et al., 2002; Nishiki and Augustine, 2004).

If Ca^{2+} ions can induce simultaneous binding of the synaptotagmin 1 C2AB fragment to negatively charged phospholipids and reconstituted SNARE complex, it is expected that this would increase the apparent membrane affinity of the synaptotagmin 1 C2AB fragment. However, directly measuring such an increase is hindered by the very high affinity of the synaptotagmin 1 C2AB fragment for negatively charged phospholipid in the presence of Ca^{2+} (for instance, binding is quantitative at 10 nM synaptotagmin 1 C2AB fragment and 1 nM concentration of 100 nm vesicles) (Arac et al., 2006). As an alternative, we designed an equilibrium partition experiment that could reveal whether the synaptotagmin 1 C2AB fragment binds preferentially to membranes containing SNARE complexes compared to protein-free membranes. Microfluidic channel technology provided a powerful tool for this

purpose. As illustrated in the diagram of Figure 5.2, we prepared a PDMS slab that, when sealed against a glass coverslip, yielded two exterior microchannels, a shorter parallel microchannel in the middle, and a perpendicular microchannel with a valving screw in the middle. Supported phospholipid bilayers lacking or containing reconstituted SNAREs complexes (molar protein to lipid ratio 1:1000) were deposited by the vesicle fusion method into the exterior microchannels with the valving screw closed to avoid mixing of the two different types of bilayers (both membranes contained 41% (w/w) POPC, 32% (w/w) DPPE, 12% (w/w) DOPS, 5% (w/w) PtdIns, and 10% (w/w) cholesterol, which approximates the lipid composition of synaptic membranes) (Rhee et al., 2005). We then added BODIPY-FL-labeled synaptotagmin 1 C2AB fragment with the valving screw open (the single native cysteine of the synaptotagmin 1 C2AB fragment, cysteine 277, was mutated to serine and a V419C mutation was introduced to yield a single exposed cysteine where the probe was attached). After washing the microchannels with buffer, binding to the plane of the bilayers was monitored with a confocal fluorescence microscope.

When we added substoichiometric amounts of the BODIPY-FL-labeled synaptotagmin 1 C2AB fragment (0.5 equivalent with respect to the reconstituted SNARE complex) in the absence of Ca^{2+}, the synaptotagmin 1 C2AB fragment did not exhibit significant binding to the membranes regardless of the presence or absence of the SNARE complex (Figure 5.3A). However, in analogous experiments performed in the presence of Ca^{2+}, most of the synaptotagmin 1 C2AB fragment partitioned quantitatively to the bilayer containing reconstituted SNARE complexes (Figure 5.3B). Quantitative analysis of the fluorescence intensities revealed that the amount of synaptotagmin 1 C2AB fragment bound

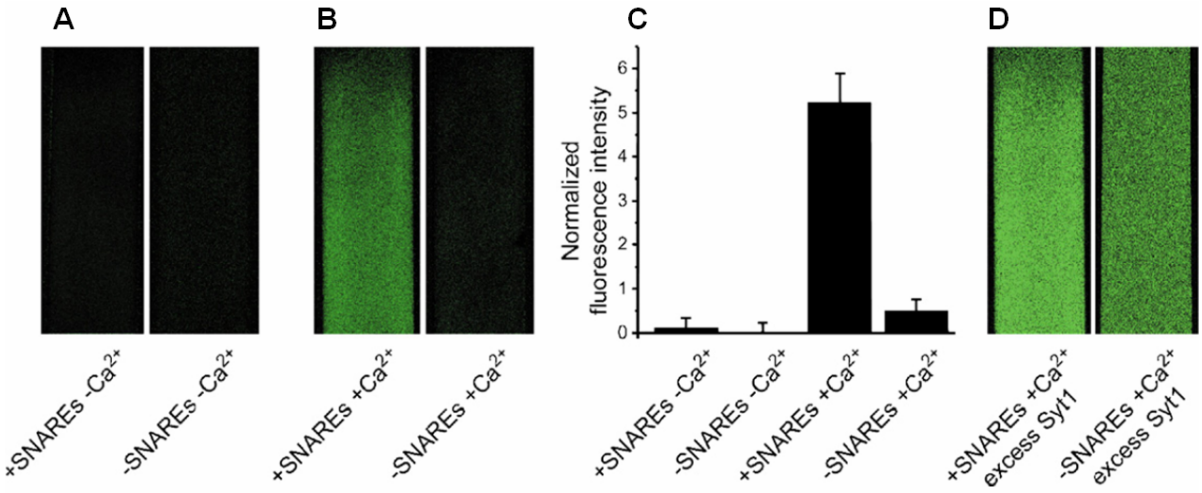

Figure 5.3 Synaptotagmin 1 C2AB fragment binds preferentially to membranes containing the reconstituted SNARE complex.

(A) Confocal micrographs of supported phospholipid bilayers (41% (w/w) POPC, 32% (w/w) DPPE, 12% (w/w) DOPS, 5% (w/w) PtdIns and 10% (w/w) cholesterol) containing or lacking reconstituted SNARE complexes, which were deposited in the external microchannels of the PDMS slab. The micrographs were obtained after injecting 0.5 equivalent of BODIPY-FL-labeled V419C-C2AB fragment (40 nM concentration) in reconstitution buffer containing 1 mM EDTA through the central microchannel with the valving screw open, incubating for 1 hour and washing the microchannels with the same buffer.

(B) Analogous experiments performed with buffer containing 1 mM Ca^{2+} and 0.5 equivalent of BODIPY-FL-labeled V419C-C2AB fragment.

(C) Quantitative analyses of the data shown in (A) and (B). Average fluorescence intensities were measured in each microchannel. The average intensity observed for the residual binding to SNARE-free membranes in the absence of Ca^{2+} (right panel in (A)) was then subtracted and used to normalize all resulting values. Error bars represent standard deviations (SDs).

(D) Partition experiment performed as in (B) but with two equivalents of BODIPY-FL-labeled V419C-C2AB fragment.

to the SNARE-containing bilayer was more than 10-fold higher than that bound to the SNARE-free bilayer (Figure 5.3C). Since the molar SNARE complex to lipid ratio was 1:1000 and the membranes contained 17% (w/w) negatively charged phospholipids, the partition coefficient between membrane sites containing SNARE complexes and sites containing negatively charged phospholipids is much higher than 10-fold. In additional experiments where we added an excess of the synaptotagmin 1 C2AB fragment (two equivalents with respect to the reconstituted SNARE complex) in the presence of Ca^{2+}, binding to both bilayers was observed but still with a clear preference for the bilayer containing SNARE complexes (Figure 5.3D), confirming that the synaptotagmin 1 C2AB fragment binds to SNARE-free phospholipid bilayers under the conditions of these experiments but with lower affinity than to membranes containing reconstituted SNARE complexes.

This result can almost certainly be attributed to simultaneous binding of the synaptotagmin 1 C2AB fragment to phospholipid and SNARE complex, as the synaptotagmin 1 C2AB fragment binds with much higher affinity to the phospholipids than to the soluble SNARE complex. However, it is possible that the SNARE complex assembled on membranes adopts an as-yet-unidentified conformation that provides a very high affinity binding site for the synaptotagmin 1 C2AB fragment, which could underlie the preferential binding to the SNARE complex containing membranes without a direct synaptotagmin 1/membrane interaction. To explore this possibility as well as to evaluate the influence of SNARE binding on the membrane penetration of the synaptotagmin 1 C2AB fragment, we used synaptotagmin 1 C2AB fragments that contained single cysteine mutations at the tip of

one of the Ca^{2+}-binding loops of the C2A domain (F234C, loop 3) or the C2B domain (V304C, loop 1) and that were labeled with an NBD probe. Both phenylalanine 234 and valine 304 contain bulky hydrophobic side chains, which have been shown to penetrate into the membrane, interact with the acyl chains of the phospholipid and make contribution to the hydrophobic interaction between synaptotagmin 1 and membrane. Moreover, biochemical and functional experiments indicated that the mutated residues insert into membranes during neurotransmitter release (Rhee et al., 2005); hence, the mutations are highly unlikely to perturb binding to the SNARE complex *in vivo*. NBD is a fluorophore which has very low fluorescence quantum yield in aqueous solution (<0.01) and exhibits a large increase in fluorescence intensity when transferred from an aqueous to a hydrophobic environment (Crowley et al., 1993). Therefore, the change in the NBD fluorescence intensity can report on the change of the environmental hydrophobicity, in our case, the membrane penetration.

The fluorescence intensities of the NBD-F234C, C277S-C2AB and NBD-V304C, C277S-C2AB fragments in the presence of liposomes increased dramatically upon addition of Ca^{2+} due to insertion of the probes into the hydrophobic interior of the bilayers, which was consistent with the Ca^{2+}-dependent phospholipid-binding of synaptotagmin 1 (Figure 5.4, black traces). Almost identical results were obtained when we performed analogous experiments using liposomes containing reconstituted SNARE complexes (Figure 5.4, red traces). In contrast, soluble SNARE complexes did not induce substantial increases in the fluorescence intensities of the NBD-labeled synaptotagmin 1 C2AB fragments in the presence or absence of Ca^{2+} (Figure 5.4; compare green and magenta traces with the black traces labeled PL - Ca^{2+}). Together with the microchannel partition experiments, these results

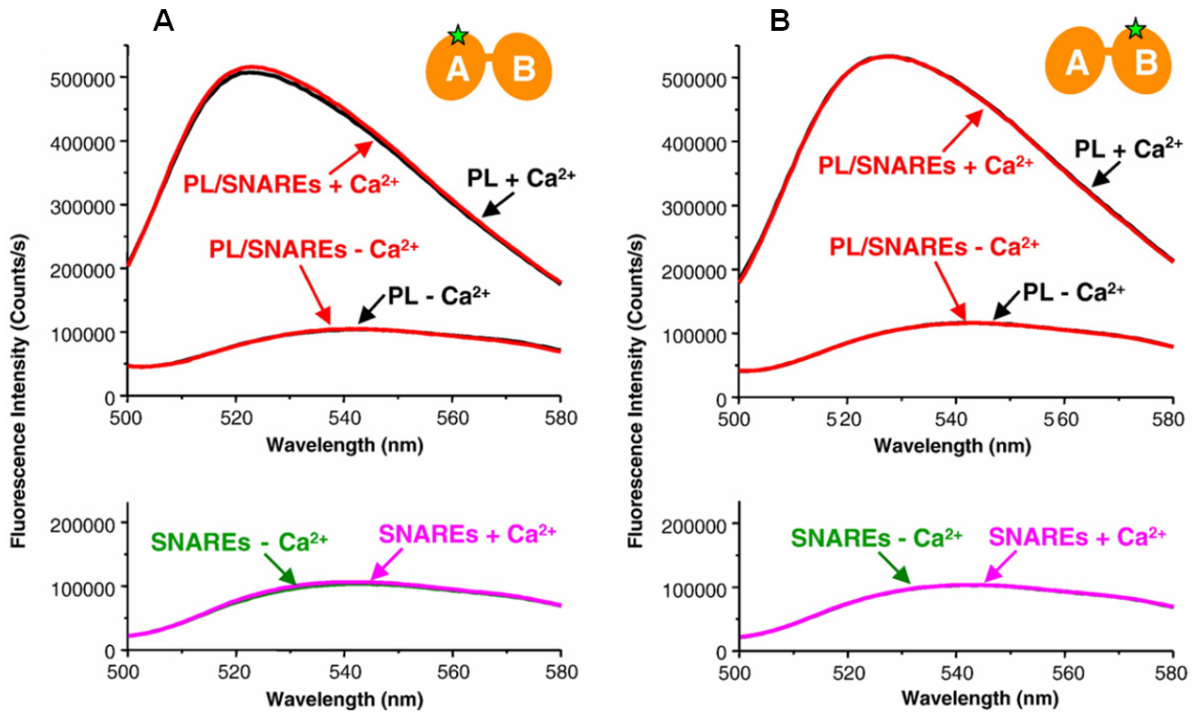

Figure 5.4 The Ca^{2+}-binding loops of the synaptotagmin 1 C2 domains remain inserted into the membrane in the presence of the reconstituted SNARE complex.

(A) Fluorescence spectra of NBD-labeled F234C, C277S double mutant synaptotagmin 1 C2AB fragment in the presence of phospholipid vesicles lacking (black traces) or containing (red traces) reconstituted SNARE complexes, acquired in 1 mM EDTA or 1 mM Ca^{2+}. The bottom panel shows analogous spectra acquired in the presence soluble SNARE complexes and 1 mM EDTA (green) or 1 mM Ca^{2+} (magenta).

(B) Analogous experiments performed with NBD-labeled V304C, C277S mutant synaptotagmin 1 C2AB fragment. The presence of phospholipid vesicles does not perturb the fluorescence spectra of both isolated C2AB fragments in 1 mM EDTA.

unambiguously demonstrated that Ca^{2+} induces simultaneous binding of the synaptotagmin 1 C2AB fragment to phospholipids and the reconstituted SNARE complexes, forming a quaternary SNARE-synaptotagmin-Ca^{2+}-phospholipid (SSCAP) complex. These data also showed that the Ca^{2+}-binding loops of both C2 domains remain inserted into the phospholipid bilayer to a similar extent upon formation of the SSCAP complex.

5.3.2 Ca^{2+}-Dependent Displacement of Complexin by Synaptotagmin 1 in a Membrane-Attached Environment

Our results clearly suggested that synaptotagmin 1 associating with the membrane is capable of SNARE binding. Since both complexin and synaptotagmin 1 are capable of SNARE binding, we wanted to determine whether they could bind simultaneously to the SNARE complex or compete with each other for SNARE binding in the membrane environment even though studies in solution described in chapter 4 suggested a mutually exclusive binding mode. In order to address this question, we monitored the interaction of a BODIPY-FL-labeled complexin fragment with SNARE complex-reconstituted supported proteolipid bilayers (molar protein to lipid ratio 1:1000) deposited into single microfluidic channels with a confocal fluorescence microscope. The complexin fragment used spans residues 26-83 and contains a single cysteine mutation V61C, which is exposed on the opposite side of the SNARE interacting interface. This fragment corresponds to the SNARE complex-interacting region of complexin and had been used to determine the complexin/SNARE complex crystal structure (Chen et al., 2002).

After incubating BODIPY-FL-labeled complexin with the blank supported phospholipid bilayer lacking the reconstituted SNARE complex and subsequently washing out unbound protein, very little green fluorescence was observed, which is consistent with no constitutive membrane association of complexin. In contrast, strong green fluorescence could be observed after washout when BODIPY-FL-labeled complexin was incubated with the SNARE complex-reconstituted supported proteolipid bilayer, indicating the interaction of complexin with the reconstituted SNARE complex and consequent association with the membrane fraction. Addition of synaptotagmin 1 in the presence of 1 mM Ca^{2+} caused a significant reduction of the green fluorescence intensity, indicating that complexin is dissociated from the reconstituted SNARE complex by synaptotagmin 1. In contrast, addition of synaptotagmin 1 in the absence of Ca^{2+} caused no observable reduction of the green fluorescence intensity (Figure 5.5A). The competition is sensitive to the ionic strength of the solution and high ionic strength inhibited the displacement of complexin from the SNARE complex by 1 μM synaptotagmin 1 in the presence of 1 mM Ca^{2+}, indicating the electrostatic nature of the interaction between synaptotagmin 1 and the SNARE complex (Figure 5.5F). A synaptotagmin 1 titration of the competition yielded a sigmoidal competition curve with EC_{50} of 23 ± 5 nM and a Hill coefficient about -1, suggesting that, in a membranous environment, synaptotagmin 1 powerfully dislodges complexin from the reconstituted SNARE complex (Figure 5.5B, 5.5C). A Ca^{2+} titration of the complexin displacement yielded an apparent Ca^{2+} affinity of 53 ± 14 μM (Figure 5.5D). The displacement of complexin from the SNARE complex in the membranous environment by synaptotagmin 1 is strictly dependent on the presence of Ca^{2+}. Even lowering the ionic strength to 0 or 50 mM KCl did not activate Ca^{2+}-

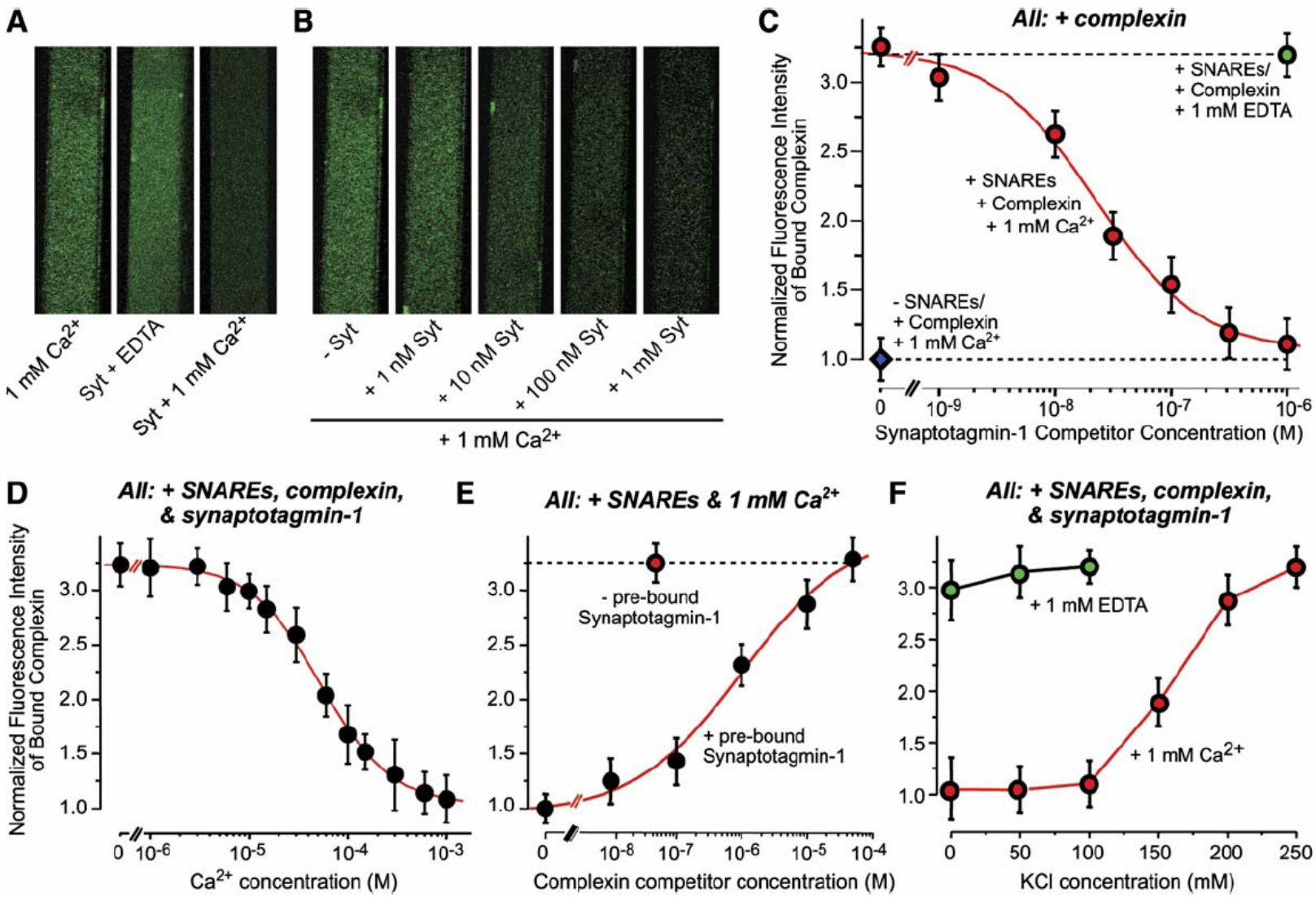
A
1 mM Ca2+
Syt + EDTA
Syt + 1 mM Ca2+
B
- Syt
+ 1 nM Syt
+ 10 nM Syt
+ 100 nM Syt
+ 1 mM Syt
+ 1 mM Ca2+
C
All: + complexin
Normalized Fluorescence Intensity of Bound Complexin
+ SNAREs/ + Complexin + 1 mM EDTA
+ SNAREs + Complexin + 1 mM Ca2+
- SNAREs/ + Complexin + 1 mM Ca2+
Synaptotagmin-1 Competitor Concentration (M)
D
All: + SNAREs, complexin, & synaptotagmin-1
Normalized Fluorescence Intensity of Bound Complexin
Ca2+ concentration (M)
E
All: + SNAREs & 1 mM Ca2+
- pre-bound Synaptotagmin-1
+ pre-bound Synaptotagmin-1
Complexin competitor concentration (M)
F
All: + SNAREs, complexin, & synaptotagmin-1
+ 1 mM EDTA
+ 1 mM Ca2+
KCl concentration (mM)

Figure 5.5 Synaptotagmin 1 displaces complexin from the reconstituted SNARE complex in a Ca^{2+}-dependent manner.

(A) Confocal micrographs of supported phospholipid bilayers containing reconstituted SNARE complexes loaded with 50 nM fluorescent complexin (residues 26–83; labeled with BODIPY-FL). Bilayers were deposited in microfluidic channels and washed with buffer containing 100 mM KCl and the indicated additions (Syt stands for 1 μM synaptotagmin 1 C2AB fragment).

(B) An analogous experiment in which the SNARE complex in the bilayer was loaded with fluorescent complexin and then washed with Ca^{2+}-containing buffer and increasing concentrations of synaptotagmin 1 as indicated. Each wash with synaptotagmin 1 was followed by a wash with buffer alone.

(C) Displacement of prebound fluorescent complexin from the SNARE complex by synaptotagmin 1. Experiments were performed as in (B); average fluorescence intensities measured under each condition were normalized to the control, in which fluorescently labeled complexin was added to a supported bilayer lacking SNARE complexes (blue diamond). Without Ca^{2+}, even the maximal synaptotagmin 1 concentration cannot displace fluorescent complexin from the SNARE complexes (green circle). Data were fitted to a dose-response curve (EC_{50} = 23 ± 5 nM; Hill coefficient = −0.96 ± 0.02). Error bars represent SDs.

(D) Ca^{2+} titration of the displacement of fluorescent complexin from the SNARE complex by 1 μM synaptotagmin 1. Experiments were performed as in (C) with increasing concentrations of free Ca^{2+} (EC_{50} = 53 ± 14 μM; Hill coefficient = −1.24 ± 0.37). Error bars represent SDs.

(E) Displacement of prebound synaptotagmin 1 from the SNARE complex by fluorescent complexin. The displacement of synaptotagmin 1 bound to the reconstituted SNARE complexes was measured in 1 mM Ca^{2+} as the binding of increasing concentrations of fluorescent complexin (EC_{50} = 1.00 ± 0.65 μM; Hill coefficient = −0.53 ± 0.18). As a control, the red circle indicates the amount of 50 nM fluorescent complexin bound in the absence of prebound synaptotagmin 1. Error bars represent SDs.

(F) Effect of ionic strength on the displacement of bound complexin from the SNARE complex by synaptotagmin 1. SNARE complexes were loaded with fluorescent complexin, and the amount of complexin remaining after washing with 1 μM synaptotagmin 1 at different KCl concentrations was quantified. Experiments were performed in the presence of 1 mM Ca^{2+} (red circles) or 1 mM EDTA (green circles). Error bars represent SDs.

independent binding of synaptotagmin 1 to the SNARE complex or enable synaptotagmin 1 to displace complexin from the SNARE complex in a Ca^{2+}-independent manner (Figure 5.5F).

We also performed the reverse competition experiments to probe whether complexin in a membranous environment could in turn displace synaptotagmin 1 from the SNARE complex by measuring the binding of fluorescently labeled complexin to membrane-attached SNARE complex in the presence of prebound synaptotagmin 1. Without prebound synaptotagmin 1, 50 nM complexin quantitatively bound to the SNARE complex. With prebound synaptotagmin 1, by contrast, micromolar complexin concentrations were required for binding, with an apparent affinity ~40-fold lower than that of the displacement of complexin by synaptotagmin 1 (EC_{50} = 1.0 ± 0.2 μM) (Figure 5.5E).

5.3.3 Structural Analysis of the Interactions between the Synaptotagmin 1 C2AB Fragment and the Soluble SNARE Complex

Structural characterization of the quaternary SSCAP complex at high resolution by X-ray crystallography or NMR spectroscopy is hindered by the necessity of including membranes in the complex and by its large molecular weight. Attempts to study Ca^{2+}-dependent interactions between the synaptotagmin 1 C2AB fragment and the soluble SNARE complex by NMR spectroscopy invariably led to precipitation even at 12 μM protein concentrations. This tendency to precipitate might arise from Ca^{2+}-induced nonspecific interactions involving the Ca^{2+}-binding loops of the synaptotagmin 1 C2AB fragment, which may bind to the highly acidic surface of the SNARE complex in the absence of membranes.

We reasoned that such nonspecific interactions may be minimized in the absence of Ca^{2+} and that Ca^{2+}-independent binding between the synaptotagmin 1 C2AB fragment and the soluble SNARE complex may reflect more faithfully the relevant interactions within the quaternary SSCAP complex, since the Ca^{2+}-binding regions of the two C2 domains interact with the membrane in this complex (Figure 5.4). However, the oligomerization tendency of SNARE complexes hindered analysis of their Ca^{2+}-independent interactions with the synaptotagmin 1 C2AB fragment in solution by NMR spectroscopy. To circumvent this problem, we used a SNARE complex with a C-terminal truncation in the syntaxin SNARE motif (at residue 253) that renders the complex monomeric (Chen et al., 2002). This SNARE complex was composed of syntaxin 1A (191-253), synaptobrevin 2 (29-93), SNAP-25 (11-82-W)/ SN I, and SNAP-25 (141-203-W)/ SN III and referred to as the short SNARE complex.

The molecular weight of both the short SNARE complex and the synaptotagmin 1 C2AB fragment is about 30 kDa and thus their 1:1 complex will be about 60 kDa. Together with the fact that SNARE complex exhibits an elongated shape and consequently has slower tumbling rate and faster transverse relaxation rate than expected for its molecular weight, regular ^{1}H-^{15}N HSQC experiments could not yield good quality spectra due to the broadened linewidths, and consequently low intensity and poor sensitivity. Therefore, we used the transverse-relaxation optimized spectroscopy (TROSY) technique, which constructively utilizes the interference between dipole-dipole (DD) coupling and chemical shift anisotropy (CSA) to suppress transverse nuclear spin relaxation (Pervushin et al., 1997; Riek et al., 2002). The two major significant sources of relaxation in proteins are CSA of each individual spin and the DD coupling. However, CSA and DD interfere with each other, and under

certain circumstances, they can almost completely cancel each other and thus eliminate the transverse relaxation effects originated from them. In the amide bond spin system, the one-bond scalar coupling between the ^{1}H nuclei and ^{15}N nuclei gives rise to four distinct multiplet components of the signal, which are combined into one signal by decoupling to boost the intensity in the conventional NMR experiments. However, each of the four components has a different transverse relaxation rate due to different degrees of interference between CSA and DD, which will also be averaged in the conventional NMR experiments. In contrast, TROSY spectra select exclusively the component with the slowest relaxation rate and narrowest linewidth, and eliminate the other components with faster relaxation rates. Theory predicts that the complete cancellation of CSA and DD for this component occurs at ^{1}H frequencies near 1 GHz due to the fact that the CSA increases with higher magnetic fields whereas the DD interaction is independent of the magnetic field. Therefore, a higher magnetic field will boost the TROSY effect. Moreover, due to the low gyromagnetic ratio of the deuteron ($\gamma D/\gamma H = 0.15$), replacement of the protons with deuterons will significantly attenuate the DD interaction and decrease amide proton transverse relaxation rate, improving the sensitivity and resolution of the spectra. Therefore, perdeuteration will help to further suppress the residual linewidth of the selected resonance due to the DD interaction with remote protons in the proteins in TROSY experiments.

Another complication of NMR spectroscopy for molecules with larger molecular weight is the increasing number of resonances and thus more crowded spectra and concomitant worse resolution. For the short SNARE complex in the presence or absence of synaptotagmin 1, selective isotope labeling can be easily carried out to alleviate this problem.

The selective labeling strategy will significantly reduce the number of NMR-visible nuclei, thus simplifying the data acquisition and processing. For example, to map the binding region in the SNARE core complex, each SNARE motif can be individually labeled and assembled with non-labeled corresponding fragments, which will generate only about 60-70 crosspeaks in the ^{1}H-^{15}N TROSY-HSQC spectra.

To gain insight into the region(s) of synaptotagmin 1 involved in binding to the SNARE complex, we first acquired TROSY-enhanced ^{1}H-^{15}N HSQC spectra of Ca^{2+}-free ^{2}H, ^{15}N-labeled synaptotagmin 1 C2AB fragment in the presence or absence of unlabeled short SNARE complex at 40 μM protein concentration as a compromise to obtain sufficient sensitivity while minimizing nonspecific interactions. These experiments were done by a previous graduate student Demet Arac from our laboratory. Previous studies from our lab showed that ^{1}H-^{15}N TROSY-HSQC spectra of the synaptotagmin 1 C2AB fragment contain two subsets of crosspeaks that precisely correspond to those of the isolated C2A and C2B domain, which suggested that the two C2 domains are flexibly linked (Arac et al., 2006). Upon addition of the short SNARE complex to the ^{2}H, ^{15}N-labeled synaptotagmin 1 C2AB fragment, the ^{1}H-^{15}N TROSY-HSQC crosspeaks from the C2B domain exhibited much more severe broadening than those from the C2A domain (Figure 5.6A, 5.6B). This observation showed that binding to the short SNARE complex is primarily mediated by the C2B domain, while the C2A domain remains flexibly linked to the C2B domain/SNARE complex. Mapping the significant crosspeak shifts and strongest broadening effects onto the structure of the C2B domain (Figure 5.6C) showed that strand 4 and its neighboring sequences are the most affected by binding to the short SNARE complex, but some perturbations are also

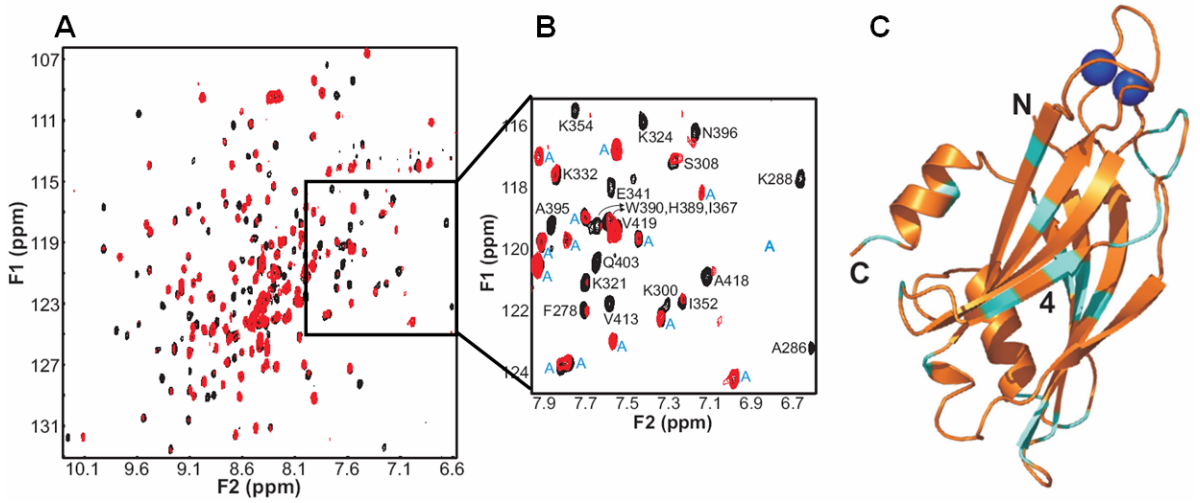

Figure 5.6 NMR analysis of Ca^{2+}-independent synaptotagmin 1/SNARE complex interactions and mapping the binding interfaces on synaptotagmin 1.

(A) Superposition of ^{1}H-^{15}N HSQC spectra of Ca^{2+}-free ^{2}H,^{15}N-labeled C2AB fragment in the absence (black contours) and presence (red contours) of unlabeled short SNARE complex. These experiments were done by a previous graduate student Demet Arac from our laboratory.

(B) Expansions of the ^{1}H-^{15}N HSQC spectra shown in (A). Crosspeaks from the C2B domain are labeled with the residue number and one letter abbreviation, whereas crosspeaks from the C2A domain are labeled with a blue 'A'.

(C) Ribbon diagram of the C2B domain summarizing the most significant perturbations in the ^{1}H-^{15}N HSQC crosspeaks of the C2B domain caused by Ca^{2+}-independent binding to the short SNARE complex. Residues corresponding to crosspeaks that exhibit significant shifts or have strong initial intensities and are broadened beyond detection upon binding are colored in cyan (disappearance of crosspeaks with weak initial intensities was not considered significant due to the overall broadening observed for most C2B domain crosspeaks). The two Ca^{2+} ions that bind to the C2B domain are shown as blue spheres to point out their binding sites, but the data were obtained in the absence of Ca^{2+}. Strand 4 of the β-sandwich is labeled.

observed in other regions of the C2B domain. These results are consistent with a previous report that a polybasic sequence in strand 4 of the C2B domain mediates Ca^{2+}-independent SNARE complex binding (Rickman et al., 2004). The widespread perturbations observed in the ^{1}H-^{15}N TROSY-HSQC crosspeaks of the C2B domain may arise from an overall (although likely subtle) structural rearrangement induced by binding. It is also possible that several regions around the C2B domain in addition to the polybasic sequence may interact with the SNARE complex under the conditions of these experiments.

To gain insight into the region(s) of the SNARE complex involved in binding to the C2B domain, we acquired ^{1}H-^{15}N TROSY-HSQC spectra of a sample of the short SNARE complex assembled with the ^{2}H, ^{15}N-labeled C-terminal SNARE motif of SNAP-25 (SN III), since some data have suggested a functional interaction between this SNARE motif and synaptotagmin 1 (Zhang et al., 2002). ^{1}H-^{15}N TROSY-HSQC spectra acquired in the presence or absence of Ca^{2+}-free unlabeled synaptotagmin 1 C2AB fragment (Figure 5.7A) showed that binding to the synaptotagmin 1 C2AB fragment induced selective broadening in subsets of crosspeaks that could be mapped to three distinct regions of the SNARE complex (Figure 5.7B): 1) an acidic central region that was previously implicated in Ca^{2+}-independent synaptotagmin 1 binding (Rickman et al., 2006); 2) another acidic region close to the C-terminus that was implicated in Ca^{2+}-dependent synaptotagmin 1 binding in a separate study (Zhang et al., 2002); and 3) a basic region at the very C-terminus. Hence these data were partially consistent with previous studies of synaptotagmin 1/SNARE complex interactions, but raised the possibility that these interactions might not be highly specific.

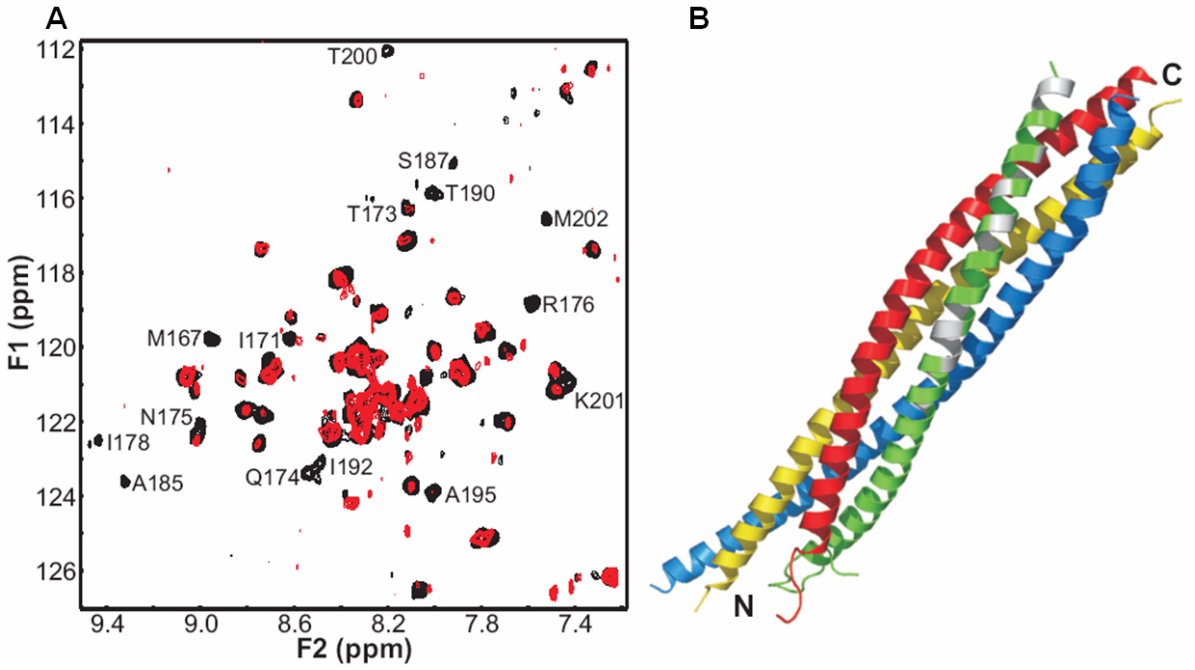

Figure 5.7 NMR analysis of Ca^{2+}-independent synaptotagmin 1/ SNARE complex interactions and mapping the binding interfaces on the SNARE complex.

(A) Superposition of ^{1}H-^{15}N TROSY-HSQC spectra of a sample of the short SNARE complex with the C-terminal SNAP-25 SNARE motif ^{2}H,^{15}N-labeled, acquired in 1 mM EDTA and the absence (black contours) or presence (red contours) of unlabeled C2AB fragment. Crosspeaks exhibiting the most significant broadening upon binding are labeled.

(B) Ribbon diagram of the SNARE complex with the SNAP-25 residues corresponding to severely broadened crosspeaks shown in white. The syntaxin SNARE motif is shown in yellow, the synaptobrevin SNARE motif is shown in red and the SNAP-25 N-terminal and C-terminal SNARE motifs are shown in blue and green, respectively.

5.3.4 Hypothetical Model of the Quaternary SSCAP Complex

The observations that phospholipid vesicles could displace the soluble SNARE complex from the synaptotagmin 1 C2AB fragment in the presence of Ca^{2+} (Arac et al., 2003), and yet Ca^{2+} could induce simultaneous binding of the synaptotagmin 1 C2AB fragment to phospholipids and membrane-anchored SNARE complex (Figure 5.3 and Figure 5.4), suggested that Ca^{2+}-dependent binding of the synaptotagmin 1 C2AB fragment to the soluble SNARE complex cannot reproduce the interactions present within the quaternary SSCAP complex and may arise from nonspecific interactions involving the C2 domain Ca^{2+}-binding loops. This notion is supported by the tendency of the SNARE complex and the synaptotagmin 1 C2AB fragment to establish nonspecific interactions, as revealed by our NMR analysis of Ca^{2+}-independent C2AB fragment/SNARE complex interactions (Figure 5.6 and Figure 5.7). Such nonspecific interactions may be exacerbated by Ca^{2+} and are likely electrostatic in nature given the high sensitivity of Ca^{2+}-dependent and Ca^{2+}-independent binding between the synaptotagmin 1 C2AB fragment and the SNARE complex to the ionic strength, and the highly uneven distribution of charges on their surfaces (Figure 5.8 and Figure 5.9A). Thus, a large part of the SNARE complex surface is highly negative and exhibits diverse types of interactions with the positively charged C-terminus of the SNARE complex itself or the highly basic C2B domain (Figure 5.8A). The C2A domain has a predominance of negative charges but its Ca^{2+}-binding region becomes highly positively charged upon binding three Ca^{2+} ions (Figure 5.8B, 5.8C). This drastic switch in electrostatic potential was shown to mediate Ca^{2+}-dependent binding to syntaxin through the C2A domain Ca^{2+}-binding loops (Shao et al., 1997) and might also underlie the observation of a

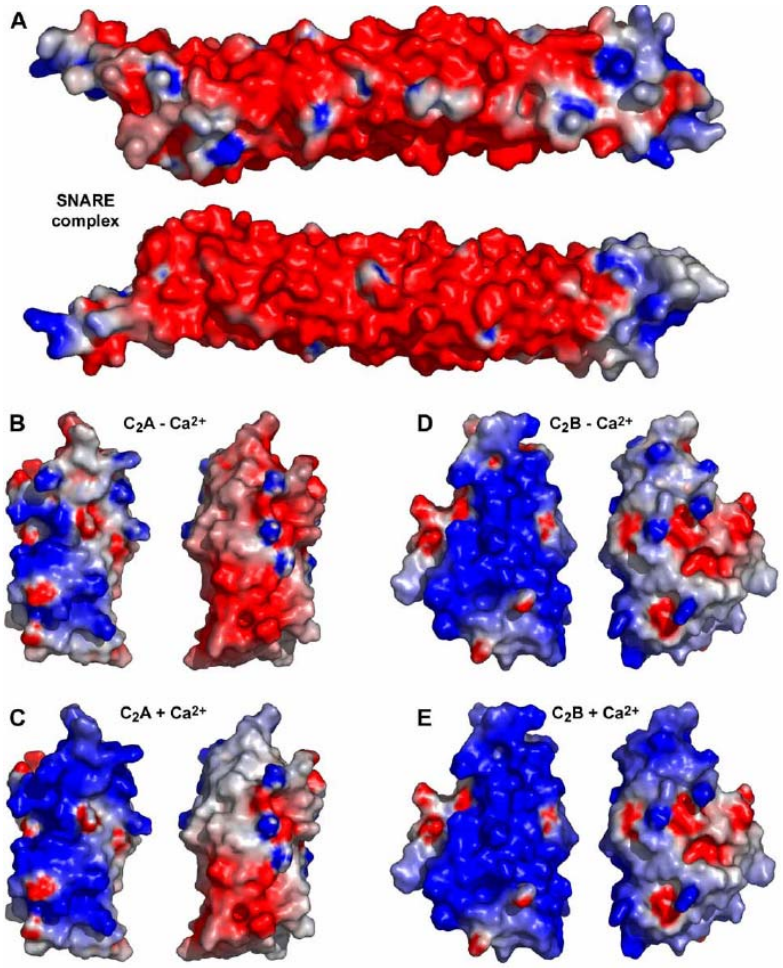

Figure 5.8 Surface electrostatic potential of the SNARE complex and the synaptotagmin 1 C2 domains.

(A) Surface electrostatic potential of the SNARE complex from two orientations representing a 90° rotation along the horizontal axis.

(B) Surface electrostatic potential of the synaptotagmin 1 C2A domain in the absence of Ca^{2+} from two orientations representing a 90° rotation along the vertical axis.

(C) Surface electrostatic potential of the synaptotagmin 1 C2A domain in the presence of Ca^{2+} from two orientations representing a 90° rotation along the vertical axis.

(D) Surface electrostatic potential of the synaptotagmin 1 C2B domain in the absence of Ca^{2+} from two orientations representing a 90° rotation along the vertical axis.

(E) Surface electrostatic potential of the synaptotagmin 1 C2B domain in the presence of Ca^{2+} from two orientations representing a 90° rotation along the vertical axis.

preponderant role for the C2A domain in Ca^{2+}-dependent binding to SNAP-25 (Gerona et al., 2000) and the SNARE complex (Davis et al., 1999). Although the Ca^{2+}-free C2B domain is already highly positively charged, Ca^{2+} also switches the electrostatic potential of its Ca^{2+}-binding region and could thus increase its affinity for negatively charged surfaces (Figure 5.8D, 5.8E). Indeed, the Ca^{2+}-binding loops of both C2 domains have been implicated in Ca^{2+}-dependent binding to SNAP-25 (Wang et al., 2003b). The incompatibility of synaptotagmin 1 C2AB fragment binding to phospholipids and the soluble SNARE complex in the presence of Ca^{2+} (Arac et al., 2003) further supported the notion that both interactions involve the same C2 domain surfaces (i.e. those of the Ca^{2+}-binding loops), and suggested that membrane anchoring of the SNARE complex is critical for the interactions with the synaptotagmin 1 C2AB fragment present in the quaternary SSCAP complex.

All these observations led us to the hypothetical model of the SSCAP complex summarized in Figure 5.9B. This model assumes that both synaptotagmin 1 C2 domains bind to the membrane through their Ca^{2+}-binding loops in a similar orientation to that observed in the absence of reconstituted SNAREs (Figure 5.4), which has been defined by EPR spectroscopy (Frazier et al., 2003; Rufener et al., 2005; Herrick et al., 2006). The model also hypothesizes that the C2AB fragment/SNARE interactions within the SSCAP complex might be partially mimicked in analyses of Ca^{2+}-independent binding of the synaptotagmin 1 C2AB fragment to soluble SNARE complex because the absence of Ca^{2+} minimizes binding modes involving the Ca^{2+}-binding loops. Hence, a prediction of the model is that the polybasic region on one side of the C2B domain β-sandwich binds to an acidic region of the membrane-anchored SNARE complex. Furthermore, key predictions of the model are that

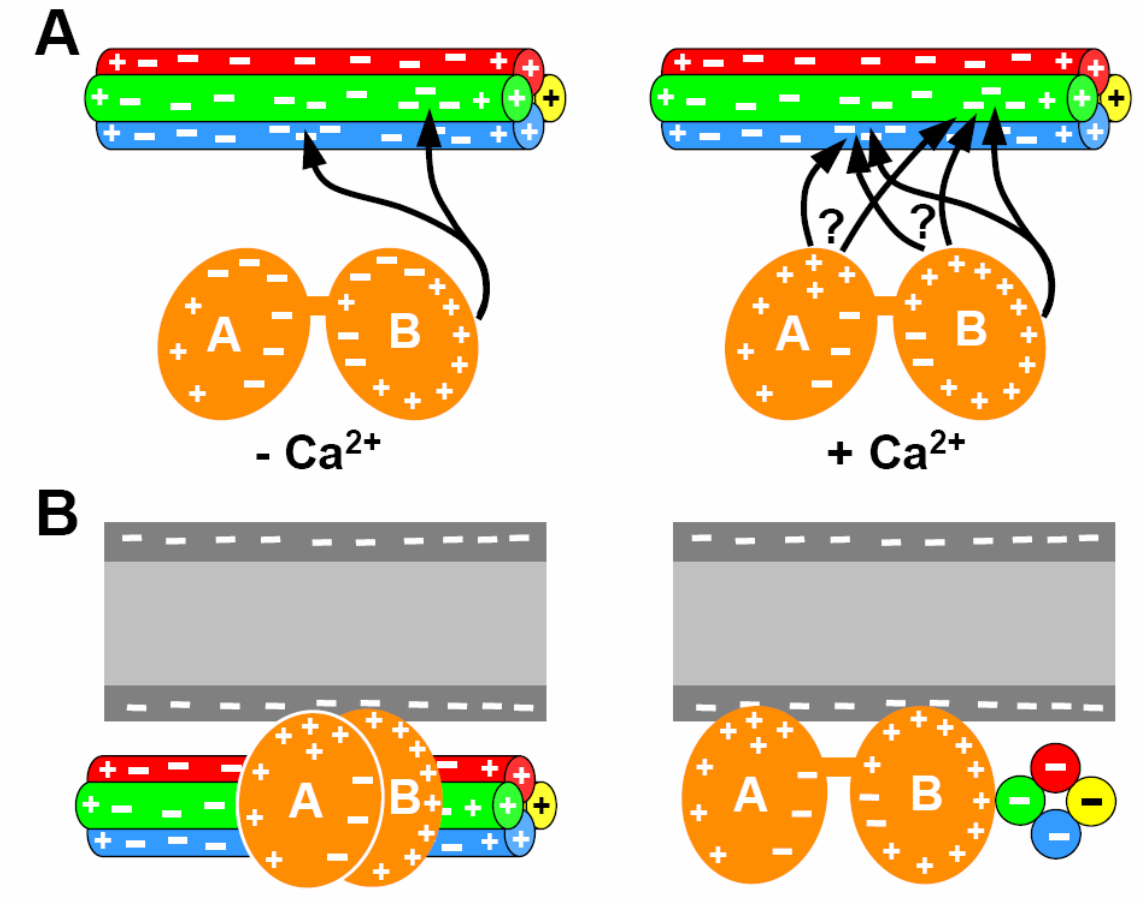

Figure 5.9 Models of synaptotagmin 1/SNARE complex interactions.

(A) Postulated Ca^{2+}-independent (left) and Ca^{2+}-dependent (right) binding modes involving soluble SNARE complexes. The syntaxin SNARE motif is shown in yellow, the synaptobrevin SNARE motif is shown in red and the SNAP-25 N-terminal and C-terminal SNARE motifs are shown in blue and green, respectively. The synaptotagmin 1 C2AB fragment is shown in orange.

(B) Model of the SSCAP complex shown from two orientations representing a 90° rotation. The models illustrate qualitatively the charge distribution in the surface of the C2 domains and the SNARE complex. The syntaxin SNARE motif is shown in yellow, the synaptobrevin SNARE motif is shown in red and the SNAP-25 N-terminal and C-terminal SNARE motifs are shown in blue and green, respectively. The synaptotagmin 1 C2AB fragment is shown in orange.

membrane anchoring of the SNARE complex increases the specificity and affinity of its interactions with the C2B domain, and that these interactions are intimately correlated with the C2B domain-phospholipid interactions within the SSCAP complex. Thus, the weaker and less specific interactions between the C2B domain and the soluble SNARE complex may not be able to persist upon Ca^{2+}-dependent binding of the synaptotagmin 1 C2AB fragment to phospholipids because the natural thermal motions of the highly elongated SNARE complex may cause steric clashes with the bilayer in the absence of membrane anchoring. This notion can explain the release of the soluble SNARE complex from the Ca^{2+}-bound synaptotagmin 1 C2AB fragment upon addition of phospholipid (Arac et al., 2003).

5.3.5 Structural Determinants of the Quaternary SSCAP Complex Formation

We have shown in section 5.3.2 that the synaptotagmin 1 C2AB fragment displaces complexin bound to membrane-anchored SNARE complex in a Ca^{2+}-dependent manner. Such displacement may be crucial to trigger membrane fusion during neurotransmitter release, as suggested by recent electrophysiological data (Tang et al., 2006) and *in vitro* membrane fusion studies (Giraudo et al., 2006; Schaub et al., 2006), and likely arises due to the quaternary SSCAP complex formation. Hence, the complexin displacement assay mentioned earlier provides a convenient means to study the structural determinants of quaternary SSCAP complex formation while mimicking a reaction that likely underlies, at least in part, the sequence of late events that lead to Ca^{2+}-triggering of neurotransmitter release. As shown before, the synaptotagmin 1 C2AB fragment quantitatively displaced complexin bound to the membrane anchored SNARE complex in the presence but not in the

absence of Ca^{2+} when we used our standard membrane composition, which includes negatively charged phospholipids (Figure 5.10A, 5.10B). However, no complexin displacement was observed even in the presence of Ca^{2+} when we substitute the neutral charged phosphotidylcholine (PC) for negatively charged phosphotidylserine (PS) and phosphotidylinositol (PtdIns) in the membranes (Figure 5.10C). The requirement of negatively charged phospholipids actually suggested that phospholipid binding of synaptotagmin 1 is a prerequisite for its efficient interaction with the SNARE complex, which also supports the notion that synaptotagmin 1 binds simultaneously to both the SNARE complex and phospholipids in the presence of Ca^{2+}. Phospholipid binding probably helps to increase the effective concentration of synaptotagmin 1 on the membrane through reducing three-dimensional (3D) diffusion to a much more efficient two-dimensional (2D) one and orientate them properly for SNARE interactions. This result showed that membrane binding and hence the quaternary SSCAP complex formation is required for the synaptotagmin 1 C2AB fragment to displace complexin from the SNARE complex.

We next monitored the displacement of complexin as a function of the concentration of different synaptotagmin 1 fragments in the presence of Ca^{2+}. The wild type synaptotagmin 1 C2AB fragment displaced complexin efficiently at submicromolar concentrations and the isolated C2B domain was also able to displace complexin, albeit at higher concentrations (Figure 5.11). However, the isolated C2A domain was basically unable to displace complexin even at 100 μM concentration. A synaptotagmin 1 C2AB fragment with a mutation that disrupts Ca^{2+} binding to the C2A domain (C2A*B) was as effective in displacing complexin as the isolated C2B domain, whereas disrupting Ca^{2+} binding to the C2B domain in the

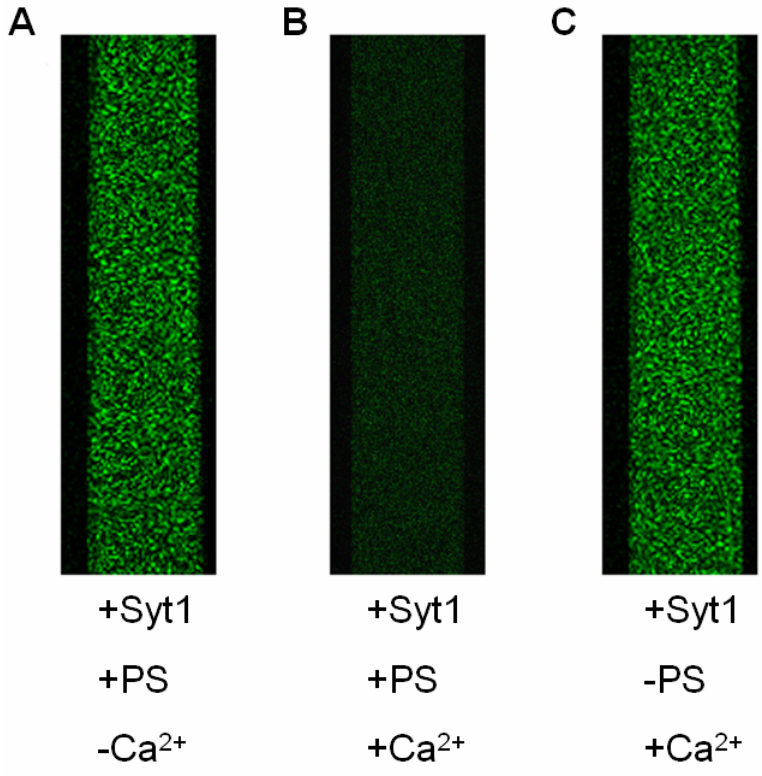

Figure 5.10 Negatively charged phospholipid is necessary for the displacement of complexin from the reconstituted SNARE complex by synaptotagmin 1.

(A) Confocal micrographs of supported bilayers containing reconstituted SNARE complexes deposited within microfluidic channels. The bilayers were loaded with 50 nM BODIPY-FL-labeled complexin fragment (residues 26-83) and washed with buffer containing 100 mM KCl, 1 μM C2AB fragment (+Syt1) and 1 mM EDTA (-Ca^{2+}).

(B) The bilayers were loaded with 50 nM BODIPY-FL-labeled complexin fragment (residues 26-83) and washed with buffer containing 100 mM KCl, 1 μM C2AB fragment (+Syt1) and 1 mM Ca^{2+} (+Ca^{2+}).

(C) The bilayers lacking PS were loaded with 50 nM BODIPY-FL-labeled complexin fragment (residues 26-83) and washed with buffer containing 100 mM KCl, 1 μM C2AB fragment (+Syt1) and 1 mM Ca^{2+} (+Ca^{2+}).

synaptotagmin 1 C2AB fragment (C2AB*) almost abolished its ability to displace complexin (Figure 5.11). These results were consistent with a model whereby the C2B domain binds directly to the SNAREs in the quaternary SSCAP complex, displacing complexin, while the C2A domain plays an auxiliary role by cooperating with the C2B domain in phospholipid binding, thereby increasing indirectly the overall affinity of the quaternary SSCAP complex and the ability of the C2B domain to displace complexin. Importantly, these results correlated with the much stronger impairment of neurotransmitter release caused by disruption of Ca^{2+} binding to the synaptotagmin 1 C2B domain compared to disruption of Ca^{2+} binding to the C2A domain (Mackler et al., 2002; Fernandez-Chacon et al., 2002; Robinson et al., 2002; Stevens and Sullivan, 2003; Nishiki and Augustine, 2004). Moreover, since the C2AB* mutant should still bind to the membrane through the C2A domain (Arac et al., 2006), the strong effect of the mutation in the C2B domain Ca^{2+} binding sites showed that formation of the quaternary SSCAP complex is not simply a result of membrane localization but requires Ca^{2+}-dependent binding of the C2B domain to phospholipids. These observations suggested that the quaternary SSCAP complex involves intimately correlated contacts of the C2B domain with the phospholipids and the SNAREs.

Since our NMR experiments and previous data reported by Davletov's group (Rickman et al., 2004) indicated that the polybasic region of the C2B domain might be involved in SNARE complex binding (Figures 5.6), we also performed the complexin displacement assay with a synaptotagmin 1 C2AB fragment containing a double lysine to alanine mutation in this region (K326A, K327A) that has been widely used in previous studies (Li et al., 2006; Rickman et al., 2004; Chapman et al., 1998; Mackler and Reist,

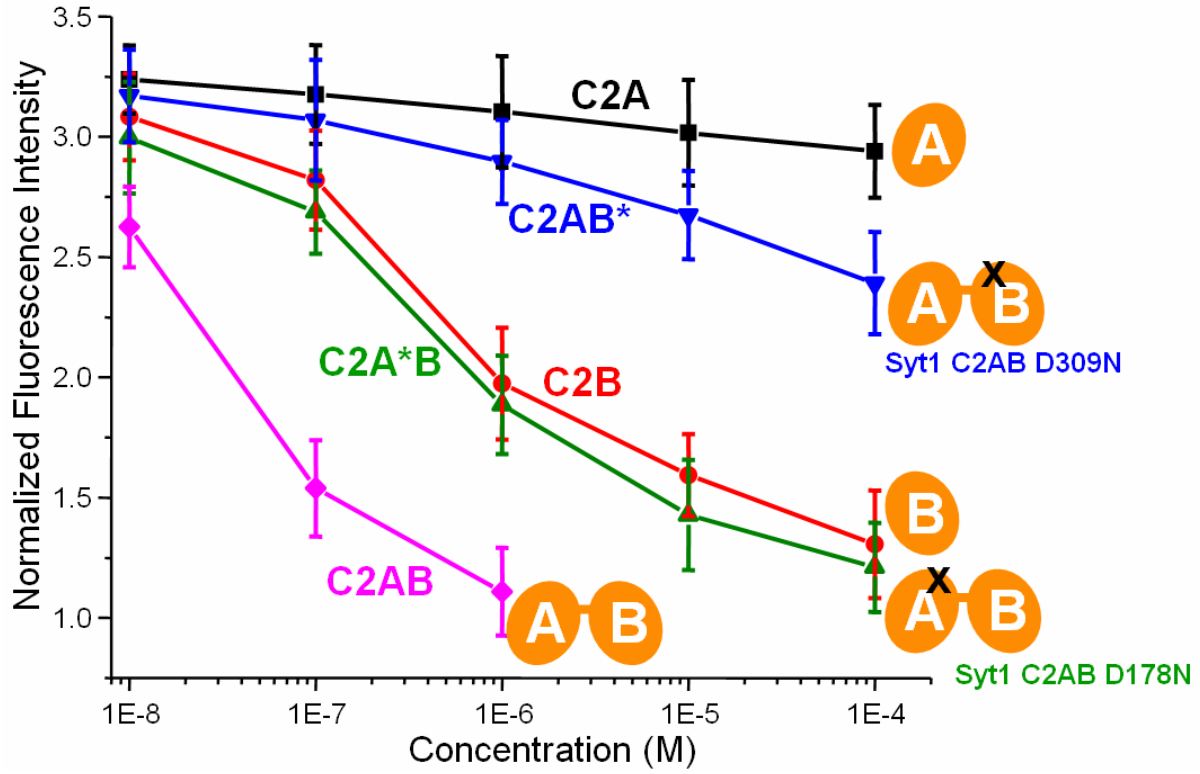

Figure 5.11 Synaptotagmin 1 C2B domain plays a preponderant role in the displacement of complexin from the reconstituted SNARE complex.

Experiments were performed as in Figure 5.10 with PS-containing membranes and 1 mM Ca^{2+}. Average fluorescence intensities measured under each condition were normalized to a control in which the fluorescently labeled complexin fragment was added to a supported bilayer lacking SNARE complexes. Error bars represent SDs. All experiments were performed with wild type SNARE complexes and additions of wild type C2AB fragment (magenta), C2A domain (black) or C2B domain (red), or mutant C2AB fragment bearing mutations that disrupt Ca^{2+}-binding to the C2A domain (D178N, green) or the C2B domain (D309N, blue).

2001). This mutation considerably decreased but did not abolish the ability of the synaptotagmin 1 C2AB fragment to displace complexin (Figure 5.12), which correlates with the partial but not complete impairment of neurotransmitter release caused by this mutation *in vivo* (Mackler and Reist, 2001; Li et al., 2006) and shows that the polybasic region of the C2B domain participates in the quaternary SSCAP complex formation. We also studied the effects of mutations in two acidic regions of SNAP-25 that have previously been implicated in synaptotagmin 1 binding (Zhang et al., 2002; Rickman et al., 2006). One mutation (D51K, E52K, E55K) is in the middle of the SNARE complex, adjacent to the central region of the SNAP-25 C-terminal SNARE motif that was perturbed by the synaptotagmin 1 C2AB fragment in our NMR experiments (Figure 5.7A, 5.7B). The other mutation (D186K, D193K) is closer to the C-terminus of the SNARE complex, in a region of the SNAP-25 C-terminal SNARE motif that was also implicated in synaptotagmin 1 C2AB fragment binding by our NMR data (Figure 5.7A, 5.7B). The mutations did not decrease the amount of complexin bound to the SNARE complex in the absence of synaptotagmin 1 C2AB fragment (Figure 5.12), showing that they did not prevent the SNARE complex assembly. Importantly, the wild type synaptotagmin 1 C2AB fragment was almost equally effective in displacing complexin from the D51K, E52K, E55K triple mutant SNARE complex as from the wild type SNARE complex (practically within experimental error), whereas the D186K, D193K double mutation strongly impaired such displacement (Figure 5.12). These results showed that the acidic region containing aspartate 186 and aspartate 193 at the C-terminus of SNAP-25 participates in binding to the synaptotagmin 1 C2AB fragment within the quaternary SSCAP complex, correlated with the impairment of exocytosis caused by mutations in this

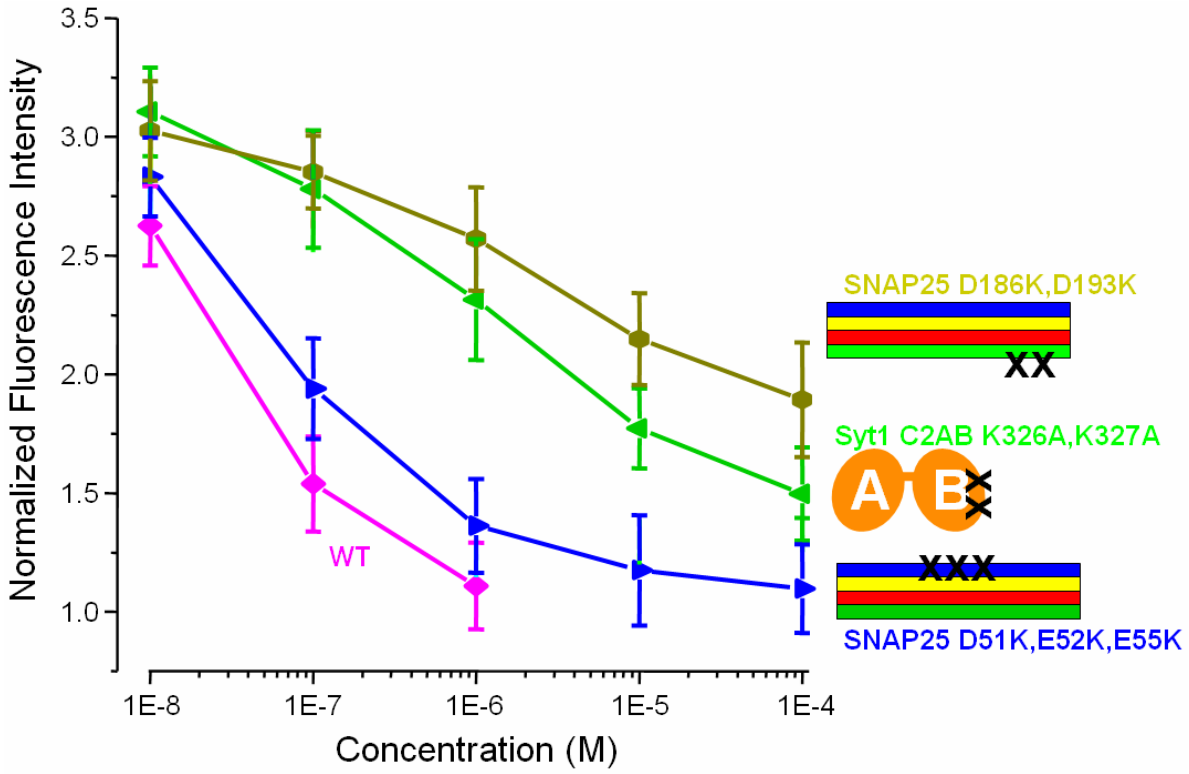

Figure 5.12 Mutagenesis analyses by the complexin displacement assay.

Experiments were performed as in Figure 5.10 with PS-containing membranes and 1 mM Ca^{2+}. Average fluorescence intensities measured under each condition were normalized to a control in which the fluorescently labeled complexin fragment was added to a supported bilayer lacking SNARE complexes. Error bars represent SDs. Experiments were performed with wild type SNARE complexes and C2AB fragment bearing the K326A, K327A mutation in the polybasic region of the C2B domain (green), or with wild type C2AB fragment and SNARE complexes bearing mutations in acidic residues of the SNAP-25 C-terminal SNARE motif (D51K, E52K, E55K blue; D186K, D193K, light green); the data obtained with wild type SNARE complexes and the C2AB fragment (magenta) is also shown in this diagram for reference.

region (Zhang et al., 2002), and suggested that membrane anchoring of the SNARE complex increases the specificity of C2AB fragment/SNARE complex interactions.

5.3.6 Model of the Quaternary SSCAP Complex

To gain further insight into the structure of the quaternary SSCAP complex, we investigated how the C2B domain might dock onto the SNARE complex using the HADDOCK program (Dominguez et al., 2003) and imposing proximity between the C2B domain polybasic region and residues aspartate 186, aspartate 193 of SNAP-25 as the sole restraints. Ribbon diagrams representing the top five clusters of models of the orientation of the C2B domain with respect to the SNARE complex yielded by the HADDOCK program are shown in Figure 5.13A. Interestingly, while there is an expected variability in the orientations observed in the five models given the paucity of restraints, the Ca^{2+}-binding loops of the C2B domain pointed in the same direction in all models (toward the top in Figure 5.13A). In addition, one of the HADDOCK models (in orange in Figure 5.13A; shown from a different view in Figure 5.13B) was similar to the top model yielded by parallel calculations performed with another docking program FTDock (Gabb et al., 1997). Clearly, these models must be considered preliminary, but they all share three interesting features in common.

First, the N-terminus of the C2B domain, where the C2A domain is attached, is oriented away from the SNARE complex (Figure 5.13C). Hence, the C2A domain cannot participate in SNARE complex binding in this orientation, but it can assist in formation of the quaternary SSCAP complex by binding to phospholipids, in correlation with the limited

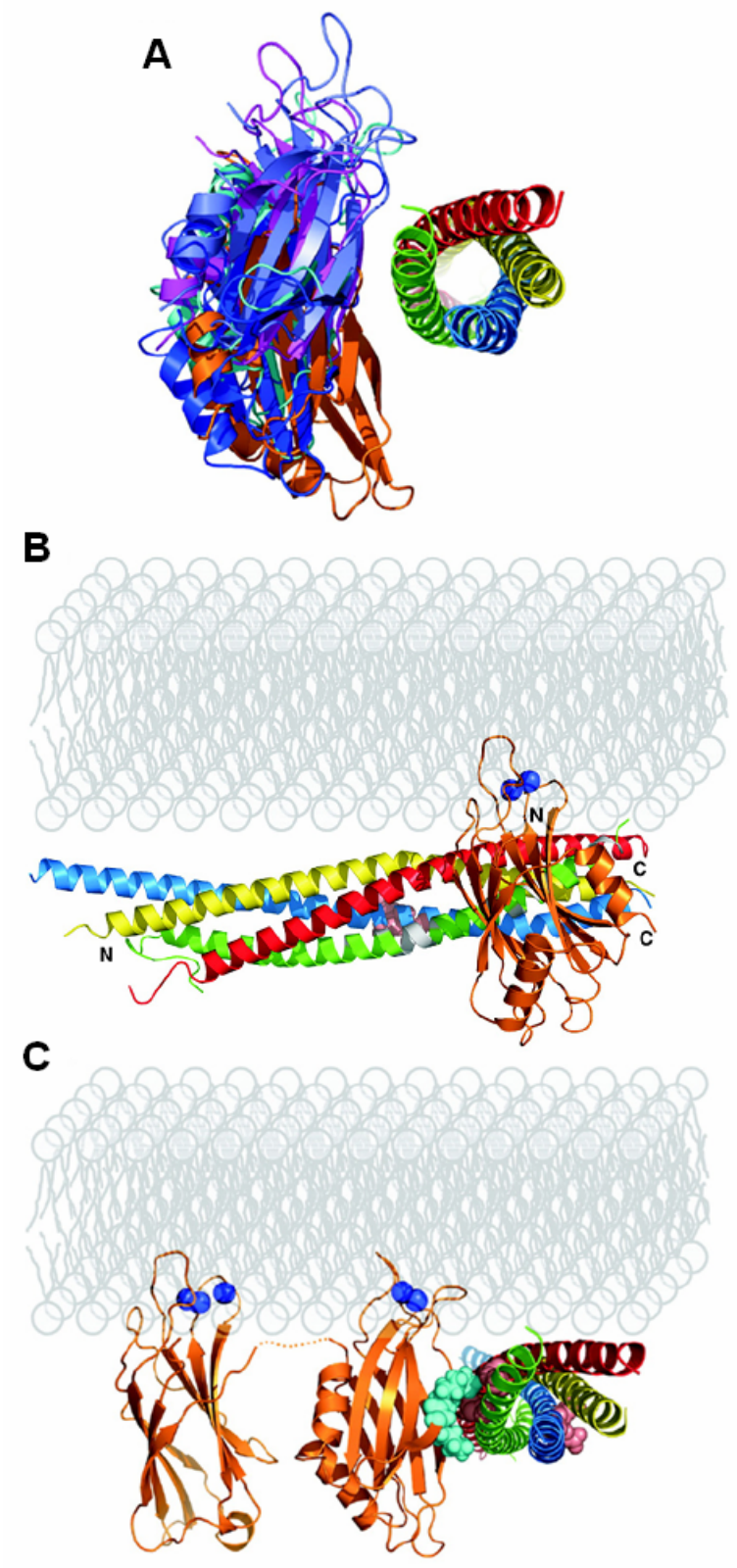
A
B
N
C
N
C
C

Figure 5.13 Computational model of the SSCAP complex.

(A) Ribbon diagrams of the five top HADDOCK models. The five models were superimposed using the coordinates of the SNARE complex to illustrate the variability in the relative orientation of the C2B domain.

(B) Ribbon diagram of the HADDOCK model that is most similar to the model obtained with FTDock, in an orientation rotated 90° with respect to that of (A). The two Ca^{2+} ions that bind to the C2B domain, which were not included in the modeling calculations, are represented as blue spheres, and the membrane phospholipids are indicated in light gray to help visualizing the relative locations of all the components of the SSCAP complex. N and C denote the N- and C-termini of the C2B domain and the SNARE complex. The residues of the SNAP-25 SNARE motif corresponding to crosspeaks that were perturbed by C2AB fragment binding in our NMR experiments are colored in white.

(C) Ribbon diagram of the same HADDOCK model shown in (B) but in a different orientation and including the C2A domain to illustrate how it emerges from the N-terminus of the C2B domain away from the SNARE complex. The linker sequence between the two C2 domains (four residues) is represented by a dashed orange curve. Residues that were mutated in our complexin displacement assays of Figure 5.12 are shown as spheres: lysine 326 and lysine 327 of the C2B domain are in blue; aspartate 51, glutamate 52, glutamate 55, aspartate 186 and aspartate 193 of SNAP-25 are in pink. Aspartate 51, glutamate 52 and glutamate 55 are also shown in (B).

effects of disrupting Ca^{2+} binding to the C2A domain on complexin displacement *in vitro* (Figure 5.11) and on neurotransmitter release *in vivo* (Fernandez-Chacon et al., 2002; Robinson et al., 2002; Stevens and Sullivan, 2003). Second, we noted that complexin binds to the SNARE complex forming a long, antiparallel α-helix that only contacts the SNARE through its C-terminal half (residues 48-70) (Chen et al., 2002). Superpositions of the HADDOCK models with the crystal structure of the complexin/SNARE complex revealed only a small overlap between the C2B domain and residues 48-70 of complexin, and a more significant overlap with the N-terminal part of the complexin helix (Figure 5.14A, 5.14B). This observation suggested that thermal fluctuations in this N-terminal part of the helix, which has some flexibility, might allow initial contact of the C2B domain with the SNARE complex and subsequent displacement of the C-terminal half of the complexin helix. This mechanism could occur at a much faster rate than mechanisms involving dissociation of complexin from the SNARE complex followed by synaptotagmin 1 binding, which are unlikely to occur *in vivo* because the off rate of complexin from membrane-attached SNARE complex (2.5 s^{-1}) is much slower than the time scale of fast release (< 0.5 ms) (Bowen et al., 2005). The third interesting feature of the HADDOCK models is that a highly positive face of the C2B domain is adjacent to the highly basic C-terminus of the SNARE complex. Hence, the strongly positive electrostatic potential generated in this region of the SSCAP complex could be critical to help bending the membranes and initiate membrane fusion, or to help opening the fusion pore if the vesicle and plasma membranes were already hemifused before Ca^{2+} influx (Figure 5.15).

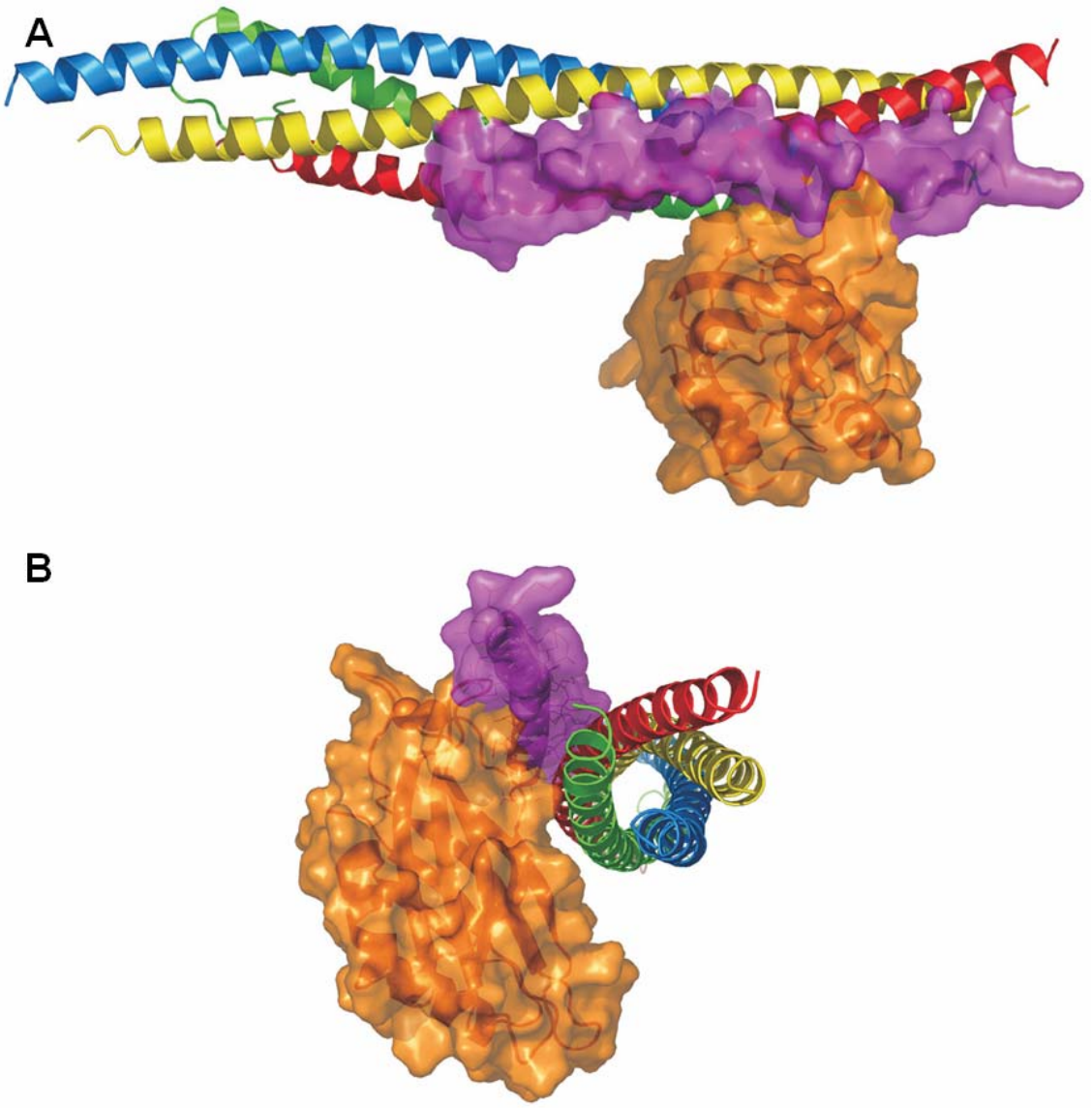

Figure 5.14 Superposition of the crystal structure of complexin/SNARE complex and the model of the synaptotagmin 1 C2B domain/SNARE complex.

(A) Partially transparent surfaces of complexin and the C2B domain are shown to illustrate the partial overlap between their binding sites on the SNARE complex. The syntaxin SNARE motif is shown in yellow, the synaptobrevin SNARE motif is shown in red and the SNAP-25 N-terminal and C-terminal SNARE motifs are shown in blue and green, respectively. The synaptotagmin 1 C2AB fragment is shown in orange. The complexin fragment is shown in magenta.

(B) The view rotated approximately 90° along the vertical axis with respect to (A).

5.4 Discussion

The role of synaptotagmin 1 as a Ca^{2+} sensor in fast neurotransmitter release and the importance of Ca^{2+}-dependent phospholipid binding for synaptotagmin 1 function have now been well established (Fernandez-Chacon et al., 2001), but the basis for the preponderant role of the C2B domain versus the C2A domain in release has not been understood. Evidence for a role of synaptotagmin 1/SNARE interactions in release was also reported (Zhang et al., 2002; Bai et al., 2004; Chapman et al., 1998), yet there were contradictory data on these interactions and it was unclear how they might be coupled with Ca^{2+}-phospholipid binding to synaptotagmin 1. The results described in this chapter show that synaptotagmin 1 forms a tight quaternary complex with the SNARE complex, Ca^{2+} and phospholipids (the SSCAP complex) and that membrane-anchoring of the SNARE complex increases the specificity of its interactions with synaptotagmin 1. The correlation between the effects of mutations in synaptotagmin 1 and SNAP-25 on the SSCAP complex formation and those of similar mutations in neurotransmitter release strongly suggest that this complex plays a critical role in neurotransmitter release and provide a clear rationale for the preponderant role of the C2B domain in Ca^{2+}-triggered fast neurotransmitter release. Furthermore, our preliminary model of the quaternary SSCAP complex suggests mechanisms for how synaptotagmin 1 might be able to displace complexin from SNARE complex in the time scale of fast release and for how the quaternary SSCAP complex might trigger synaptic vesicle exocytosis.

A vast amount of research has investigated synaptotagmin 1/SNARE interactions, but it was unclear whether the target of synaptotagmin 1 is syntaxin, SNAP-25, syntaxin/SNAP-25 heterodimers or the ternary SNARE complex, and to what extent these interactions are

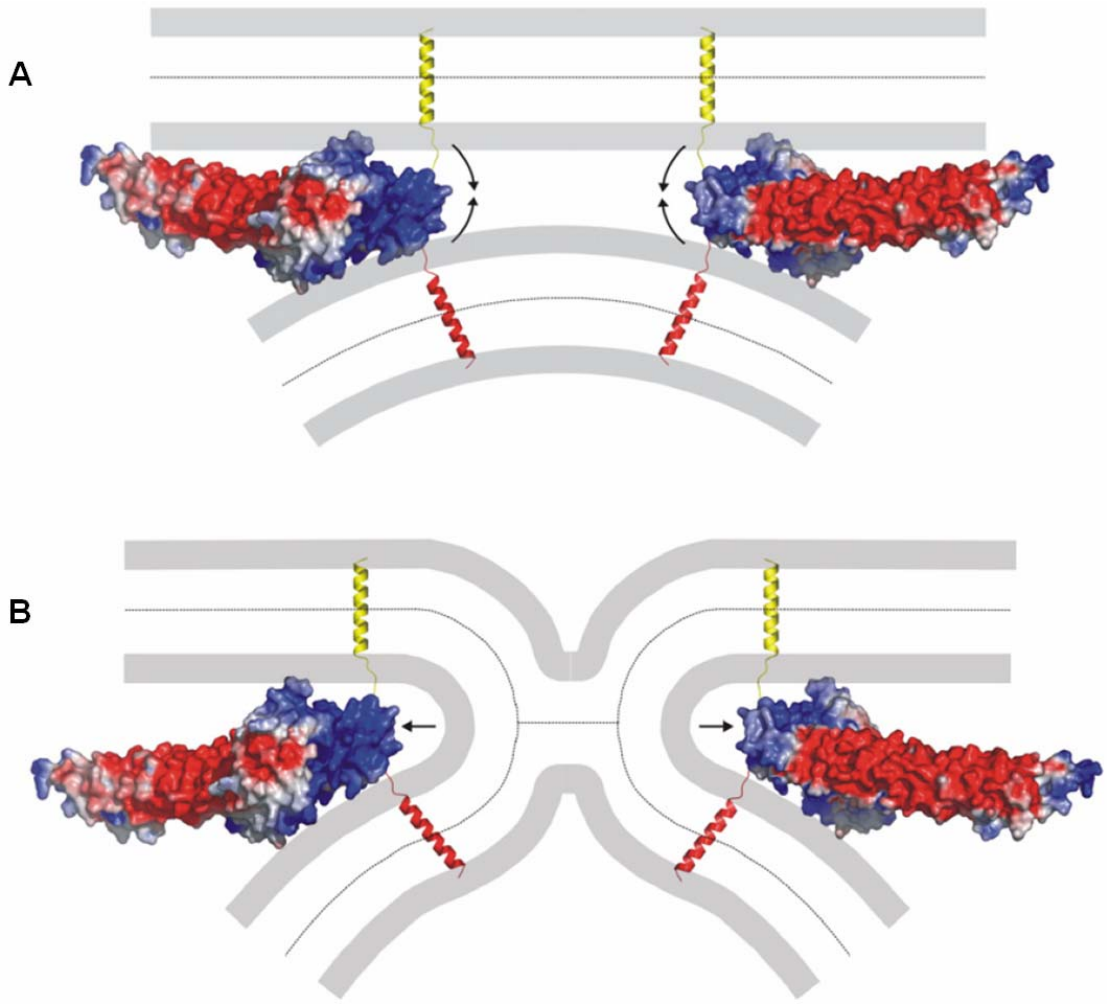

Figure 5.15 Models illustrating how the SSCAP complex could trigger neurotransmitter release.

(A) The diagram shows the surface electrostatic potential of two copies of the modeled C2B domain/SNARE complex and how the highly positive potential at the tips of the complexes could help to bend the membranes to initiate membrane fusion. The model on the left was slightly rotated to better show the highly positive surface at the tip. The model on the right is rotated 180° around the vertical axis with respect to that on the left. The TM regions of syntaxin and synaptobrevin are in yellow and red, respectively. The electrostatic surface potential was computed with GRASP. The models were rendered with PyMol. The electrostatic potential is contoured at the 5 kT/e level, with red denoting negative potential and blue denoting positive potential.

(B) The diagram shows an alternative model how the highly positive potential at the tips of the complexes could help opening the fusion pore if the vesicle and plasma membranes were already hemifused before Ca^{2+} influx.

Ca^{2+} dependent and are compatible with phospholipid binding. As this field has developed, reasons for some of the contradictions have emerged. Thus, it is now clear that SNARE interactions identified with brain homogenates may result simply from the sticky nature of the SNAREs and their abundance in brain (more than 100 SNARE targets have been reported) (Jahn and Scheller, 2006). Similarly, synaptotagmin 1 is very sticky and its C2B domain binds avidly to polyacidic molecules such as DNA and RNA, which can promote irrelevant interactions and hinder relevant ones (Ubach et al., 2001). It also became clear that the widely used GST pulldown assays can yield diverse artifacts arising among other reasons from insufficient characterization of the purity and proper folding of the GST fusion proteins (Rizo et al., 2006). In addition, differences observed in the Ca^{2+}-dependence of synaptotagmin 1/SNARE complex interactions likely arise because fusion of GST to synaptotagmin 1 enhances Ca^{2+}-independent binding. This finding can be attributed to a weak interaction of GST with the SNARE complex that can be detected by ITC (described in chapter 4), but would not be detectable in pulldown assays. Conversely, synaptotagmin 1/SNARE complex interactions are highly sensitive to ionic strength and therefore the weaker Ca^{2+}-independent component may not be observed in GST pulldowns at 100 mM or higher salt concentrations because bound proteins may be removed during the washing steps.

^{1}H-^{15}N HSQC spectra provided a powerful tool to detect both weak and strong interactions in solution without protein tags. Although the relatively high concentrations used to acquire these spectra can promote nonspecific interactions, the information obtained on the regions involved in the interactions is critical to understand their nature and test their relevance. For instance, early NMR and mutagenesis studies showed that the Ca^{2+}-binding

region of the C2A domain mediates binding to phospholipids (Zhang et al., 1998), the cytoplasmic region of syntaxin and its N-terminal Habc domain (Shao et al., 1997; Fernandez et al., 1998), thus revealing a promiscuity for negatively charged surfaces that reflects a general tendency of highly charged surfaces to nonspecific interactions. A key concept that emerged at the same time from these studies is that electrostatic interactions may play a crucial role in Ca^{2+}-triggered fast neurotransmitter release because the fast switch in electrostatic potential caused by Ca^{2+} binding to C2 domains is particularly well suited for the fast speed of this process. The picture that emerges from all these observations and the results described in this chapter is that synaptotagmin 1 and the SNAREs have multiple surfaces with high charge density, some of which participate in formation of the quaternary SSCAP complex but can also engage in diverse interactions in the absence of their natural targets. For instance, in our model of the quaternary SSCAP complex, synaptotagmin 1 binds primarily to the C-terminus of SNAP-25, as suggested previously (Zhang et al., 2002), but does not interact directly with the syntaxin SNARE motif, which is located in the opposite side of the SNARE complex (Figure 5.13). Hence, binary synaptotagmin 1/syntaxin interactions may be observed in the absence of other components of the SSCAP complex, but may not be physiologically relevant. On the other hand, detergent solubilization of native proteins disrupts membranes and thus may also lead to artifacts, given the key role of the membrane in the quaternary SSCAP complex formation. Moreover, just separating the SNARE complex from membranes can also lead to misleading results, as 1D NMR experiments conclusively showed that the synaptotagmin 1 C2AB fragment cannot bind simultaneously to phospholipid and the soluble SNARE complex (Arac et al., 2003) and yet

it is now clear that such simultaneous binding occurs when the SNARE complexes are anchored to membranes (Figure 5.3 and Figure 5.4).

Interactions of synaptotagmin 1 with liposomes and SNAREs were proposed to underlie the observed enhancement of the SNARE-mediated liposome fusion caused by synaptotagmin 1 in the presence of Ca^{2+} (Bhalla et al., 2006; Tucker et al., 2004), leading to the claim that Ca^{2+}-dependent membrane fusion was reconstituted (Tucker et al., 2004). However, it is unclear to what extent these experiments reproduced the events that occur *in vivo*, as the modest magnitude of such enhancement (2-4 fold) was in contrast to the much higher increase in the rate of neurotransmitter release induced by Ca^{2+} *in vivo* (ca. 18,000-fold) (Rhee et al., 2005), and the stronger disruption of liposome fusion enhancement by mutations in the C2A domain Ca^{2+}-binding sites compared to analogous mutations in the C2B domain (Bhalla et al., 2005) contrasted with the preponderant role of the C2B domain in neurotransmitter release (Mackler and Reist, 2001; Fernandez-Chacon et al., 2002; Robinson et al., 2002; Stevens and Sullivan, 2003; Nishiki and Augustine, 2004). Perhaps the best evidence for simultaneous binding of synaptotagmin 1 to SNAREs and membranes was provided by the finding that Ca^{2+} and the synaptotagmin 1 C2AB fragment increased the rate of formation of syntaxin/SNAP-25 heterodimers on membranes, which led to a model whereby Ca^{2+} influx promotes formation of such heterodimers followed by synaptobrevin binding and membrane fusion (Bhalla et al., 2006). While the rate enhancement was rather modest (ca. 5-fold) and this model seems inconsistent with the fast time scale of release, it is plausible that the enhancement reflects the same interactions that underlie formation of the SSCAP complex revealed by our data.

Characterizing the quaternary SSCAP complex at atomic resolution will require challenging structural studies, and its physiological relevance could be questioned since the complex still lacks the membrane anchor of synaptotagmin 1 as well as other key components of the release machinery. However, our results and preliminary model allowed us to rationalize a variety of available functional data and to formulate a number of important predictions that will need to be tested with further experiments. Multiple correlations had strongly suggested a critical role of Ca^{2+}-dependent phospholipid binding for synaptotagmin 1 function in Ca^{2+}-triggered fast neurotransmitter release (Fernandez-Chacon et al., 2001; Rhee et al., 2005; Li et al., 2006), but this activity could not explain by itself the preponderant role of the C2B domain for release. Whereas the finding that the C2B domain could bind simultaneously to two membranes yielded a potential basis for this apparent paradox and suggested a model whereby the highly positive electrostatic potential of the C2B domain could bend the membranes to initiate fusion (Arac et al., 2006), it was unclear how this action could be coordinated with the proposed role of the SNAREs in exerting mechanical force to induce the membrane fusion. The critical role of Ca^{2+}-binding to the C2B domain for the SSCAP complex formation (Figure 5.11) reveals an additional rationale for the key function of the C2B domain that incorporates interactions between synaptotagmin 1 and the SNARE complex, thus providing a mechanism to couple their functions. It is actually plausible that the C2B domain interacts simultaneously with the SNARE complex through the side of the β-sandwich, and with both membranes through the Ca^{2+}-binding loops and the opposite tip of the β-sandwich, which are positively charged (Figure 5.15). Interestingly, the previously proposed role of the C2B domain in bending the membranes to

initiate fusion (Arac et al., 2006), which has been supported by theoretical calculations (Zimmerberg et al., 2006), could be played in a similar fashion and even more efficiently by the SSCAP complex, as the positive charge of the C-termini of the SNARE complex adds to that of the C2B domain to form a continuous, highly positive surface (Figure 5.15). This surface is located at the tip of the SSCAP complex that is expected to exert mechanical forces on the membranes and is thus in an ideal position to perform this action. In an alternative model entailing a hemifusion state before Ca^{2+} influx, this positive surface could provide an attractive force on the membranes to open the fusion pore, as proposed previously for the role of the C2B domain (Rizo et al., 2006; Zimmerberg et al., 2006).

Our data also provide a sound explanation for the auxiliary rather than critical role of Ca^{2+} binding to the C2A domain for neurotransmitter release. Hence, the orientation of the N-terminus of the C2B domain facing away from the SNARE complex (Figure 5.13C) determined that the C2A domain couldn't contact the SNARE complex directly but could contribute to the overall stability of the quaternary SSCAP complex by binding to Ca^{2+}-phospholipids. This feature likely underlies the limited effects of disrupting Ca^{2+} binding to the C2A domain on the SSCAP complex formation (Figure 5.11) and on Ca^{2+}-triggered neurotransmitter release (Fernandez-Chacon et al., 2002; Robinson et al., 2002; Stevens and Sullivan, 2003). Similarly, the partial disruption of the SSCAP complex formation induced by the K326A, K327A mutation in the C2B domain polybasic region (Figure 5.12) paralleled the partial impairment of neurotransmitter release caused by this mutation (Li et al., 2006; Mackler and Reist, 2001). The polybasic region had been implicated in many interactions, such as phosphatidylinositol phosphates, syntaxin/SNAP-25 heterodimer, and AP-2, *etc*. (Li

et al., 2006; Rickman et al., 2004; Chapman et al., 1998), likely because of its promiscuity in the absence of the correct target, but it was unclear which this target was. An intriguing possibility was that the polybasic region could participate directly in phospholipid binding, but it was difficult to envisage how this region and the Ca^{2+}-binding loops could contact one or even two membranes simultaneously (Arac et al., 2003; Li et al., 2006). In contrast, it is easy to visualize how the polybasic region can contact the SNARE complex while the Ca^{2+} binding loops insert into one membrane (Figure 5.13B, 5.13C). Furthermore, the participation of the polybasic region in SNARE binding within the SSCAP complex bodes well with the acidic nature of the C-terminal region of SNAP-25 involved in the SSCAP complex formation (Figure 5.12).

Another correlation with functional data is provided by the impairment of the SSCAP complex formation caused by mutations in the SNAP-25 C-terminus and the reduction of Ca^{2+}-triggered exocytosis in PC12 cells induced by similar mutations (Zhang et al., 2002). Moreover, our model of the SSCAP complex allows a clear rationalization for the differential inhibitory effects of botulinum neurotoxins (BoNT) A and E in neurotransmitter release (Pellizzari et al., 1999). BoNT E, which severely blocks neurotransmitter release, cleaves SNAP-25 between residues 180 and 181, effectively removing the SNAP-25 C-terminal sequence that is key for synaptotagmin 1 binding. BoNT A produces a milder inhibition of neurotransmitter release and cleaves SNAP-25 between residues 197 and 198, which leaves the synaptotagmin 1 binding region intact according to our model. This milder inhibition and the fact that it could be overcome by increasing the Ca^{2+} concentration (Keller and Neale, 2001) likely arises from the expected destabilization of the C-terminus of the SNARE

complex caused by the cleavage and the intimate cooperativity of Ca^{2+}, synaptotagmin 1 and the SNAREs in forming the quaternary complex with phospholipid. This close cooperativity is reflected in the finding that SSCAP complex formation was strongly hampered by either disrupting Ca^{2+}-binding to the C2B domain (Figure 5.11) or a lack of SNARE membrane anchoring (Arac et al., 2003), and could arise from phospholipid binding at the basic C2B domain/SNARE complex interface or from conformational changes in the C2B domain upon Ca^{2+}-phospholipid binding that might be required for SNARE complex binding.

The tight nature of the C2B domain/SNARE complex interactions within the SSCAP complex was also emphasized by the fact that the synaptotagmin 1 C2AB fragment can displace complexin from the SNARE complex (Figure 5.5). As explained above, our model of the SSCAP complex indicated that such displacement arose from only a small degree of overlap between the complexin and synaptotagmin 1 binding regions on the SNARE complex (Figure 5.14A, 5.14B), suggesting a mechanism for rapid displacement of complexin by synaptotagmin 1 that could occur in the fast time scale of neurotransmitter release and does not require initial dissociation of complexin, which is too slow for this time scale (Bowen et al., 2005). Interestingly, a homodimer-heterodimer switch involving Munc13-1 and α-RIM, two proteins that function in synaptic vesicle priming, also arises from only a small overlap between the Munc13-1 surfaces involved in both complexes (Lu et al., 2006). Hence, this may be a common theme in transitions between different protein complexes that need to occur with a fast speed such as those involved in synaptic vesicle exocytosis.

Our studies also illustrate the importance of including membranes in studies of interactions between proteins involved in neurotransmitter release, which in retrospective is not surprising, given the very nature of this process. Microfluidic channel technology, which had already been shown to be very useful for biological studies (Sia and Whitesides, 2003), was instrumental for the design of the experiments that revealed the formation of the SSCAP complex (Figure 5.1 and Figure 5.2) and the analysis of complexin displacement by synaptotagmin 1 (Figure 5.5). Particularly useful features of this approach to study interactions on membrane surfaces are that it allows high surface-to-volume ratios for easy access and favorable partition of the reagents to the bilayers, as well as easy delivery of reagents and quick, efficient removal of unbound materials. These features and the small reaction volumes involved facilitate the performance of multiple experiments in a relatively short time using limited amounts of reagents that may be scarce or expensive. Thus, it can be anticipated that this and similar approaches can be applied to investigate a wide variety of biological processes that occur on membrane surfaces.

Overall, the results described in this chapter suggest the following mechanism of Ca^{2+}-triggered fast synchronous neurotransmitter release: After the synaptic vesicle docking and initial priming on the active zone, the SNARE complex assembles from the N-terminus to the C-terminus to bring the two opposing membranes to apposition, binding of complexin helps to accomplish the zippering and full assembly of the SNARE complex, finishing the priming process, yet suspending the primed vesicles in this highly energized metastable state. Upon Ca^{2+} influx, synaptotagmin 1 binds simultaneously to phospholipid and the C-terminus

of the SNARE complex, forming the quaternary SSCAP complex, displacing complexin, and leading to the final stage of fusion pore opening (Figure 5.16).

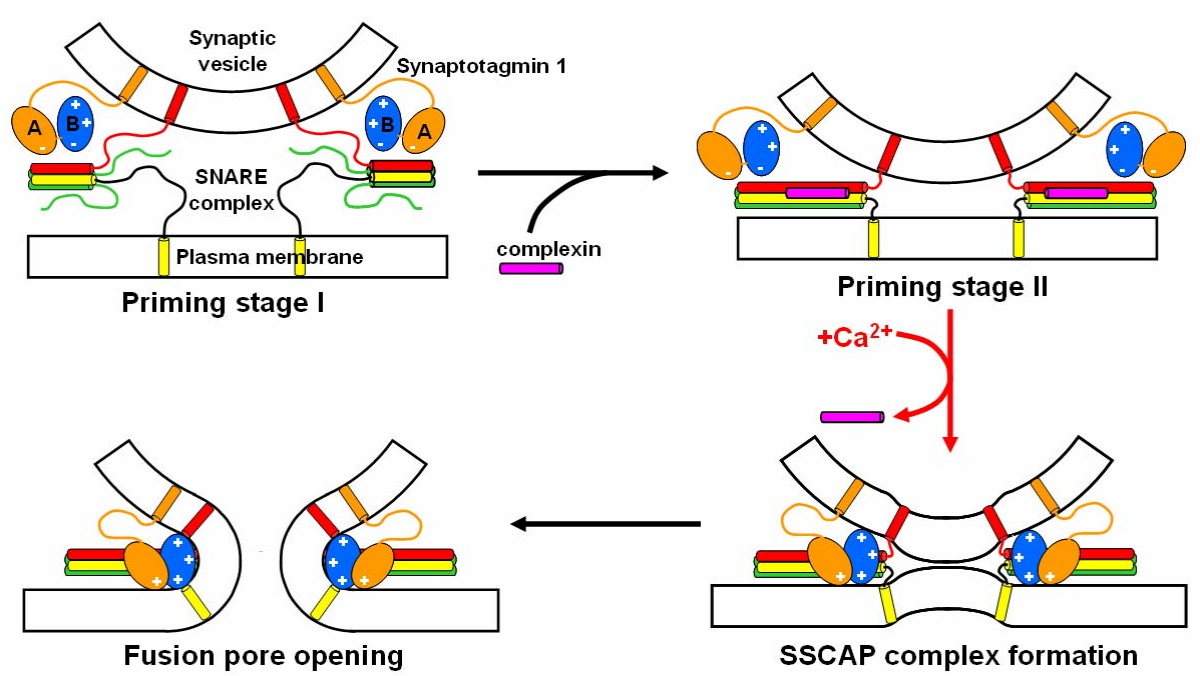

Figure 5.16 Model of Ca^{2+}-triggered synchronous neurotransmitter release.

The model involves several stages: 1) priming stage I in which the SNARE complex assembles from N-terminus to C-terminus, to bring the two opposing membranes to apposition; 2) priming stage II in which binding of complexin helps to accomplish the full assembly of the SNARE complex, finishing the priming process, yet suspending the primed vesicles in this highly energized metastable state; 3) the SSCAP complex formation in which Ca^{2+} influx causes synaptotagmin 1 to bind simultaneously to phospholipid and the C-terminus of the SNARE complex, displace complexin, and form the quaternary SSCAP complex; and 4) fusion pore opening in which the synaptic vesicle membrane fuses with the presynaptic plasma membrane and releases the neurotransmitters. Syntaxin, synaptobrevin, and SNAP-25 are shown in yellow, red, and green, respectively. The C2A and C2B domain of synaptotagmin 1 are shown in orange and blue, respectively. Complexin is shown in magenta. The cylinders inside the lipid bilayers represent the transmembrane regions of syntaxin, synaptobrevin and synaptotagmin 1.

Chapter 6 Summary and Future Directions

6.1 Summary and Future Directions of Studies on Synaptotagmin 4

In chapter 2, we have described a systematic analysis of the Ca^{2+} and phospholipid binding properties of both vertebrate (rat) and invertebrate (*Drosophila*) synaptotagmin 4. These studies revealed that in contrast to predictions from sequence alignment, both C2 domains of *Drosophila* synaptotagmin 4 exhibit Ca^{2+}-dependent phospholipid binding, whereas neither C2 domain of rat synaptotagmin 4 does, indicating that synaptotagmin 4 is a Ca^{2+} sensor in *Drosophila* but not in rat. We also learned that proteins clearly identified as orthologues by sequence analyses may not preserve the same function during evolution. The structural basis of the inability of the rat synaptotagmin 4 C2B domain to bind Ca^{2+} and phospholipid was revealed by X-ray crystallography and NMR spectroscopy studies. However, the question of how the *Drosophila* synaptotagmin 4 C2A domain binds to phospholipids in a Ca^{2+}-dependent manner even though it only retains residual Ca^{2+} binding remains open. The only clue that we currently have is the unique 14-residue insertion in its loop 1. Further studies using site-directed mutagenesis and loop swapping will be needed to understand the structural basis of this puzzling observation.

6.2 Summary and Future Directions of Studies on the RIM C2A domain

In chapter 3, we have described the structural and functional analyses of the RIM2 C2A domain. The functional studies revealed that the RIM2 C2A domain does not bind to Ca^{2+}, phospholipids, and its putative binding partner synaptotagmin 1 and SNAP-25. The

crystal structure of the RIM2 C2A domain as well as the sequence conservation pattern suggest the existence of a potential target binding site around the bottom 3_{10} helix. Several lines of evidence suggest that the arginine 805 in the bottom 3_{10} helix is potentially critical for the as-yet-unidentified interactions of the RIM2 C2A domain. However, further studies will be needed to test these ideas and identify which interaction(s) mediates the function of the RIM C2A domain. Crosslinking between the RIM2 C2A domain wild type or R805H mutant and rat brain homogenate will be used to identify its potential binding partners. The crosslinking products observed selectively for wild type but not for R805H mutant will be submitted to mass spectrometry for protein identification. The common crosslinking products will also be submitted to mass spectrometry if no obvious difference is observed. Once the potential candidates are identified, NMR spectroscopy will be used to test and study the interactions between them and the RIM2 C2A domain. If a convincing complex formation between the candidate and the RIM2 C2A domain is observed, X-ray crystallography will be used to determine the complex structures.

6.3 Summary and Future Directions of Studies on the SSCAP complex

In chapters 4 and 5, we have described the studies of synaptotagmin 1/SNARE complex interaction both in solution and in the membrane environment and revealed the existence of a quaternary SSCAP complex formed by simultaneous binding of synaptotagmin 1 to phospholipids and reconstituted SNARE complex in the presence of Ca^{2+}. Based on limited information from site-directed mutagenesis data, docking was carried out to generate a hypothetical atomic model of the SSCAP complex, the validity of which still awaits

corroboration. More mutations will be designed, based on the SSCAP complex docking model, to test more rigorously the validity of the model using complexin displacement assay. EPR spectroscopy will be used to probe the membrane penetration mode of synaptotagmin 1 in the context of the SSCAP complex. Ultimately, 2D crystallography on the phospholipid membranes will be attempted to determine the atomic resolution structure of the SSCAP complex.

BIBLIOGRAPHY

Adolfsen,B., Saraswati,S., Yoshihara,M., and Littleton,J.T. (2004). Synaptotagmins are trafficked to distinct subcellular domains including the postsynaptic compartment. J. Cell Biol. *166*, 249-260.

Antonin,W., Fasshauer,D., Becker,S., Jahn,R., and Schneider,T.R. (2002). Crystal structure of the endosomal SNARE complex reveals common structural principles of all SNAREs. Nat. Struct. Biol. *9*, 107-111.

Arac,D., Chen,X., Khant,H.A., Ubach,J., Ludtke,S.J., Kikkawa,M., Johnson,A.E., Chiu,W., Sudhof,T.C., and Rizo,J. (2006). Close membrane-membrane proximity induced by Ca(2+)-dependent multivalent binding of synaptotagmin-1 to phospholipids. Nat. Struct. Mol. Biol. *13*, 209-217.

Arac,D., Murphy,T., and Rizo,J. (2003). Facile detection of protein-protein interactions by one-dimensional NMR spectroscopy. Biochemistry *42*, 2774-2780.

Augustine,G.J., Burns,M.E., DeBello,W.M., Pettit,D.L., and Schweizer,F.E. (1996). Exocytosis: proteins and perturbations. Annu. Rev. Pharmacol. Toxicol. *36*, 659-701.

Bai,J., Earles,C.A., Lewis,J.L., and Chapman,E.R. (2000). Membrane-embedded synaptotagmin penetrates cis or trans target membranes and clusters via a novel mechanism. J. Biol. Chem. *275*, 25427-25435.

Bai,J., Wang,C.T., Richards,D.A., Jackson,M.B., and Chapman,E.R. (2004). Fusion Pore Dynamics Are Regulated by Synaptotagmin*t-SNARE Interactions. Neuron *41*, 929-942.

Bailey,S. (1994). The Ccp4 Suite - Programs for Protein Crystallography. Acta Crystallographica Section D-Biological Crystallography *50*, 760-763.

Banerjee,A., Kowalchyk,J.A., DasGupta,B.R., and Martin,T.F.J. (1996). SNAP-25 is required for a late postdocking step in Ca2+-dependent exocytosis. Journal of Biological Chemistry *271*, 20227-20230.

Basanez,G., Goni,F.M., and Alonso,A. (1998). Effect of single chain lipids on phospholipase C-promoted vesicle fusion. A test for the stalk hypothesis of membrane fusion. Biochemistry *37*, 3901-3908.

Bashir,R., Britton,S., Strachan,T., Keers,S., Vafiadaki,E., Lako,M., Richard,I., Marchand,S., Bourg,N., Argov,Z., Sadeh,M., Mahjneh,I., Marconi,G., Passos-Bueno,M.R., Moreira,E.S., Zatz,M., Beckmann,J.S., and Bushby,K. (1998). A gene related to Caenorhabditis elegans spermatogenesis factor fer-1 is mutated in limb-girdle muscular dystrophy type 2B. Nat. Genet. *20*, 37-42.

Baumert,M., Maycox,P.R., Navone,F., Decamilli,P., and Jahn,R. (1989). Synaptobrevin - An Integral Membrane-Protein of 18000 Daltons Present in Small Synaptic Vesicles of Rat-Brain. Embo Journal *8*, 379-384.

Benes,C.H., Wu,N., Elia,A.E., Dharia,T., Cantley,L.C., and Soltoff,S.P. (2005). The C2 domain of PKCdelta is a phosphotyrosine binding domain. Cell *121*, 271-280.

Bennett,M.K. and Scheller,R.H. (1993). The molecular machinery for secretion is conserved from yeast to neurons. Proc. Natl. Acad. Sci. U. S. A *90*, 2559-2563.

Bennett,M.K., Calakos,N., and Scheller,R.H. (1992). Syntaxin: a synaptic protein implicated in docking of synaptic vesicles at presynaptic active zones. Science *257*, 255-259.

Berton,F., Cornet,V., Iborra,C., Garrido,J., Dargent,B., Fukuda,M., Seagar,M., and Marqueze,B. (2000). Synaptotagmin I and IV define distinct populations of neuronal transport vesicles. Eur. J. Neurosci. *12*, 1294-1302.

Betz,A., Thakur,P., Junge,H.J., Ashery,U., Rhee,J.S., Scheuss,V., Rosenmund,C., Rettig,J., and Brose,N. (2001). Functional interaction of the active zone proteins Munc13-1 and RIM1 in synaptic vesicle priming. Neuron *30*, 183-196.

Bhalla,A., Chicka,M.C., Tucker,W.C., and Chapman,E.R. (2006). Ca(2+)-synaptotagmin directly regulates t-SNARE function during reconstituted membrane fusion. Nat. Struct. Mol. Biol. *13*, 323-330.

Bhalla,A., Tucker,W.C., and Chapman,E.R. (2005). Synaptotagmin isoforms couple distinct ranges of Ca2+, Ba2+, and Sr2+ concentration to SNARE-mediated membrane fusion. Mol. Biol. Cell *16*, 4755-4764.

Blasi,J., Chapman,E.R., Link,E., Binz,T., Yamasaki,S., De Camilli,P., Sudhof,T.C., Niemann,H., and Jahn,R. (1993a). Botulinum neurotoxin A selectively cleaves the synaptic protein SNAP-25. Nature *365*, 160-163.

Blasi,J., Chapman,E.R., Yamasaki,S., Binz,T., Niemann,H., and Jahn,R. (1993b). Botulinum neurotoxin C1 blocks neurotransmitter release by means of cleaving HPC-1/syntaxin. EMBO J. *12*, 4821-4828.

Bock,J.B., Matern,H.T., Peden,A.A., and Scheller,R.H. (2001). A genomic perspective on membrane compartment organization. Nature *409*, 839-841.

Bollmann,J.H., Sakmann,B., and Borst,J.G. (2000). Calcium sensitivity of glutamate release in a calyx-type terminal. Science *289*, 953-957.

Bowen,M.E., Weninger,K., Ernst,J., Chu,S., and Brunger,A.T. (2005). Single-molecule studies of synaptotagmin and complexin binding to the SNARE complex. Biophys. J. *89*, 690-702.

Bracher,A., Kadlec,J., Betz,H., and Weissenhorn,W. (2002). X-ray structure of a neuronal complexin-SNARE complex from squid. J. Biol. Chem. *277*, 26517-26523.

Brenner,S. (1974). The genetics of Caenorhabditis elegans. Genetics *77*, 71-94.

Brian,A.A. and Mcconnell,H.M. (1984). Allogeneic Stimulation of Cyto-Toxic T-Cells by Supported Planar Membranes. Proceedings of the National Academy of Sciences of the United States of America-Biological Sciences *81*, 6159-6163.

Broadie,K., Prokop,A., Bellen,H.J., O'Kane,C.J., Schulze,K.L., and Sweeney,S.T. (1995). Syntaxin and synaptobrevin function downstream of vesicle docking in Drosophila. Neuron *15*, 663-673.

Brose,N., Petrenko,A.G., Sudhof,T.C., and Jahn,R. (1992). Synaptotagmin: a calcium sensor on the synaptic vesicle surface. Science *256*, 1021-1025.

Brunger,A.T. (2005). Structure and function of SNARE and SNARE-interacting proteins. Q. Rev. Biophys. *38*, 1-47.

Brunger,A.T., Adams,P.D., Clore,G.M., DeLano,W.L., Gros,P., Grosse-Kunstleve,R.W., Jiang,J.S., Kuszewski,J., Nilges,M., Pannu,N.S., Read,R.J., Rice,L.M., Simonson,T., and Warren,G.L. (1998). Crystallography & NMR system: A new software suite for macromolecular structure determination. Acta Crystallogr. D. Biol. Crystallogr. *54 (Pt 5)*, 905-921.

Burri,L. and Lithgow,T. (2004). A complete set of SNAREs in yeast. Traffic. *5*, 45-52.

Butz,S., Fernandez-Chacon,R., Schmitz,F., Jahn,R., and Sudhof,T.C. (1999). The subcellular localizations of atypical synaptotagmins III and VI. Synaptotagmin III is enriched in synapses and synaptic plasma membranes but not in synaptic vesicles. J. Biol. Chem. *274*, 18290-18296.

Calakos,N., Schoch,S., Sudhof,T.C., and Malenka,R.C. (2004). Multiple roles for the active zone protein RIM1alpha in late stages of neurotransmitter release. Neuron *42*, 889-896.

Castillo,P.E., Janz,R., Sudhof,T.C., Tzounopoulos,T., Malenka,R.C., and Nicoll,R.A. (1997). Rab3A is essential for mossy fibre long-term potentiation in the hippocampus. Nature *388*, 590-593.

Castillo,P.E., Schoch,S., Schmitz,F., Sudhof,T.C., and Malenka,R.C. (2002). RIM1alpha is required for presynaptic long-term potentiation. Nature *415*, 327-330.

Chapman,E.R. (2002). Synaptotagmin: a Ca(2+) sensor that triggers exocytosis? Nat. Rev. Mol. Cell Biol. *3*, 498-508.

Chapman,E.R. and Davis,A.F. (1998). Direct interaction of a Ca^{2+}-binding loop of synaptotagmin with lipid bilayers. J. Biol. Chem. *273*, 13995-14001.

Chapman,E.R., An,S., Edwardson,J.M., and Jahn,R. (1996). A novel function for the second C2 domain of synaptotagmin. Ca2+-triggered dimerization. J. Biol. Chem. *271*, 5844-5849.

Chapman,E.R., Desai,R.C., Davis,A.F., and Tornehl,C.K. (1998). Delineation of the oligomerization, AP-2 binding, and synprint binding region of the C2B domain of synaptotagmin. J. Biol. Chem. *273*, 32966-32972.

Chapman,E.R., Hanson,P.I., An,S., and Jahn,R. (1995). Ca^{2+} regulates the interaction between synaptotagmin and syntaxin 1. J. Biol. Chem. *270*, 23667-23671.

Chen,X., Tang,J., Sudhof,T.C., and Rizo,J. (2005). Are neuronal SNARE proteins Ca2+ sensors? J. Mol. Biol. *347*, 145-158.

Chen,X., Tomchick,D.R., Kovrigin,E., Arac,D., Machius,M., Sudhof,T.C., and Rizo,J. (2002). Three-dimensional structure of the complexin/SNARE complex. Neuron *33*, 397-409.

Chen,Y., Xu,Y., Zhang,F., and Shin,Y.K. (2004). Constitutive versus regulated SNARE assembly: a structural basis. EMBO J. *23*, 681-689.

Chen,Y.A. and Scheller,R.H. (2001). SNARE-mediated membrane fusion. Nat. Rev. Mol. Cell Biol. *2*, 98-106.

Chernomordik,L. (1996). Non-bilayer lipids and biological fusion intermediates. Chem. Phys. Lipids *81*, 203-213.

Chernomordik,L.V., Melikyan,G.B., and Chizmadzhev,Y.A. (1987). Biomembrane fusion: a new concept derived from model studies using two interacting planar lipid bilayers. Biochim. Biophys. Acta *906*, 309-352.

Chieregatti,E., Witkin,J.W., and Baldini,G. (2002). SNAP-25 and synaptotagmin 1 function in Ca2+-dependent reversible docking of granules to the plasma membrane. Traffic. *3*, 496-511.

Clary,D.O., Griff,I.C., and Rothman,J.E. (1990). SNAPs, a family of NSF attachment proteins involved in intracellular membrane fusion in animals and yeast. Cell *61*, 709-721.

Coppola,T., Magnin-Luthi,S., Perret-Menoud,V., Gattesco,S., Schiavo,G., and Regazzi,R. (2001). Direct interaction of the Rab3 effector RIM with Ca2+ channels, SNAP-25, and synaptotagmin. J. Biol. Chem. *276*, 32756-32762.

Crowley,K.S., Reinhart,G.D., and Johnson,A.E. (1993). The signal sequence moves through a ribosomal tunnel into a noncytoplasmic aqueous environment at the ER membrane early in translocation. Cell *73*, 1101-1115.

Dai,H., Shin,O.H., Machius,M., Tomchick,D.R., Sudhof,T.C., and Rizo,J. (2004). Structural basis for the evolutionary inactivation of Ca2+ binding to synaptotagmin 4. Nature Structural & Molecular Biology *11*, 844-849.

Dai,H., Tomchick,D.R., Garcia,J., Sudhof,T.C., Machius,M., and Rizo,J. (2005). Crystal structure of the RIM2 C2A-domain at 1.4 A resolution. Biochemistry *44*, 13533-13542.

Dai,H., Shen,N., Arac,D., and Rizo,J. (2007). A Quaternary SNARE-Synaptotagmin-Ca(2+)-Phospholipid Complex in Neurotransmitter Release. J. Mol. Biol. *367*, 848-863.

Davis,A.F., Bai,J., Fasshauer,D., Wolowick,M.J., Lewis,J.L., and Chapman,E.R. (1999). Kinetics of synaptotagmin responses to Ca2+ and assembly with the core SNARE complex onto membranes. Neuron *24*, 363-376.

Davletov,B., Perisic,O., and Williams,R.L. (1998). Calcium-dependent membrane penetration is a hallmark of the C2 domain of cytosolic phospholipase A2 whereas the C2A domain of synaptotagmin binds membranes electrostatically. J. Biol. Chem. *273*, 19093-19096.

Davletov,B.A. and Sudhof,T.C. (1993). A single C2 domain from synaptotagmin I is sufficient for high affinity Ca2+/phospholipid binding. J. Biol. Chem. *268*, 26386-26390.

Deken,S.L., Vincent,R., Hadwiger,G., Liu,Q., Wang,Z.W., and Nonet,M.L. (2005). Redundant localization mechanisms of RIM and ELKS in Caenorhabditis elegans. J. Neurosci. *25*, 5975-5983.

Dekker,L.V. and Parker,P.J. (1997). Regulated binding of the protein kinase C substrate GAP-43 to the V0/C2 region of protein kinase C-delta. J. Biol. Chem. *272*, 12747-12753.

Delaglio,F., Grzesiek,S., Vuister,G.W., Zhu,G., Pfeifer,J., and Bax,A. (1995). Nmrpipe - A Multidimensional Spectral Processing System Based on Unix Pipes. Journal of Biomolecular Nmr *6*, 277-293.

Delaglio,F., Grzesiek,S., Vuister,G.W., Zhu,G., Pfeifer,J., and Bax,A. (1995). Nmrpipe - A Multidimensional Spectral Processing System Based on Unix Pipes. Journal of Biomolecular Nmr *6*, 277-293.

Dessen,A., Tang,J., Schmidt,H., Stahl,M., Clark,J.D., Seehra,J., and Somers,W.S. (1999). Crystal structure of human cytosolic phospholipase A2 reveals a novel topology and catalytic mechanism. Cell *97*, 349-360.

DiAntonio,A. and Schwarz,T.L. (1994). The effect on synaptic physiology of synaptotagmin mutations in Drosophila. Neuron *12*, 909-920.

Dominguez,C., Boelens,R., and Bonvin,A.M. (2003). HADDOCK: a protein-protein docking approach based on biochemical or biophysical information. J. Am. Chem. Soc. *125*, 1731-1737.

Dulubova,I., Sugita,S., Hill,S., Hosaka,M., Fernandez,I., Sudhof,T.C., and Rizo,J. (1999). A conformational switch in syntaxin during exocytosis: role of munc18. EMBO J. *18*, 4372-4382.

Earles,C.A., Bai,J., Wang,P., and Chapman,E.R. (2001). The tandem C2 domains of synaptotagmin contain redundant Ca2+ binding sites that cooperate to engage t-SNAREs and trigger exocytosis. J. Cell Biol. *154*, 1117-1123.

Eastwood,S.L. and Harrison,P.J. (2000). Hippocampal synaptic pathology in schizophrenia, bipolar disorder and major depression: a study of complexin mRNAs. Mol. Psychiatry *5*, 425-432.

Edwards,A.S. and Newton,A.C. (1997). Regulation of protein kinase C betaII by its C2 domain. Biochemistry *36*, 15615-15623.

Edwardson,J.M., Wang,C.T., Gong,B., Wyttenbach,A., Bai,J., Jackson,M.B., Chapman,E.R., and Morton,A.J. (2003). Expression of mutant huntingtin blocks exocytosis in PC12 cells by depletion of complexin II. J. Biol. Chem. *278*, 30849-30853.

Essen,L.O., Perisic,O., Cheung,R., Katan,M., and Williams,R.L. (1996). Crystal structure of a mammalian phosphoinositide-specific phospholipase C delta. Nature *380*, 595-602.

Essen,L.O., Perisic,O., Lynch,D.E., Katan,M., and Williams,R.L. (1997). A ternary metal binding site in the C2 domain of phosphoinositide-specific phospholipase C-delta1. Biochemistry *36*, 2753-2762.

Fasshauer,D., Eliason,W.K., Brunger,A.T., and Jahn,R. (1998a). Identification of a minimal core of the synaptic SNARE complex sufficient for reversible assembly and disassembly. Biochemistry *37*, 10354-10362.

Fasshauer,D., Otto,H., Eliason,W.K., Jahn,R., and Brunger,A.T. (1997). Structural changes are associated with soluble N-ethylmaleimide-sensitive fusion protein attachment protein receptor complex formation. J. Biol. Chem. *272*, 28036-28041.

Fasshauer,D., Sutton,R.B., Brunger,A.T., and Jahn,R. (1998b). Conserved structural features of the synaptic fusion complex: SNARE proteins reclassified as Q- and R-SNAREs. Proc. Natl. Acad. Sci. U. S. A *95*, 15781-15786.

Ferguson,G.D., Anagnostaras,S.G., Silva,A.J., and Herschman,H.R. (2000). Deficits in memory and motor performance in synaptotagmin IV mutant mice. Proc. Natl. Acad. Sci. U. S. A *97*, 5598-5603.

Ferguson,G.D., Thomas,D.M., Elferink,L.A., and Herschman,H.R. (1999). Synthesis degradation, and subcellular localization of synaptotagmin IV, a neuronal immediate early gene product. J. Neurochem. *72*, 1821-1831.

Fernandez,I., Arac,D., Ubach,J., Gerber,S.H., Shin,O., Gao,Y., Anderson,R.G., Sudhof,T.C., and Rizo,J. (2001). Three-dimensional structure of the synaptotagmin 1 c(2)b-domain. Synaptotagmin 1 as a phospholipid binding machine. Neuron *32*, 1057-1069.

Fernandez,I., Ubach,J., Dulubova,I., Zhang,X., Sudhof,T.C., and Rizo,J. (1998). Three-dimensional structure of an evolutionarily conserved N-terminal domain of syntaxin 1A. Cell *94*, 841-849.

Fernandez-Chacon,R., Konigstorfer,A., Gerber,S.H., Garcia,J., Matos,M.F., Stevens,C.F., Brose,N., Rizo,J., Rosenmund,C., and Sudhof,T.C. (2001). Synaptotagmin I functions as a calcium regulator of release probability. Nature *410*, 41-49.

Fernandez-Chacon,R., Shin,O.H., Konigstorfer,A., Matos,M.F., Meyer,A.C., Garcia,J., Gerber,S.H., Rizo,J., Sudhof,T.C., and Rosenmund,C. (2002). Structure/function analysis of Ca2+ binding to the C2A domain of synaptotagmin 1. J. Neurosci. *22*, 8438-8446.

Ferro-Novick,S. and Jahn,R. (1994). Vesicle fusion from yeast to man. Nature *370*, 191-193.

Frazier,A.A., Roller,C.R., Havelka,J.J., Hinderliter,A., and Cafiso,D.S. (2003). Membrane-bound orientation and position of the synaptotagmin I C2A domain by site-directed spin labeling. Biochemistry *42*, 96-105.

Fukuda,M., Ibata,K., and Mikoshiba,K. (2001). A unique spacer domain of synaptotagmin IV is essential for Golgi localization. J. Neurochem. *77*, 730-740.

Fung,B.K. and Stryer,L. (1978). Surface density determination in membranes by fluorescence energy transfer. Biochemistry *17*, 5241-5248.

Gabb,H.A., Jackson,R.M., and Sternberg,M.J. (1997). Modelling protein docking using shape complementarity, electrostatics and biochemical information. J. Mol. Biol. *272*, 106-120.

Garcia,J., Gerber,S.H., Sugita,S., Sudhof,T.C., and Rizo,J. (2004). A conformational switch in the Piccolo C2A domain regulated by alternative splicing. Nat. Struct. Mol. Biol. *11*, 45-53.

Garcia,R.A., Forde,C.E., and Godwin,H.A. (2000). Calcium triggers an intramolecular association of the C2 domains in synaptotagmin. Proc. Natl. Acad. Sci. U. S. A *97*, 5883-5888.

Garner,C.C., Kindler,S., and Gundelfinger,E.D. (2000). Molecular determinants of presynaptic active zones. Curr. Opin. Neurobiol. *10*, 321-327.

Geppert,M., Goda,Y., Hammer,R.E., Li,C., Rosahl,T.W., Stevens,C.F., and Sudhof,T.C. (1994). Synaptotagmin I: a major Ca2+ sensor for transmitter release at a central synapse. Cell *79*, 717-727.

Gerber,S.H., Rizo,J., and Sudhof,T.C. (2002). Role of electrostatic and hydrophobic interactions in ca(2+)-dependent phospholipid binding by the c(2)a-domain from synaptotagmin I. Diabetes *51 Suppl 1*, S12-S18.

Gerona,R.R., Larsen,E.C., Kowalchyk,J.A., and Martin,T.F. (2000). The C terminus of SNAP25 is essential for Ca(2+)-dependent binding of synaptotagmin to SNARE complexes. J. Biol. Chem. *275*, 6328-6336.

Giraudo,C.G., Eng,W.S., Melia,T.J., and Rothman,J.E. (2006). A clamping mechanism involved in SNARE-dependent exocytosis. Science *313*, 676-680.

Gray,M.O., Karliner,J.S., and Mochly-Rosen,D. (1997). A selective epsilon-protein kinase C antagonist inhibits protection of cardiac myocytes from hypoxia-induced cell death. J. Biol. Chem. *272*, 30945-30951.

Hanson,P.I., Roth,R., Morisaki,H., Jahn,R., and Heuser,J.E. (1997). Structure and conformational changes in NSF and its membrane receptor complexes visualized by quick-freeze/deep-etch electron microscopy. Cell *90*, 523-535.

Hayashi,T., McMahon,H., Yamasaki,S., Binz,T., Hata,Y., Sudhof,T.C., and Niemann,H. (1994). Synaptic vesicle membrane fusion complex: action of clostridial neurotoxins on assembly. EMBO J. *13*, 5051-5061.

Helm,C.A. and Israelachvili,J.N. (1993). Forces between phospholipid bilayers and relationship to membrane fusion. Methods Enzymol. *220*, 130-143.

Herrick,D.Z., Sterbling,S., Rasch,K.A., Hinderliter,A., and Cafiso,D.S. (2006). Position of synaptotagmin I at the membrane interface: cooperative interactions of tandem C2 domains. Biochemistry *45*, 9668-9674.

Hess,D.T., Slater,T.M., Wilson,M.C., and Skene,J.H. (1992). The 25 kDa synaptosomal-associated protein SNAP-25 is the major methionine-rich polypeptide in rapid axonal transport and a major substrate for palmitoylation in adult CNS. J. Neurosci. *12*, 4634-4641.

Hibino,H., Pironkova,R., Onwumere,O., Vologodskaia,M., Hudspeth,A.J., and Lesage,F. (2002). RIM binding proteins (RBPs) couple Rab3-interacting molecules (RIMs) to voltage-gated Ca(2+) channels. Neuron *34*, 411-423.

Hodgkin,A.L. (1964). The ionic basis of nervous conduction. Science *145*, 1148-1154.

Holm,L. and Sander,C. (1993). Protein structure comparison by alignment of distance matrices. J. Mol. Biol. *233*, 123-138.

Hu,K., Carroll,J., Fedorovich,S., Rickman,C., Sukhodub,A., and Davletov,B. (2002). Vesicular restriction of synaptobrevin suggests a role for calcium in membrane fusion. Nature *415*, 646-650.

Hubbard,S.J., Campbell,S.F., and Thornton,J.M. (1991). Molecular recognition. Conformational analysis of limited proteolytic sites and serine proteinase protein inhibitors. J. Mol. Biol. *220*, 507-530.

Hunt,D.M., Johnson,S., Halford,S., Morris,A.M., Patel,R., Zhang,K., Hardcastle,A., and Moore,A.T. (2002). Genomic structure and pattern of alternate splicing for RIM1. A candidate gene for CORD7. Investigative Ophthalmology & Visual Science *43*, U180.

Huxley,A.F. (1964). Excitation and conduction in nerve: quantitative analysis. Science *145*, 1154-1159.

Ishizuka,T., Saisu,H., Odani,S., and Abe,T. (1995). Synaphin: a protein associated with the docking/fusion complex in presynaptic terminals. Biochem. Biophys. Res. Commun. *213*, 1107-1114.

Jackson,R.M., Gabb,H.A., and Sternberg,M.J. (1998). Rapid refinement of protein interfaces incorporating solvation: application to the docking problem. J. Mol. Biol. *276*, 265-285.

Jahn,R. and Scheller,R.H. (2006). SNAREs--engines for membrane fusion. Nat. Rev. Mol. Cell Biol. *7*, 631-643.

Jahn,R. and Sudhof,T.C. (1999). Membrane fusion and exocytosis. Annu. Rev. Biochem. *68*, 863-911.

Jahn,R., Lang,T., and Sudhof,T.C. (2003). Membrane fusion. Cell *112*, 519-533.

Jessell,T.M. and Kandel,E.R. (1993). Synaptic transmission: a bidirectional and self-modifiable form of cell-cell communication. Cell *72 Suppl*, 1-30.

Johnson,B.A. and Blevins,R.A. (1994). Nmr View - A Computer-Program for the Visualization and Analysis of Nmr Data. Journal of Biomolecular Nmr *4*, 603-614.

Johnson,S., Halford,S., Morris,A.G., Patel,R.J., Wilkie,S.E., Hardcastle,A.J., Moore,A.T., Zhang,K., and Hunt,D.M. (2003). Genomic organisation and alternative splicing of human RIM1, a gene implicated in autosomal dominant cone-rod dystrophy (CORD7). Genomics *81*, 304-314.

Jones,T.A., Zou,J.Y., Cowan,S.W., and Kjeldgaard,M. (1991). Improved Methods for Building Protein Models in Electron-Density Maps and the Location of Errors in These Models. Acta Crystallographica Section A *47*, 110-119.

Katz,B. and Miledi,R. (1968). The role of calcium in neuromuscular facilitation. J. Physiol *195*, 481-492.

Kee,Y. and Scheller,R.H. (1996). Localization of synaptotagmin-binding domains on syntaxin. J. Neurosci. *16*, 1975-1981.

Keller,J.E. and Neale,E.A. (2001). The role of the synaptic protein snap-25 in the potency of botulinum neurotoxin type A. J. Biol. Chem. *276*, 13476-13482.

Knable,M.B., Barci,B.M., Bartko,J.J., Webster,M.J., and Torrey,E.F. (2002). Molecular abnormalities in the major psychiatric illnesses: Classification and Regression Tree (CRT) analysis of post-mortem prefrontal markers. Mol. Psychiatry *7*, 392-404.

Koushika,S.P., Richmond,J.E., Hadwiger,G., Weimer,R.M., Jorgensen,E.M., and Nonet,M.L. (2001). A post-docking role for active zone protein Rim. Nat. Neurosci. *4*, 997-1005.

Kozlov,M.M. and Markin,V.S. (1983). [Possible mechanism of membrane fusion]. Biofizika *28*, 242-247.

Kweon,D.H., Kim,C.S., and Shin,Y.K. (2003). Regulation of neuronal SNARE assembly by the membrane. Nat. Struct. Biol. *10*, 440-447.

Lee,H.J., Song,J.Y., Kim,J.W., Jin,S.Y., Hong,M.S., Park,J.K., Chung,J.H., Shibata,H., and Fukumaki,Y. (2005). Association study of polymorphisms in synaptic vesicle-associated genes, SYN2 and CPLX2, with schizophrenia. Behav. Brain Funct. *1*, 15.

Lee,J. and Lentz,B.R. (1997). Evolution of lipidic structures during model membrane fusion and the relation of this process to cell membrane fusion. Biochemistry *36*, 6251-6259.

Li,C., Ullrich,B., Zhang,J.Z., Anderson,R.G., Brose,N., and Sudhof,T.C. (1995). Ca(2+)-dependent and -independent activities of neural and non-neural synaptotagmins. Nature *375*, 594-599.

Li,L., Shin,O.H., Rhee,J.S., Arac,D., Rah,J.C., Rizo,J., Sudhof,T., and Rosenmund,C. (2006). Phosphatidylinositol phosphates as co-activators of Ca2+ binding to C2 domains of synaptotagmin 1. J. Biol. Chem. *281*, 15845-15852.

Lin,R.C. and Scheller,R.H. (1997). Structural organization of the synaptic exocytosis core complex. Neuron *19*, 1087-1094.

Lin,R.C. and Scheller,R.H. (2000). Mechanisms of synaptic vesicle exocytosis. Annu. Rev. Cell Dev. Biol. *16*, 19-49.

Link,E., Edelmann,L., Chou,J.H., Binz,T., Yamasaki,S., Eisel,U., Baumert,M., Sudhof,T.C., Niemann,H., and Jahn,R. (1992). Tetanus toxin action: inhibition of neurotransmitter release linked to synaptobrevin proteolysis. Biochem. Biophys. Res. Commun. *189*, 1017-1023.

Littleton,J.T., Serano,T.L., Rubin,G.M., Ganetzky,B., and Chapman,E.R. (1999). Synaptic function modulated by changes in the ratio of synaptotagmin I and IV. Nature *400*, 757-760.

Littleton,J.T., Stern,M., Perin,M., and Bellen,H.J. (1994). Calcium dependence of neurotransmitter release and rate of spontaneous vesicle fusions are altered in Drosophila synaptotagmin mutants. Proc. Natl. Acad. Sci. U. S. A *91*, 10888-10892.

Littleton,J.T., Stern,M., Schulze,K., Perin,M., and Bellen,H.J. (1993). Mutational analysis of Drosophila synaptotagmin demonstrates its essential role in Ca(2+)-activated neurotransmitter release. Cell *74*, 1125-1134.

Llinas,R., Sugimori,M., and Silver,R.B. (1992). Microdomains of high calcium concentration in a presynaptic terminal. Science *256*, 677-679.

Llinas,R., Sugimori,M., and Silver,R.B. (1995). The concept of calcium concentration microdomains in synaptic transmission. Neuropharmacology *34*, 1443-1451.

Lu,J., Machius,M., Dulubova,I., Dai,H., Sudhof,T.C., Tomchick,D.R., and Rizo,J. (2006). Structural basis for a Munc13-1 homodimer to Munc13-1/RIM heterodimer switch. PLoS. Biol. *4*, e192.

Mackler,J.M. and Reist,N.E. (2001). Mutations in the second C2 domain of synaptotagmin disrupt synaptic transmission at Drosophila neuromuscular junctions. J. Comp Neurol. *436*, 4-16.

Mackler,J.M., Drummond,J.A., Loewen,C.A., Robinson,I.M., and Reist,N.E. (2002). The C(2)B Ca(2+)-binding motif of synaptotagmin is required for synaptic transmission in vivo. Nature *418*, 340-344.

Margittai,M., Fasshauer,D., Pabst,S., Jahn,R., and Langen,R. (2001). Homo- and heterooligomeric SNARE complexes studied by site-directed spin labeling. J. Biol. Chem. *276*, 13169-13177.

Marqueze,B., Boudier,J.A., Mizuta,M., Inagaki,N., Seino,S., and Seagar,M. (1995). Cellular localization of synaptotagmin I, II, and III mRNAs in the central nervous system and pituitary and adrenal glands of the rat. J. Neurosci. *15*, 4906-4917.

Matos,M.F., Rizo,J., and Sudhof,T.C. (2000). The relation of protein binding to function: what is the significance of munc18 and synaptotagmin binding to syntaxin 1, and where are the corresponding binding sites? Eur. J. Cell Biol. *79*, 377-382.

Matthew,W.D., Tsavaler,L., and Reichardt,L.F. (1981). Identification of a synaptic vesicle-specific membrane protein with a wide distribution in neuronal and neurosecretory tissue. J. Cell Biol. *91*, 257-269.

McMahon,H.T., Missler,M., Li,C., and Sudhof,T.C. (1995). Complexins: cytosolic proteins that regulate SNAP receptor function. Cell *83*, 111-119.

Melia,T.J., Weber,T., McNew,J.A., Fisher,L.E., Johnston,R.J., Parlati,F., Mahal,L.K., Sollner,T.H., and Rothman,J.E. (2002). Regulation of membrane fusion by the membrane-proximal coil of the t-SNARE during zippering of SNAREpins. J. Cell Biol. *158*, 929-940.

Misura,K.M., Gonzalez,L.C., Jr., May,A.P., Scheller,R.H., and Weis,W.I. (2001a). Crystal structure and biophysical properties of a complex between the N-terminal SNARE region of SNAP25 and syntaxin 1a. J. Biol. Chem. *276*, 41301-41309.

Misura,K.M., Scheller,R.H., and Weis,W.I. (2001b). Self-association of the H3 region of syntaxin 1A. Implications for intermediates in SNARE complex assembly. J. Biol. Chem. *276*, 13273-13282.

Moont,G., Gabb,H.A., and Sternberg,M.J. (1999). Use of pair potentials across protein interfaces in screening predicted docked complexes. Proteins *35*, 364-373.

Morton,A.J. and Edwardson,J.M. (2001). Progressive depletion of complexin II in a transgenic mouse model of Huntington's disease. J. Neurochem. *76*, 166-172.

Murshudov,G.N., Vagin,A.A., and Dodson,E.J. (1997). Refinement of macromolecular structures by the maximum-likelihood method. Acta Crystallographica Section D-Biological Crystallography *53*, 240-255.

Nalefski,E.A. and Falke,J.J. (1996). The C2 domain calcium-binding motif: structural and functional diversity. Protein Sci. *5*, 2375-2390.

Nalefski,E.A. and Falke,J.J. (1998). Location of the membrane-docking face on the Ca2+-activated C2 domain of cytosolic phospholipase A2. Biochemistry *37*, 17642-17650.

Nalefski,E.A., McDonagh,T., Somers,W., Seehra,J., Falke,J.J., and Clark,J.D. (1998). Independent folding and ligand specificity of the C2 calcium-dependent lipid binding domain of cytosolic phospholipase A2. J. Biol. Chem. *273*, 1365-1372.

Navaza,J. (1994). Amore - An Automated Package for Molecular Replacement. Acta Crystallographica Section A *50*, 157-163.

Nishiki,T. and Augustine,G.J. (2004). Dual roles of the C2B domain of synaptotagmin I in synchronizing Ca2+-dependent neurotransmitter release. J. Neurosci. *24*, 8542-8550.

Nonet,M.L., Grundahl,K., Meyer,B.J., and Rand,J.B. (1993). Synaptic function is impaired but not eliminated in C. elegans mutants lacking synaptotagmin. Cell *73*, 1291-1305.

Otwinowski,Z. and Minor,W. (1997). Processing of X-ray diffraction data collected in oscillation mode. Macromolecular Crystallography, Pt A *276*, 307-326.

Oyler,G.A., Higgins,G.A., Hart,R.A., Battenberg,E., Billingsley,M., Bloom,F.E., and Wilson,M.C. (1989). The identification of a novel synaptosomal-associated protein, SNAP-25, differentially expressed by neuronal subpopulations. J. Cell Biol. *109*, 3039-3052.

Pabst,S., Hazzard,J.W., Antonin,W., Sudhof,T.C., Jahn,R., Rizo,J., and Fasshauer,D. (2000). Selective interaction of complexin with the neuronal SNARE complex. Determination of the binding regions. J. Biol. Chem. *275*, 19808-19818.

Pabst,S., Margittai,M., Vainius,D., Langen,R., Jahn,R., and Fasshauer,D. (2002). Rapid and selective binding to the synaptic SNARE complex suggests a modulatory role of complexins in neuroexocytosis. J. Biol. Chem. *277*, 7838-7848.

Pellizzari,R., Rossetto,O., Schiavo,G., and Montecucco,C. (1999). Tetanus and botulinum neurotoxins: mechanism of action and therapeutic uses. Philos. Trans. R. Soc. Lond B Biol. Sci. *354*, 259-268.

Perin,M.S., Brose,N., Jahn,R., and Sudhof,T.C. (1991a). Domain structure of synaptotagmin (p65). J. Biol. Chem. *266*, 623-629.

Perin,M.S., Fried,V.A., Mignery,G.A., Jahn,R., and Sudhof,T.C. (1990). Phospholipid binding by a synaptic vesicle protein homologous to the regulatory region of protein kinase C. Nature *345*, 260-263.

Perin,M.S., Johnston,P.A., Ozcelik,T., Jahn,R., Francke,U., and Sudhof,T.C. (1991b). Structural and functional conservation of synaptotagmin (p65) in Drosophila and humans. J. Biol. Chem. *266*, 615-622.

Perisic,O., Fong,S., Lynch,D.E., Bycroft,M., and Williams,R.L. (1998). Crystal structure of a calcium-phospholipid binding domain from cytosolic phospholipase A2. J. Biol. Chem. *273*, 1596-1604.

Pervushin,K., Riek,R., Wider,G., and Wuthrich,K. (1997). Attenuated T2 relaxation by mutual cancellation of dipole-dipole coupling and chemical shift anisotropy indicates an avenue to NMR structures of very large biological macromolecules in solution. Proc. Natl. Acad. Sci. U. S. A *94*, 12366-12371.

Poirier,M.A., Hao,J.C., Malkus,P.N., Chan,C., Moore,M.F., King,D.S., and Bennett,M.K. (1998a). Protease resistance of syntaxin.SNAP-25.VAMP complexes. Implications for assembly and structure. J. Biol. Chem. *273*, 11370-11377.

Poirier,M.A., Xiao,W., Macosko,J.C., Chan,C., Shin,Y.K., and Bennett,M.K. (1998b). The synaptic SNARE complex is a parallel four-stranded helical bundle. Nat. Struct. Biol. *5*, 765-769.

Powell,C.M., Schoch,S., Monteggia,L., Barrot,M., Matos,M.F., Feldmann,N., Sudhof,T.C., and Nestler,E.J. (2004). The presynaptic active zone protein RIM1alpha is critical for normal learning and memory. Neuron *42*, 143-153.

Reim,K., Mansour,M., Varoqueaux,F., McMahon,H.T., Sudhof,T.C., Brose,N., and Rosenmund,C. (2001). Complexins regulate a late step in Ca2+-dependent neurotransmitter release. Cell *104*, 71-81.

Reim,K., Wegmeyer,H., Brandstatter,J.H., Xue,M., Rosenmund,C., Dresbach,T., Hofmann,K., and Brose,N. (2005). Structurally and functionally unique complexins at retinal ribbon synapses. J. Cell Biol. *169*, 669-680.

Rhee,J.S., Betz,A., Pyott,S., Reim,K., Varoqueaux,F., Augustin,I., Hesse,D., Sudhof,T.C., Takahashi,M., Rosenmund,C., and Brose,N. (2002). Beta phorbol ester- and diacylglycerol-induced augmentation of transmitter release is mediated by Munc13s and not by PKCs. Cell *108*, 121-133.

Rhee,J.S., Li,L.Y., Shin,O.H., Rah,J.C., Rizo,J., Sudhof,T.C., and Rosenmund,C. (2005). Augmenting neurotransmitter release by enhancing the apparent Ca2+ affinity of synaptotagmin 1. Proc. Natl. Acad. Sci. U. S. A *102*, 18664-18669.

Rickman,C. and Davletov,B. (2003). Mechanism of calcium-independent synaptotagmin binding to target SNAREs. J. Biol. Chem. *278*, 5501-5504.

Rickman,C., Archer,D.A., Meunier,F.A., Craxton,M., Fukuda,M., Burgoyne,R.D., and Davletov,B. (2004). Synaptotagmin Interaction with the Syntaxin/SNAP-25 Dimer Is Mediated by an Evolutionarily Conserved Motif and Is Sensitive to Inositol Hexakisphosphate. J. Biol. Chem. *279*, 12574-12579.

Rickman,C., Jimenez,J.L., Graham,M.E., Archer,D.A., Soloviev,M., Burgoyne,R.D., and Davletov,B. (2006). Conserved prefusion protein assembly in regulated exocytosis. Mol. Biol. Cell *17*, 283-294.

Riek,R., Fiaux,J., Bertelsen,E.B., Horwich,A.L., and Wuthrich,K. (2002). Solution NMR techniques for large molecular and supramolecular structures. J. Am. Chem. Soc. *124*, 12144-12153.

Rigaud,J.L. and Levy,D. (2003). Reconstitution of membrane proteins into liposomes. Methods Enzymol. *372*, 65-86.

Rigaud,J.L., Pitard,B., and Levy,D. (1995). Reconstitution of membrane proteins into liposomes: application to energy-transducing membrane proteins. Biochim. Biophys. Acta *1231*, 223-246.

Rizo,J. and Sudhof,T.C. (1998). C2-domains, structure and function of a universal Ca2+-binding domain. J. Biol. Chem. *273*, 15879-15882.

Rizo,J. and Sudhof,T.C. (2002). Snares and munc18 in synaptic vesicle fusion. Nat. Rev. Neurosci. *3*, 641-653.

Rizo,J., Chen,X., and Arac,D. (2006). Unraveling the mechanisms of synaptotagmin and SNARE function in neurotransmitter release. Trends Cell Biol. *16*, 339-350.

Robinson,I.M., Ranjan,R., and Schwarz,T.L. (2002). Synaptotagmins I and IV promote transmitter release independently of Ca(2+) binding in the C(2)A domain. Nature *418*, 336-340.

Ron,D., Luo,J., and Mochly-Rosen,D. (1995). C2 region-derived peptides inhibit translocation and function of beta protein kinase C in vivo. J. Biol. Chem. *270*, 24180-24187.

Rothman,J.E. (1994). Mechanisms of intracellular protein transport. Nature *372*, 55-63.

Rufener,E., Frazier,A.A., Wieser,C.M., Hinderliter,A., and Cafiso,D.S. (2005). Membrane-bound orientation and position of the synaptotagmin C2B domain determined by site-directed spin labeling. Biochemistry *44*, 18-28.

Schaub,J.R., Lu,X., Doneske,B., Shin,Y.K., and McNew,J.A. (2006). Hemifusion arrest by complexin is relieved by Ca2+-synaptotagmin I. Nat. Struct. Mol. Biol. *13*, 748-750.

Schekman,R. and Orci,L. (1996). Coat proteins and vesicle budding. Science *271*, 1526-1533.

Schiavo,G., Benfenati,F., Poulain,B., Rossetto,O., Polverino,d.L., DasGupta,B.R., and Montecucco,C. (1992). Tetanus and botulinum-B neurotoxins block neurotransmitter release by proteolytic cleavage of synaptobrevin. Nature *359*, 832-835.

Schiavo,G., Gu,Q.M., Prestwich,G.D., Sollner,T.H., and Rothman,J.E. (1996). Calcium-dependent switching of the specificity of phosphoinositide binding to synaptotagmin. Proc. Natl. Acad. Sci. U. S. A *93*, 13327-13332.

Schiavo,G., Stenbeck,G., Rothman,J.E., and Sollner,T.H. (1997). Binding of the synaptic vesicle v-SNARE, synaptotagmin, to the plasma membrane t-SNARE, SNAP-25, can explain docked vesicles at neurotoxin-treated synapses. Proc. Natl. Acad. Sci. U. S. A *94*, 997-1001.

Schneggenburger,R. and Neher,E. (2000). Intracellular calcium dependence of transmitter release rates at a fast central synapse. Nature *406*, 889-893.

Schoch,S., Castillo,P.E., Jo,T., Mukherjee,K., Geppert,M., Wang,Y., Schmitz,F., Malenka,R.C., and Sudhof,T.C. (2002). RIM1 alpha forms a protein scaffold for regulating neurotransmitter release at the active zone. Nature *415*, 321-326.

Schoch,S., Deak,F., Konigstorfer,A., Mozhayeva,M., Sara,Y., Sudhof,T.C., and Kavalali,E.T. (2001). SNARE function analyzed in synaptobrevin/VAMP knockout mice. Science *294*, 1117-1122.

Schulze,K.L., Broadie,K., Perin,M.S., and Bellen,H.J. (1995). Genetic and electrophysiological studies of Drosophila syntaxin-1A demonstrate its role in nonneuronal secretion and neurotransmission. Cell *80*, 311-320.

Serra-Pages,C., Medley,Q.G., Tang,M., Hart,A., and Streuli,M. (1998). Liprins, a family of LAR transmembrane protein-tyrosine phosphatase-interacting proteins. J. Biol. Chem. *273*, 15611-15620.

Shao,X., Davletov,B.A., Sutton,R.B., Sudhof,T.C., and Rizo,J. (1996). Bipartite Ca^{2+}-binding motif in C2 domains of synaptotagmin and protein kinase C. Science *273*, 248-251.

Shao,X., Fernandez,I., Sudhof,T.C., and Rizo,J. (1998). Solution structures of the Ca2+-free and Ca2+-bound C2A domain of synaptotagmin I: does Ca2+ induce a conformational change? Biochemistry *37*, 16106-16115.

Shao,X., Li,C., Fernandez,I., Zhang,X., Sudhof,T.C., and Rizo,J. (1997). Synaptotagmin-syntaxin interaction: the C2 domain as a Ca2+-dependent electrostatic switch. Neuron *18*, 133-142.

Shin,O.H., Rhee,J.S., Tang,J., Sugita,S., Rosenmund,C., and Sudhof,T.C. (2003). Sr2+ binding to the Ca2+ binding site of the synaptotagmin 1 C2B domain triggers fast exocytosis without stimulating SNARE interactions. Neuron *37*, 99-108.

Shin,O.H., Rizo,J., and Sudhof,T.C. (2002). Synaptotagmin function in dense core vesicle exocytosis studied in cracked PC12 cells. Nat. Neurosci. *5*, 649-656.

Sia,S.K. and Whitesides,G.M. (2003). Microfluidic devices fabricated in poly(dimethylsiloxane) for biological studies. Electrophoresis *24*, 3563-3576.

Sollner,T., Bennett,M.K., Whiteheart,S.W., Scheller,R.H., and Rothman,J.E. (1993a). A protein assembly-disassembly pathway in vitro that may correspond to sequential steps of synaptic vesicle docking, activation, and fusion. Cell *75*, 409-418.

Sollner,T., Whiteheart,S.W., Brunner,M., Erdjument-Bromage,H., Geromanos,S., Tempst,P., and Rothman,J.E. (1993b). SNAP receptors implicated in vesicle targeting and fusion. Nature *362*, 318-324.

Sollner,T.H. (2003). Regulated exocytosis and SNARE function (Review). Mol. Membr. Biol. *20*, 209-220.

Stevens,C.F. and Sullivan,J.M. (2003). The synaptotagmin C2A domain is part of the calcium sensor controlling fast synaptic transmission. Neuron *39*, 299-308.

Sudhof,T.C. (1995). The synaptic vesicle cycle: a cascade of protein-protein interactions. Nature *375*, 645-653.

Sudhof,T.C. (2002). Synaptotagmins: why so many? J. Biol. Chem. *277*, 7629-7632.

Sudhof,T.C. (2004). The synaptic vesicle cycle. Annual Review of Neuroscience *27*, 509-547.

Sudhof,T.C. and Rizo,J. (1996). Synaptotagmins: C2-domain proteins that regulate membrane traffic. Neuron *17*, 379-388.

Sugita,S., Han,W., Butz,S., Liu,X., Fernandez-Chacon,R., Lao,Y., and Sudhof,T.C. (2001). Synaptotagmin VII as a plasma membrane Ca(2+) sensor in exocytosis. Neuron *30*, 459-473.

Sugita,S., Hata,Y., and Sudhof,T.C. (1996). Distinct Ca(2+)-dependent properties of the first and second C2-domains of synaptotagmin I. J. Biol. Chem. *271*, 1262-1265.

Sugita,S., Shin,O.H., Han,W., Lao,Y., and Sudhof,T.C. (2002). Synaptotagmins form a hierarchy of exocytotic Ca(2+) sensors with distinct Ca(2+) affinities. EMBO J. *21*, 270-280.

Sutton,R.B. and Sprang,S.R. (1998). Structure of the protein kinase Cbeta phospholipid-binding C2 domain complexed with Ca2+. Structure. *6*, 1395-1405.

Sutton,R.B., Davletov,B.A., Berghuis,A.M., Sudhof,T.C., and Sprang,S.R. (1995). Structure of the first C2 domain of synaptotagmin I: a novel Ca^{2+}/phospholipid-binding fold. Cell *80*, 929-938.

Sutton,R.B., Ernst,J.A., and Brunger,A.T. (1999). Crystal structure of the cytosolic C2A-C2B domains of synaptotagmin III. Implications for Ca(+2)-independent snare complex interaction. J. Cell Biol. *147*, 589-598.

Sutton,R.B., Fasshauer,D., Jahn,R., and Brunger,A.T. (1998). Crystal structure of a SNARE complex involved in synaptic exocytosis at 2.4 A resolution. Nature *395*, 347-353.

Takahashi,S., Yamamoto,H., Matsuda,Z., Ogawa,M., Yagyu,K., Taniguchi,T., Miyata,T., Kaba,H., Higuchi,T., Okutani,F., and . (1995). Identification of two highly homologous presynaptic proteins distinctly localized at the dendritic and somatic synapses. FEBS Lett. *368*, 455-460.

Takao-Rikitsu,E., Mochida,S., Inoue,E., guchi-Tawarada,M., Inoue,M., Ohtsuka,T., and Takai,Y. (2004). Physical and functional interaction of the active zone proteins, CAST, RIM1, and Bassoon, in neurotransmitter release. J. Cell Biol. *164*, 301-311.

Tang,J., Maximov,A., Shin,O.H., Dai,H., Rizo,J., and Sudhof,T.C. (2006). A complexin/synaptotagmin 1 switch controls fast synaptic vesicle exocytosis. Cell *126*, 1175-1187.

Tannenberg,R.K., Scott,H.L., Tannenberg,A.E., and Dodd,P.R. (2006). Selective loss of synaptic proteins in Alzheimer's disease: evidence for an increased severity with APOE varepsilon4. Neurochem. Int. *49*, 631-639.

Thomas,D.M., Ferguson,G.D., Herschman,H.R., and Elferink,L.A. (1999). Functional and biochemical analysis of the C2 domains of synaptotagmin IV. Mol. Biol. Cell *10*, 2285-2295.

Tocco,G., Bi,X., Vician,L., Lim,I.K., Herschman,H., and Baudry,M. (1996). Two synaptotagmin genes, Syt1 and Syt4, are differentially regulated in adult brain and during postnatal development following kainic acid-induced seizures. Brain Res. Mol. Brain Res. *40*, 229-239.

Tokumaru,H., Umayahara,K., Pellegrini,L.L., Ishizuka,T., Saisu,H., Betz,H., Augustine,G.J., and Abe,T. (2001). SNARE complex oligomerization by synaphin/complexin is essential for synaptic vesicle exocytosis. Cell *104*, 421-432.

Trimble,W.S., Cowan,D.M., and Scheller,R.H. (1988). Vamp-1 - A Synaptic Vesicle-Associated Integral Membrane-Protein. Proceedings of the National Academy of Sciences of the United States of America *85*, 4538-4542.

Tucker,W.C. and Chapman,E.R. (2002). Role of synaptotagmin in Ca2+-triggered exocytosis. Biochem. J. *366*, 1-13.

Tucker,W.C., Weber,T., and Chapman,E.R. (2004). Reconstitution of Ca2+-Regulated Membrane Fusion by Synaptotagmin and SNAREs. Science.

Ubach,J., Garcia,J., Nittler,M.P., Sudhof,T.C., and Rizo,J. (1999). Structure of the Janus-faced C2B domain of rabphilin. Nat. Cell Biol. *1*, 106-112.

Ubach,J., Lao,Y., Fernandez,I., Arac,D., Sudhof,T.C., and Rizo,J. (2001). The C2B domain of synaptotagmin I is a Ca2+-binding module. Biochemistry *40*, 5854-5860.

Ubach,J., Zhang,X., Shao,X., Sudhof,T.C., and Rizo,J. (1998). Ca^{2+} binding to synaptotagmin: how many Ca^{2+} ions bind to the tip of a C2-domain? EMBO J. *17*, 3921-3930.

Ullrich,B., Li,C., Zhang,J.Z., McMahon,H., Anderson,R.G., Geppert,M., and Sudhof,T.C. (1994). Functional properties of multiple synaptotagmins in brain. Neuron *13*, 1281-1291.

Verdaguer,N., Corbalan-Garcia,S., Ochoa,W.F., Fita,I., and Gomez-Fernandez,J.C. (1999). Ca(2+) bridges the C2 membrane-binding domain of protein kinase Calpha directly to phosphatidylserine. EMBO J. *18*, 6329-6338.

Verhage,M., Maia,A.S., Plomp,J.J., Brussaard,A.B., Heeroma,J.H., Vermeer,H., Toonen,R.F., Hammer,R.E., van den Berg,T.K., Missler,M., Geuze,H.J., and Sudhof,T.C. (2000). Synaptic assembly of the brain in the absence of neurotransmitter secretion. Science *287*, 864-869.

Vician,L., Lim,I.K., Ferguson,G., Tocco,G., Baudry,M., and Herschman,H.R. (1995). Synaptotagmin IV is an immediate early gene induced by depolarization in PC12 cells and in brain. Proc. Natl. Acad. Sci. U. S. A *92*, 2164-2168.

von Poser,C., Ichtchenko,K., Shao,X., Rizo,J., and Sudhof,T.C. (1997). The evolutionary pressure to inactivate. A subclass of synaptotagmins with an amino acid substitution that abolishes Ca2+ binding. J. Biol. Chem. *272*, 14314-14319.

Wang,C.T., Grishanin,R., Earles,C.A., Chang,P.Y., Martin,T.F., Chapman,E.R., and Jackson,M.B. (2001a). Synaptotagmin modulation of fusion pore kinetics in regulated exocytosis of dense-core vesicles. Science *294*, 1111-1115.

Wang,C.T., Lu,J.C., Bai,J., Chang,P.Y., Martin,T.F., Chapman,E.R., and Jackson,M.B. (2003a). Different domains of synaptotagmin control the choice between kiss-and-run and full fusion. Nature *424*, 943-947.

Wang,P., Wang,C.T., Bai,J., Jackson,M.B., and Chapman,E.R. (2003b). Mutations in the effector binding loops in the C2A and C2B domains of synaptotagmin I disrupt exocytosis in a nonadditive manner. J. Biol. Chem. *278*, 47030-47037.

Wang,X., Hu,B., Zimmermann,B., and Kilimann,M.W. (2001b). Rim1 and rabphilin-3 bind Rab3-GTP by composite determinants partially related through N-terminal alpha -helix motifs. J. Biol. Chem. *276*, 32480-32488.

Wang,Y. and Sudhof,T.C. (2003). Genomic definition of RIM proteins: evolutionary amplification of a family of synaptic regulatory proteins(small star, filled). Genomics *81*, 126-137.

Wang,Y., Liu,X., Biederer,T., and Sudhof,T.C. (2002). A family of RIM-binding proteins regulated by alternative splicing: Implications for the genesis of synaptic active zones. Proc. Natl. Acad. Sci. U. S. A *99*, 14464-14469.

Wang,Y., Okamoto,M., Schmitz,F., Hofmann,K., and Sudhof,T.C. (1997). Rim is a putative Rab3 effector in regulating synaptic-vesicle fusion. Nature *388*, 593-598.

Wang,Y., Sugita,S., and Sudhof,T.C. (2000). The RIM/NIM family of neuronal C2 domain proteins. Interactions with Rab3 and a new class of Src homology 3 domain proteins. J. Biol. Chem. *275*, 20033-20044.

Washbourne,P., Thompson,P.M., Carta,M., Costa,E.T., Mathews,J.R., Lopez-Bendito,G., Molnar,Z., Becher,M.W., Valenzuela,C.F., Partridge,L.D., and Wilson,M.C. (2002). Genetic ablation of the t-SNARE SNAP-25 distinguishes mechanisms of neuroexocytosis. Nat. Neurosci. *5*, 19-26.

Weber,T., Zemelman,B.V., McNew,J.A., Westermann,B., Gmachl,M., Parlati,F., Sollner,T.H., and Rothman,J.E. (1998). SNAREpins: minimal machinery for membrane fusion. Cell *92*, 759-772.

Weimbs,T., Mostov,K., Low,S.H., and Hofmann,K. (1998). A model for structural similarity between different SNARE complexes based on sequence relationships. Trends Cell Biol. *8*, 260-262.

Wu,Y., He,Y., Bai,J., Ji,S.R., Tucker,W.C., Chapman,E.R., and Sui,S.F. (2003). Visualization of synaptotagmin I oligomers assembled onto lipid monolayers. Proc. Natl. Acad. Sci. U. S. A *100*, 2082-2087.

Xia,Y.N. and Whitesides,G.M. (1998). Soft lithography. Angewandte Chemie-International Edition *37*, 551-575.

Xu,G.Y., McDonagh,T., Yu,H.A., Nalefski,E.A., Clark,J.D., and Cumming,D.A. (1998). Solution structure and membrane interactions of the C2 domain of cytosolic phospholipase A2. J. Mol. Biol. *280*, 485-500.

Zhang,X., Kim-Miller,M.J., Fukuda,M., Kowalchyk,J.A., and Martin,T.F. (2002). Ca2+-dependent synaptotagmin binding to SNAP-25 is essential for Ca2+-triggered exocytosis. Neuron *34*, 599-611.

Zhang,X., Rizo,J., and Sudhof,T.C. (1998). Mechanism of phospholipid binding by the C2A-domain of synaptotagmin I. Biochemistry *37*, 12395-12403.

Zhen,M. and Jin,Y. (1999). The liprin protein SYD-2 regulates the differentiation of presynaptic termini in C. elegans. Nature *401*, 371-375.

Zimmerberg,J., Akimov,S.A., and Frolov,V. (2006). Synaptotagmin: fusogenic role for calcium sensor? Nat. Struct. Mol. Biol. *13*, 301-303.

VITAE

Han Dai was born in Nanjing, Jiangsu Province, People's Republic of China on September 30, 1979, the son of Zhenjia Dai and Xiumin Guo. After completing his work at Jinling Middle School, Nanjing, Jiangsu in 1997, he entered Nanjing University in Nanjing, Jiangsu. He received the degree of Bachelor of Science with a major in Biochemistry from Nanjing University in June, 2001. Then he continued his graduate study in Nanjing University for one more year. He entered the Graduate School of Biomedical Sciences at the University of Texas Southwestern Medical Center at Dallas in July, 2002. In May 2003, he joined Dr. Rizo-Rey's laboratory. After five-year hard work, he was awarded the degree of Doctor of Philosophy in April 2007 from the Molecular Biophysics Program at the University of Texas Southwestern Medical Center at Dallas.

Permanent Address: 5454 Amesbury Dr., Apt. 903
Dallas TX, 75206